THEORETICAL AND EXPERIMENTAL STUDIES OF THE DYNAMICS AND
ACOUSTICS OF FORCED ORDERED GRANULAR NETWORKS

BY

YIJING ZHANG

DISSERTATION

Submitted in partial fulfillment of the requirements
for the degree of Doctor of Philosophy in Theoretical and Applied Mechanics
in the Graduate College of the
University of Illinois at Urbana-Champaign, 2017

Urbana, Illinois

Doctoral Committee:

Professor Alexander F. Vakakis, Chair & Director of Research
Research Professor Lawrence A. Bergman
Research Professor D. Michael McFarland
Assistant Professor Sameh Tawfick

Abstract

Ordered arrays of granular particles (beads) have attracted considerable attention in recent years due to their rich dynamical behaviors and interesting properties. Depending on the ratio of static to dynamic deformations between particles the dynamics of granular media is highly tunable ranging from being strongly nonlinear and non-smooth in the absence of static pre-compression, to reducing to weakly nonlinear and smooth for large static pre-compression. The nonlinearity in uncompressed granular media arises from two sources: First, nonlinear Hertzian interactions, which can be modeled mathematically, between beads in contact, and second, bead separations in the absence of compressive forces between them leading to collisions between adjacent beads. When no applied pre-compression exists there is complete absence of linear acoustics in ordered granular media, which results in zero speed of sound as defined in the sense of linear acoustics through the classical wave equation; thus, these media have been characterized as "sonic vacua". However, various nonlinear waves can still propagate in these media with energy tunable properties.

The first part of this dissertation aims to study the frequency responses of a single homogenous granular chain. We consider a one-dimensional uncompressed granular chain composed of a finite number of identical spherical elastic beads with Hertzian interactions. The chain is harmonically excited by an amplitude- and frequency-dependent boundary drive at its left end and has a fixed boundary at its right end. We computationally and experimentally detect time-periodic, strongly nonlinear resonances whereby the particles (beads) of the granular chain respond at integer multiples of the excitation period, and which correspond to local peaks of the maximum transmitted force at the chain's right, fixed end. In between these resonances we detect local minima of the maximum transmitted forces corresponding to anti-resonances, where chimera

states (i.e., coexistence of different stationary and nonstationary waveforms) are noted, in the steady-state dynamics. Furthermore, we construct a mathematical model which can completely capture the rich and complex dynamics of the system.

The second part of the study is primarily concerned with the propagatory dynamics of geometrically coupled ordered granular media. In particular, we focus on primary pulse transmission in a two-dimensional granular network composed of two ordered chains that are nonlinearly coupled through Hertzian interactions. Impulsive excitation is applied to one of the chains (denoted as "excited chain"), and the resulting transmitted primary pulses in both chains are considered, especially in the non-directly excited chain (denoted as "absorbing chain"). A new type of mixed nonlinear solitary pulses – shear waves is predicted for this system, leading to primary pulse equi-partition between chains, indicating strong energy exchange between two chains through the geometric coupling. Then, an analytical reduced model for primary pulse transmission is derived to study the strongly nonlinear acoustics in the small-amplitude approximation. In contrast to the full equations of motion the simplified model is re-scalable with energy and parameter-free, and is asymptotically solved by extending the one-dimensional nonlinear mapping technique. The nonlinear maps, which are derived for this two-dimensional system and governing the amplitudes of the mixed-type waves, accurately capture the primary pulse propagation in this system and predict the first occurrence of energy or pulse equi-partition in the network. Moreover, to confirm the theoretical results we experimentally test a series of two-dimensional granular networks, and prove the occurrence of strong energy exchanges leading to eventual pulse equi-partition between the excited and absorbing chains, provided that the number of beads is sufficiently large.

Then we analyze the dynamics of a granular network composed of two semi-infinite, ordered homogeneous granular chains mounted on linear elastic foundations and coupled by weak linear stiffnesses under periodic excitation. We first review the acoustic filtering properties of linear and nonlinear semi-infinite periodic media containing two attenuation zones (AZs) and one propagation zone (PZ) in the frequency domain. In both linear and nonlinear systems, under suddenly applied, high-frequency harmonic excitations, "dynamic overshoot" phenomena are realized whereby coherent traveling responses are propagating to the far fields of these media despite the fact that the high frequencies of the suddenly applied excitations lie well within the stop bands of these systems. For the case of the linear system we show that the transient dynamic overshoot can be approximately expressed in terms of the Green's function at its free end. A different type of propagating wave in the form of a "pure" traveling breather, i.e., of a single propagating oscillatory wavepacket with a localized envelope, is realized in the transient responses of a nonlinear granular network. The pure breather is asymptotically studied by a complexification/averaging technique, showing nearly complete but reversible energy exchanges between the excited and absorbing chains as the breather propagates to the far field. We analytically prove that the reason for this dynamic overshoot phenomenon in both linear and nonlinear networks is the high rate of application of the high-frequency harmonic excitation, which, in essence, amounts approximately to an impulsive excitation of the periodic medium. Verification of the analytical approximations with direct numerical simulations is performed.

We further study passive pulse redirection and nonlinear targeted energy transfer in the aforementioned weakly coupled granular network. Periodic excitation in the form of repetitive half-sine pulses is applied to the excited chain. The frequency of excitation is within the pass band of the granular system. At the steady state nearly complete but reversible energy exchanges

between the two chains are noted. We show that passive pulse redirection and targeted energy transfer from the excited to the absorbing chain can be achieved by macro-scale realization of the spatial analog of the Landau-Zener quantum tunneling effect. This is realized by finite stratification of the elastic foundation of the excited chain, and depends on the system parameters (e.g., the percentage of stratification) and on the parameters of the periodic excitation. We detect the existence of two distinct nonlinear phenomena in the periodically forced network; namely, (i) energy localization in the absorbing chain due to sustained 1:1 resonance capture leading to irreversible pulse redirection from the excited chain, and (ii) continuous energy exchanges in the form of nonlinear beats between the two chains in the absence of resonance capture. Our results demonstrate that steady state passive pulse redirection in these networks can be robustly achieved under periodic excitation.

The final part of present work is concerned with propagating breathers in granular networks under impulsive excitation. We apply a complexification-averaging methodology leading to smooth slow flow reduced models of the dynamics to reveal the nature of 1:1 resonance at fundamental steady-state responses of the system. The primary aim of this analytical study is to provide a predictive way to excite the system at its resonance conditions. In addition to the fundamental resonance we numerically verify the occurrences of subharmonic steady-state responses in such granular networks. We experimentally detect the propagating breathers in a single chain mounted on elastic foundations. Our experimental measurements show good correspondence with the computational results which validate our previous theoretical predications. The results of this work contribute to the design of practical nonlinear acoustic metamaterials and provide a new avenue for understanding ofthe complex nonlinear dynamics of granular media.

Acknowledgements

First and foremost, I would like to express my sincere gratitude to my advisor Prof. Alexander F. Vakakis for his continuous support of my Ph.D research in the last four years, for his patience, motivation and encouragement. His immense knowledge and thorough guidance have helped me in all the time of study and writing of this dissertation. I was very impressed by his teaching abilities and have been so fortunate to take three enormously well organized and delivered courses with him. I could not have imagined having a better advisor and mentor for my Ph.D study.

I would like to thank Prof. Yuli Starosvetsky of Technion – Israel Institute of Technology, for his advice and help in the analytical derivation of the mapping technique discussed in Chapter 3. His valuable advice and support are greatly acknowledged. Also, I would like to give special thanks to Prof. McFarland and Dr. Hasan for their effort to advise me. I would like to thank Prof. McFarland for his invaluable and constructive suggestions. His support helped me overcome many obstacles in my research and illuminated my work. I was also so grateful to have Dr. Hasan as a colleague and friend when I first joined the group. I have learnt a lot from him. He was always patient to look at every details in my work and answered every "naïve" question I asked.

I would also like to thank my committee members Prof. Vakakis, Prof. Lawrence Bergman, Prof. McFarland, and Prof. Sameh Tawfick for their time and contributions. I would like to acknowledge the Mechanical Science and Engineering Department (MechSE) at University of Illinois at Urbana-Champaign for giving me an opportunity to complete the doctoral program.

I would also like to thank my colleagues Arif Hasan, Jayaprakash Kalkunte, Mehmet Kurt, Kevin Remick, Bongwon Jeong, Randi Potekin, Antoine Blanchard, Keegan Moore and Zhen Zhang for their great advice, for providing a friendly work environment and all the laughs along

the way. Special thanks are due to Keegan Moore for his contributions in Chapter 4 regarding the resonance capture analysis and the numerical empirical mode decompositions.

Table of Contents

Chapter 1. Introduction

Granular media are collections of finite numbers of distinct granules or beads. These unique media are usually considered to possess the properties of solid, liquid and gas states of matter. The evolution of the motion of the granules follows Newton's 2nd law and the compressive forces between granules are non-zero only when there are contacts between them. The particle distribution in the granular system can range from packed or ordered to randomly dispersed or disordered. In this dissertation, we primarily focus on ordered granular systems, i.e., the arrangements of granules in the systems follow certain patterns or paths.

1.1 Literature review and research objectives

Ordered arrays of granular beads are known to exhibit rich nonlinear dynamical and acoustical behaviors, so they have received considerable attention in diverse fields of applied mathematics, applied physics and mechanics. This field of research originated from the papers of Nesterenko (1983) and Lazaridi and Nesterenko (1985), and was further explored by other researchers (Sinkovits et al., 1995; Coste et al. 1997; Sen et al., 1998; Daraio et al., 2006; Sen et al., 2008; Spadoni et al., 2010; James, 2011; Kevrekidis, 2011; Porter et al., 2015).

It is well-known that granular media are a highly complex and distinct class of dynamical systems. The dynamics of granular media is highly tunable, ranging from strongly nonlinear and non-smooth in the absence of static pre-compression, to weakly nonlinear and smooth for large static pre-compression (Nesterenko, 2001; Daraio et al., 2006; Sen et al., 2008; Sun et al., 2011). The nonlinearity in granular media arises from two sources: First, due to nonlinear Hertzian interactions between beads in contact; and second, due to bead separations in the absence of compressive forces between them leading to collisions between adjacent beads. With applied pre-

compression a linear component in the acoustics is generated and the problem becomes linearizable, whereas for strong pre-compression and under the assumption of small amplitude oscillations, the dynamics of granular chains can be effectively described by the well-known Fermi-Paste-Ulam (FPU) model (Poggi et al., 1997; Rink and Verhulst, 2000; Chechin et. al., 2002; Flach et al., 2005; Dauxois et al., 2005, Berman and Izrailev, 2005; Henrici and Kappeler, 2008) which in a long-wave approximation is reduced to the well-known integrable Kortweg-de Vries (KdV) model (Nesterenko, 2001; Sen et al., 2008). When no pre-compression exists and separation between beads is possible, there is complete absence of linear acoustics in ordered granular media, which results in zero speed of sound as defined in the sense of linear acoustics through the classical wave equation; hence, these uncompressed media have been characterized by Nesterenko (2001) as "sonic vacua". Despite the absence of linear acoustics, however, it has been shown that these essentially nonlinear sonic vacua possess highly complex nonlinear responses with no counterparts in linear theory. Moreover, even in the strongly nonlinear regime (i.e., in the absence of any pre-compression) computational and analytical techniques have been developed for studying solitary waves (Lazaridi, and Nesterenko, 1985; Coste et al., 1997; MacKay, 1999; Sen and Manciu, 2001; Sen et al., 2008), traveling waves (Starosvetsky and Vakakis, 2010), resonances and anti-resonances (Pozharskiy et al., 2015; Zhang et al., 2016), frequency bands (Jayaprakash et al., 2011a; Lydon et al., 2013; Hasan et al., 2015), traveling and standing breathers (Sen and Mohan, 2009; Starosvetsky et al., 2012a), targeted energy transfers (Hasan et al., 2013a), and other strongly nonlinear dynamical and acoustical phenomena.

Much emphasis has been given to the analysis of wave propagation in one-dimensional homogenous granular chains. Nesterenko (1983) was the first to discover the propagation of a special class of solitary pulses in one-dimensional homogeneous granular chains that do not

involve bead separations, and, hence, can be studied by asymptotic techniques in the continuum limit using long-wave approximations; in this work these solitary pulses will be denoted as *Nesterenko solitary pulses*. These waves span 6-7 beads (Lazaridi and Nesterenko, 1985; Nesterenko, 2001; Sen et al., 2008) with amplitude-dependent shapes and speeds, and were referred to as compactons (Rosenau and Hyman, 1993, Porter et al., 2008) exhibiting super-exponential decay in their tails (Chatterjee, 1999). Solitary waves provide the fundamental mechanism for energy and momentum transfer in ordered granular networks, and have been well-studied both theoretically (Friesecke and Wattis, 1994; Ji and Hong, 1999; MacKay, 1999; Sen and Manciu, 2001; English and Pego, 2005; Stefanov and Kevrekidis, 2012; Starosvetsky, 2012) and experimentally (Lazaridi and Nesterenko, 1985; Coste et al., 1997; Daraio et al., 2006; Job et al., 2007). Solitary pulses have been used in various applications, such as sound bullets and acoustic lenses (Spadoni and Daraio, 2010) and nondestructive evaluation (Yang et al., 2012).

Although few works have considered dissipation effects in granular chains, the highly complex granular dynamics is very sensitive to damping, since for low-enough dissipation the granular chain possesses chaotic dynamics due to separations and ensuing collisions between beads (Lydon et al., 2013; Hooheboom et al., 2013; Charalampidis et al., 2015). Despite numerous efforts (Rosas et al., 2007; Carretero-Gonzalez et al. 2009; Vergara 2010), a universal model capturing quantitatively the phenomenology of dissipative losses is still not available. Nevertheless, modeling the dissipation with (linear) velocity-dependent damping is very successful as proved experimentally (Herbold and Nesterenko, 2007; Potekin et al., 2012).

In spatially periodic systems resonances and anti-resonances are the main mechanism to facilitate or restrict energy transmission. In impulsively excited one-dimensional diatomic granular chains resonances and anti-resonances were also noted. Periodic diatomic chains are composed of

3

pairs of different types of beads, for example, chains consisting of alternating ("heavy" and "light") beads with dissimilar mass and/or stiffness. The dynamics of one-dimensional diatomic granular chains have been studied in previous works (Nesterenko, 2001; Porter et al., 2008; Herbold et al., 2009). In an appropriately designed dimer chain with no pre-compression, the existence of countable infinities of resonances and anti-resonances was proved theoretically (Jayaprakash et al., 2011b; Jayaprakash et al., 2013) and verified experimentally (Potekin et al., 2012). At discrete values of the mass ratio of light and heavy beads anti-resonances are realized, leading to unattenuated energy transmission through the dimer chain. At other discrete values of the mass ratio, resonances can be realized when the initial applied impulse leads to strong but localized oscillations of the light beads; these resonances lead to strong passive attenuation of propagating pulses, which restricts energy transmission to the far field (Jayaprakash et al., 2011b). This is a clear practical application for passive shock mitigation devices which are commonly used in engineering practice.

Although the majority of works have focused on "dry" granular media, i.e., granular networks where the interstitial space between granules is unfilled and granules are not connected to any attachments, the effect of elastic foundations on the free (unforced) and forced dynamics of spatially periodic media can be significant, e.g., giving rise to a special class of time-periodic nonlinear responses with highly localized envelopes referred to as discrete traveling breathers (Sievers and Takeno, 1988; Campbell and Peyrard, 1990). A traveling breather is defined as a nonlinear oscillatory wavepacket propagating in a nonlinear medium, with its envelope possessing localized characteristics (either in amplitude or in slope). It has been demonstrated that discrete standing or propagating breathers form in nonlinear lattices due to discreteness, dispersion and nonlinearity (Aubry, 1997; Flach and Willis, 1998; Flach and Gorbach, 2008).

4

The formation of discrete breathers in ordered granular media is a relatively unexplored area of study. The realization of transient breathers due to the presence of the small mass intruder (Starosvetsky et al., 2012b), and intrinsic energy localization by exciting breathers under pre-compression (i.e., taking into account the linear component in the dynamics) (Theocharis et al., 2010) were studied, whereas experimental proof of discrete breathers in a one-dimensional diatomic granular crystal has been reported by Boechler et al. (2010). Some other works related to discrete breathers in ordered granular media include discrete breathers at the interface between a diatomic and a monoatomic granular chain with pre-compression (Hoogeboom et al., 2010); and wave localization in Hertzian chains with mass defect (Job et al., 2009). Furthermore, analytical techniques have been developed for studying the highly complex dynamics of discrete breathers in granular media (James, 2011; James et al., 2013). Starosvetsky et al. (2012a) analytically studied the dynamics of two weakly coupled, homogeneous granular chains without precompression, each supported by a linear distributed elastic foundation, in which complete and recurrent energy exchanges between the chains through the excitation of nonlinear beat phenomena were detected. In a continuation of that work Hasan et al. (2013) introduced the concept of targeted energy transfer, i.e., of directed energy transfer (Vakakis et al. 2008), from a primary oscillating system to a secondary attachment, where this energy is locally confined without scattering back to the identical granular network, leading to passive, irreversible pulse redirection from the directly excited chain to the chain to which it is weakly coupled. The nonlinear dynamical mechanism governing this interesting phenomenon was found to be a macroscopic analog (in space) of the Landau-Zener quantum tunneling effect (in time). Landau-Zener tunneling is a dynamical transition of a two-level quantum mechanical system where the quantum system tunnels across an energy gap between two energy states (Zener, 1932; Razavy, 2003). Such a macroscopic analog of Landau-Zener

tunneling in time was first studied by Kosevich et al. (2010) and Manevitch et al. (2011). Moreover, in two recent works (Vortnikov and Starosvetsky, 2015a,b) the efficacy of nonlinear energy channeling was demonstrated in two-dimensional nonlinear networks of coupled oscillators consisting of periodic arrays of locally resonant unit-cells incorporating internal rotators. In ordered granular media the practical realization of the Landau-Zener effect was achieved by spatial stratification (variation) of the weak coupling between the chains or of the elastic foundation of the directly excited chain. The propagation of discrete breathers proved to be the fundamental component of this passive energy redirection and targeted energy transfer (Hasan et al., 2013; Zhang et al., 2015b). In addition, experimental verification of traveling breathers was performed by Hasan et al. (2015) in harmonically forced granular chains embedded in viscoelastic material matrices.

The acoustic filtering properties of linear systems with spatially periodic structure have been well studied. The dispersion relation of linear periodic systems contains two stop-bands and one pass-band in the frequency domain (Brillouin, 1953; Mead, 1975; Vakakis et al., 2008). In similarity to linear periodic systems, ordered granular media also support acoustic bands (i.e., pass- and stop-bands) which are passively tunable with energy (Jayaprakash et al., 2011a; Lydon et al., 2013; Hasan et al., 2015). The structure of the pass- and stop-bands strongly affects the transmission of disturbances in the far fields of the media, since frequency components in stop-bands are blocked from transmission, whereas components in pass-bands propagate through these media unattenuated. In turn, these acoustic filtering properties drastically affect the forced responses of these media under harmonic excitations, since only frequencies in pass-bands can lead to spatially extended forced responses, whereas frequencies in stop-bands lead to near-field motions that are spatially localized close to the excitation source. Due to the strong energy

dependencies of acoustic zones of granular media much focus is devoted to the application of granular lattices in diverse fields (Donahue et al., 2014; Leonard et al., 2014), such as tunable vibration filters and acoustic switches (Boechler et al., 2011).

Motivated by these pioneering achievements in the area of strongly nonlinear dynamics of granular media reviewed above, in this dissertation we aim to explore and analyze the nonlinear dynamics of one-dimensional and multi-dimensional networks of uncompressed, highly discontinuous granular metamaterials. The dynamical systems in this study follow the essentially nonlinear inter-particle Hertzian interaction law. In addition, another form of strong nonlinearity in the interaction law originates from the possible separations between neighboring beads because of the tensionless character of the system, which implies there are no forces when beads are not in contact. The ensuing collisions between beads lead to interesting nonlinear dynamical phenomena and introduce non-smooth effects to the systems. In the context of our discussion this work aims to be one of the first comprehensive studies of nonlinear resonances and propagatory behaviors of ordered granular media.

The main objectives of this dissertation are summarized as: (a) To study the nonlinear dynamical mechanisms governing strong energy transfer phenomena and energy redistribution in granular networks; (b) To investigate and construct a predictive mathematical framework of wave propagation in granular networks and acoustic metamaterials for effective wave tailoring; and (c) To theoretically design and experimentally establish practical realizations to employ granular media as shock transmitters or attenuators.

1.2 Outline of the thesis

We begin our study in Chapter 2 by considering the dynamics of a homogenous one-dimensional granular chain. We particularly consider nonlinear resonances and anti-resonances in finite granular chains under harmonic excitations. The boundaries of the system under consideration consist of an actuator exciting the bead with prescribed harmonic displacement at one end and a rigid wall at the other end (Pozharskiy et al., 2015). The nonlinear nature of the system makes the dynamics energy dependent and sensitive to external excitations. We analyze the dynamics of the homogenous chain for varying driving frequency under constant forcing amplitude, wherein distinguishable resonances and anti-resonances between the resonances are studied. In Section 2.1 we present an experimental study of this one-dimensional uncompressed granular chain. We experimentally detect time-periodic, strongly nonlinear resonances and anti-resonances, which correspond to local peaks and dips of the maximum transmitted force at the chain's fixed end, respectively. Furthermore, the experimental results are verified by direct numerical simulations.

In Chapter 3 we focus on primary pulse transmission in a two-dimensional granular network composed of two ordered homogeneous chains that are nonlinearly coupled through Hertzian interactions with rigid boundaries (Zhang et al., 2015a). One of the chains is excited by impulsive excitation (designated as the "excited chain"), and the resulting transmitted primary pulses in both chains are considered, especially in the non-directly excited chain (the "absorbing chain"). In Section 3.1, we numerically study the propagatory and oscillatory responses of coupled granular networks where a new type of mixed wave involving nonlinear solitary-like pulses in the longitudinal direction and oscillatory shear waves in the transverse direction is formed. We show strong energy exchanges between the two coupled granular chains, leading to eventual primary pulse equi-partition. In Section 3.2 we extend the one-dimensional nonlinear mapping technique

developed in (Starosvetsky, 2012) to analytically study the strongly nonlinear acoustics in the small-amplitude approximation in the coupled granular systems by introducing an analytical reduced model for primary pulse transmission. The amplitudes of the mixed-type waves of the primary pulse propagation in this system are accurately captured by the extended nonlinear maps. Furthermore, these asymptotic results predict the first occurrence of energy equipartition in the network as presented in Section 3.2. Finally, in Section 3.3 a series of experimental tests of two-dimensional coupled granular networks is performed to verify the strong energy exchanges between the excited and abosbing chains.

A systematic analysis of the frequency response of weakly coupled granular networks is presented in Chapter 4. We first briefly review the well-known acoustic filtering properties of linear systems with spatially periodic structure in Section 4.1. We show that in linear systems under high-frequency suddenly applied excitations, dynamic overshoot phenomena are realized and the responses can be asymptotically approximated in terms of the Green's function at the free ends. Then, in Section 4.2 dynamic overshoot phenomena in the form of "pure" traveling breathers in a two-dimensional strongly nonlinear granular network composed of two semi-infinite, ordered homogeneous granular lattices mounted on linear elastic foundations and coupled by weak linear coupling terms are demonstrated (Zhang and Vakakis, 2016). The pure breathers are asymptotically studied by a complexification/averaging technique (Manevitch, 1999) revealing nearly complete but reversible energy exchanges between the excited and absorbing lattices as the breather propagates to the far field. In Section 4.3 we extend this work by exciting this two-dimensional granular network in the intermediate frequency range. We find that sequential series of nonlinear beats in terms of propagating breathers in both chains lead to strong and recurring energy exchanges. In addition, we show that passive pulse redirection and targeted energy transfer

is possible from the directly excited lattice to the absorbing one by introducing a macro-scale analog of the Landau-Zener quantum tunneling effect in the spatial domain. Moreover, we reveal the nonlinear mechanism, i.e., sustained resonance capture, leading to irreversible pulse redirection in this periodically forced network.

Granular networks mounted on linear elastic foundations are considered as good candidates as effective shock mitigators due to the realization of passive energy redirection and targeted energy transfer, and the propagation of discrete breathers is proved to be the fundamental component which enables the realization of these interesting phenomena. However, very few works reported analytical results of propagating breathers in granular networks and no experimental evidence of the existence of such propagating breathers has been reported to date. Hence, in Chapter 5, we analytically and experimentally study the formation of propagating breathers in granular networks. Smooth slow flow reduced models of the dynamics are developed in Section 5.1.1 for the fundamental resonance responses, whereas the existence of higher-order resonances is numerically shown in Section 5.1.2. Further, in Section 5.2 a series of experimental tests is performed to study propagating breathers in ordered steel granular chains, and the proposed theoretical model fully captures the experimentally detected responses.

Finally, in Chapter 6 we provide a summary of all the results presented in this dissertation and discuss their potential application to practical design. In addition, we provide some suggestions for further development of the ideas based on the topics of this dissertation.

1.3 References

Aubry, S., "Breathers in Nonlinear Lattices: Existence, Linear Stability and Quantization," *Physica D*, **103**, 201-250, 1997.

Berman, G., Izrailev, F., "The Fermi–Pasta–Ulam Problem: Fifty Years of Progress," *Chaos Interdiscip. J. Nonl. Sci.*, **15**(1), 015104, 2005.

Boechler, N., Theocharis, G., Job, S., Kevrekidis, P., Porter M., Daraio, C., "Discrete Breathers in One-Dimensional Diatomic Granular Crystals," *Phys. Rev. Lett.*, **104**(24), 244302, 2010.

Boechler, N., Theocharis, G., Daraio, C., "Bifurcation-based Acoustic Switching and Rectification," *Natural Materials*, **10**(9), 665-668, 2011.

Brillouin, L., *Wave Propagation in Periodic Structures*, Dover Publication, New York, 1953.

Carretero-Gonzalez, R., Khatri, D., Porter, M., Kevrekidis, P., Daraio, C., "Dissipative Solitary Waves in Granular Crystals," *Phys. Rev. Lett.*, **102**, 024102, 2009.

Campbell, D., Peyrard, M., *CHAOS-Soviet American Perspectives on Nonlinear Science*, American Institute of Physics, 1990.

Charalampidis, E., Li, F., Chong, C., Yang, J., Kevrekidis, P., "Time-periodic Solutions of Driven Damped Trimer Granular Crystals," *Math. Problems in Engr.,* **830978**, 2015

Chatterjee, A., "Asymptotic Solution for Solitary Waves in a Chain of Elastic Spheres," *Phys. Rev. E*, **59**(5), 5912-5919, 1999.

Chechin, G., Novikova, N., Abramenko, A., "Bushes of Vibrational Modes for Fermi-Pasta-Ulam Chains," *Physica D*, **166**(3), 208-238, 2002.

Coste, C., Falcon, E., Fauve, S., "Solitary Waves in a Chain of Beads under Hertz Contact," *Phys. Rev. E*, **56** (5), 6104–6117, 1997.

Daraio, C., Nesterenko, V., Herbold, B., Jin, S., "Tunability of Solitary Wave Properties in One-dimensional Strongly Nonlinear Phononic Crystals," *Phys. Rev. E*, **73**(2), 026610, 2006.

Dauxois, T., Khomeriki, R., Piazza, F., Ruffo, S., "The Anti-FPU Problem," *Chaos*, **15**(1), 015110, 2005.

Donahue, C., Anzel, P., Bonanomi, L., Keller, T., Daraio, C., "Experimental Realization of a Nonlinear Acoustic Lens with a Tunable Focus," *J. Appl. Phys.*, **104**, 014103, 2014.

English, J., Pego, R., "On the Solitary Wave Pulse in a Chain of Beads," *Proc. Amer. Math. Soc.*, **133**(6), 1763-1768, 2005.

Flach S., Willis C., "Discrete Breathers," *Phys. Rep.,* **295**, 181-264, 1998.

Flach, S., Ivanchenko, M., Kanakov, O., "q-breathers and the Fermi-Pasta-Ulam Problem," *Phys. Rev. Lett.*, **95**(6). 064102, 2005.

Flach S., Gorbach A., "Discrete Breathers — Advances in Theory and Applications," *Phys. Rep.,* **467**(1–3), 1–116, 2008.

Friesecke, G., Wattis, J., "Existence Theorem for Solitary Waves on Lattices," *Comm. in Math. Phys.*, **161**(2), 391-418, 1994.

Hasan, M., Starosvetsky, Y., Vakakis, A., Manevitch, L., "Nonlinear Targeted Energy Transfer and Macroscopic Analog of the Quantum Landau–Zener Effect in Coupled Granular Chains," *Physica D*, **252**, 46–58, 2013.

Hasan, M., Cho, S., Remick, K., Vakakis, A., McFarland, D., Kriven, W., "Experimental Study of Nonlinear Acoustic Bands and Propagating Breathers in Ordered Granular Media Embedded in Matrix," *Gran. Matter*, **17**, 49–72, 2015.

Henrici, A., Kappeler, T., "Results on Normal Forms for FPU Chains," *Comm. Math. Phys.*, **278**(1), 145-177, 2008.

Herbold, E., Nesterenko, V., "Shock Wave Structure in a Strongly Nonlinear Lattice with Viscous Dissipation," *Phys. Rev. E,* **75**(2), 021304, 2007.

Herbold, E., Kim, J., Nesterenko, V., Wang, S., Daraio, C., "Pulse Propagation in a Linear and Nonlinear Diatomic Periodic Chain: Effects of Acoustic Frequency Band-gap," *Acta Mech.*, **205**(1-4), 85–103, 2009.

Hoogeboom, C., Theocharis, G., Kevrekidis, P., "Discrete Breathers at the Interface between a Diatomic and a Monoatomic Granular Chain," *Phys. Rev. E*, **82**(6), 061303, 2010.

Hoogeboom, C., Man, Y., Boechler, N., Theocharis, G., Kevrekidis, P., Kevrekidis, I., Daraio, C., "Hysteresis Loops and Multi-stability: From Periodic Orbits to Chaotic Dynamics (and back) in Diatomic Granular Crystals," *EPL,* **101,** 44003, 2013.

James, G., "Nonlinear Waves in Newton's Cradle and the Discrete p-Schrödinger Equation," *Math. Mod. Meth. Appl. Sci.*, **21**, 2335-2377, 2011.

James, G., Kevrekidis, P., Cuevas J., "Breathers in Oscillator Chains with Hertzian Interactions," *Physica D*, **251**, 39–59, 2013.

Jayaprakash, K., Starosvetsky, Y., Vakakis, A., Peeters, M., Kerschen, G., "Nonlinear Normal Modes and Band Zones in Granular Chains with No Precompression," *Nonl. Dyn.*, **63**(3), 359-385, 2011a.

Jayaprakash, K., Starosvetsky, Y., Vakakis, A., "New Family of Solitary Waves in Granular Dimer Chains with No Precompression," *Phys. Rev. E*, **83**(3), 036606, 2011b.

Jayaprakash, K., Starosvetsky, Y., Vakakis, A., Gendelman, O., "Nonlinear Resonances Leading to Strong Pulse Attenuation in Granular Dimer Chains," *J. Nonl. Sci.*, **23**(3), 363–392, 2013.

Ji, J.Y., Hong, J., "Existence Criterion of Solitary Waves in a Chain of Grains," *Phys. Lett. A*, **260**(1-2), 60-61, 1999.

Job, S., Melo, F., Sokolow, A., Sen, S., "Solitary Wave Trains in Granular Chains: Experiments, Theory and Simulations," *Granul. Matter*, **10**(1), 13-20, 2007.

Job, S., Santibanez, F., Tapia, F., Melo, F., "Wave Localization in Strongly Nonlinear Hertzian Chains with Mass Defect," *Phys. Rev. E*, **80**(2), 025602, 2009.

Kevrekidis, P., "Non-linear Waves in Lattices: Past, Present, Future," *IMA J. Appl. Math.*, **76**, 389-423, 2011.

Kosevich, Y., Manevitch, L., Manevitch, E., "Vibrational Analogue of Nonadiabatic Landau-Zener Tunneling and a Possibility for the Creation of a New Type of Energy Trap," *Phys. Usp.*, **53,** 1281-1286, 2010.

Lazaridi, A., Nesterenko, V., "Observation of a New Type of Solitary Waves in a One-Dimensional Granular Medium," *J. Appl. Mech. Tech. Phys.*, **26**(3), 405-408, 1985.

Leonard, A., Ponson, L., Daraio, C., "Exponential Stress Mitigation in Structured Granular Composites," *Extr. Mech. Lett*., **1**, 23-28, 2014.

Lydon, J., Jayaprakash, K., Ngo, D., Starosvetsky, Y., Vakakis, A., and Daraio, C., "Frequency Bands of Strongly Nonlinear Homogeneous Granular Systems," *Phys. Rev. E*, **88**(1), 012206, 2013.

MacKay, R., "Solitary Waves in a Chain of Beads under Hertz Contact," *Phys. Lett. A*, **251**(3), 191-192, 1999.

Manevitch, L., "Complex Representation of Dynamics of Coupled Nonlinear Oscillators," in *Mathematical Models of Non-Linear Excitations: Transfer, Dynamics, and Control in Condensed Systems and Other Media*, Kluwer Academic, 1999.

Manevitch, L., Kosevich, Y., Mane, M., Sigalov, G., Bergman, L., Vakakis, A., "Towards a New Type of Energy Trap: Classical Analog of Quantum Landau-Zener Tunneling," *Int. J. Nonl. Mech.*, **46,** 247-252, 2011.

Mead, D., "Wave Propagation and Natural Modes in Periodic Systems: I Mono-coupled Systems," *J. Sound Vib.*, **40**(1), 1–18, 1975.

Nesterenko, V., "Propagation of Nonlinear Compression Pulses in Granular Media," *J. Appl. Mech. Techn. Phys.*, **24**(5), 733-743, 1983.

Nesterenko, V., *Dynamics of Heterogeneous Materials*, Springer Verlag, 2001.

Poggi, P., Ruffo, S., "Exact Solutions in the FPU Oscillator Chain," *Physica D*, **103**(1), 251-272, 1997.

Porter, M., Daraio, C., Herbold, E., Szelengowicz, I., Kevrekidis, P., "Highly Nonlinear Solitary Waves in Periodic Dimer Granular Chains," *Phys. Rev. E*, **77**(1), 015601, 2008.

Porter, M., Kevrekidis, P., Daraio, C., "Granular Crystals: Nonlinear Dynamics Meets Materials Engineering," *Phys. Today,* **68,** 44-50, 2015.

Potekin, R., Jayaprakash, K., McFarland, D., Remick, K., Bergman, L., Vakakis, A., "Experimental Study of Strongly Nonlinear Resonances and Anti-resonances in Granular Dimer Chains," *Exp. Mech.*, **53**(5), 861–870, 2012.

Pozharskiy, D., Zhang, Y., Williams, M., McFarland, D., Kevrekidis, P., Vakakis, A., Kevrekidis, I., "Nonlinear Resonances and Antiresonances of a Forced Sonic Vacuum," *Phys. Rev. E*, **92**(6), 063203; and arXiv:1507.01025, 2015.

Razavy, M., *Quantum Theory of Tunneling*, World Scientific, 2003.

Rink, B., Verhulst, F., "Near-integrability of Periodic FPU-chains," *Physica A*, **285**(3), 467-482, 2000.

Rosenau, P., Hyman, J., "Compactons: Solitons with Finite Wavelength," *Phys. Rev. Lett.*, **70**(5), 564-567, 1993.

Rosas, A., Romero, A., Nesterenko, V., Lindenberg, K., "Observation of Two-wave Structure in Strongly Nonlinear Dissipative Granular Chains," *Phys. Rev. Lett.*, **98**, 164301, 2007.

Sen, S., Manciu, M., Wright, J., "Soliton-like Pulses in Perturbed and Driven Hertzian Chains and Their Possible Applications in Detecting Buried Impurities," *Phys. Rev. E,* **57** (2), 2386–2397, 1998.

Sen, S., Manciu, M., "Thermalizing an Impulse," *Physica A*, **299**(3), 551-558, 2001.

Sen, S., Hong, J., Bang, J., Avalos, E., Doney, R., "Solitary Waves in the Granular Chain," *Phys. Rep.,* **462** (2), 21–66, 2008.

Sen, S., Mohan, T., "Dynamics of Metastable Breathers in Nonlinear Chains in Acoustic Vacuum," *Phys. Rev. E*, **79**(3), 036603, 2009.

Sievers, A., Takeno, S., "Intrinsic Localized Modes in Anharmonic Crystals," *Phys. Rev. Lett.*, **61**(8), 970-973, 1988.

Sinkovits, R., Sen, S., "Nonlinear Dynamics in Granular Columns," *Phys. Rev. Lett.,* **74** (14), 2686–2689, 1995.

Spadoni, A., Daraio, C., "Generation and Control of Sound Bullets with a Nonlinear Acoustic Lens," *Proc. Natl. Acad. Sci.,* **107** (16), 7230–7234, 2010.

Starosvetsky, Y., Vakakis, A., "Traveling Waves and Localized Modes in One-Dimensional Homogeneous Granular Chains With no Pre-Compression," *Phys. Rev. E*, **82**(2), 026603, 2010.

Starosvetsky Y., "Evolution of the Primary Pulse in One-dimensional Granular Crystals Subject to On-site Perturbations: Analytical study," *Phys. Rev. E*, **85**(5), 051306, 2012.

Starosvetsky, Y., Hasan, M., Vakakis, A., Manevitch, L., "Strongly Nonlinear Beat Phenomena and Energy Exchanges in Weakly Coupled Granular Chains on Elastic Foundations," *SIAM J. Appl. Math.*, **72**(1), 337–361, 2012a.

Starosvetsky, Y., Jayaprakash, K., Vakakis, A., "Scattering of Solitary Waves and Excitation of Transient Breathers in Granular Media by Light Intruders," *J. Appl. Mech.*, **79**, 011001, 1-12, 2012b.

Stefanov, A., Kevrekidis, P., "On the Existence of Solitary Traveling Waves for Generalized Hertzian Chains," *J. Nonl. Sci.*, **22**(3), 327-349, 2012.

Sun, D., Daraio, C., Sen, S., "Nonlinear Repulsive Force between Two Solids with Axial Symmetry," *Phys. Rev. E,* **83** (6), 066605, 2011.

Theocharis, G., Boechler, N., Kevrekidis, P., Job, S., Porter, M., Daraio, C., "Intrinsic Energy Localization Through Discrete Gap Breathers in One-Dimensional Diatomic Granular Crystals," *Phys. Rev. E*, **82**(5), 056604, 2010.

Vakakis, A., Gendelman, O., Bergman, L., McFarland, D., Kerschen, G., Lee, Y., *Passive Nonlinear Targeted Energy Transfer in Mechanical and Structural Systems*, Springer Verlag, 2008.

Vergara, L., "Model for Dissipative Highly Nonlinear Waves in Dry Granular Crystals," *Phys. Rev. Lett.,* **104,** 244302, 2010.

Vorotnikov, K., Starosvetsky, Y., "Nonlinear Energy Channeling in the Two-dimensional, Locally Resonant, Unit-cell Model. I. High Energy Pulsations and Routes to Energy Localization," *Chaos*, **25**, 073106, 2015a.

Vorotnikov, K., Starosvetsky, Y., "Nonlinear Energy Channeling in the Two-dimensional, Locally Resonant, Unit-cell Model. II. Low Energy Excitations and Unidirectional Energy Transport," *Chaos*, **25**, 073107, 2015b.

Yang, J., Silverstro, C., Sangiorgio, S., Borkowski, S., Ebramzadeh, E., Nardo, L., Daraio, C., "Nondestructive Evaluation of Orthopaedic Implant Stability in THA Using Highly Nonlinear Solitary Waves," *Smart Mater. Struct.,* **21**, 012002, 2012.

Zener, C., "Non-Adiabatic Crossing of Energy Levels," *Proc. Royal Soc. London A*, **137**(833), 696-702, 1932.

Zhang, Y., Hasan, M., Starosvetsky, Y., McFarland, D., Vakakis, A., "Nonlinear Mixed Solitary—Shear Waves and Pulse Equi-partition in a Granular Network," *Physica D*, **291**, 45-61, 2015a.

Zhang, Y., Moore, K., McFarland, D., Vakakis, A., "Targeted Energy Transfers and Passive Acoustic Wave Redirection in a Two-dimensional Granular Network Under Periodic Excitation," *J. Appl. Phys*., **118**, 234901, 2015b.

Zhang, Y., Pozharskiy, D., McFarland, D., Kevrekidis, P., Kevrekidis, I., Vakakis, A., "Experimental Study of Nonlinear Resonances and Antiresonances in a Forced, Ordered Granular Chain," *Exp. Mech*. (in press); and arXiv:1606.09305, 2016.

Zhang, Y., Vakakis, A., "High-Frequency Dynamic Overshoot in Linear and Nonlinear Periodic Media," *J. Comput*. *Nonl. Dynam.*, **12**, 011012, 2016.

Chapter 2. One-dimensional granular network under harmonic excitation: Resonances, anti-resonances, and chimera states

One-dimensional ordered arrays of granular beads are known to exhibit rich nonlinear dynamical and acoustical behavior, so they have received considerable recent attention in diverse fields of applied mathematics, applied physics and mechanics. Most published works on ordered granular media focus on impulsive inputs which often are simplified as prescribed initial conditions. Only a few works have studied the responses of granular particles to harmonic excitations (Lydon et al., 2013; Hoogeboom et al., 2013; Chong et al., 2014; Charalampidis et al., 2015). As essentially nonlinear systems, the dynamics and acoustics of uncompressed granular media are highly tunable with energy and depend on the frequency and energy content of the external excitation. In this chapter, we perform a systematic study of a one-dimensional granular medium under harmonic excitation. Resonance is the main mechanism for energy transmission in spatially periodic systems. To study the frequency responses in single granular networks, a scalar model is developed, where all beads are constrained to move only in the horizontal direction, so the network is one-dimensional; under this condition additional effects due to rotations of the beads can be neglected, so such rotational effects are not taken into account in the model. We numerically show that in this system there occur resonances and anti-resonances in the long-term responses, in the form of traveling and standing waves. Moreover, to model dissipative effects in the granular chain due to inherent internal structural damping within the beads and frictional effects during bead interactions, we introduce linear damping terms in the system. This type of viscous damping has been shown to be adequate in modeling granular dynamics (Herbold and Nesterenko, 2007; Rosas et al., 2007; Carretero-Gonzalez et al., 2009; Potekin et al., 2012).

We also experimentally examine the existence of resonances and anti-resonances by slightly modifying the configuration of the system through the addition of soft flexures in Section 2.2. We show that the very rich and complex dynamics of this system can be reproduced by our experimental setup, with good agreement between experimental and numerical results. In a more general context, the material in this chapter aims to experimentally prove the realization of strongly nonlinear resonances and anti-resonances in an uncompressed granular medium, even if the medium itself has a complete absence of any linear resonance spectrum.

2.1 Computational study

In Section 2.1, we construct a mathematical model of an uncompressed granular chain consisting of 11 identical particles (beads), and a right fixed boundary. A prescribed harmonic displacement with constant amplitude is applied at the left boundary through the (prescribed) motion of a "zero-th" bead. A systematic computational study is performed to investigate the stationary-state nonlinear responses of the network under different excitation frequencies. We show that in spite of the fact that the applied excitation has constant amplitude the amount of energy transmitted to the right end of the system varies with respect to excitation frequencies. In particular, we measure the maximum of the transmitted force at the right end for varying driving frequency where local peaks ("resonances") and dips ("anti-resonances") are identified.

2.1.1 System description

A schematic of the considered one-dimensional granular system is presented in Figure 2.1. The beads are of spherical shape and are composed of linearly elastic material; moreover, it is assumed that the developed stresses due to bead-to-bead interactions are within the elastic limit of the material of the beads. Under compressive internal forces the interactions between beads obey the

essentially nonlinear Hertzian law, with some added dissipative effects as discussed below. In the absence of compressive forces, bead separations and ensuing collisions between them may occur, providing an additional source of strong nonlinearity in the dynamics.
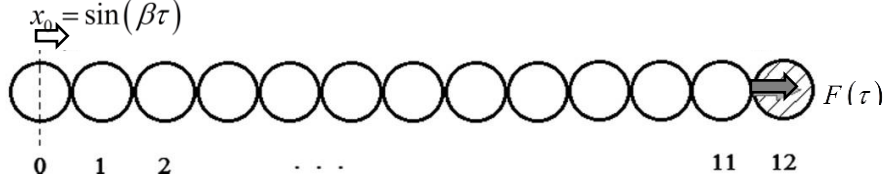

Figure 2.1. The one-dimensional granular network under periodic excitation.

According to the previous assumptions, the granular medium can be theoretically approximated by a discrete model consisting of concentrated point masses (the beads) with nearest-neighbor coupling stiffnesses obeying the Hertzian (3/2) power force law in local compression, and exerting zero force (i.e., allowing for separation between beads) in the absence of any such compression. Accordingly, the equations of motion of the granular system of Figure 2.1 can be approximately expressed as,

$$
\begin{aligned}
& m\frac{d^2u_1}{dt^2} = \frac{E\sqrt{2R}}{3(1-\nu^2)}\left\{\left(A_0\sin(2\pi ft)-u_1\right)_+^{3/2} - \left(u_1-u_2\right)_+^{3/2}\right\} \\
& +D\left\{\left[2\pi fA_0\cos(2\pi ft)-\dot{u}_1\right]\mathrm{H}\left(A_0\sin(2\pi ft)-u_1\right) - \left(\dot{u}_1-\dot{u}_2\right)\mathrm{H}\left(u_1-u_2\right)\right\} \\
& m\frac{d^2u_i}{dt^2} = \frac{E\sqrt{2R}}{3(1-\nu^2)}\left\{\left(u_{i-1}-u_i\right)_+^{3/2} - \left(u_i-u_{i+1}\right)_+^{3/2}\right\} \\
& +D\left\{\left(\dot{u}_{i-1}-\dot{u}_i\right)\mathrm{H}\left(u_{i-1}-u_i\right) - \left(\dot{u}_i-\dot{u}_{i+1}\right)\mathrm{H}\left(u_i-u_{i+1}\right)\right\}, \quad i=2,3,...,N-1 \\
& m\frac{d^2u_N}{dt^2} = \frac{E\sqrt{2R}}{3(1-\nu^2)}\left\{\left(u_{N-1}-u_N\right)_+^{3/2} - (u_N)_+^{3/2}\right\} \\
& +D\left\{\left(\dot{u}_{N-1}-\dot{u}_N\right)\mathrm{H}\left(u_{N-1}-u_N\right) - \left(\dot{u}_N\right)\mathrm{H}\left(u_N\right)\right\}
\end{aligned}
\tag{2.1}
$$

where m is the mass of one spherical bead, E and ν the elastic modulus and Poisson's ratio of its material, R its radius (for material density denoted by ρ), and D the viscous damping coefficient;

the variable u_i , $i = 1,2, ..., N = 11$, denotes the axial displacement of the $i - th$ bead of the granular chain. The amplitude (in m) and frequency (in Hz) of the prescribed displacement excitation are represented by A_0 and f. The subscript (+) denotes that a negative argument in the corresponding parenthesis should be replaced by zero, whereas $H(\cdot)$ denotes the Heaviside function. These terms appear due to the absence of tensile stresses in the granular chain, implying the possibility of bead separations in the absence of compressive forces. Moreover, zero initial conditions are assumed at the time instant of application of the periodic excitation.

The equations of motion (2.1) are in dimensional form. For our preliminary computational study reported in this section we consider a granular system composed of steel beads with parameters $m = 28.84 \times 10^{-3} \, Kg$, $E = 193 \times 10^9 \, Pa$, $v = 0.3$, $R = 9.525 \times 10^{-3}m$; and damping $D = 100 \, Ns/m$. At this point we would like to emphasize that the system considered in this section is not tied to any specific physical setup since our primary purpose is to highlight the strongly nonlinear resonance and anti-resonance phenomena that can occur the forced granular chain. Moreover, we assume that the harmonic displacement excitation has constant amplitude $A_0 = 5 \times 10^{-7}m$, which ensures that the elastic deformations of the beads are sufficiently small (within the elastic limit of steel). The dimensional equations of motion can be normalized by dividing each equation by the common mass of the beads, m, and introducing the following rescalings,

$$x_i = u_i \, / \, A_0, \tau = \varphi t, \lambda = D \, / \, (m\varphi) \text{ and } \beta = 2\pi f \, / \, \varphi$$

where the scaling factor is defined as $\varphi = \left\{ \dfrac{\sqrt{2RA_0} \, \mathrm{E}}{3(1-v^2)m} \right\}^{1/2}$. Then the non-dimensional equations of motion for this system can be expressed in the following form,

$$\ddot{x}_1 = \left(\sin(\beta\tau) - x_1\right)_+^{3/2} - \left(x_1 - x_2\right)_+^{3/2}$$
$$+\lambda\left\{\left(\beta\cos(\beta\tau) - \dot{x}_1\right)H\left(\sin(\beta\tau) - x_1\right) - \left(\dot{x}_1 - \dot{x}_2\right)H\left(x_1 - x_2\right)\right\}$$
$$\ddot{x}_i = \left(x_{i-1} - x_i\right)_+^{3/2} - \left(x_i - x_{i+1}\right)_+^{3/2} \qquad (2.2)$$
$$+\lambda\left\{\left(\dot{x}_{i-1} - \dot{x}_i\right)H\left(x_{i-1} - x_i\right) - \left(\dot{x}_i - \dot{x}_{i+1}\right)H\left(x_i - x_{i+1}\right)\right\}, \quad i = 2,...,N-1$$
$$\ddot{x}_N = \left(x_{N-1} - x_N\right)_+^{3/2} - \left(x_N\right)_+^{3/2} + \lambda\left\{\left(\dot{x}_{N-1} - \dot{x}_N\right)H\left(x_{N-1} - x_N\right) - \left(\dot{x}_N\right)H\left(x_N\right)\right\}$$

where the variables x_i denote the normalized displacement of the $i-th$ bead of the chain, and τ is the new normalized time. These equations indicate that the only nondimensional parameter governing the nonlinear dynamics is the normalized frequency β. We study the frequency response of the granular chain by fixing the amplitude of the displacement excitation and recording the maximum of the transmitted force at the rigid wall on the right end for varying frequency. We focus on the stationary-state response of this granular network, i.e., on the state of the dynamics that is eventually reached after a sufficiently long time, so that any initial transients have died out due to dissipative effects.

2.1.2 Computational results

As an example of the nonlinear stationary-state dynamics of the granular chain, in Figure 2.2 we present the maximum of the transmitted force at the right end of the 11 bead homogeneous chain for varying driving frequency in the range $30Hz \leq f \leq 3000Hz$ and constant amplitude $A_0 = 5\times10^{-7}\,m$. In this particular example there are five distinguishable peaks or "resonances," corresponding to frequencies where maximal force is transmitted to the right end of the chain. The diagram of Figure 2.2 also features dips or "anti-resonances" between the resonances, associated with frequencies of minimal force transmission. In recent studies it was theoretically (Jayaprakash et al., 2011) and experimentally (Hasan et al., 2015) shown that ordered granular media such as the granular chain of Figure 2.1 possess energy-tunable pass and stop bands similar to linear

24

spatially periodic systems. These strongly nonlinear frequency bands are due to the periodic structure of the granular system, and the essentially nonlinear bead-to-bead interactions, and correspond to frequency and energy ranges where disturbances will either propagate (pass bands) or attenuate (stop bands) in the medium. Indeed, in low-frequency acoustic pass-bands, these highly discontinuous media support solitary-like pulses (Lazaridi and Nesterenko, 1985; Coste et al., 1997; MacKay, 1999; Sen and Manciu, 2001; Sen et al., 2008), or spatially extended wave transmission (Starosvetsky et al., 2012; Hasan et al., 2013). Referring to the plot of Figure 2.2, the frequency range (coinciding with the pass band) where these resonances and anti-resonances occur lies within the nonlinear pass band of the granular chain of Figure 2.1, whereas for frequencies above 2000Hz (in the stop band) there is negligible force transmission due to the incapacity of the granular crystal to transmit energy at high frequency. Focusing on the responses within the pass bands where resonances and anti-resonances occur, we explore these features in detail to fully understand the strongly nonlinear mechanisms governing these interesting stationary-state phenomena.
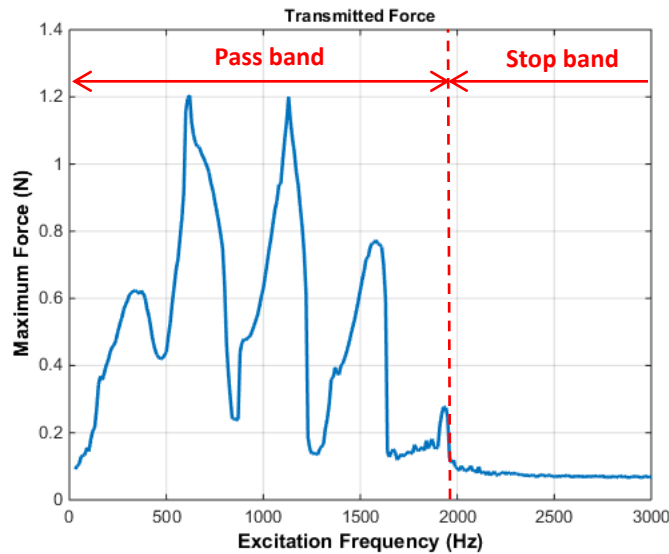

Figure 2.2. Maximum force transmitted on the right fixed boundary.

As a representative example of the dynamic response of the forced granular chain in a resonance, in Figure 2.3 we depict the spatiotemporal variation of the kinetic energies of the 11 beads in the regime of 1:1 and 1:3 resonance peaks, together with the corresponding displacement waveforms for every bead during one period. It is apparent that the response of the chain is in the form of waves that are initiated on the left (forced) end of the chain, and reflected at the right fixed end. The third component of each figure summarizes this pulse traveling in the form of an effective phase variation in the response of each bead: What is plotted is the time difference between the first occurrence during a period (at stationarity), of positive velocity for each bead, and for the leftmost bead of the chain; the almost perfect straight line plot clearly implies the traveling pulse nature of the long-term, stationary dynamics in the resonance peaks considered. This provides some insight into the nature of the relevant periodic, nonlinear solutions that dominate the response at resonance of the crystal lattice under the periodic external excitation. Focusing at the resonance depicted in Figure 2.3a we note that the zero-th bead exerts a strong impulse-like excitation at precisely the time instant when the traveling pulse reflected from the right, immovable boundary reaches the left end; one deduces that there is a strong excitation exerted at the granular chain at each period of the prescribed displacement excitation, so that the traveling pulses in the chain fully synchronize with the excitation source. Accordingly, this peak is designated as a 1:1 resonance.

On the contrary, at the resonance depicted in Figure 2.3b (corresponding to the third peak of Figure 2.2), one notes that there is one strong impulse-like excitation every three periods of the zero-th bead oscillation, since the time needed by the traveling pulse to fully traverse twice the length of the chain is three times the period of the excitation; hence, this is designated as a 1:3 resonance. We note that whereas secondary, weaker impulses also occur in between the strong impulse excitations in this case, these are too weak to initiate new identifiable traveling pulses in
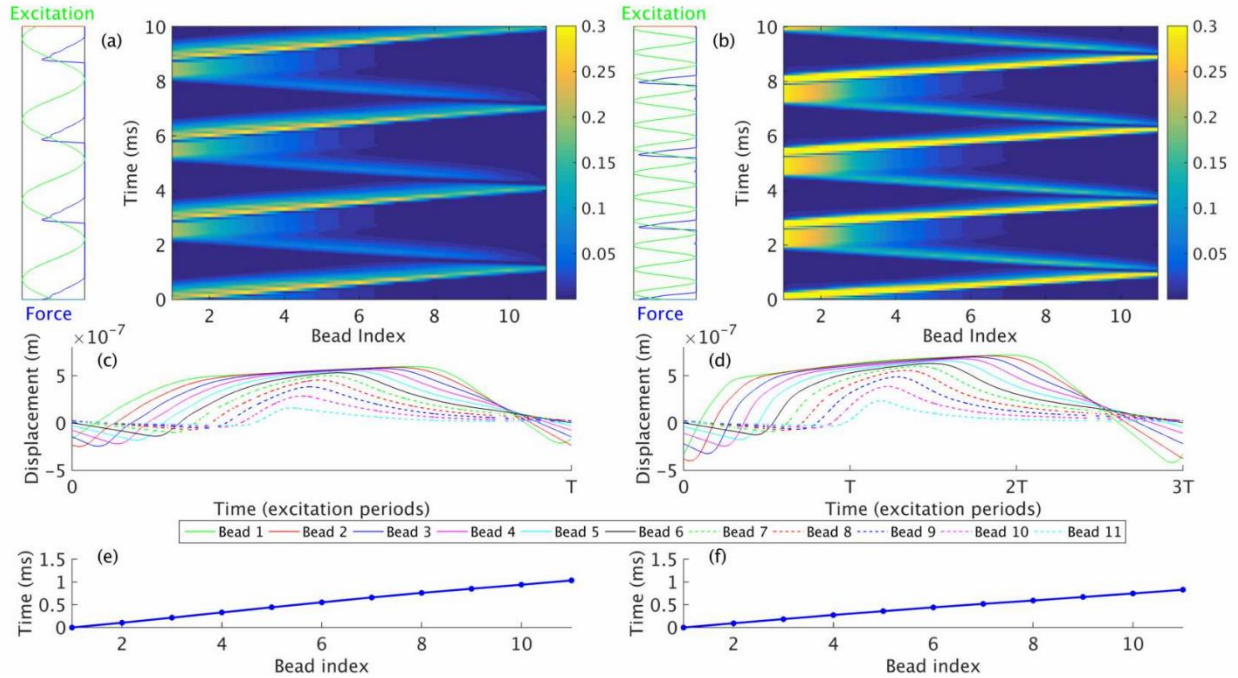
26

Figure 2.3. Long-term, stationary spatiotemporal variation of the kinetic energy (scaled $\times 10^7$) for (a) 1:1 resonance and (b) 1:3 resonance, where the input harmonic displacement and applied force excitations for each case are also shown on the left of each plot; (c,d) Displacement waveforms of every bead during one full period of the crystal motion, and (e,f) effective phase variation of the individual bead responses (computed by the time instants when each bead's velocity first becomes positive and when the leftmost bead's velocity first becomes positive); this highlights the "traveling pulse" nature of the long-term, stationary dynamics of the granular chain at the resonance peaks.

the granules. Using this classification the resonance peaks of Figure 2.2 can be classified as $1:n$ resonances for $n = 1, \dots, 5$, whereas higher-order resonances are eliminated due to dissipative effects. Moreover, all these nonlinear resonances occur in the pass band of the granular medium of Figure 2.1, since only in that frequency range can traveling pulses propagate from the left to the right boundary and vice versa.

In anti-resonances, as shown in Figure 2.4, there occurs strong attenuation of the propagating pulses caused by destructive interference between right- and left-going pulses
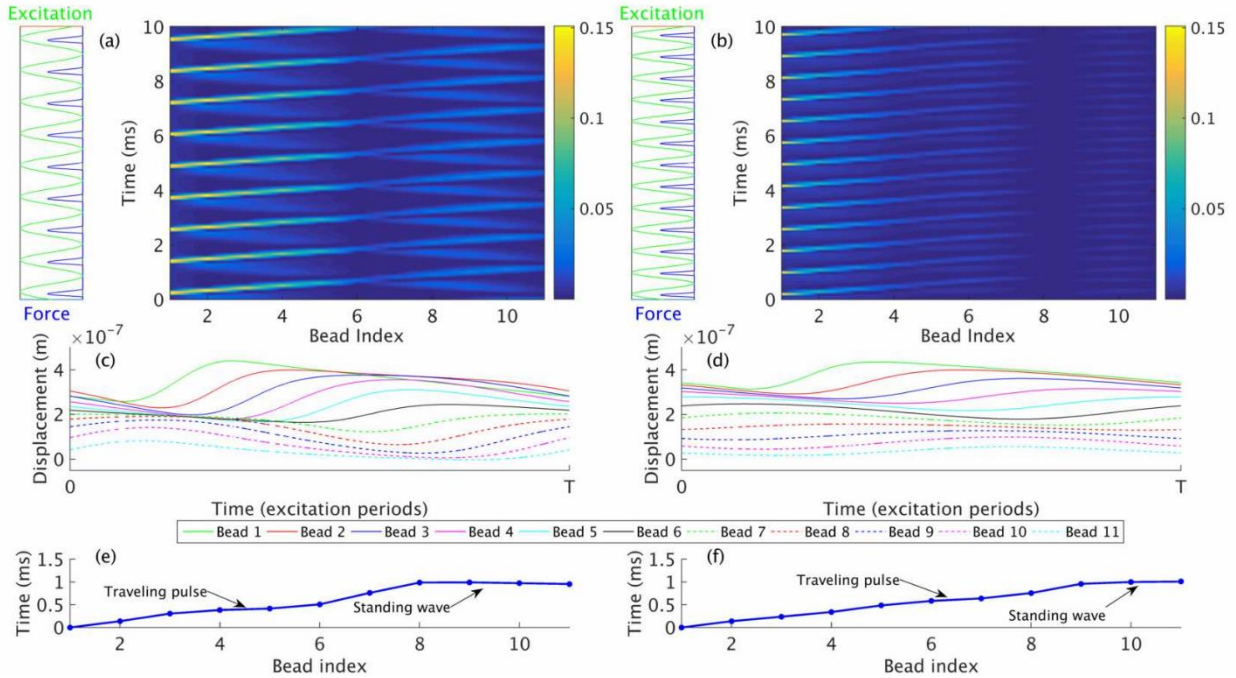
27

Figure 2.4. Long-term, stationary spatiotemporal variation of the kinetic energy (scaled $\times 10^7$) for (a) the second antiresonance and (b) the third antiresonance, where the input harmonic displacement and applied force excitations for each case are also shown on the left of each plot; (c,d) Displacement waveforms of every bead during one full period of the crystal motion, and (e,f) Effective phase variation of the individual bead responses (computed by the time instants when each bead reaches maximum positive displacement and when the leftmost bead does); this highlights the chimera-like, partially "traveling pulse" and partially "standing wave" nature of the long-term, stationary dynamics of the granular chain at antiresonances.

propagating through the granular chain. The negative interference of traveling pulses propagating in opposite directions in the granule is responsible for the "low-intensity" impulses delivered by the exciting source in these cases resulting the minimization of transmitted force. Moreover, all anti-resonances are located within the pass band, and correspond to 1:1 synchronization between the prescribed amplitude excitation and the resulting pulses in the medium. In such case a type of mixed traveling pulses (similar as in the resonance cases) and apparent nonlinear standing waves (traveling on the left side, standing on the right side) is observed here. This coexistence of

apparently traveling and standing waves highlights the essentially nonlinear nature and the high complexity of the long-term, stationary response and is corroborated by the results presented in Figures 2.4e and 2.4f. States of coexistence of different waveforms have been referred to as chimera states in other contexts (Abrams and Strogatz, 2004; Panaggio and Abrams, 2015). It was believed that identical oscillators exhibit either in-phase synchronization or incoherent drifting before the recovery of chimera states. A chimera state is a state of broken symmetry and has been defined as coexisting regions of coherent and incoherent oscillation in identical oscillators. The dynamics of these states have studied theoretically (Panaggio and Abrams, 2015) and experimentally (Martens et al., 2013).

2.2 Experimental tests, results and comparisons

In Section 2.1 we numerically examined and explained the existence of resonances and anti-resonances in a single granular chain under harmonic excitation. In this section, we present an experimental study of such a forced single granular chain aiming to verify the computational results in the previous section. For this study we consider harmonic excitation at one end of the granular network and study the steady state responses. Moreover, we focus only on low-frequency regimes where dissipative effects are less pronounced, and where low-order resonances and anti-resonances are realized. We experimentally confirm two types of resonance motions involving harmonic or subharmonic traveling pulses in the granular chain, as well as a state of anti-resonance. Hence, we experimentally prove that a strongly nonlinear medium (with complete absence of linear acoustics and with no linear resonance spectrum) can still support a nonlinear resonance spectrum that is tunable with energy. To our knowledge this is the first such experimental result reported in the area of granular media.

In addition, we modify our computational model to compare with the experimental measurements in the stationary-state responses which verifies that theoretically predicted resonances and anti-resonances can be realized experimentally. The results reported in this work have multiple potential applications in the design of acoustic metamaterials which are strongly nonlinear. These media can be used as energy absorbers when they are excited at anti-resonance frequencies, but, on the contrary, can intensify energy transmission at resonance frequencies.

2.2.1 Experimental setup and procedures

The experimental fixture is shown in Figure 2.5, and represents the practical realization of the forced granular medium depicted in Figure 2.1. It consists of two sturdy pillars connected through threaded shafts. To host the flexures, stainless steel holders with slots are placed on these shafts. Each bead in the granular chain is rigidly attached to the one end of a thin steel flexure and aligned horizontally and vertically. This alignment is crucial in order to experimentally realize the one-dimensionality of the granular dynamics and minimize frictional effects due to relative rotations between adjacent beads. The other end of the aforementioned flexure is placed in a slot of the holders assembled on the threaded shafts. The thin flexures, made of spring steel grade 1095, are designed to be much softer than the stiff beads, so that the time scales of the dynamics of the flexure responses and the dynamics of the bead-to-bead interactions (through Hertzian contact) are separable. It follows that the dynamics of the flexures should minimally affect the granular dynamics, so their contributions to the measured responses should be small. Nevertheless, as discussed below, the theoretical model needs to be modified by adding weak grounded stiffness in order to account for "ringing effects" in the measured responses due to the dynamics of the supporting flexures. After completing the alignment of the granular chain the holders are firmly bolted and rigidly fastened to the support structures.
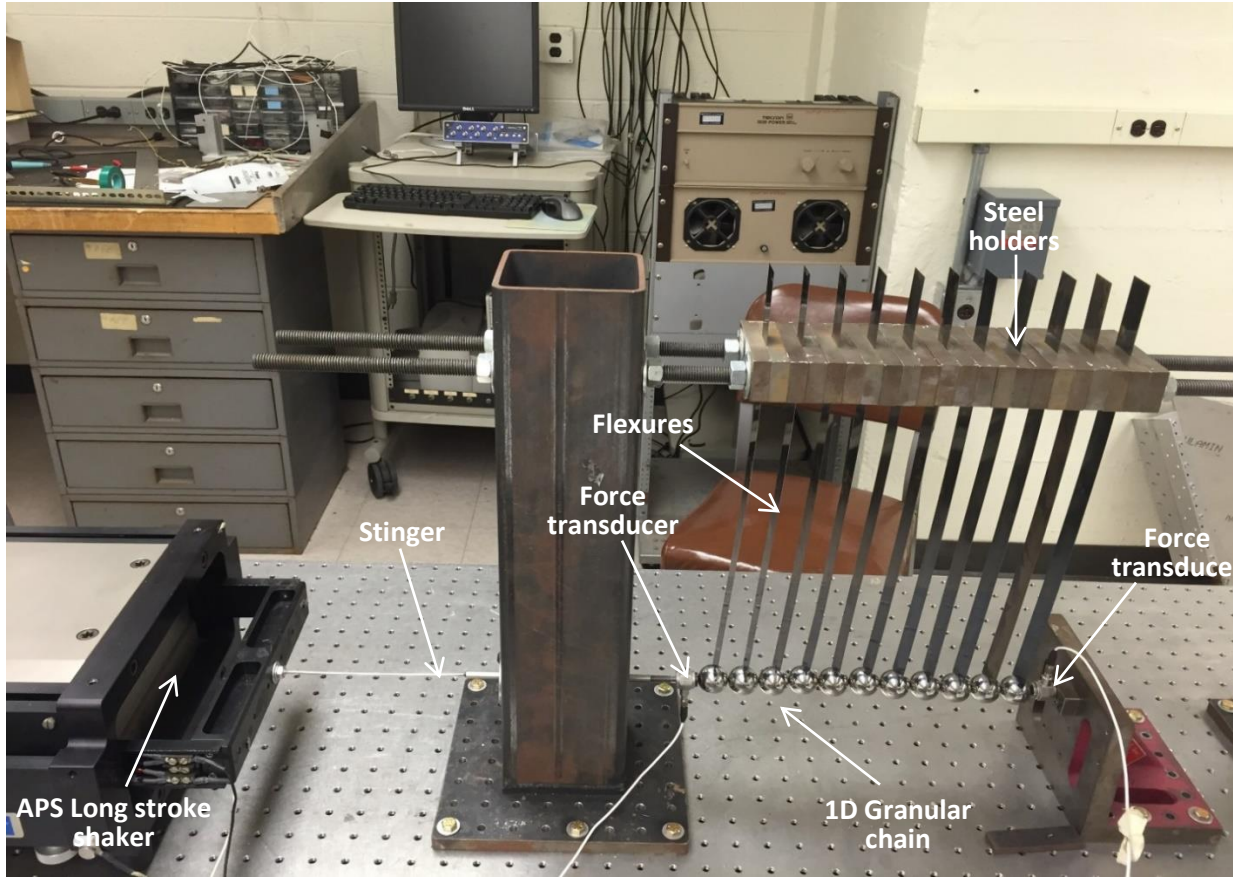
Figure 2.5. Experimental fixture of the forced granular chain.

The homogeneous granular chain consists of 11 spherical granules composed of bearing-quality aircraft-grade E52100 alloy steel of common radius $R = 12.7\ mm$, modulus of elasticity $E = 210\ GPa$, density $\rho = 7850\ Kg\ /\ m^3$ and Poisson's ratio $\nu = 0.3$. The supporting flexure is inserted to a depth of about $1/8^{\text{th}}$ of its diameter and permanently glued. Controlled excitation to the first particle (at the left end) is provided by means of an APS® long-stroke shaker. The stinger of the shaker is guided to excite the chain horizontally, and a piezoelectric force transducer (PCB® model 208C03, with sensitivity 2,248mV/kN) is attached at the point of contact of the stinger with the sample in order to measure the applied force. Due to the strong nonlinear bead-stinger dynamic interaction during the measurement, the measured applied force is affected by the measured

response since the force sensor is not glued to the first particle, which raises the possibility of losing contact with the chain as we will see below. Hence, a laser vibrometer (Polytec® model PSV-300-U) is employed here to record the velocity of the armature of the shaker which is unaffected by the measured dynamics and enables accurate measurement of the amplitude and frequency of the applied harmonic motion. As a measured output signal, the transmitted force at the right end of the chain is recorded by an additional piezoelectric force transducer (PCB® model 208C02, with sensitivity 11,241mV/kN). To summarize, three measurements (applied force, input velocity and output force) are recorded in the testing of this granular chain. The data is then post processed using Matlab®.

2.2.2 Experimental results

As mentioned above, our experimental study considers the forced dynamics of the granular chain under low-frequency harmonic excitation. We aim to maintain the shaker's displacement amplitude as constant as the frequency varies, but this amplitude cannot be recorded directly due to the limitation of the experimental setup. Assuming that the motion of the shaker is ideally harmonic and its initial phase is zero, its velocity can be expressed as $V(t) = V_0\cos(2\pi ft)$, and the corresponding displacement as $A(t) = A_0\sin(2\pi ft)$ where f is the driving frequency and $A_0 = V_0/2\pi f$. In Figure 2.6 we depict the experimental measurements of the amplitude of the velocity of the shaker (V_0) in the range $20Hz \le f \le 160Hz$, along with the corresponding displacement amplitude of the shaker (A_0). Clearly, the displacement amplitude (cf. Figure 2.6b) remains nearly constant under different drive frequencies. By maintaining the amplitude of the excitation to a nearly constant level, the only factor that affects the response of the tested system

is the driving frequency. Hence, all experimental measurements can be plotted and analyzed as functions of the external frequency.

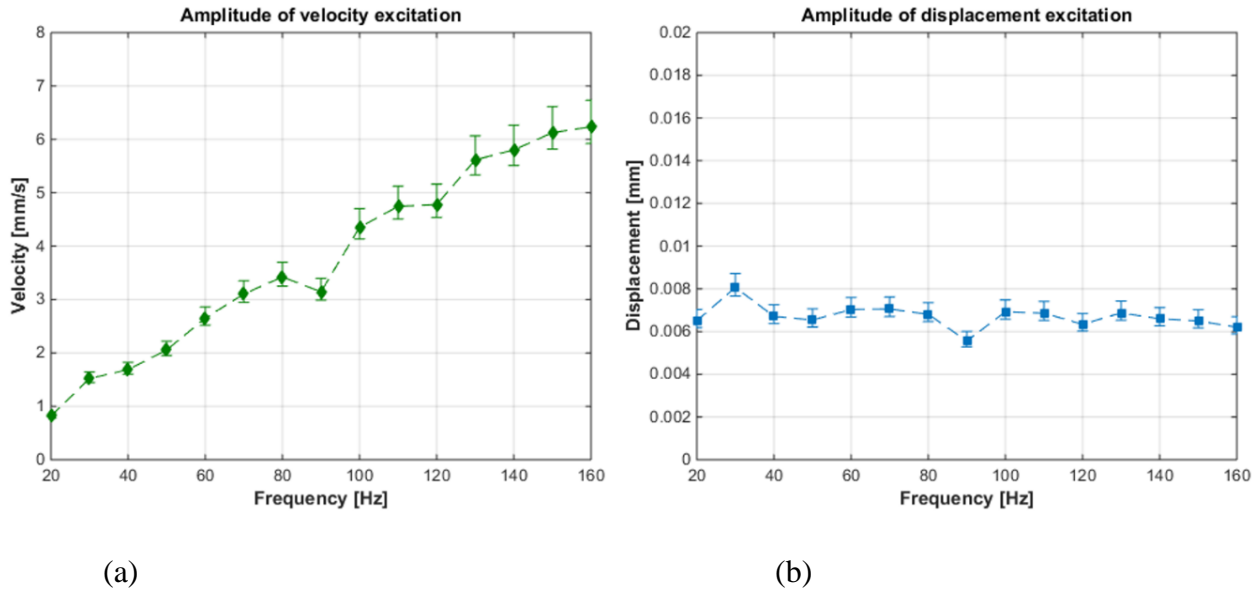(a)   (b)

Figure 2.6. Experimental shaker output over the frequency range of the tests: (a) Measured velocity amplitude, and (b) derived displacement amplitude of the armature of the shaker.

The study of the force transmitted by the 11th (farthest to the right) bead to the force transducer at the right boundary allows us to identity the resonances and anti-resonances in the stationary-state dynamics: local peaks of the maximum transmitted force correspond to maxima of energy transmission through the granular medium, whereas local valleys of the maximum transmitted force indicate weak energy transmission. The central result of the experimental study is summarized in Figure 2.7a, depicting the maxima of the experimentally measured transmitted force at the right of the granular chain for varying drive frequency in the range $20Hz \leq f \leq 160Hz$. Within this range we are able to detect two clear local peaks or resonances (located at $60Hz$ and $100Hz$), and one valley or anti-resonance in between the two peaks
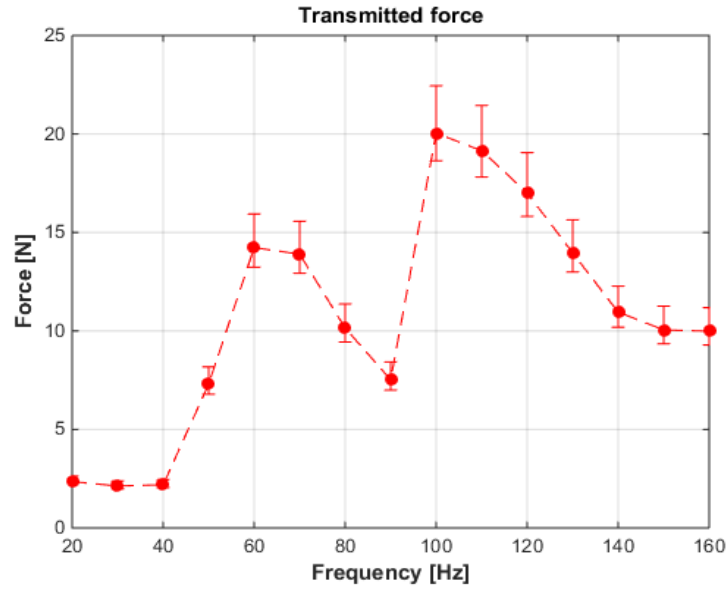
(a)
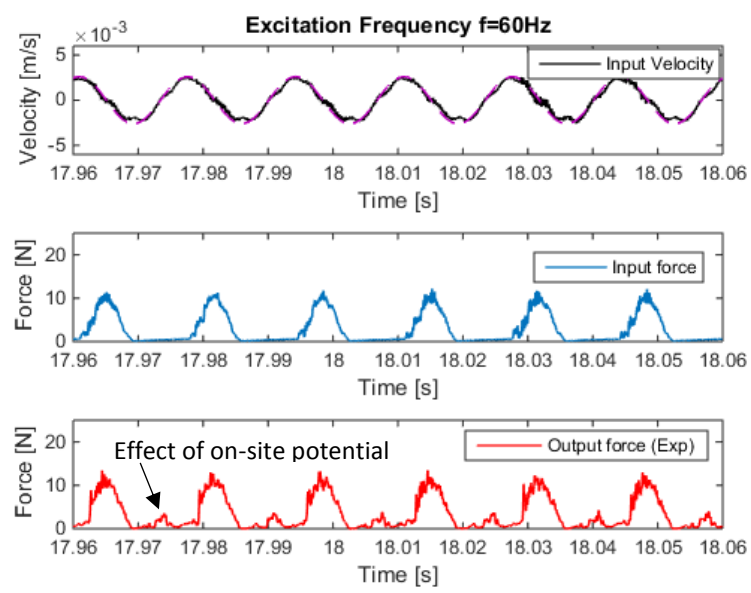
(b)

Figure 2.7. Experimental response of the granular chain under harmonic excitation: (a) Maximum of the transmitted force measured by the force transducer at the right end for $20Hz \leq f \leq 160Hz$; (b) experimental velocity time series of the armature of the shaker measured by laser vibrometry (*top*), time series of input force applied at the first bead measured by the force transducer at the left end (*middle*), and time series of the transmitted force by the 11th bead measured by the force transducer at the right end (*bottom*), under harmonic excitation at 60 Hz (1:1 resonance).
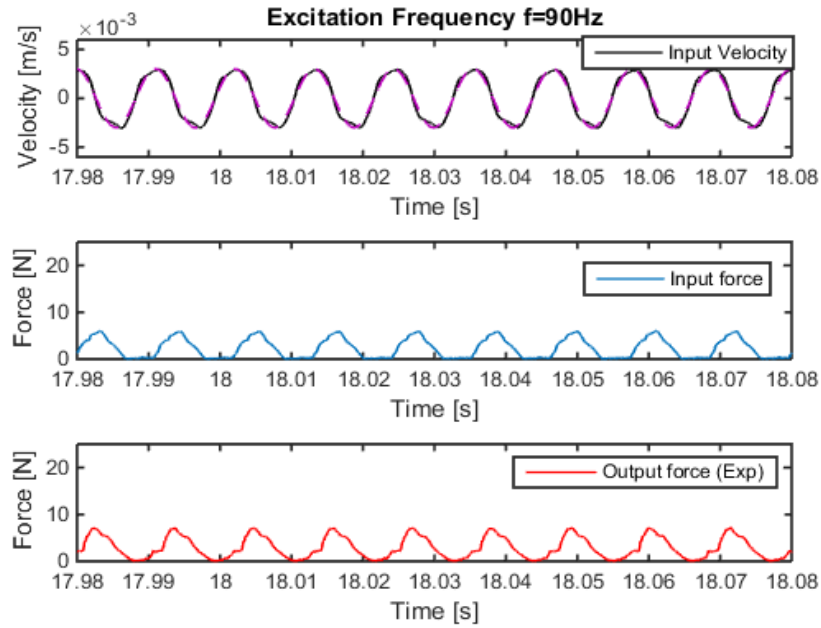
(a)
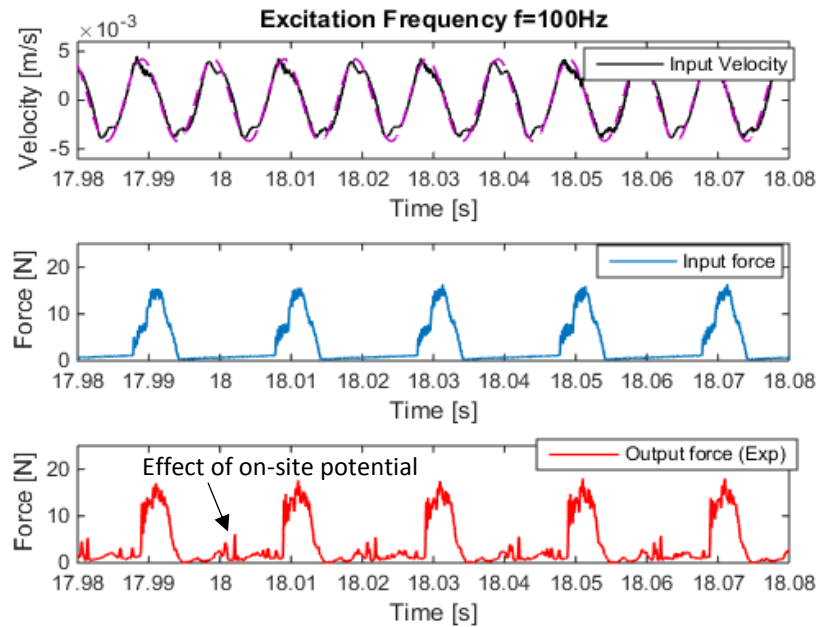
(b)

Figure 2.8. Experimental velocity time series of the armature of the shaker measured by laser vibrometry (*top*), time series of input force applied at the first bead measured by the force transducer at the left end (*middle*), and time series of the transmitted force by the 11th bead measured by the force transducer at the right end (*bottom*), under harmonic excitation at (a) 90 Hz (1:1 anti-resonance), and (b) 100 Hz (1:2 resonance).

(located at $90Hz$). Based on the theoretical study of Section 2.1 we identify that these two peaks of transmitted force are 1:1 and 1:2 resonances, respectively, whereas the valley in between is a 1:1 anti-resonance. To ensure repeatability of the experimental results, three different tests were repeated at every frequency, except for the two resonance peaks and the anti-resonance valley, for which five repeated tests were performed at each frequency. Even though the amplitude of the excitation was maintained almost constant in each of the repeated tests, some small variation was still unavoidable during the experiments. Accordingly, the averages of the different trial tests were computed to determine the final measured responses for varying frequency. The extreme measured values of these tests were also indicated in Figures 2.6 and 2.7 through the error bars.

A special note is warranted at this point concerning the force excitation exerted by the stinger of the shaker to the first bead of the granular chain. As discussed in previous works (Hasan et al., 2015; Pozharskiy et al., 2015), at the low-frequency pass band, even though the stinger has a prescribed harmonic motion, it does not maintain continuous contact with the first bead of the granular chain; as a result, the force excitation applied to the granular chain consists of a periodic or quasi-periodic series of force pulses as shown in the time series of input force in Figure 2.7b. In the pass band each applied force pulse generates a transmitted pulse in the granular chain (cf. Figure 2.3) which propagates almost unattenuated (except for dissipative effects) through the chain. This is verified by the force pulses transmitted to the right end of the chain and recorded by the force transducer at the right end (cf. Figure 2.7b).

In Figures 2.7b and 2.8a, b we depict experimentally measured time series for three distinct forcing frequencies, namely $60Hz$, $90Hz$ and $100Hz$, corresponding to 1:1 resonance, 1:1 anti-resonance, and 1:2 resonance, respectively. In particular, we depict the velocity time series of the armature of the shaker measured by a non-contacting laser vibrometer with reference to numerical

36

harmonic signals at corresponding frequencies; this time series is nearly harmonic, verifying that the applied displacement excitation of the shaker stinger is harmonic. In addition, we depict the time series of the input force applied by the stinger to the first bead of the granular chain and measured by the force transducer located at the left end of the chain; the time series verifies the pulse-like excitation of the granular chain in the low-frequency pass band, as discussed previously. Finally, the time series of the force transmitted by the 11th (furthest to the right) bead to the force transducer at the right end of the chain; we note that the transmitted force is again in the form of pulses since each applied impulse pulse on the left end gives rise to a transmitted force pulse at the right end. The recording of the maxima of the transmitted force pulses for varying frequency generates the transmitted force plot of Figure 2.7a.

Clear "silent zones" between any two successive input force pulses are due to the separations between the stinger and the first bead. However, a different result is observed considering the region between two successive transmitted force pulses in the two resonance peaks (cf. Figures 2.7b and 2.8b) since instead of silent zones we note the realization of distinct small peaks of transmitted force between the main transmitted pulses. These small residual force pulses (or "ringing") are mainly contributed by the presence of the on-site potential (elastic foundation) in the nonlinear dynamics due to the fact that each of the beads of the granular chain is supported (grounded) by the "soft" steel flexures. Even though there is time scale separation between the "soft" dynamics of the flexures and the "stiff" dynamics of the bead-bead interactions, there is still a measured dynamic effect contributed by the supporting flexures. As a result, the 11th bead does not fully relax after each interaction with the force transducer (which generates the main transmitted force pulse), but due to the restoring effect of the flexure foundation the bead regains contact with the force transducer, resulting in the small force pulse which occurs after the

37

transmission of the main force pulse. We note, however, that this ringing residual effect is small compared to the main transmitted force pulse train, a result that verifies the adequate time scale separation of the stiff/soft dynamics.

In our study we focus only on the main transmitted forced pulses caused by the Hertzian interactions between beads. Considering first the case of excitation frequency at 60 Hz, there occurs 1:1 resonance in the dynamics (cf. Figures 2.7a,b). At this resonance peak the stinger of the shaker exerts a strong force pulse at every period of the harmonic oscillation of the shaker armature, so there is 1:1 synchronization between the displacement of the shaker and the resulting input force to the granular chain. By increasing the excitation frequency to 90 Hz (1:1 anti-resonance), a different type of forced dynamics of the granular chain is identified, where the maximum transmitted force plot reaches a local valley (cf. Figures 2.7a and 2.8a). At that frequency input force pulses delivered by the excitation source have a 1:1 correspondence with low-intensity transmitted force pulses, due to destructive interference of left- and right-going pulses in the granular chain. Interestingly enough, by further increasing the frequency to 100 Hz we notice a second resonance peak in the transmitted force plot which corresponds to an 1:2 resonance; in this case the granular chain undergoes a period-2 subharmonic motion. Indeed, at this resonance peak (cf. Figures 2.7a and 2.8b) the excitation source exerts a strong force pulse at every second period of the harmonic oscillation of the shaker armature. As a result, the input force pulse measured at the left end of the granular chain repeats itself every two periods of the prescribed harmonic oscillation of the armature of the shaker. Between two successive input force pulses, clear silent zones are again noticed due to the loss of contact between the stinger and the first bead of the granular chain. The cause of this 1:2 resonance (similarly for all higher order resonances) is the relative phase between the periodic motions of the stinger and the first bead of the chain which

38

leads to loss of contact at every period of the prescribed displacement excitation of the shaker armature; rather, following one cycle of oscillation (period) after a strong force pulse is exerted on the chain, the stinger motion becomes out-of-phase with respect to the motion of the first bead of the chain, so no contact is possible at that time instant. However, after another cycle, the motion of the shaker and of the first bead are in-phase (condition for resonance) so a strong force impulse is exerted again by the stinger of the shaker to the chain. Moreover, similar to the case of 1:1 resonance (cf. Figure 2.7b), small residual force pulses are introduced in the transmitted force measurement due to the soft dynamics of the flexures (cf. Figure 2.8b).

Hence, our experimental results fully verify previous theoretical predictions and confirm the existence of strongly nonlinear resonance motions in the granular chain of Figure 2.5. We note at this point that since the granular chain has no prior compression, it represents a sonic vacuum with complete lack of any linear resonance spectrum. It follows that the experimentally measured resonance spectrum is strongly nonlinear and fully tunable with energy, so the detected resonances and anti-resonances are highly sensitive to the applied energy input. Moreover, due to the highly complex granular dynamics the nonlinear resonance spectrum is highly sensitive to damping, since for low-enough dissipation the granular chain possesses chaotic dynamics (due to separations and ensuing collisions between beads) so no detectable resonance spectrum can be observed. This was the case of a previous study (Lydon et al., 2013) where chaotic resonance motions were experimentally detected in a two-bead granular system, and no discernable resonance spectrum similar to the one presented here (cf. Figure 2.7a) could be experimentally detected. This was due to sensitive dependence on initial conditions of the chaotic motions of that system. Chaotic dynamics was also observed systematically in distributed versions of relevant driven-damped granular chains e.g., in (Hooheboom et al., 2013; Charalampidis et al., 2015).

39

2.2.3 Theoretical modeling and comparisons

As a further step we aim to reconstruct computationally the experimental measurements. Based on the previous discussion it is clear that the mathematical model (2.1-2.2) should be augmented by stiffness terms in order to model the "soft" dynamics of the supporting flexures that give rise to the "ringing" effects in the transmitted force time series of Figure 2.7b and 2.8b. To this end, the augmented configuration depicted in Figure 2.9 is considered, which, compared to the model of Figure 2.1, possesses weak grounding linear stiffnesses for each bead of the granular chain.
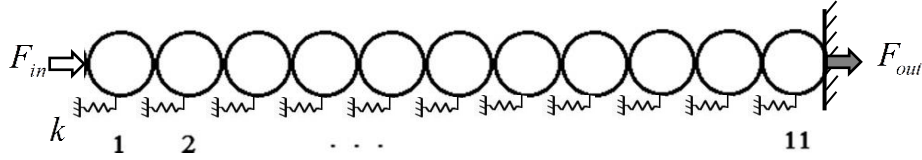

Figure 2.9. Augmented mathematical model for the forced granular chain incorporating the weak on-site foundation generated by the supporting flexures.

Maintaining the notation of the model (2.1-2.2), the augmented equations of motion (in dimensional form) of this system are expressed as:

$$m\frac{d^2u_1}{dt^2} = F_{in} - \frac{E\sqrt{2R}}{3(1-v^2)}\left\{(u_1-u_2)_+^{3/2}\right\} + D\left\{-(\dot{u}_1-\dot{u}_2)\mathrm{H}(u_1-u_2)\right\} - ku_1$$

$$m\frac{d^2u_i}{dt^2} = \frac{E\sqrt{2R}}{3(1-v^2)}\left\{(u_{i-1}-u_i)_+^{3/2} - (u_i-u_{i+1})_+^{3/2}\right\}$$

$$+D\left\{(\dot{u}_{i-1}-\dot{u}_i)\mathrm{H}(u_{i-1}-u_i)-(\dot{u}_i-\dot{u}_{i+1})\mathrm{H}(u_i-u_{i+1})\right\} - ku_i, \quad i=2,3,...10 \qquad (2.3)$$

$$m\frac{d^2u_{11}}{dt^2} = \frac{E\sqrt{2R}}{3(1-v^2)}\left\{(u_{10}-u_{11})_+^{3/2} - \sqrt{2}(u_{11})_+^{3/2}\right\}$$

$$+D\left\{(\dot{u}_{10}-\dot{u}_{11})\mathrm{H}(u_{10}-u_{11})-(\dot{u}_{11})\mathrm{H}(u_{11})\right\} - ku_{11}$$

The first term, F_{in}, on the right-hand-side of the equation of motion of the first bead is taken directly from the experimental measurements (cf. Figures 2.7b, 2.8a and 2.8b), in order to ensure

that the computational model is excited by the same pulse train excitation exerted in the experimental fixture. This turns our modeling into a data assimilation problem, since the response of the system is driven by an experimentally obtained signal; the model predictions will then become nonlinear observations of the experimental system state. The numerical values of all parameters in the model (2.3) were previously defined, except for the damping coefficient D and the (soft) foundation stiffness k. The viscous damping in a one dimensional homogenous chain composed of steel beads has been estimated by Herbold et al. (2007) as 32.15 Ns/m, and by Potekin et al. (2013), as 35.4 Ns/m. Regarding the numerical value of the damping coefficient, we consider the estimated value by Potekin et al. (2013) which was derived for the identical experimental setup. Accordingly, we set $D = 35.4$ Ns/m and use this numerical damping value in all of the following computational simulations that are performed for comparing with the experimental results. To simulate the weak foundation effect resulting from the thin steel flexures, we choose k as 0.1% of the Hertzian contact stiffness between particles, and set $k = E\sqrt{2R}\big/3000(1-\nu^2)$.

In Figure 2.10 we compare the experimental transmitted forces directly recorded by the force transducer with direct numerical simulations of the granular network (2.3) with a fixed boundary condition at the end; in the computational model the output force is calculated as $F_{out} = 2E\sqrt{R}(u_{11})_+^{3/2}\big/3(1-\nu^2)$. In Figure 2.10a the maximum of the numerical output force at the right end of the chain is superimposed on the experimental results in the frequency range $20Hz \leq f \leq 160Hz$. Satisfactory agreement is inferred, with the computational predictions fully capturing the two resonances and the anti-resonance in-between of the experimental measurements. Moreover, comparisons of the experimental and computational time series of the transmitted force
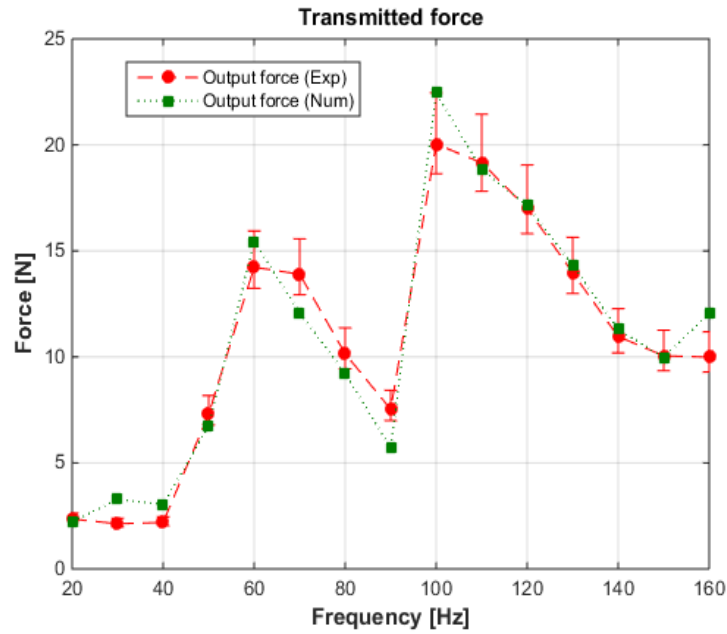
(a)
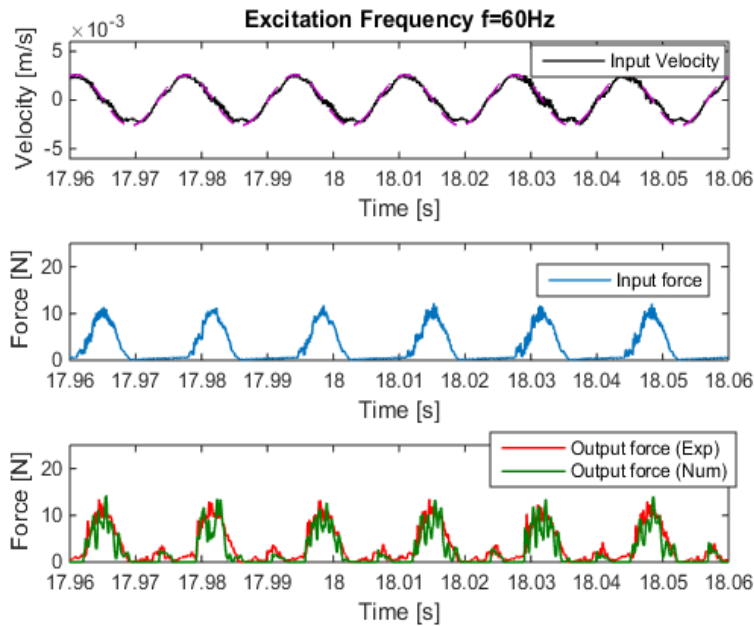
(b)

Figure 2.10. Comparisons between experimental measurements (red) and numerical results (green) from the model (3): (a) Maximum of the transmitted force at the right end of the granular chain in the frequency range $20Hz \leq f \leq 160Hz$; (b) experimental velocity time series of the armature of the shaker (*top*), experimental input force at the left end of the first granule (*middle*) and transmitted force at the right end (*bottom*) for 1:1 resonance at 60 Hz.
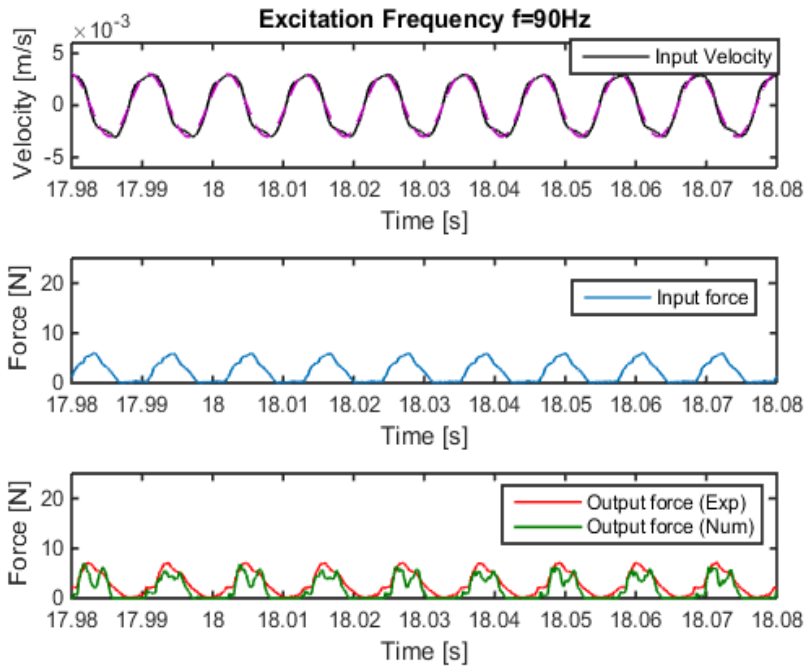
(a)
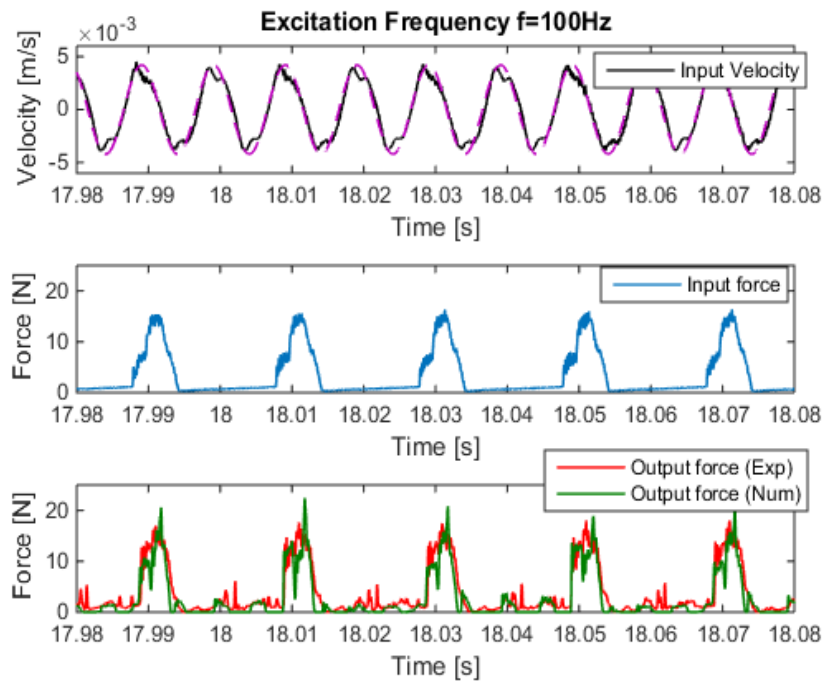

(b)

Figure 2.11. Comparisons between experimental measurements (red) and numerical results (green) from the model (3): Experimental velocity time series of the armature of the shaker (*top*), experimental input force at the left end of the first granule (*middle*) and transmitted force at the right end (*bottom*) for (a) 1:1 anti-resonance at 90 Hz, and (b) 1:2 resonance at 100 Hz.

at 60 Hz (1:1 resonance), 90 Hz (1:1 anti-resonance) and 100 Hz (1:2 resonance) are depicted in Figures 2.10b, 2.11a and 2.11b, respectively. Examining the force pulse trains depicted in these plots, we clearly deduce that all numerical simulations reproduce accurately the experimental measurements, following the same trends and even reproducing the ringing effects due to the flexural supports at the two resonances (cf. Figures 2.10b and 2.11b). It follows that the augmented mathematical model (2.3) is capable of accurately reproducing the experimental measurements, fully validating the experimentally detected strongly nonlinear resonance and anti-resonance steady state responses.

The deviations between the experimental and computational results may be attributed to the approximation of dissipative effects by linear viscous damping used in the numerical model (2.3) which is incapable of fully modeling nonlinear dissipative effects such as friction and plasticity. Despite numerous efforts (Rosas et al., 2007; Carretero-Gonzalez et al. 2009; Vergara 2010), a universal model capturing quantitatively the phenomenology of dissipative losses is still not available. In addition, possible inherent bead misalignments in the experimental fixture can affect the force pulses transmitted to the right end of the granular chain, as well as the theoretical modeling of the right boundary condition as fixed, i.e., of infinite stiffness. It is clear that in the practical realization of the granular chain, the right boundary is a force transducer which has a finite stiffness. Nevertheless, the computational results are in satisfactory agreement with the experimental measurements, both in the frequency and the time domains, fully recovering the resonances and anti-resonances in the stationary-state responses.

2.3 Conclusions

In this chapter, we have studied the stationary-state dynamics of a one-dimensional finite homogeneous granular chain, without prior compression and under time-periodic excitation. Two types of resonance motions in the granular chain, i.e., harmonic or subharmonic traveling pulses, and states of anti-resonances have been identified experimentally. These results, which correspond to local maxima and minima, respectively, of the maximum transmitted force at the right end of the chain, validate theoretical studies. In particular, in agreement with previous theoretical predictions we experimentally verified the existence of two strongly nonlinear resonance peaks and one anti-resonance valley between them within the frequency range of $20 - 160 \, Hz$, which indicated that a strongly nonlinear medium can possess an energy-tunable nonlinear resonance spectrum. Furthermore, we revisited the mathematical model of the experimental fixture and were able to confirm the existence of aforementioned interesting dynamic responses by direct numerical simulations.

We emphasize that due to the strong nonlinearity of the granular dynamics, the detected resonance spectra are dependent on the intensities (magnitudes) of the applied excitations, so the stationary-state dynamics are passively tunable with energy. Moreover, such designs can be extended to higher dimensions, exploring the concepts of resonance and anti-resonance in these setups as well, e.g., in hexagonal or square lattices. In general, the results of this work contribute to the design of practical nonlinear acoustic metamaterials with properties adaptive to different types of external excitations.

2.4 References

Abrams, D., Strogatz, S., "Chimera States for Coupled Oscillators," *Phys. Rev. Lett.*, **93**, 174102, 2004.

Carretero-Gonzalez, R., Khatri, D., Porter, M., Kevrekidis, P., Daraio, C., "Dissipative Solitary Waves in Granular Crystals," *Phys. Rev. Lett.*, **102**, 024102, 2009.

Charalampidis, E., Li, F., Chong, C., Yang, J., Kevrekidis, P., "Time-periodic Solutions of Driven Damped Trimer Granular Crystals," *Math. Problems in Engr.*, 830978, 2015.

Chong, C., Li, F., Yang, J., Williams, M., Kevrekidis, I., Kevrekidis, P., Daraio, C., "Damped-driven Granular Chains: An Ideal Playground for Dark Breathers and Multibreathers," *Phys. Rev. E*, **89**(3), 032924, 2014.

Coste, C., Falcon, E., Fauve, S., "Solitary Waves in a Chain of Beads under Hertz Contact," *Phys. Rev. E*, **56**(5), 6104–6117, 1997.

Hasan, M., Cho, S., Remick, K., Vakakis, A., McFarland, D., Kriven, W., "Experimental Study of Nonlinear Acoustic Bands and Propagating Breathers in Ordered Granular Media Embedded in Matrix," *Gran. Matter*, 17, 49–72, 2015.

Hasan, M., Starosvetsky, Y., Vakakis, A., Manevitch, L., "Nonlinear Targeted Energy Transfer and Macroscopic Analog of the Quantum Landau–Zener Effect in Coupled Granular Chains," *Physica D*, **252**, 46–58, 2013.

Herbold, E., Nesterenko, V., "Shock Wave Structure in a Strongly Nonlinear Lattice with Viscous Dissipation," *Phys. Rev. E*, **75**(2), 021304, 2007.

Hoogeboom, C., Man, Y., Boechler, N., Theocharis, G., Kevrekidis, P.G., Kevrekidis, I.G., Daraio, C., "Hysteresis loops and multi-stability: From periodic orbits to chaotic dynamics (and back) in diatomic granular crystals," *EPL,* **101,** 44003, 2013.

Jayaprakash, K., Starosvetsky, Y., Vakakis, A., Peeters, M., Kerschen, G., "Nonlinear Normal Modes and Band Zones in Granular Chains with No Precompression," *Nonl. Dyn.*, **63**(3), 359-385, 2011.

Lazaridi, A.N., Nesterenko, V.F., "Observation of a new type of solitary waves in a one-dimensional granular medium," *J. Appl. Mech. Tech. Phys.*, **26**(3), 405–408, 1985.

Lydon, J., Jayaprakash, K., Ngo, D., Starosvetsky, Y., Vakakis, A.F., Daraio, C., "Frequency Bands of Strongly Nonlinear Finite Homogeneous Granular Chains," *Phys. Rev. E*, **88**, 012206, 2013.

MacKay, R.S., "Solitary waves in a chain of beads under hertz contact," *Phys. Lett. A*, **251**(3), 191-192, 1999.

Martens, E., Thutupalli, S., Fourriere, A., Hallatschek, O., "Chimera states in mechanical oscillator networks", *Proc. Natl. Acad. Sci. U.S.A*, **110**(26), 10563-10567, 2013.

Panaggio, M., Abrams, D., "Chimera states: Coexistence of coherence and incoherence in networks of coupled oscillators", *Nonlineraity*, **28**(3); and arXiv: 1403.6204v3, 2015.

Potekin, R., Jayaprakash, K., McFarland, D., Remick, K., Bergman, L., and Vakakis, A., "Experimental study of strongly nonlinear resonances and anti-resonances in granular dimer chains," *Exp. Mech.*, **53**(5), 861–870, 2012.

Pozharskiy, D., Zhang, Y., Williams, M., McFarland, D., Kevrekidis, P., Vakakis, A., Kevrekidis, I., "Nonlinear Resonances and Antiresonances of a Forced Sonic Vacuum," *Phys. Rev. E*, **92**(6), 063203; and arXiv:1507.01025, 2015.

Rosas, A., Romero, A.H., Nesterenko, V.F., Lindenberg, K., "Observation of two-wave structure in strongly nonlinear dissipative granular chains," *Phys. Rev. Lett*., **98**, 164301, 2007.

Sen, S., Hong, J., Bang, J., Avalos, E., Doney, R., "Solitary waves in the granular chain," *Phys. Rep.,* **462** (2), 21–66, 2008.

Sen, S., Manciu, M., "Solitary wave dynamics in generalized hertz chains: An improved solution of the equation of motion," *Phys. Rev. E*, **64**(5), 056605, 2001.

Starosvetsky, Y., "Evolution of the primary pulse in one-dimensional granular crystals subject to on-site perturbations: Analytical study," *Phys. Rev. E*, **85**(5), 051306, 2012.

Vergara, L., "Model for dissipative highly nonlinear waves in dry granular crystals," *Phys. Rev. Lett.,* **104,** 244302, 2010.

Chapter 3. Two-dimensional granular network under impulsive excitation

It is evident from the discussions of Chapter 2 that ordered arrays of granular particles (beads) possess rich dynamical behavior, including passive adaptivity and tunabilty with energy. The propagatory dynamics of such one-dimensional granular networks has been well studied (Chatterjee, 1999; Coste et al., 1997; Daraio et al., 2005; Job et al., 2007; Mackay, 1999). Nesterenko (2001) was the first to discover the propagation of a special class of solitary pulses in one-dimensional homogeneous granular chains that do not involve bead separations, and, hence, can be studied by asymptotic techniques in the continuum limit using long-wave approximations; here these solitary pulses will be denoted as Nesterenko solitary pulses. However, the many current applications of ordered granular crystals, such as shock and vibration mitigation (Jayaprakash et al., 2013), shock energy trapping and absorption (Sen et al., 2001; Daraio et al., 2006b; Doney and Sen, 2006; Fraternali et al., 2009), tunability of solitary waves (Daraio et al., 2006a) and frequency filtering (Jayaprakash et al., 2011), mainly focus on one-dimensional systems.

In this chapter, we extend our studies to two-dimensional coupled granular chains. We numerically, analytically and experimentally examine primary wave transmission in a system of impulsively excited, coupled, finite granular chains, and show strong energy exchanges through excitation of transverse primary pulses (or shear waves) and the formation of a new type of mixed waves involving both solitary pulse propagation in the longitudinal direction and oscillatory shear waves in the orthogonal direction. We emphasize that in this chapter we are only interested in primary pulse propagation, that is in the early time wave transmission of nonlinear waves, before any reflections from the axial boundaries of the system occur and secondary waves are generated. In that context, our analysis extends the one-dimensional nonlinear mapping technique developed by Starosvetsky (2012), and Ben-Meir and Starosvetsky (2013), and clarifies the strongly

nonlinear dynamical mechanisms that govern the formation and evolution of these mixed primary waves. Moreover, our developed mathematical model is validated with experimental measurements and contributes to the predictive design of multi-dimensional granular media in applications in practical acoustic metamaterials.

3.1 Computational study

In this section, we report on the strongly nonlinear dynamics of a system of uncompressed, coupled, finite granular chains. For this study we consider impulsive excitation of one of the chains of the granular network. We show that in spite of the fact that the impulse is only applied to one of the granular chains, strong transient energy transfer from this directly excited chain to its neighboring absorbing chain is obtained. Eventually, the initially applied impulse is spread in two chains and evolves towards a final stationary state of formation of solitary waves with same amplitudes that propagate in each of the chains. Moreover, by examining time series of two chains' responses in horizontal and vertical directions, which are parallel and normal to the orientation of the chain, respectively, two types of wave forms, namely solitary-like pulses and shear oscillatory waves, are noted.

3.1.1 System description

We depict our considered system of ordered granular chains in Figure 3.1. The system is composed of two coupled homogeneous granular chains with no prior compression. All beads are identical, spherical in shape, composed of linearly elastic material, and in point contact with each other. Strongly nonlinear Hertzian dynamic interactions between beads are assumed with no dissipative effects, such as those attributed to material damping, plasticity or dry friction. One of the chains is excited by an impulse of intensity V_0 applied at $t = 0+$, and is designated as the "excited chain,"

whereas the other is designated as the "absorbing chain." Rigid-wall boundary conditions are imposed on three sides of the system, with the fourth side being free, and the system is assumed to be at rest at $t = 0 -$. As discussed below, these boundary conditions play an important role in the complex wave phenomena that evolve in this system.
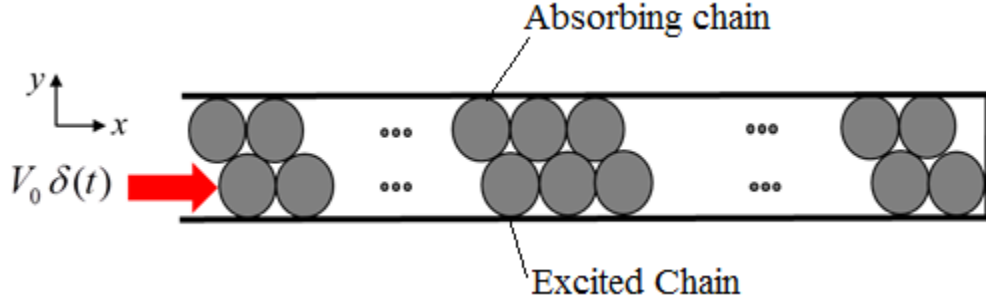

Figure 3.1. Impulsively excited system of two coupled granular chains.

Denoting by z_i and w_i the horizontal and vertical components, respectively, of the displacement of the $i\,th$ bead of the excited chain, and by ξ_i and η_i the corresponding displacement components of the $i\,th$ bead of the absorbing chain (with $i = 1, ..., n$), the strongly nonlinear and coupled equations of motion can be derived explicitly, and are listed in equation (3.1). Similar to equation (2.2), the equations of motion (3.1) have been normalized by introducing the re-scalings $z_i \rightarrow z_i/R$, $w_i \rightarrow w_i/R$, $\xi_i \rightarrow \xi_i/R$, $\eta_i \rightarrow \eta_i/R$, $\tau = t/\sqrt{A}$, $\bar{\lambda} = \sqrt{A}\lambda/m$, $\bar{V}_0 = \sqrt{A}V_0/R$, where the scaling factor is $A = 2\sqrt{2}\pi\rho R^2(1 - v^2)/E$. Then all parameters except for the damping coefficients can be removed from the re-scaled equations since the mass-normalized Hertzian coefficient re-scales as $\alpha = 1$, and the undamped problem becomes parameter-free.

$$\ddot{z}_i = \alpha \left[\frac{z_i - z_{i-1} + 2}{\sqrt{(z_i - z_{i-1} + 2)^2 + (w_i - w_{i-1})^2}} (2 - \sqrt{(z_i - z_{i-1} + 2)^2 + (w_i - w_{i-1})^2})_+^{3/2} + \right.$$

$$\left. \frac{z_i - z_{i+1} - 2}{\sqrt{(z_i - z_{i+1} - 2)^2 + (w_i - w_{i+1})^2}} (2 - \sqrt{(z_i - z_{i+1} - 2)^2 + (w_i - w_{i+1})^2})_+^{3/2} \right] +$$

$$\alpha \left[\frac{z_i - \xi_{i-1} + 1}{\sqrt{(z_i - \xi_{i-1} + 1)^2 + (w_i - \eta_{i-1} - \sqrt{3})^2)}} (2 - \sqrt{(z_i - \xi_{i-1} + 1)^2 + (w_i - \eta_{i-1} - \sqrt{3})^2})_+^{3/2} + \right.$$

$$\left. \frac{z_i - \xi_i - 1}{\sqrt{(z_i - \xi_i - 1)^2 + (w_i - \eta_i - \sqrt{3})^2)}} (2 - \sqrt{(z_i - \xi_i - 1)^2 + (w_i - \eta_i - \sqrt{3})^2})_+^{3/2} \right] +$$

$$\lambda \left[(\dot{z}_{i-1} - \dot{z}_i)(2 - \sqrt{(z_i - z_{i-1} + 2)^2 + (w_i - w_{i-1})^2})_+ - \right.$$

$$(\dot{z}_i - \dot{z}_{i+1})(2 - \sqrt{(z_i - z_{i+1} - 2)^2 + (w_i - w_{i+1})^2})_+ +$$

$$(\dot{\xi}_{i-1} - \dot{z}_i)(2 - \sqrt{(z_i - \xi_{i-1} + 1)^2 + (w_i - \eta_{i-1} - \sqrt{3})^2})_+ -$$

$$\left. (\dot{z}_i - \dot{\xi}_i)(2 - \sqrt{(z_i - \xi_i - 1)^2 + (w_i - \eta_i - \sqrt{3})^2})_+ \right]$$

$$\ddot{w}_i = \alpha \left[\frac{w_i - w_{i-1}}{\sqrt{(w_i - w_{i-1} + 2)^2 + (w_i - w_{i-1})^2}} (2 - \sqrt{(z_i - z_{i-1} + 2)^2 + (w_i - w_{i-1})^2})_+^{3/2} + \right.$$

$$\left. \frac{w_i - w_{i+1}}{\sqrt{(z_i - z_{i+1} - 2)^2 + (w_i - w_{i+1})^2}} (2 - \sqrt{(z_i - z_{i+1} - 2)^2 + (w_i - w_{i+1})^2})_+^{3/2} \right] +$$

$$\alpha \left[\frac{w_i - \eta_{i-1} - \sqrt{3}}{\sqrt{(z_i - \xi_{i-1} + 1)^2 + (w_i - \eta_{i-1} - \sqrt{3})^2)}} (2R - \sqrt{(z_i - \xi_{i-1} + 1)^2 + (w_i - \eta_{i-1} - \sqrt{3})^2})_+^{3/2} + \right.$$

$$\left. \frac{w_i - \eta_i - \sqrt{3}}{\sqrt{(z_i - \xi_i -)^2 + (w_i - \eta_i - \sqrt{3})^2)}} (2 - \sqrt{(z_i - \xi_i - 1)^2 + (w_i - \eta_i - \sqrt{3})^2})_+^{3/2} \right] +$$

$$\lambda \left[(\dot{w}_{i-1} - \dot{w}_i)(2 - \sqrt{(z_i - z_{i-1} + 2)^2 + (w_i - w_{i-1})^2})_+ - \right.$$

$$(\dot{w}_i - \dot{w}_{i+1})(2 - \sqrt{(z_i - z_{i+1} - 2)^2 + (w_i - w_{i+1})^2})_+ +$$

$$(\dot{\eta}_{i-1} - \dot{w}_i)(2 - \sqrt{(z_i - \xi_{i-1} + 1)^2 + (w_i - \eta_{i-1} - \sqrt{3})^2})_+ -$$

$$\left. (\dot{w}_i - \dot{\eta}_i)(2 - \sqrt{(z_i - \xi_i - 1)^2 + (w_i - \eta_i - \sqrt{3})^2})_+ \right] + 2^{3/2} \alpha (-w_i)_+^{3/2} \qquad (3.1)$$

$$\ddot{\xi}_i = \alpha \left[\frac{\xi_i - \xi_{i-1} + 2}{\sqrt{(\xi_i - \xi_{i-1} + 2)^2 + (\eta_i - \eta_{i-1})^2}} (2 - \sqrt{(\xi_i - \xi_{i-1} + 2)^2 + (\eta_i - \eta_{i-1})^2})_+^{3/2} + \right.$$

$$\left. \frac{\xi_i - \xi_{i+1} - 2}{\sqrt{(\xi_i - \xi_{i+1} - 2)^2 + (\eta_i - \eta_{i+1})^2}} (2 - \sqrt{(\xi_i - \xi_{i+1} - 2)^2 + (\eta_i - \eta_{i+1})^2})_+^{3/2} \right] +$$

$$\alpha \left[\frac{\xi_i - z_i + 1}{\sqrt{(\xi_i - z_i + 1)^2 + (\eta_i - w_i + \sqrt{3})^2}} (2 - \sqrt{(\xi_i - z_i + 1)^2 + (\eta_i - w_i + \sqrt{3})^2})_+^{3/2} + \right.$$

$$\left. \frac{\xi_i - z_{i+1} - 1}{\sqrt{(\xi_i - z_{i+1} - 1)^2 + (\eta_i - w_{i+1} + \sqrt{3})^2}} (2 - \sqrt{(\xi_i - z_{i+1} - 1)^2 + (\eta_i - w_{i+1} + \sqrt{3})^2})_+^{3/2} \right] +$$

$$\lambda \left[\left(\dot{\xi}_{i-1} - \dot{\xi}_i \right) (2 - \sqrt{(\xi_i - \xi_{i-1} + 2)^2 + (\eta_i - \eta_{i-1})^2})_+ - \right.$$

$$\left(\dot{\xi}_i - \dot{\xi}_{i+1} \right) (2 - \sqrt{(\xi_i - \xi_{i+1} - 2)^2 + (\eta_i - \eta_{i+1})^2})_+ +$$

$$(\dot{z}_i - \dot{\xi}_i)(2 - \sqrt{(\xi_i - z_i + 1)^2 + (\eta_i - w_i + \sqrt{3})^2})_+ -$$

$$\left. (\dot{\xi}_i - \dot{z}_{i+1})(2 - \sqrt{(\xi_i - z_{i+1} - 1)^2 + (\eta_i - w_{i+1} + \sqrt{3})^2})_+ \right]$$

$$\ddot{\eta}_i = \alpha \left[\frac{\eta_i - \eta_{i-1}}{\sqrt{(\xi_i - \xi_{i-1} + 2)^2 + (\eta_i - \eta_{i-1})^2}} (2 - \sqrt{(\xi_i - \xi_{i-1} + 2)^2 + (\eta_i - \eta_{i-1})^2})_+^{3/2} + \right.$$

$$\left. \frac{\eta_i - \eta_{i+1}}{\sqrt{(\xi_i - \xi_{i+1} - 2)^2 + (\eta_i - \eta_{i+1})^2}} (2 - \sqrt{(\xi_i - \xi_{i+1} - 2)^2 + (\eta_i - \eta_{i+1})^2})_+^{3/2} \right] +$$

$$\alpha \left[\frac{\eta_i - w_i + \sqrt{3}}{\sqrt{(\xi_i - z_i + 1)^2 + (\eta_i - w_i + \sqrt{3})^2}} (2 - \sqrt{(\xi_i - z_i + 1)^2 + (\eta_i - w_i + \sqrt{3})^2})_+^{3/2} + \right.$$

$$\left. \frac{\eta_i - w_{i+1} + \sqrt{3}}{\sqrt{(\xi_i - z_{i+1} - 1)^2 + (\eta_i - w_{i+1} + \sqrt{3})^2}} (2 - \sqrt{(\xi_i - z_{i+1} - 1)^2 + (\eta_i - w_{i+1} + \sqrt{3})^2})_+^{3/2} \right] +$$

$$\lambda \left[(\dot{\eta}_{i-1} - \dot{\eta}_i)(2 - \sqrt{(\xi_i - \xi_{i-1} + 2)^2 + (\eta_i - \eta_{i-1})^2})_+ - \right.$$

$$(\dot{\eta}_i - \dot{\eta}_{i+1})(2 - \sqrt{(\xi_i - \xi_{i+1} - 2)^2 + (\eta_i - \eta_{i+1})^2})_+ +$$

$$(\dot{w}_i - \dot{\eta}_i)(2 - \sqrt{(\xi_i - z_i + 1)^2 + (\eta_i - w_i + \sqrt{3})^2})_+ -$$

$$\left. (\dot{\eta}_i - \dot{w}_{i+1})(2 - \sqrt{(\xi_i - z_{i+1} - 1)^2 + (\eta_i - w_{i+1} + \sqrt{3})^2})_+ \right] - 2^{3/2} \alpha (\eta_i)_+^{3/2}$$

(3.1 cont.)

53

Hence, the results can be extended to the general class of granular networks possessing the configuration of Figure 3.1. We note that this set of equations is not re-scalable with energy since not all terms are proportional to the same power of the displacement components. It follows that the nonlinear dynamics of the system can change qualitatively with energy (i.e., with varying intensity of applied impulse). As discussed later, this can be rectified in the limit of small applied impulses by deriving a reduced model which is fully re-scalable with energy (see Section 3.2). In any case, the intensity of the applied impulse should be sufficiently small in order that the resulting deformations of the elastic beads of the coupled granular chains conform to the assumptions necessary for the mathematical model (3.1), and the (small) rotations of the beads can be neglected.

3.1.2 Mixed solitary-shear waves and pulse equi-partition

In the following computational study of this section we consider undamped granular chains composed of a number of identical stainless steel beads with parameters $\rho = 7958 \; kg/m^3$, $E = 1.93 \times 10^{11} \; Pa$, $v = 0.3$, $R = 4.75 \times 10^{-3} m$, $\lambda = 0 \; Nm/s$, $A = 754.8 \times 10^{-12} sec^2$ and $V_0 = 172.9 \; \bar{V}_0 \; mm/sec$. In Figure 3.2 we depict the time series of the normalized horizontal and vertical velocity components (e.g., in the normalized velocity $z'(\tau)$, prime denotes differentiation with respect to normalized time τ) of the leading beads of the excited and absorbing chains, each composed of $n = 20$ beads for normalized impulse intensity $\bar{V}_0 = 1 \times 10^{-4}$. In these plots we depict the early-time primary wave and pulse propagation in the two nonlinearly coupled chains, that is, the nonlinear waves and pulses that evolve immediately after the application of the applied impulse before reflections from the right boundary take place. Our main motivation is to study the perturbations of the Nesterenko solitary waves that would develop in the one- dimensional chains in the absence of coupling between chains and the lateral fixed boundary conditions.
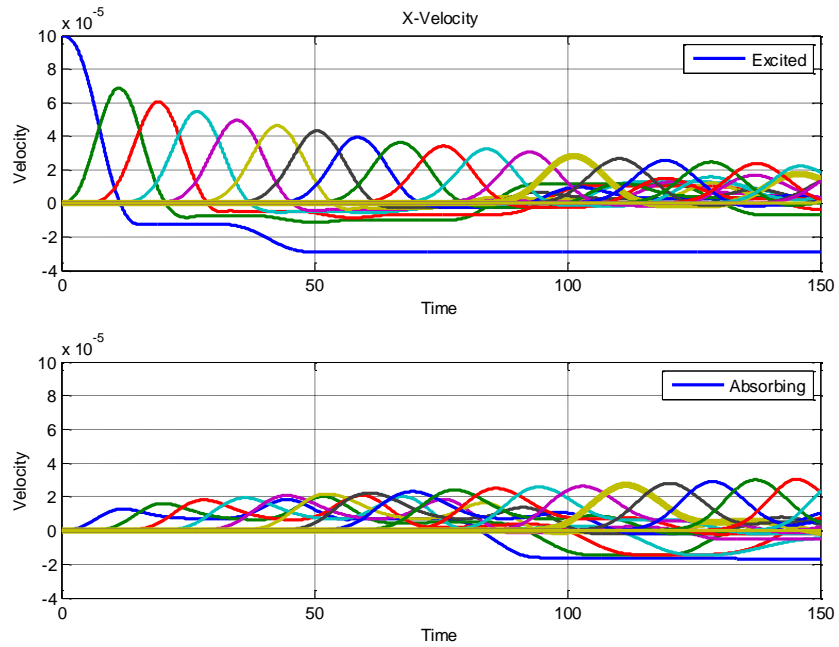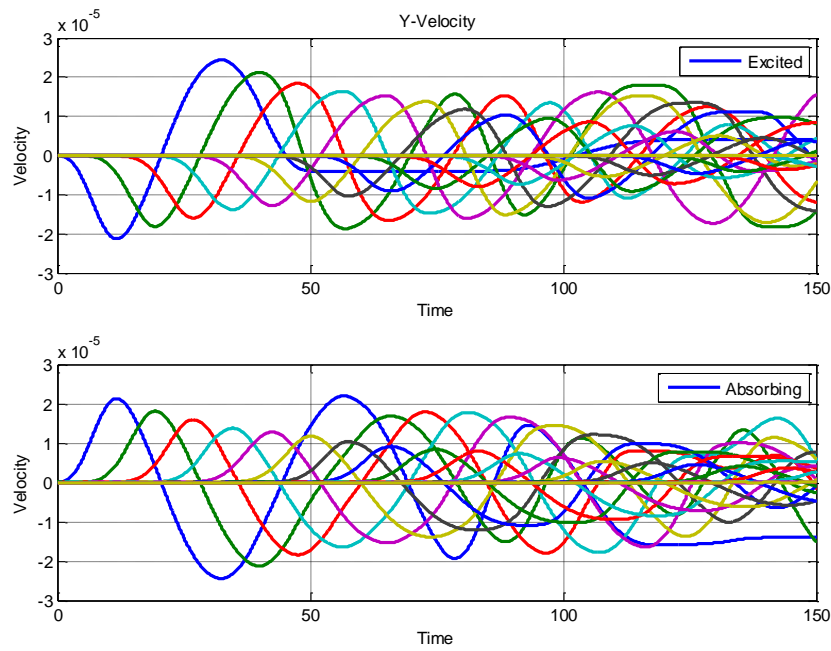
Figure 3.2. Re-scaled early-time velocity components of the leading beads of the system with $n = 20$ and normalized impulse intensity $\bar{V}_0 = 1 \times 10^{-4}$: (a) Horizontal components ($P-$pulses), and (b) vertical components ($S-$waves) in the excited and absorbing granular chains.

Certain conclusions can be drawn from the results of Figure 3.2. As an initial observation, two distinct types of propagating pulses and waves are realized involving predominantly horizontal and vertical velocity components, respectively. Focusing first on primary pulses involving the horizontal velocity components (denoted for obvious reasons as "P −pulses" (solitary pulses), see Figure 3.2a), we note that two traveling solitary pulses develop in each of the two chains, which are similar to the Nesterenko solitary pulses realized in single homogeneous granular chains and studied in (Nesterenko, 2001) using a long wave approximation analysis. These horizontal pulses are primarily responsible for momentum and energy transfer in the axial directions of the two chains, and can be considered as perturbations of the Nesterenko solitary pulses of the uncoupled one-dimensional granular chains. When coupling exists, strong energy exchanges between the two chains is inferred, as demonstrated by the primary pulse equi-partition that occurs when the two P −pulses reach the 13th beads of the excited and absorbing chains (see Figure 3.2a). Note that due to the geometry of the coupled granular system there is a time delay in the arrival of the primary P −pulse at the 13th bead of the absorbing chain.

This strong energy exchange and pulse equi-partition is more clearly viewed in Figure 3.3 where the contour plots of the total instantaneous kinetic energies of the beads of the excited and absorbing chains are depicted separately as they evolve in space and time. From these plots it is concluded that following the application of the impulse, energy is transferred from the excited to the absorbing chain, leading to eventual energy equi-partition between the two chains. We note that this energy transfer is not recurring in time, as in systems where nonlinear beat phenomena or discrete breathers are realized. Discrete breathers (Kopidakis and Aubry, 2000) were reported in other configurations of ordered granular systems, including homogeneous granular chains on elastic foundations (James, 2011; James et al., 2013), and systems of linearly coupled chains on

56

elastic foundations (Starosvetsky et al., 2012); in these works it was shown that these recurrent strongly nonlinear motions caused by 1:1 resonance captures, are effective mechanisms for strong energy transfer between components of a weakly coupled system, and, with appropriate structural modifications, can lead to passive energy redirection (i.e., one-way targeted energy transfer) from the excited chain to the absorbing one (Hasan et al., 2013a).
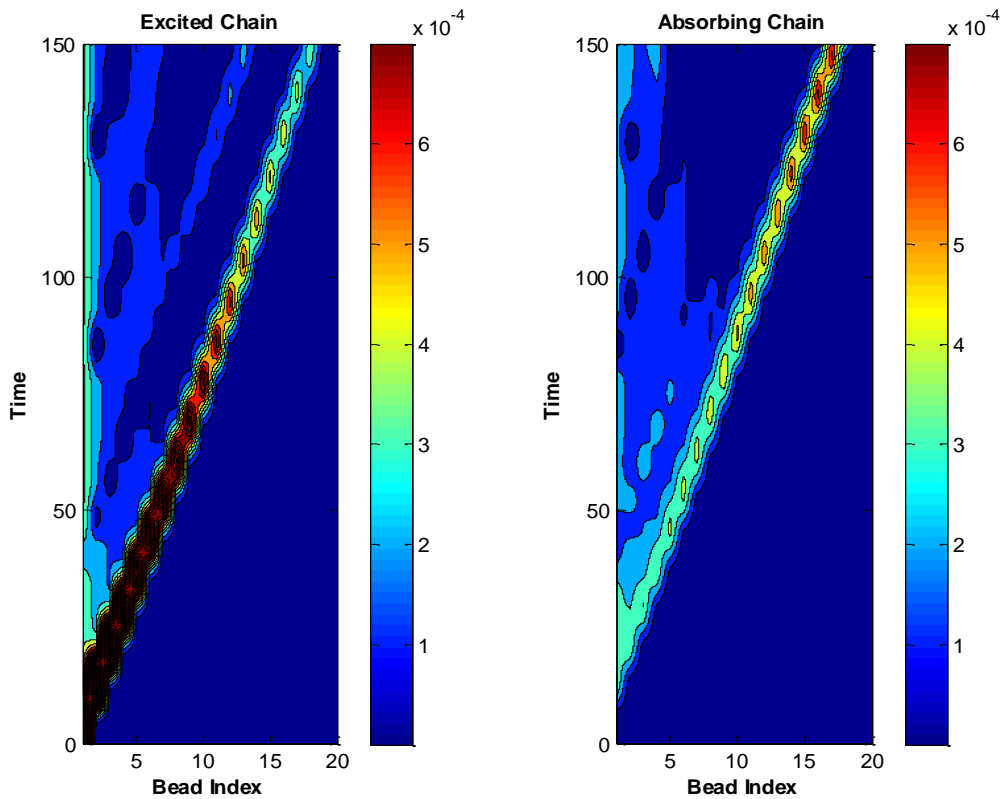
Figure 3.3. Contour plots of total kinetic energy (scaled $\times 10^6$) of the re-scaled granular system with $n = 20$ and normalized impulse intensity $\bar{V}_0 = 1 \times 10^{-4}$; strong energy exchange between the excited and absorbing granular chains is noted leading to eventual energy equi-partition.
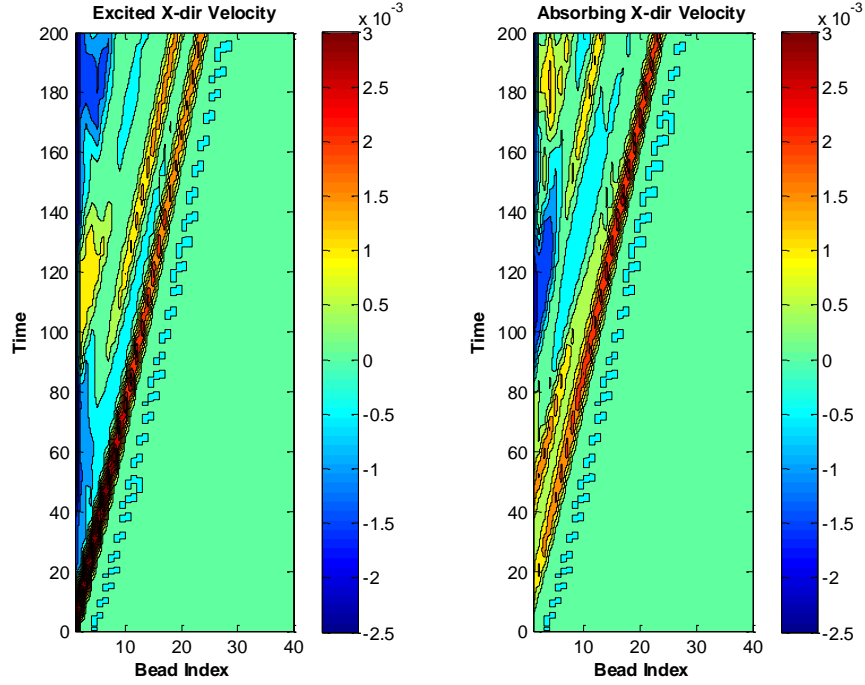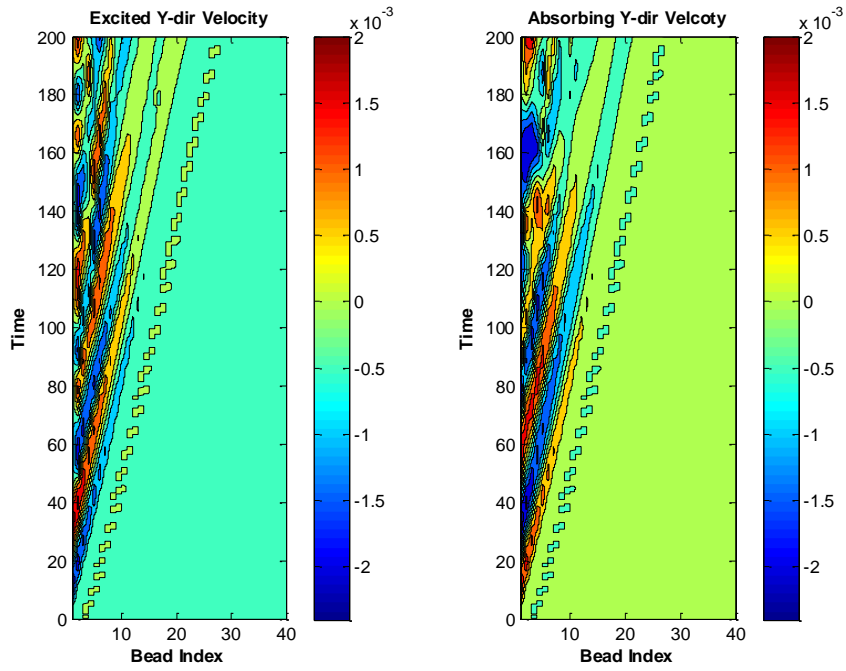
Figure 3.4. Contour plots of amplitudes of re-scaled velocity components (scaled $\times 10^2$) of the coupled granular system with $n = 40$ and re-scaled impulse intensity $\bar{V}_0 = 1 \times 10^{-4}$: (a) Horizontal components ($P-$pulses), (b) vertical components ($S-$waves).

The studies involving discrete breathers will be discussed in Chapter 4. On the contrary, in the present coupled chain configuration, once energy equi-partition occurs following initial transients, it is preserved during the entire primary pulse transmission, leading to the propagation of two independent solitary P −waves of equal magnitudes in each chain. Indeed, following the application of the impulse there is an initial phase during which waves of mixed type are realized giving rise to complex energy exchanges between the two chains; however, after these initial transients propagating pulses develop in the x −direction in each of the two chains and propagate unattenuated to the far field. Hence, the present system resembles more the impulsively excited system of weakly coupled granular chains considered in (Starosvetsky et al., 2013), and the granular system with intruders considered in (Szelengowicz et al., 2013), where weak coupling leads to pulse equi-partition. In this case, however, it is the geometry and kinematics of the network that provide the necessary coupling between the two granular chains that induces eventual pulse equi-partition (at least for the small intensity impulses considered in the presented simulations).

Additional interesting conclusions can be drawn considering the y −components of the velocities depicted in Figure 3.2b. In particular, we deduce the formation of a different type of nonlinear waves involving oscillations in the y −direction, i.e., in the direction transverse to the axial direction of pulse propagation. These secondary oscillatory waves will be denoted as 'S − waves' (shear waves), to emphasize their resemblance to shear waves of classical linear elasticity theory. These transverse higher-frequency oscillations of the beads in the vertical direction (contrasting the near-zero frequency of the P −solitary pulses propagating axially) are generated by Hertzian interactions with the fixed bounding walls, so the resulting motions constitute strongly nonlinear shear-type waves. The overall result is the formation of near-field nonlinear shear waves, which indicates that the propagation of P −pulses in the x −direction is associated with transverse

oscillations of the beads in the transverse $y-$direction. The formation of nonlinear shear waves can be better viewed in Figure 3.4 where contour plots of the re-scaled amplitudes of the horizontal and vertical velocity components of the excited and absorbing chains are depicted in space and time for a system with $n = 40$, and re-scaled impulse intensity $\bar{V}_0 = 1 \times 10^{-4}$. As mentioned previously, these waves are near-field motions (i.e., they are spatially localized close to the point of application of the impulse) and are formed during the initial transients, when $P-$pulses propagate in both chains. We conclude that nonlinear shear waves are produced by the nonlinear coupling of the horizontal and vertical motions of the beads during the initial highly energetic phase of the motion (i.e., when the nonlinear effects are more pronounced), and cannot be transmitted to the far field (downstream) of the coupled system.

We note, however, that due to the geometric configuration of the coupled granular network of Figure 3.1, in the vicinity of the point of application of the impulse the $P-$pulses and $S-$waves become coupled, and together form a mixed mode of wave propagation involving coupled near-zero frequency horizontal propagatory pulses, and higher-frequency vertical shear oscillatory waves. In essence, the nonlinear $S-$waves correspond to oscillatory dynamics and the $P-$pulses to propagatory acoustics. Moreover, whereas the $P-$pulses constitute the primary mechanism for momentum and energy transfer along the longitudinal direction of the coupled granular system (similar to the Nesterenko solitary waves in isolated one-dimensional homogeneous granular chains), the $S-$ waves provide the mechanism for partial higher-frequency scattering of the applied impulsive energy in a direction orthogonal to the primary direction of momentum transfer. Hence, these secondary oscillatory waves play an important role in the nonlinear acoustics of the problem, by reducing the amount of impulsive energy that is eventually transferred to the far field of the coupled system. Close to the point of application of the impulse the mixed wave mode is

composed of both propagatory acoustics and oscillatory dynamics, whereas away from that point the wave mode becomes purely propagatory, composed of only P −pulses.

As mentioned previously, the strongly nonlinear dynamics of the coupled granular system (3.1) is not re-scalable with energy, so it is expected to depend on the magnitude of the intensity of the applied impulse. Therefore, the previous results are tied to the assumption of small applied impulse intensities, or, equivalently, of small-energy nonlinear acoustics. Precisely in this small-energy limit, however, and under certain additional restrictions, it is possible to perform simplifications of the full equations of motion (3.1) and reduce them to a system that is amenable to asymptotic analysis. Moreover, it is possible to make the reduced system fully re-scalable with energy, so that its dynamics and acoustics become independent of the (small) intensity of the applied impulse. In the following section we perform this analytical reduction, and study asymptotically the responses of the reduced system by extending the nonlinear mapping technique first developed by Starosvetsky (2012), and Ben-Meir and Starosvetsky (2013). Our analysis theoretically recovers the formation of the mixed wave mode close to the point of application of the applied impulse leading to the formation of coupled P − and S − waves, reveals the nonlinear dynamical mechanisms governing the formation of the mixed wave mode, and correctly predicts the first instance of primary pulse equi-partition in the two granular chains.

3.2 Analytical study

Considering the strongly nonlinear equations of motion (3.1), we will restrict our study to the regime of primary pulse propagation and disregard secondary waves formed in the tail of the primary propagating pulses or after reflection of the primary pulses from the rigid boundaries. In addition, we will assume that the horizontal and vertical deformations (and their time derivatives)

61

are sufficiently small, so simplifications of the strongly nonlinear terms can be carried out. Under these assumptions we focus on the regime of the acoustics corresponding to the propagating front of the primary pulse where strong compressive forces between beads are realized. Clearly, in the propagating front of the primary pulse no bead separations or collisions can occur, the acoustics is smooth, and the (+) subscripts can be disregarded in equations (3.1). This simplifies significantly the analysis.

3.2.1 Reduced system

Based on the physics of the problem, and motivated by the previous computational results, we expect that the x −components of the responses of the beads of the excited chain will represent the dominant acoustics of primary pulse propagation, and drive the other components of the response of the coupled granular system. Moreover, for primary pulse transmission we anticipate that the effects of damping can be neglected, since dissipative effects are minimal in the early time response of the system (i.e., during primary pulse transmission); numerical simulations confirmed the validity of this assumption.

As the first step in the analysis to asymptotically model primary P −pulse propagation in the excited chain, we set $w_i = \xi_i = \eta_i = 0$ in equations (3.1), neglect the damping terms, and implement the re-scalings mentioned therein to get the normalized equations for $z_i, \quad i = 1, \dots n$:

$$z_i'' = \left[\frac{z_i - z_{i-1} + 2}{\sqrt{(z_i - z_{i-1} + 2)^2}} \left(2 - \sqrt{(z_i - z_{i-1} + 2)^2}\right)_+^{3/2} + \right.$$

$$\left. \frac{z_i - z_{i+1} - 2}{\sqrt{(z_i - z_{i+1} - 2)^2}} \left(2 - \sqrt{(z_i - z_{i+1} - 2)^2}\right)_+^{3/2} \right] +$$

$$\left[\frac{z_i + 1}{\sqrt{(z_i + 1)^2 + (\sqrt{3})^2}} \left(2 - \sqrt{(z_i + 1)^2 + (\sqrt{3})^2}\right)_+^{3/2} + \right.$$

$$\left. \frac{z_i - 1}{\sqrt{(z_i - 1)^2 + (\sqrt{3})^2}} \left(2 - \sqrt{(z_i - 1)^2 + (\sqrt{3})^2}\right)_+^{3/2} \right]$$

(3.2)

Note that we have introduced the re-scaled time variable $\tau = t/\sqrt{A}$, where $A = 2\sqrt{2}\pi\rho R^2(1 - \nu^2)/E$, as discussed in Section 3.1. Assuming that $(z_{i-1} - z_i) \ll 1$ and $z_i \ll 1$ we perform the following Taylor series expansions,

$$\sqrt{(z_i \pm 1)^2 + (\sqrt{3})^2} = \{4 \pm 2z_i + ...\}^{1/2} = \left\{2 \pm \frac{1}{2}(4)^{-1/2} 2z_i + ...\right\} = 2 \pm \frac{1}{2} z_i + ...$$

$$(2 - \sqrt{(z_i \pm 1)^2 + (\sqrt{3})^2})_+^{3/2} = \left(2 - \{4 \pm 2z_i\}^{1/2} + ...\right)_+^{3/2}$$

$$= \left(2 - \left\{2 \pm \frac{1}{2}(4)^{-1/2} 2z_i + ...\right\}\right)_+^{3/2} = \left(\mp \frac{1}{2} z_i + ...\right)_+^{3/2}$$

(3.3)

$$\frac{z_i \pm 1}{2 \pm \frac{1}{2} z_i} = (z_i \pm 1)\left\{2 \pm \frac{1}{2} z_i\right\}^{-1} = (z_i \pm 1)\left\{(2)^{-1} \mp (2)^{-2}(\frac{1}{2} z_i) + ...\right\} =$$

$$(z_i \pm 1)\frac{(4 \mp z_i)}{8} + ... = \frac{1}{2} \mp \frac{3z_i}{8} \mp \frac{z_i^2}{8} + ...$$

Substituting into (3.2) we obtain the following simplified system:

$$z_i'' = \left[(z_{i-1} - z_i)_+^{3/2} - (z_i - z_{i+1})_+^{3/2}\right] + \left[\frac{z_i + 1}{2 + \frac{1}{2} z_i}\left(-\frac{1}{2} z_i\right)_+^{3/2} + \frac{z_i - 1}{2 - \frac{1}{2} z_i}\left(\frac{1}{2} z_i\right)_+^{3/2} \right] + ...$$

(3.4)

63

Then, disregarding nonlinear terms of order higher than the Hertzian exponent, (3/2), from equations (3.4), we obtain the following reduced equation of motion for the axial components of the responses of the beads of the excited chain,

$$z_i'' = \left[(z_{i-1} - z_i)_+^{3/2} - (z_i - z_{i+1})_+^{3/2} \right] + \frac{1}{2^{5/2}} \left[-(z_i)_+^{3/2} \right] + ... \tag{3.5}$$

where we have recognized that $(-z_i)_+^{3/2} = 0$ for primary pulse propagation, since no bead separations can occur in that highly compressed local regime of the acoustics.

The solution of this reduced system provides the main approximation for the primary $P-$wave (solitary pulse) in the excited chain, driving the nonlinear acoustics by exciting primary $S-$ waves in both chains and primary $P-$waves in the absorbing chain. Adopting this causality argument, we can formulate similar reduced systems governing the other response components of the granular network. To this end, we assume that $(w_{i-1} - w_i) \ll 1$, $(z_i - \xi_i) \ll 1$, $(w_i - \eta_i) \ll 1$, and $w_i, \xi_i, \eta_i \ll 1$ and perform similar Taylor series expansions to obtain the governing equations for the other components of the bead responses,

$$w_i'' = -\frac{\sqrt{3}}{2^{5/2}} \left\{ \left[-(z_i - \xi_{i-1}) + \sqrt{3}(w_i - \eta_{i-1}) \right]_+^{3/2} + \left[(z_i - \xi_i) + \sqrt{3}(w_i - \eta_i) \right]_+^{3/2} \right\} + 2^{3/2}(-w_i)_+^{3/2} + ... \tag{3.6}$$

$$\xi_i'' = \left[(\xi_{i-1} - \xi_i)_+^{3/2} - (\xi_i - \xi_{i+1})_+^{3/2} \right] + $$
$$\frac{1}{2^{5/2}} \left\{ \left[(z_i - \xi_i) + \sqrt{3}(w_i - \eta_i) \right]_+^{3/2} - \left[-(z_{i+1} - \xi_i) + \sqrt{3}(w_{i+1} - \eta_i) \right]_+^{3/2} \right\} + ... \tag{3.7}$$

$$\eta_i'' = \frac{\sqrt{3}}{2^{5/2}} \left\{ \left[(z_i - \xi_i) + \sqrt{3}(w_i - \eta_i) \right]_+^{3/2} + \left[-(z_{i+1} - \xi_i) + \sqrt{3}(w_{i+1} - \eta_i) \right]_+^{3/2} \right\} - 2^{3/2}(\eta_i)_+^{3/2} + ... \tag{3.8}$$

The reduced system (3.5-3.8) can be further simplified by imposing the symmetry argument that the vertical components of the displacements of the excited and absorbing chains

are equal but out-of-phase, $\xi_i = -\eta_i$, $i = 1, 2, ..., n$. Hence, the final reduced system is composed of the following three equations:

$$z_i'' = \left[(z_{i-1} - z_i)_+^{3/2} - (z_i - z_{i+1})_+^{3/2} \right] + \frac{1}{2^{5/2}} \left[-(z_i)_+^{3/2} \right] + ... \qquad (3.9a)$$

$$w_i'' = -\frac{\sqrt{3}}{2^{5/2}} \left(\left[(z_i - \xi_i) + 2\sqrt{3}w_i \right]_+^{3/2} \right) + 2^{3/2} (-w_i)_+^{3/2} + ... \qquad (3.9b)$$

$$\xi_i'' = \left[(\xi_{i-1} - \xi_i)_+^{3/2} - (\xi_i - \xi_{i+1})_+^{3/2} \right] + \frac{1}{2^{5/2}} \left[(z_i - \xi_i) + 2\sqrt{3}w_i \right]_+^{3/2} + ... \qquad (3.9c)$$
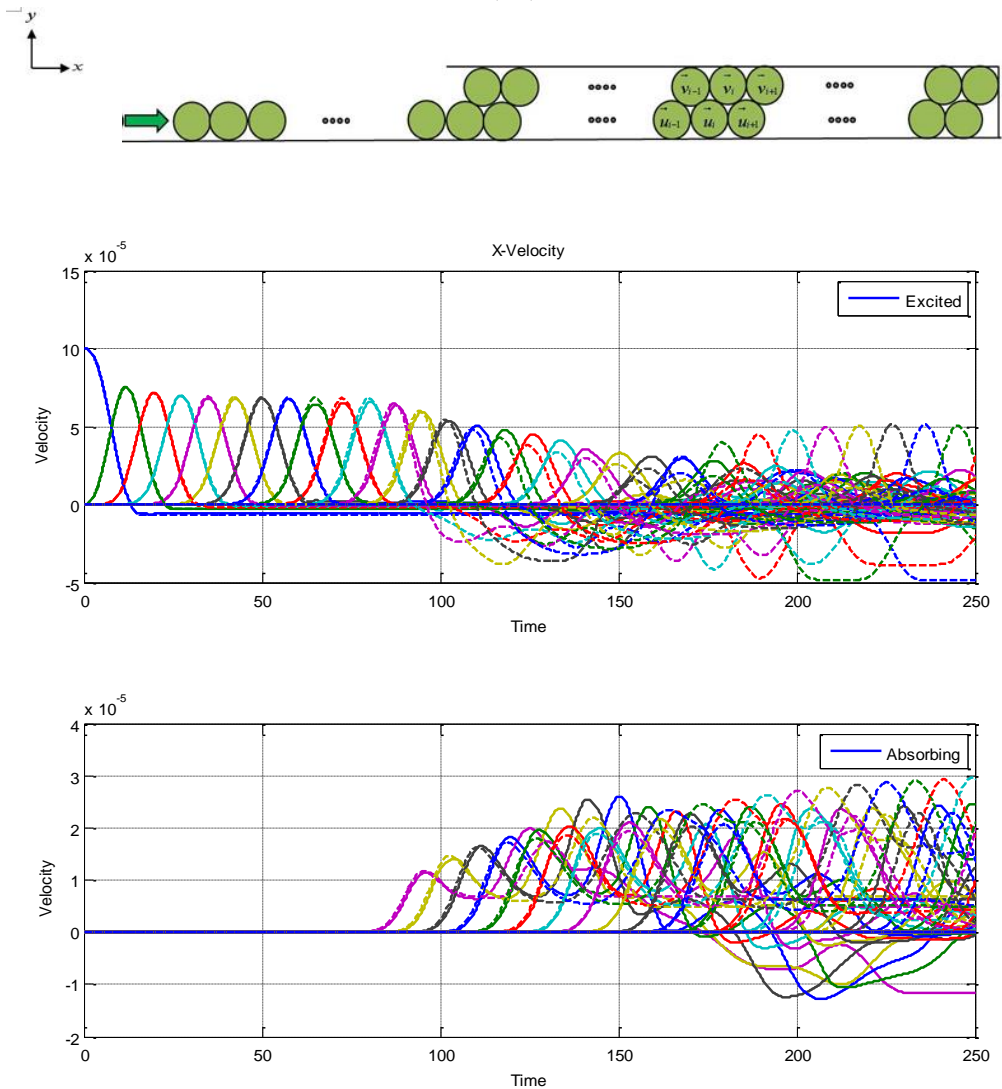
$$i = 1, ..., n$$

Figure 3.5. Comparison of the responses of the exact re-scaled system (3.1) (———), and the reduced system (3.9a-c) (-----------): Re-scaled horizontal velocity components (P −pulses).
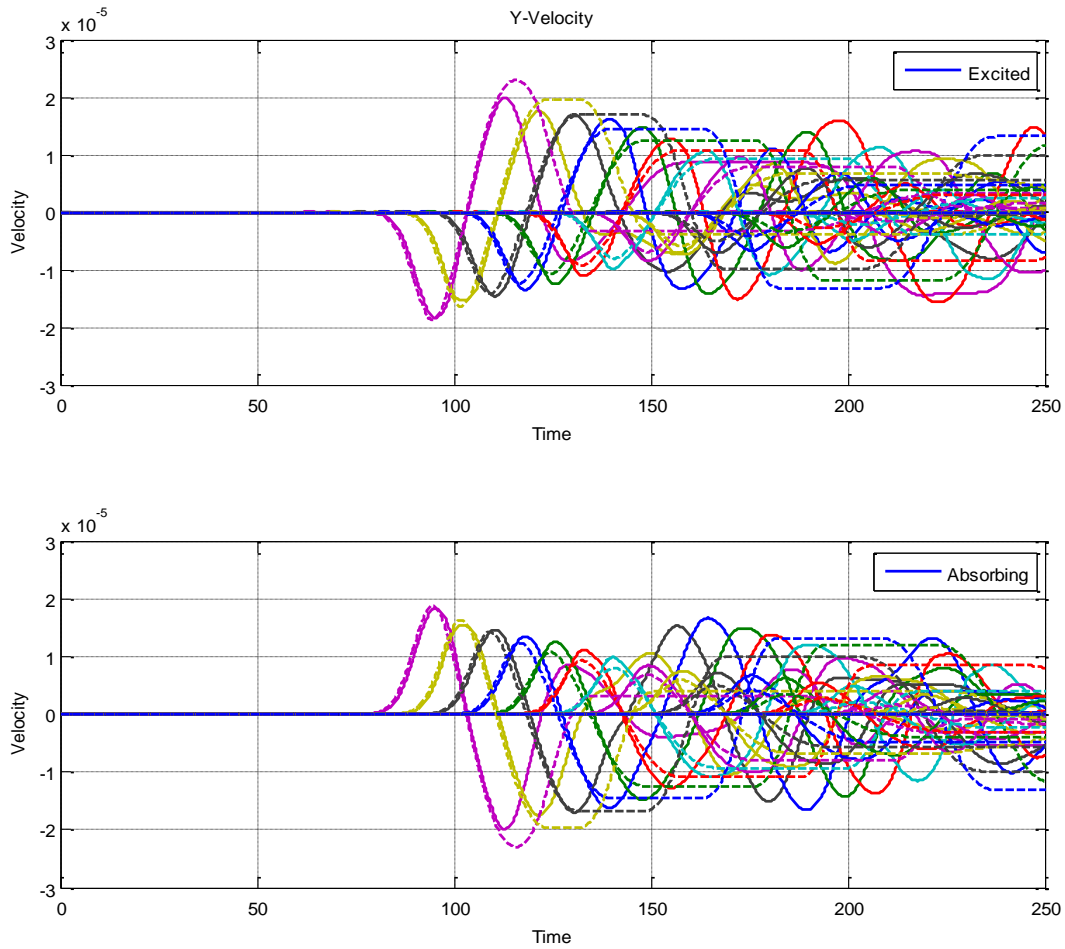
Figure 3.6. Comparison of the responses of the exact re-scaled system (3.1) (————), and the reduced system (3.9a-c) (-----------):Re-scaled vertical velocity components (S −waves).

By construction, equation (3.9a) governing the formation of the primary pulse in the excited chain is uncoupled from the other two equations and serves as the "driver" of the nonlinear acoustics of the system in the neighborhood of excitation. That is, after approximating the primary P −wave propagation in the excited chain by approximately solving (3.9a), we will consider the derived solution as the excitation for the other two equations (3.9b) and (3.9c) governing the formation of primary P − pulse propagation in the absorbing chain and primary S − wave propagation in both chains, respectively. Moreover, we note that since all nonlinear terms in the

reduced system (3.9) have the same power (3/2), the dynamics and acoustics are fully re-scalable with energy; this is in contrast to the original system (3.1), which as discussed previously is not re-scalable with energy. It follows that the results of our asymptotic analysis are independent of the intensity of the applied impulse, provided that it is sufficiently small in order to conform to our previous assumptions.

In Figures 3.5 and 3.6 we depict the comparison of the reduced system with the original system (3.1) for a coupled granular system with $n = 50$, and normalized impulse intensity $\bar{V}_0 = 1 \times 10^{-4}$. We have slightly modified the configuration of the system by adding an auxiliary one-dimensional homogeneous granular chain on the left side of the excited chain and applying the impulse to the left end of this auxiliary chain; the rationale for this modification is our wish to excite the coupled granular chain by a "pure" Nesterenko solitary wave instead of an impulse, so that we can study the scattering of the impeding solitary wave by the two-dimensional granular system under consideration. In addition, it turns out that the nonlinear mapping methodology developed below works best with this type of "pure" Nesterenko solitary pulse excitation instead of impulse excitation; this is due to the fact that it is based on a perturbation of the Nesterenko solitary pulse which is used as the generating solution in the asymptotics. The comparisons of the $P-$pulses and $S-$waves depicted in Figures 3.5 and 3.6 indicate that the reduced model accurately captures the formation of the primary pulses/waves in the coupled granular system and validates our reduction.

3.2.2 Solitary-like wave approximation and analytical results

In this section, we proceed to analyze the reduced system (3.9a-c) in order to study the nonlinear dynamical mechanisms governing the formation of primary pulses/waves, and the mixed wave

mode in the neighborhood of the point of the impeding Nesterenko solitary wave. Towards this end, we will extend to multiple dimensions the nonlinear mapping technique developed by Starosvetsky (2012), and Ben-Meir and Starosvetsky (2013) for studying primary pulse transmission in one-dimensional granular chains.

Considering first the primary $P-$pulse governed by (3.9a), we note that by defining the small parameter $\varepsilon \equiv 1/2^{5/2} \ll 1$, this equation represents a perturbation of a one-dimensional homogeneous granular chain which admits as a solution the Nesterenko solitary pulse. It follows that we can use this well-known solitary solution as a generating function in order to develop asymptotic approximations for $\varepsilon \ll 1$ by perturbation expansions. Motivated by this observation we introduce the relative displacement $\delta_i \equiv \left(z_i - z_{i+1} \right)$ and express this equation as follows (where higher order terms arising due to the previous Taylor series expansions are omitted from further consideration):

$$\delta_i'' + \varepsilon \left[\left\{ \left(z_i \right)_+^{3/2} - \left(z_{i+1} \right)_+^{3/2} \right\} \right] = \left(\delta_{i-1} \right)_+^{3/2} - 2 \left(\delta_i \right)_+^{3/2} + \left(\delta_{i+1} \right)_+^{3/2} + ... \qquad (3.10)$$

In the asymptotic analysis ε will be regarded as the small parameter of the problem. Furthermore, assuming that the amplitude variation between adjacent bead responses in (3.9a) is sufficiently small, we express $z_i = \delta_i + \delta_{i+1} + o(\varepsilon)$, and express (3.10) in the following form:

$$\delta_i'' + \varepsilon \left[\left\{ \left(\delta_i + \delta_{i+1} \right)_+^{3/2} - \left(\delta_{i+1} \right)_+^{3/2} \right\} \right] = \left(\delta_{i-1} \right)_+^{3/2} - 2 \left(\delta_i \right)_+^{3/2} + \left(\delta_{i+1} \right)_+^{3/2} + o(\varepsilon) \qquad (3.11)$$

In the limit $\varepsilon \to 0$ equation (3.11) describes the homogeneous granular chain and the solution is the Nesterenko solitary pulse; although no exact analytical solution for this pulse exists there have been developed a number of approximations (Nesterenko, 1983; Lazaridi and Nesterenko, 1985;

68

Sen et al., 2008; Ahnert et al., 2009; Starosvetsky and Vakakis, 2010). Motivated by these observations and following Starosvetsky (2012), we assume that for primary pulse propagation the developing $P-$solitary pulse in the excited chain can be regarded as a perturbation of the Nesterenko solitary pulse, and express the relative displacements $\delta_i(\tau)$ and $\delta_{i-1}(\tau)$ as

$$\delta_i(\tau) \approx A_i \tilde{S}(A_i^{1/4}\tau) \implies \delta_i'(\tau) \approx A_i^{5/4}\tilde{S}'(A_i^{1/4}\tau) \implies \delta_i''(\tau) \approx A_i^{3/2}\tilde{S}''(A_i^{1/4}\tau)$$
$$\delta_{i-1}(\tau) \approx A_{i-1}\tilde{S}(A_{i-1}^{1/4}\tau + 1) \tag{3.12}$$

where by $\tilde{S}(\bullet)$ we denote the approximation for the Nesterenko solitary pulse of the homogeneous granular chain, and by A_i the amplitude of the primary pulse at the $i\,th$ bead of the excited chain.

Considering now the construction of the nonlinear map governing the amplitudes A_i of the solitary approximations of expressions (3.12), we work as follows. Substituting (3.12) into (3.11) we obtain:

$$A_i^{3/2}\tilde{S}''(A_i^{1/4}\tau) = \left[A_{i-1}^{3/2}\left\{\tilde{S}\left(A_{i-1}^{1/4}\tau+1\right)\right\}^{3/2} - 2A_i^{3/2}\left\{\tilde{S}\left(A_i^{1/4}\tau\right)\right\}^{3/2} + A_{i+1}^{3/2}\left\{\tilde{S}\left(A_{i+1}^{1/4}\tau-1\right)\right\}^{3/2} \right] -$$
$$\varepsilon\left\{\left[A_i\,\tilde{S}\left(A_i^{1/4}\tau\right) + A_{i+1}\tilde{S}\left(A_{i+1}^{1/4}\tau-1\right)\right]^{3/2} - \left[A_{i+1}\tilde{S}\left(A_{i+1}^{1/4}\tau-1\right)\right]^{3/2}\right\} + o(\varepsilon) \tag{3.13}$$

Integrating this expression with respect to time in the interval $-\infty < \tau \le 0$, shifting time so that the maximum of the primary propagating pulse at the $i\,th$ bead is realized at $\tau = 0$, taking into account the limit $\lim_{\tau\to-\infty}\tilde{S}'(A_i^{1/4}\tau) = 0$ and that $\tilde{S}'(0) = 0$ (since $\tau = 0$ corresponds to the maximum of the primary propagating pulse at the $i\,th$ bead), and introducing the new scaled time $\tilde{\tau} = A_i^{1/4}\tau$ in the integrals, we obtain the approximate expression:

$$0 = \left[A_{i-1}^{5/4} \int_{-\infty}^{0} \left\{ \tilde{S}(\tilde{\tau}+1) \right\}^{3/2} d\tilde{\tau} - 2A_i^{5/4} \int_{-\infty}^{0} \left\{ \tilde{S}(\tilde{\tau}) \right\}^{3/2} d\tilde{\tau} + A_{i+1}^{5/4} \int_{-\infty}^{0} \left\{ \tilde{S}(\tilde{\tau}-1) \right\}^{3/2} d\tilde{\tau} \right] -$$

$$\varepsilon \left\{ \int_{-\infty}^{0} \left[A_i \tilde{S}\left(A_i^{1/4}\tau\right) + A_{i+1}\tilde{S}\left(A_{i+1}^{1/4}\tau -1\right) \right]^{3/2} d\tau - A_{i+1}^{5/4} \int_{-\infty}^{0} \left\{ \tilde{S}_{i+1}(\tilde{\tau}-1) \right\}^{3/2} d\tilde{\tau} \right\} + o(\varepsilon) \tag{3.14}$$

Recognizing that the following expressions are numerical constants depending only on the approximation for the Nesterenko solitary pulse $\tilde{S}(\bullet)$,

$$\int_{-\infty}^{0} \tilde{S}(u+1)^{3/2} du \equiv f_1, \quad \int_{-\infty}^{0} \tilde{S}(u)^{3/2} du \equiv f_2, \quad \int_{-\infty}^{0} \tilde{S}(u-1)^{3/2} du \equiv f_3, \quad \int_{-\infty}^{0} \tilde{S}(u-1) du \equiv f_4 \tag{3.15}$$

we write (3.15) as:

$$0 = \left[A_{i-1}^{5/4} - 2A_i^{5/4} \frac{f_2}{f_1} + A_{i+1}^{5/4} \frac{f_3}{f_1} \right] -$$

$$\frac{\varepsilon}{f_1} \left\{ \int_{-\infty}^{0} \left[A_i \tilde{S}\left(A_i^{1/4}\tau\right) + A_{i+1}\tilde{S}\left(A_{i+1}^{1/4}\tau -1\right) \right]^{3/2} d\tau - A_{i+1}^{5/4} f_4 \right\} + o(\varepsilon) \tag{3.16}$$

Due to the assumed small variation of the amplitude of the primary $P-$pulse in the excited chain, it is possible to assume that $A_{i+1} = A_i + O(\varepsilon)$, which combined with the fact that $f_1 = 2.5052$, $f_3 = 0.1378$, and $\mu = \dfrac{f_3}{f_1} \approx 0.06 \ll 1$ (Starosvetsky, 2012), leads to further simplification of (3.17),

$$0 = \left[A_{i-1}^{5/4} - 2A_i^{5/4} \frac{f_2}{f_1} + A_i^{5/4} \frac{f_3}{f_1} \right] -$$

$$\frac{\varepsilon}{f_1} \left\{ \int_{-\infty}^{0} \left[A_i \tilde{S}\left(A_i^{1/4}\tau\right) + A_i \tilde{S}\left(A_i^{1/4}\tau -1\right) \right]^{3/2} d\tau - A_i^{5/4} f_4 \right\} + O(\varepsilon\mu) \tag{3.18}$$

or,

$$\left[A_{i-1}^{5/4} - \left(2\frac{f_2}{f_1} - \mu\right)A_i^{5/4}\right] + \frac{\varepsilon}{f_1}\left(f_4 - f_5\right)A_i^{5/4} = 0 + O(\varepsilon\mu) \tag{3.19}$$

where $f_5 \equiv \int_{-\infty}^{0}\left[\tilde{S}(u) + \tilde{S}(u-1)\right]^{3/2} du$. By evaluating this map in a recurring way (starting from the

"initial condition" $A_0 = A$, where A is the maximum relative response for the impeding

Nesterenko solitary pulse) we obtain an asymptotic approximation of the spatial variation of the

maximum amplitude of the primary P −pulse in the excited chain at each of the leading beads

following the arrival of the Nesterenko solitary pulse that is generated by the impulse excitation

on the auxiliary homogeneous chain on the left of the coupled granular system. The actual spatial

and temporal variation of the primary pulse in the excited chain (up to the shifted time instant $\tau =$

0 when it reaches its maximum amplitude at each bead) can then be approximated by the relations

(3.12).

In Figure 3.7 we present the numerical solution computed by the nonlinear map (3.19) for

the 20 leading beads of the excited granular chain, subject to a normalized impulse of intensity

$\bar{V}_0 = 1 \times 10^{-4}$ applied to the auxiliary homogeneous chain. By comparing these results with the

corresponding maxima of the relative displacements between beads computed from the exact re-

scaled system (3.1) we observe good agreement, which validates our previous asymptotic

approximation.

Following the analytic approximation of primary pulse generation in the excited chain, in

the next step of our study we consider the remaining two equations (3.9b) and (3.9c) of the reduced

system, and regard terms depending on z_i as excitations. By noting the mathematical structures of

these equations we conclude that the primary P − pulse in the exciting chain acts as parametric

forcing for both primary $S-$waves and primary $P-$pulses in the absorbing chain. In addition, we note that the $S-$waves are nonlinearly coupled to the $P-$pulse in the absorbing chain, so these secondary waves are simultaneously excited by the initial primary $P-$pulse in the excited chain.
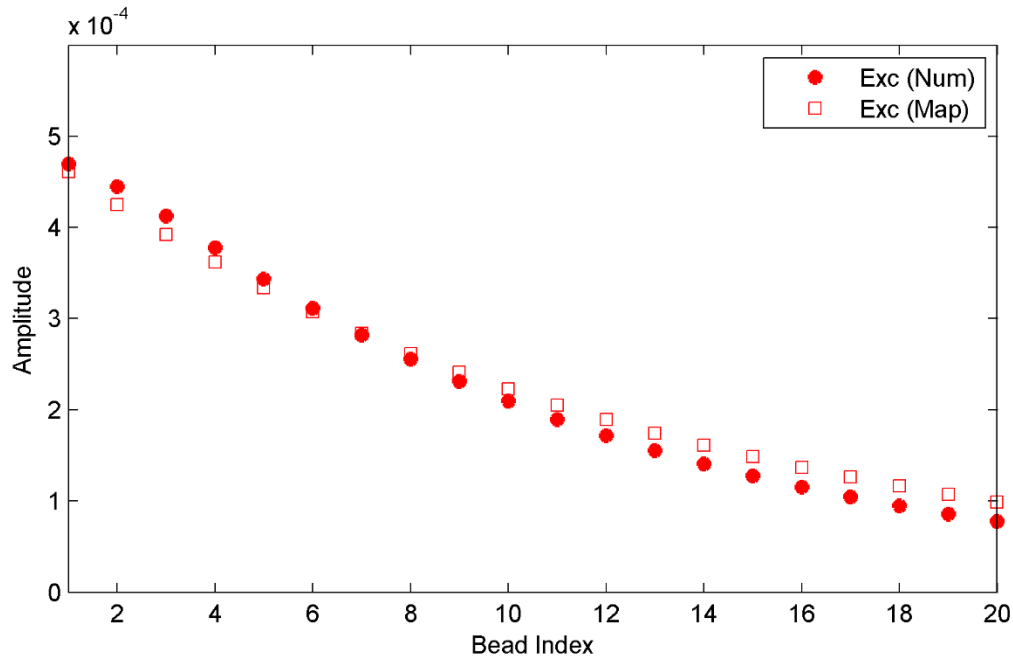

Figure 3.7. Primary $P-$pulse propagation in the excited chain: Maximum amplitudes of re-scaled relative $x-$displacements between leading beads for normalized impulse intensity $\bar{V}_0 = 1 \times 10^{-4}$; ($\square$) Asymptotic predictions based on the reduced system (3.19), compared to ($\bullet$) exact solutions based on the re-scaled equations (3.1).

The nonlinear coupled equations (3.9b) and (3.9c) are difficult to analyze so at this point we make an additional simplifying assumption which will allow us further analytical treatment of the problem; namely, we will assume that the mutual interaction between the driven primary $S-$waves and $P-$pulses in the absorbing chain is much weaker than the interaction of each of these waves and the driver primary $P-$pulse in the excited chain. Accordingly we proceed to omit these mutual interactions from further analysis (i.e., the coupling terms in (3.9b,c)), and consider instead the further simplified equations:

$$w_i'' = -\frac{\sqrt{3}}{2^{5/2}}\left(\left[z_i + 2\sqrt{3}w_i\right]_+^{3/2}\right) + 2^{3/2}(-w_i)_+^{3/2} + \dots \tag{3.20}$$

$$\xi_i'' = \left[\left(\xi_{i-1} - \xi_i\right)_+^{3/2} - \left(\xi_i - \xi_{i+1}\right)_+^{3/2}\right] + \frac{1}{2^{5/2}}\left[(z_i - \xi_i)\right]_+^{3/2} + \dots \tag{3.21}$$

$$i = 1, \dots, n$$

We note that this last simplification (which can be justified from a physical point of view) provides results that are consistent with numerical simulations.

Starting from equation (3.20) governing the evolution of the primary $S-$waves in both excited and absorbing chains and imposing the previous approximations, $z_i = \delta_i + \delta_{i+1} + o(\varepsilon)$, $\delta_i(t) = A_i\tilde{S}(A_i^{1/4}t)$, $A_{i+1} = A_i + O(\varepsilon)$, we obtain the expression:

$$w_i'' - 2^{3/2}(-w_i)_+^{3/2} = -\sqrt{3}\varepsilon\left[A_i\tilde{S}(A_i^{1/4}\tau) + A_i\tilde{S}(A_i^{1/4}\tau - 1) + 2\sqrt{3}w_i\right]_+^{3/2} + O(\varepsilon^2) \tag{3.22}$$

Interestingly enough this can be completely renormalized, so the amplitudes A_i can be scaled out of the equation. To show this, we introduce the following transformation of variables $w_i = A_i\tilde{w}$, $A_i^{1/4}\tau = \tilde{\tau}$, yielding

$$\tilde{w}'' - 2^{3/2}(-\tilde{w})_+^{3/2} = -\sqrt{3}\varepsilon\left[\tilde{S}(\tilde{\tau}) + \tilde{S}(\tilde{\tau} - 1) + 2\sqrt{3}\tilde{w}\right]_+^{3/2} + O(\varepsilon^2) \tag{3.23}$$

Hence, the global dynamics of shear waves in the granular chain is effectively reduced to the single degree-of-freedom (DOF) nonlinear oscillator (3.23) which is independent of the strength of the excitation provided by the excited chain (the driver), and thus can be solved once and for all for the entire class of granular systems considered herein. This also means that by solving (3.23) one may obtain the functional form $\tilde{w}(\tilde{\tau})$ and the amplitude of the primary response (that is, $\tilde{w}(\tilde{\tau}^*)$,

where $\tilde{\tau}^*$ corresponds to the time point where the primary response reaches its maximum value).

Here we note in passing that an analytical approximation of the primary response of (3.23) can be derived by various well known techniques of perturbation theory (e.g., Padé approximants or other successive approximations). Then, to derive the response of the transversal pulse propagating down the chain, one applies to the previous transformation, $w_i(\tau) = A_i \tilde{w}(A_i^{1/4}\tau)$.
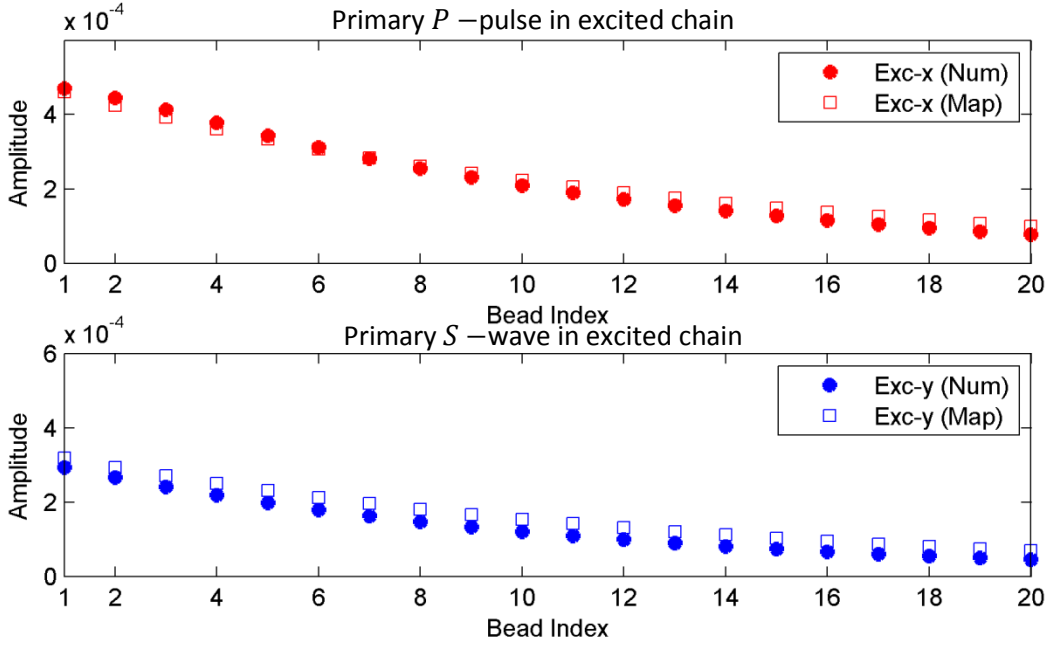

Figure 3.8. Primary $P-$ pulse and $S-$ wave transmission in the excited chain: Maximum amplitudes of re-scaled $y-$ displacements of the leading beads for normalized impulse intensity $\bar{V}_0 = 1 \times 10^{-4}$; Asymptotic predictions based on the reduced system (3.22) ($\square$), compared to exact solutions based on the re-scaled equations (3.1) ($\bullet$); the results of Figure 3.7 are reproduced here for comparison.

We also note that equation (3.23) describes a weak perturbation corresponding to the primary phase of the response of an asymmetric, strongly nonlinear oscillator. In fact this asymmetry is caused by the two distinct types of interaction (depending on the phase); namely, interaction with the rigid wall (primary phase – the first half period), and also interaction with the

neighboring beads (secondary phase − the second half period). This justifies the oscillatory dynamics of the primary $S-$waves, compared to the propagatory dynamics of the primary $P-$pulses which are governed by equations (3.9a) and (3.21), and are not in the form of perturbed oscillators. This underscores the different nature of the generated waves and pulses in the $x-$ and $y-$directions. First, we need to solve equation (3.23) for the global variable $\tilde{w}$, and then we can obtain the responses of the $y-$components of all beads of the excited chain using the expression $w_i = A_i \tilde{w}$. In Figure 3.8 we depict the maxima of the amplitudes of the re-scaled $y-$displacements of the leading beads of the excited chain for normalized impulse intensity $\bar{V}_0 = 1 \times 10^{-4}$, from which satisfactory agreement with direct numerical simulations of the exact model (3.1) of Section 3.1 is noted.

Finally, considering the evaluation of the $P-$pulse in the absorbing chain governed by equation (3.21), we introduce the results of the map (3.19) into that equation and perform direct numerical integration of the resulting equation:

$$\xi_i'' = \left[\left(\xi_{i-1} - \xi_i \right)_+^{3/2} - \left(\xi_i - \xi_{i+1} \right)_+^{3/2} \right] + \frac{1}{2^{5/2}} \left[A_i \tilde{S}(A_i^{1/4}\tau) + A_i \tilde{S}(A_i^{1/4}\tau - 1) - \xi_i \right]_+^{3/2}$$
$$i = 1,...,n$$

(3.24)

Again, following the same idea of driving and driven variables we retain solely the terms of the excited chain (z_i) corresponding to the driving variable. It is worthwhile noting that unlike equation (3.22), equation (3.24) cannot be reduced to a single degree-of-freedom system (i.e. a forced nonlinear oscillator). Therefore, the primary response of (3.24) cannot be expressed in reduced form, so we cannot express ξ_i in terms of the solution of a single, forced oscillator scaled with respect to its corresponding amplitude of oscillation A_i (which is derived from the nonlinear
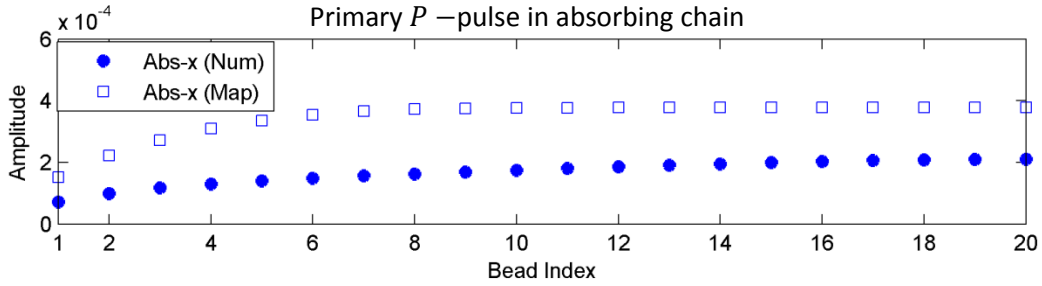
Figure 3.9. Primary $P-$pulse propagation in the absorbing chain, maximum amplitudes of re-scaled relative $x-$displacements between leading beads for normalized impulse intensity $\bar{V}_0 = 1 \times 10^{-4}$: Asymptotic predictions based on the reduced system (3.21) ($\square$), compared to exact solutions based on the re-scaled equations (3.1) ($\bullet$).

map (3.19)). Thus, equation (3.24) can only be solved numerically. Results of the numerical simulations are shown in Figure 3.9. We note that there is discrepancy between the analytical predictions and the direct numerical simulations, which can be attributed to the approximations involved in the derivation of the reduced order model, especially the elimination of the cross-coupling terms between the driven variables. The build-up of the $P-$pulse in the absorbing chain, however, is fully captured by the analytical model, although it overestimates its amplitude.

3.3 Experimental study

In Section 3.1 we computationally presented strong energy exchange between two coupled chains. Then, we developed a semi-analytical method for studying the primary pulse transmission in such a nonlinearly coupled system of granular chains subjected to impulsive excitation in Section 3.2. To test the previous theoretical and analytical results we designed an experimental fixture to study the impulsive response of a two-dimensional, uncompressed granular network such as the one depicted in Figure 3.1. The impulsive excitation was provided by means of a pendulum with a similar bead at its end, which excited the first bead at one end of the excited chain. Moreover, in

76

similarity to the theoretical analysis, in the experimental tests we only focused on primary pulse transmission, that is, on the early-time evolution of propagating pulses in the axial directions of the two coupled chains of the granular network, and not on secondary pulses developing the wake of the primary pulses or formed after the reflections of the primary pulses from the boundaries.

3.3.1 Experimental setup

In similarity to the theoretical study, we considered a number of identical beads composed of type 302 stainless steel (McMaster Carr®, 9291K31) for the excited and absorbing chains, as depicted in Figure 3.10. Each bead had a radius of $R = 9.5\ mm$, modulus of elasticity $E = 193\ GPa$, density $\rho = 8,000\ Kg/m^3$, and Poisson's ratio $\nu = 0.3$. The lateral boundaries were also composed of stainless steel in order to conform to the previous theoretical models. The transduction mechanism consisted of a piezoelectric force transducer (PCB® model 208C02 with sensitivity 11,241 mV/kN) at the left boundary of the excited chain to measure the transmitted force at that location, and two non-contacting laser vibrometers (Polytec® models PSV-300-U and PSV-400) to measure the initial input velocity provided to the system by the pendulum, and the velocity of the last bead of the free left end of the absorbing chain, respectively. The force transducer was firmly mounted on a pedestal and rigidly fixed onto the base (cf. Figure 3.10).

Comparing the experimental granular network of Figure 3.10 with the theoretical network of Figure 3.1 we highlight the difference that in the experimental network the number of beads of the excited chain exceeded the number of beads of the absorbing chain by one. This slightly modified configuration allowed enough space to place the excitation mechanism (the pendulum) to impact the first bead of the excited chain without contacting the absorbing chain, and reduced

77

friction effects due to possible bead misalignments in the experiment. As in the theoretical model of the network of Figure 3.1 the fixed boundary condition in the experiment was posed at the end
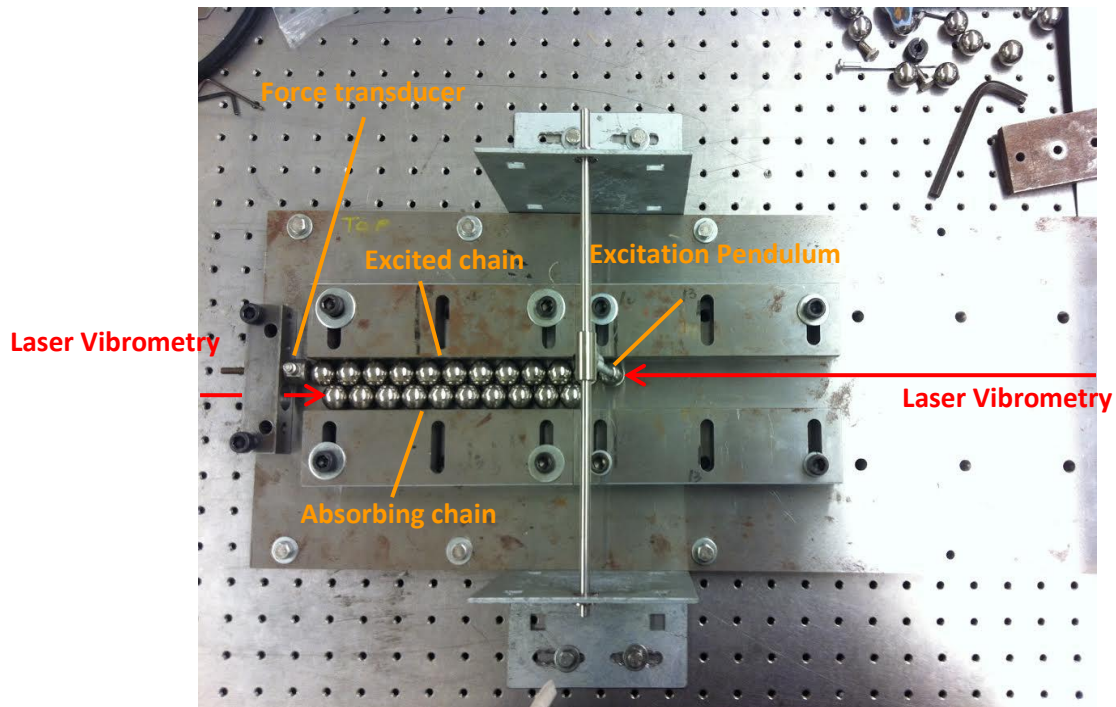

Figure 3.10. Top view of experimental fixture for testing the impulsively excited granular network.

of the excited chain, so the end of the absorbing chain was traction-free. As discussed below, the traction-free boundary condition at the end of the absorbing chain introduced end-effects in the response of its bead, which needed to be taken into account in our study of primary pulse equi-partition in the network.

A series of experimental tests was performed with varying numbers of beads in each of the network configurations that was tested. In the tests we used a combination of 4-3, 7-6, 10-9 and 13-12 numbers of beads in the excited and absorbing chains, respectively. For example, in the configuration shown in Figure 3.10 there are a total of 13 beads in the excited chain and 12 beads in the absorbing chain. As mentioned previously at the one end of the excited chain a pendulum

was used to provide the initial impulse excitation. We recorded the initial input velocity provided to the excited chain by aiming a laser vibrometer directly at the bead of the pendulum, similar to (Hasan et al., 2013b). To measure the velocity response of the last bead of the absorbing chain, another laser vibrometer was used in synchronization with the first one. In addition, the transmitted force signal measured at the end of the excited chain was fed to a 24-bit m+p International® VibPilot data acquisition system, allowing for direct visualization of the transmitted force. The data was then post-processed using Matlab®. These measurements were used to study the nonlinear dynamics of the granular network and verify the results predicted by the theoretical models of the previous Sections 3.1 and 3.2. As shown below energy transfer from the excited to the absorbing chain intensifies with increasing number of beads. Moreover, the realization of strong energy exchange between the two coupled granular chains and the verification of the theoretically predicted eventual pulse equi-partition in the two chains can be inferred by measuring the transmitted force at the end of the excited chain and the velocity of the last bead of the absorbing chain; this will be performed by computing the velocity of the end bead of the excited chain in terms of the measured transmitted force, and comparing it to the directly measured velocity of the last bead of the absorbing chain.

A last note concerning the experimental setup has to do with the dissipative effects in the dynamics, which are always present in any practical fixtures. Although an attempt was made to minimize the frictional contacts in the experimental fixture, complete elimination of friction and other sources of damping in the experiments could not be accomplished. In fact, friction forces are expected due to relative rotations between adjacent beads or between beads and side boundaries; moreover, inherent internal structural damping in the material of the beads is anticipated as an additional source of damping in the experimental system. Given that in the previous theoretical

models we did not take into account such dissipative effects, we anticipate discrepancies when comparing the predictions of the theoretical models to experimental measurements. To address this issue, linear viscous damping terms proportional to the relative velocities between adjacent beads and between beads and the rigid boundaries were introduced in the theoretical models used for comparisons with direct experimental measurements. The determination of the viscous damping parameter was performed by reconciling the theoretical and experimental results for an impulsively excited, isolated homogeneous granular chain composed of 7 beads. Such viscous damping models have been proven to provide a good approximation to the dissipative effects in the granular dynamics (Rosas et al., 2007; Herbold and Nesterenko, 2007; Potekin et al., 2013; Hasan et al., 2013b).

3.3.2 Experimental results and comparisons with numerical simulation

As discussed previously, we have carried out five different sets of experiments for granular networks composed of different number of beads. To test the repeatability of the experimental results, at least 5 trials were performed for each of the considered experimental configurations. In all cases impulsive excitation was applied to the first bead of the excited chain by means of a pendulum with a bead attached to its end. The applied initial impulse (and, approximately, the initial velocity of the first bead of the excited chain) was measured by a laser vibrometer; this measurement is important in order to accurately reproduce theoretically the experimental tests and obtain the corresponding comparisons. A typical measurement of the velocity of the bead of the pendulum is depicted in Figure 3.11, from which we deduce approximately the initial velocity of the first bead of the excited chain. In the experimental tests the measured initial velocities were in the range $115 - 134 \, mm/s$.
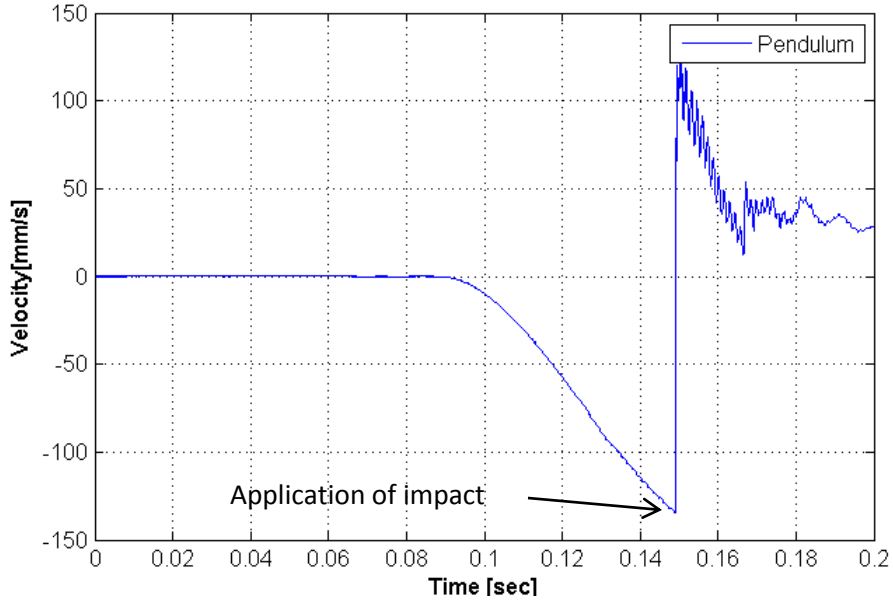
Figure 3.11. Typical laser vibrometer measurement of the velocity of the pendulum used to apply the impulsive excitation.

After application of the initial impulse to the first bead of the excited chain, mixed primary $P-$pulses and $S-$waves propagate in the coupled chains as described in Sections 3.1 and 3.2. Clearly, the transduction mechanism employed in this series of experiments is incapable of directly measuring these mixed primary wave phenomena that evolve in the early-time dynamics of the granular network; rather, only the force transmitted by the end bead of the excited chain and the velocity of the end bead of the absorbing chain can be recorded and these are the only measurements that can be used for comparisons with theoretical predictions. We emphasize at this point, that similar to the theoretical study carried out in Sections 3.1 and 3.2, we are only interested in measuring primary pulse transmission in the experimental network, i.e., the early-time dynamics of the system, with our principal aim being to verify experimentally the theoretically predicted primary pulse equi-partition between the two chains when the number of beads of each chain increases. In order to achieve this it is necessary to estimate the velocity pulse arriving at the end

81

of the excited chain and compare it to the directly measured velocity pulse arriving at the end of the absorbing chain.

This is performed by considering that the transmitted force recorded by the force transducer at the end of the excited chain is given by, $F_n = \sqrt{2}(z_n)_+^{3/2}$, where z_n is the displacement between the end bead of the excited chain with respect to the (fixed) force transducer. From this expression the velocity of the last bead of the excited chain may be computed as, $\dot{z}_{n_+} = \frac{d}{dt}\left[\left(\frac{F_n}{\sqrt{2}}\right)^{2/3}\right]$. Note that since the force transducer is only capable of recording compressive forces, the estimated velocity profiles are "chopped" after the time instant when the recorded force is zero, i.e., at the time instant when the end bead separates from the force transducer. This experimental velocity estimate, when compared to the directly measured velocity of the last bead of the absorbing chain, will be used to study pulse equi-partition in the network of Figure 3.10 as discussed below.

In a preliminary experimental test we considered the impulsive response of an isolated homogeneous chain composed of 7 beads; the transmitted force at the end of the chain is shown in Figure 3.12. In this plot the experimental transmitted force (solid line) is reconciled with the theoretical prediction incorporating no viscous damping (light dashed line) and viscous damping (bold dashed line) by selecting the viscous damping coefficient of the theoretical model as $\lambda = 20\ Ns/m$ and corresponding normalized damping coefficient $\bar{\lambda} = 0.0038$. These damping values are used throughout in this section for the simulations used for comparing theoretical and experimental results. A total of 7 trial tests are superimposed in Figure 3.12, from which the repeatability of the experiment is deduced. For consistency this viscous damping parameter was kept fixed in all numerical simulations presented below, and the comparisons of the theoretical

predictions derived by the models and the experimental messurements validate this damping estimation.
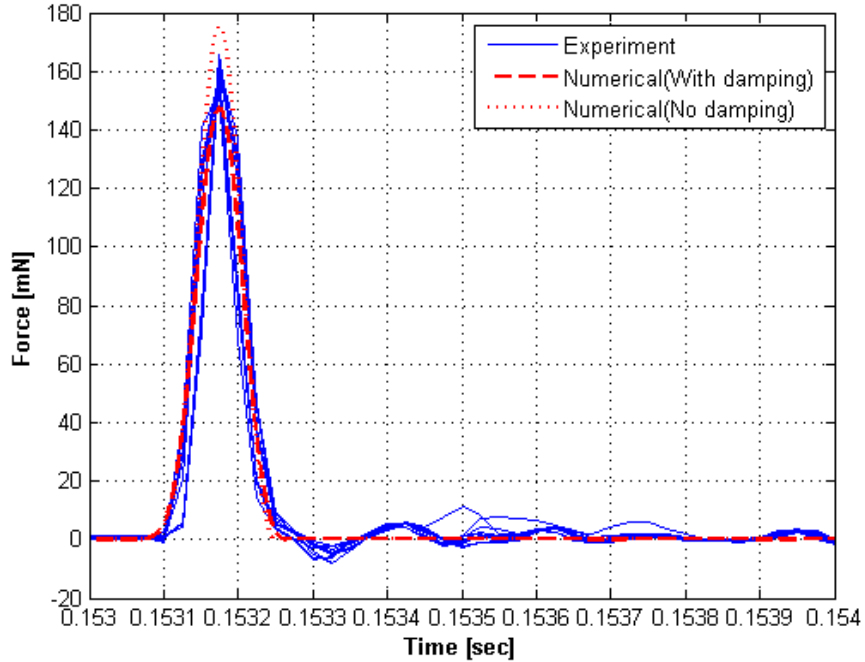

Figure 3.12. Experimental (solid line) and numerical (dashed line for the damped system, dotted line for the undamped system) transmitted force at the end of an isolated homogeneous granular chain of 7 beads in order to estimate the viscous damping coefficient in the model.

In Figure 3.13 we compare the experimental measurements and numerical predictions for the granular network with 4 beads in the excited chain and 3 beads in the absorbing chain. The numerical results were obtained by numerically integrating the theoretical model (3.1) of Section 3.1 modified for the different configuration of the experimental fixture (i.e., the fixed boundary condition at the end of the excited chain and the fact that the number of beads of the excited chain exceeds that of the absorbing chain by one), and the viscous dissipative effects as discussed previously. For this specific configuration we performed 12 experimental trials and noticed good repeatability of the experimental results. In addition, satisfactory agreement between the experimental measurements and the theoretical predictions is inferred.
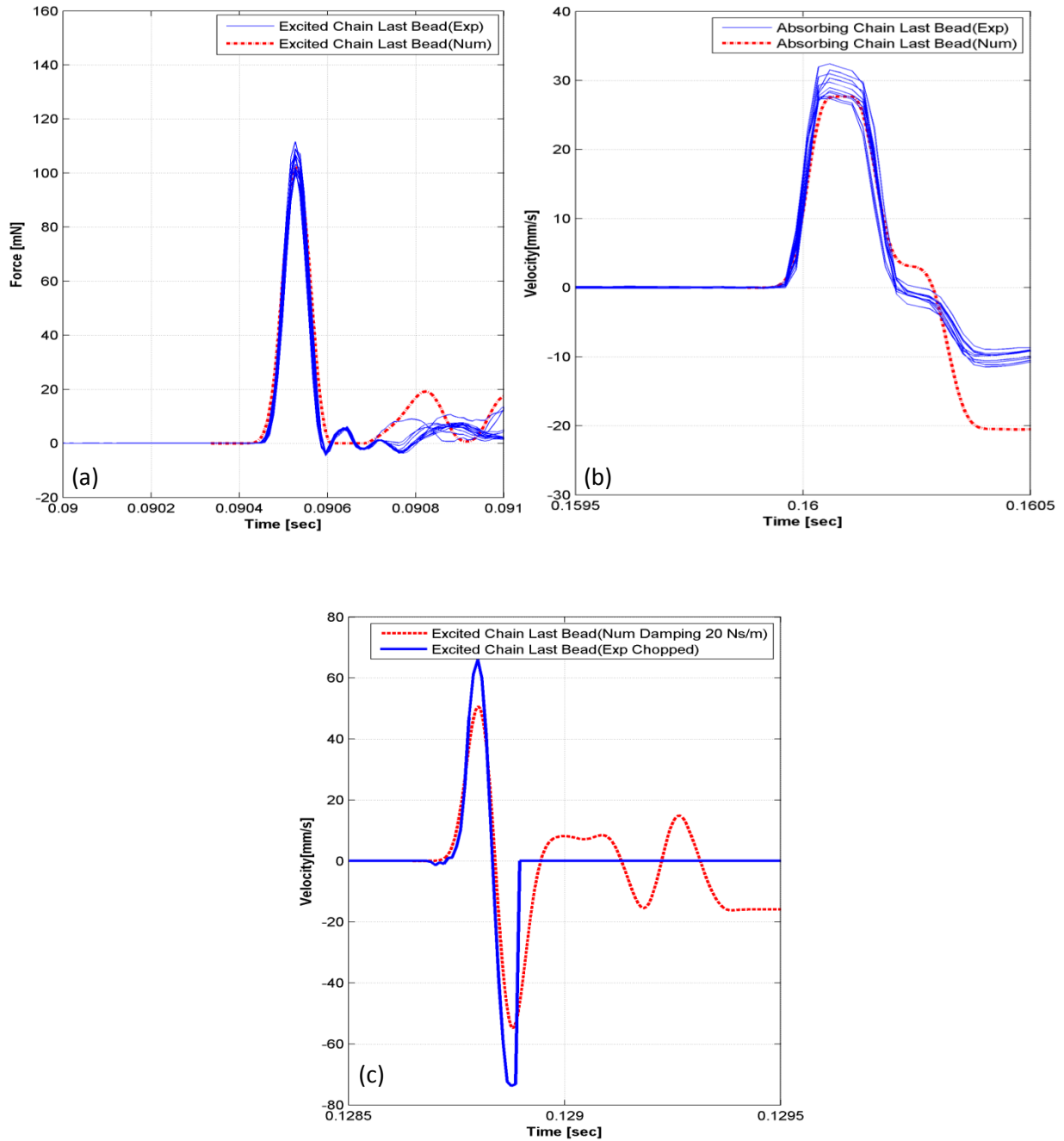
Figure 3.13. Comparisons between experimental measurements (solid lines) and numerical results (dashed lines) for the granular network with 4 beads in the excited chain and 3 beads in the absorbing chain: (a) Transmitted force at the end of the excited chain, (b) velocity of the last bead of the absorbing chain, and (c) velocity of the last bead of the excited chain derived from the force measurement in (a) as explained in the text.

Figure 3.14. Comparisons between experimental measurements (solid lines) and numerical results (dashed lines) for the granular network with 7 beads in the excited chain and 6 beads in the absorbing chain: (a) Transmitted force at the end of the excited chain, (b) velocity of the last bead of the absorbing chain, and (c) velocity of the last bead of the excited chain derived from the force measurement in (a) as explained in the text.
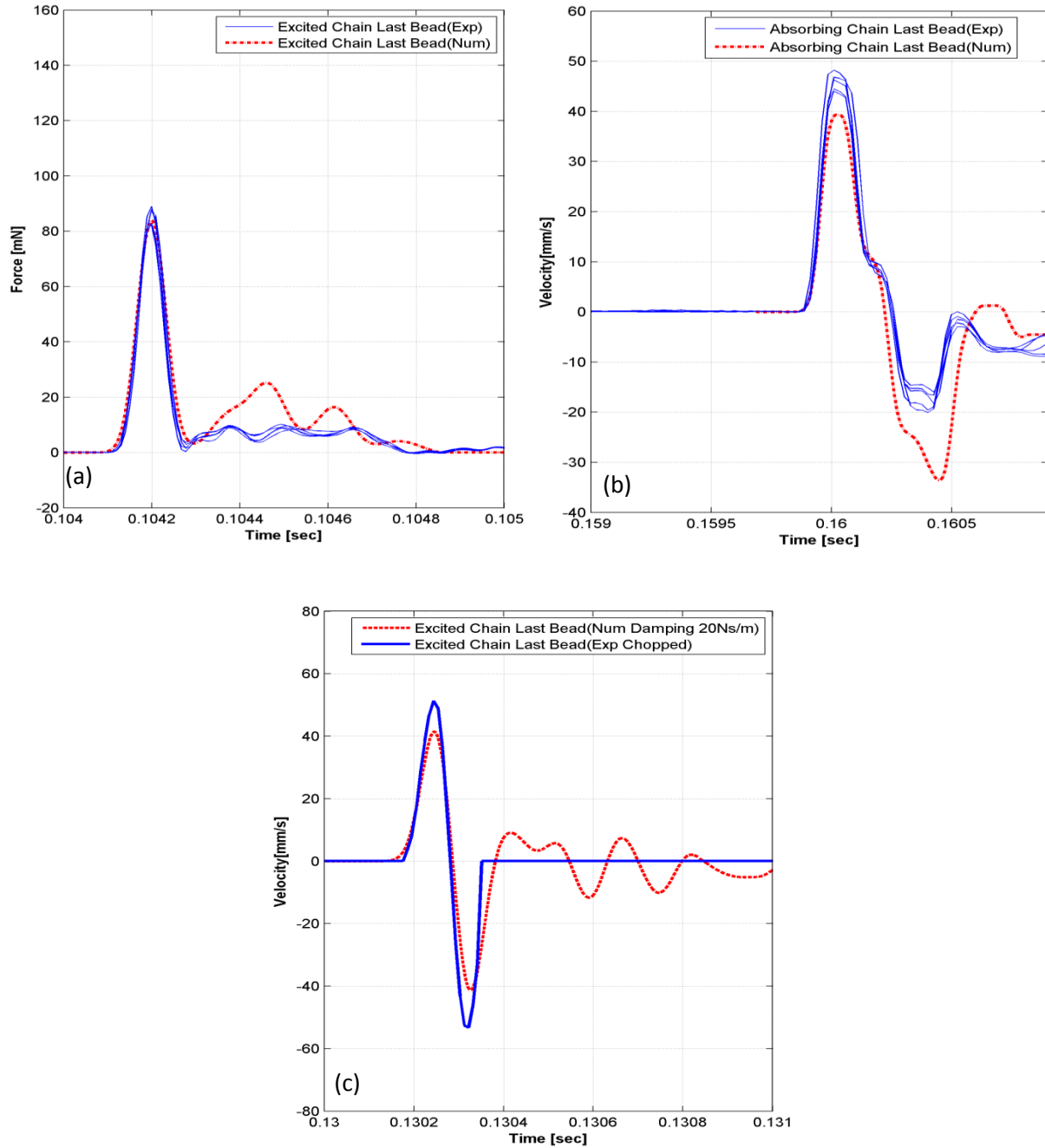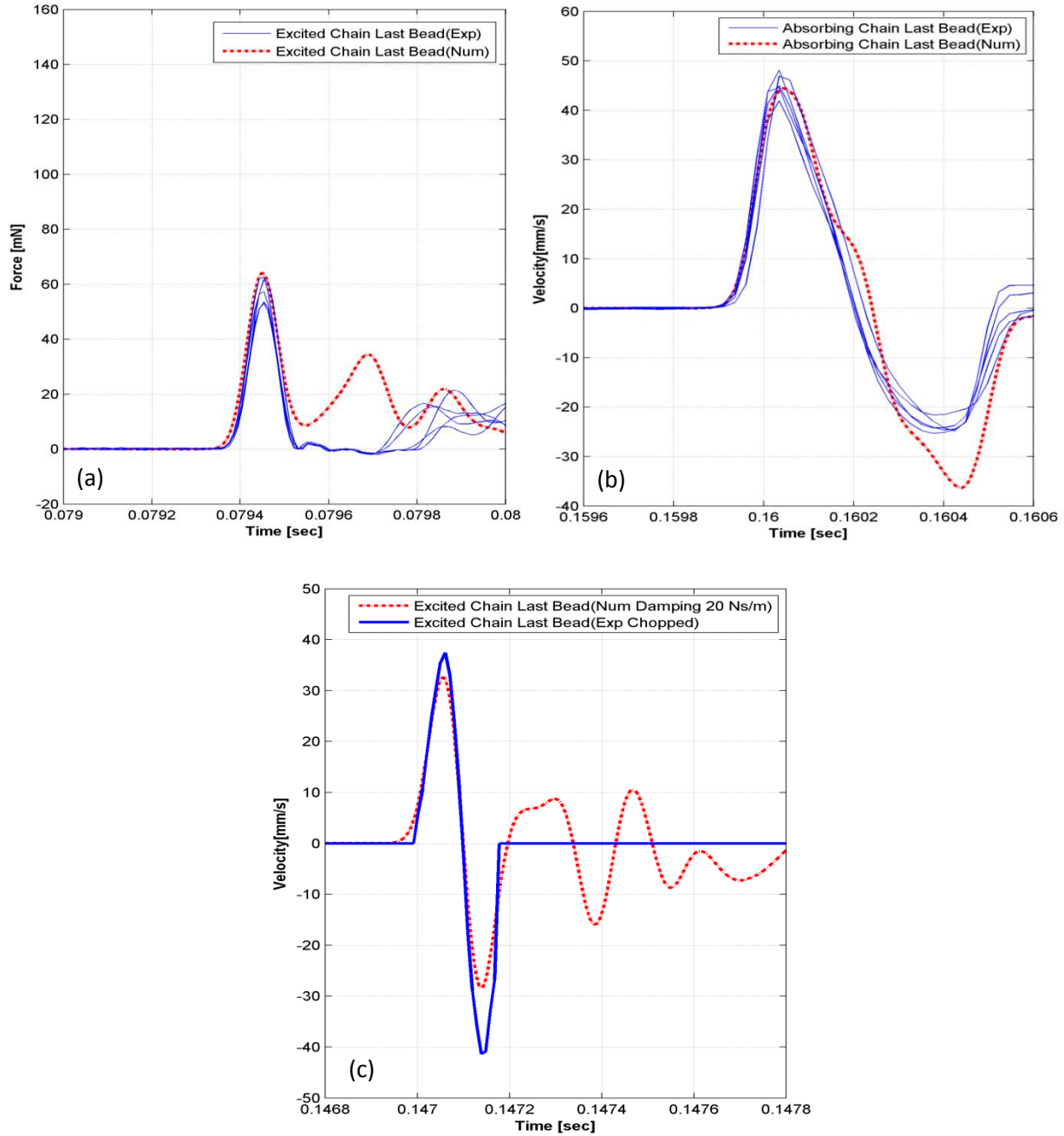
Figure 3.15. Comparisons between experimental measurements (solid lines) and numerical results (dashed lines) for the granular network with 10 beads in the excited chain and 9 beads in the absorbing chain: (a) Transmitted force at the end of the excited chain, (b) velocity of the last bead of the absorbing chain, and (c) velocity of the last bead of the excited chain derived from the force measurement in (a) as explained in the text.

Figure 3.16. Comparisons between experimental measurements (solid lines) and numerical results (dashed lines) for the granular network with 13 beads in the excited chain and 12 beads in the absorbing chain: (a) Transmitted force at the end of the excited chain, (b) velocity of the last bead of the absorbing chain, and (c) velocity of the last bead of the excited chain derived from the force measurement in (a) as explained in the text.
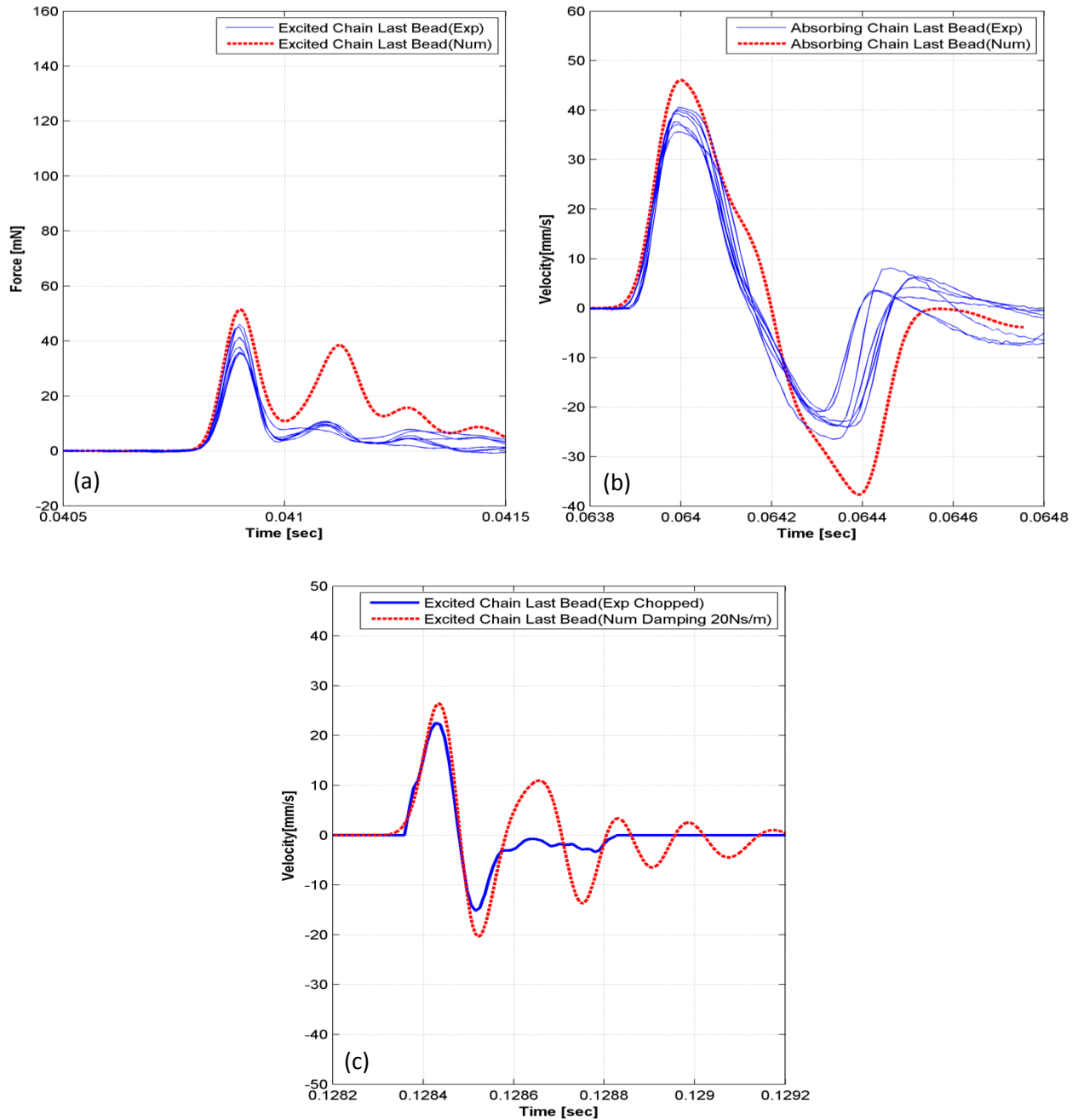
Similarly, we compared the experimental and numerical results for the other three network configurations with varying number of beads in the excited and absorbing chains, and the results are depicted in Figures 3.14-3.16. In all cases the theoretical predictions of the dissipative model (3.1) are in satisfactory agreement with experimental measurements, which validates the computational and analytical results presented in Sections 3.1 and 3.2. All numerical simulations follow the same trends with the experimental results. The deviations between theory and experiment may be attributed to the approximation of viscous damping in the theoretical model which is incapable of fully modeling nonlinear dissipative effects such as friction and plasticity; and also to inherent bead misalignments in the experimental networks that can have an effect on the experimental results. Even more important, perhaps, is that these results enable the experimental study of primary pulse equi-partition in the two chains with increasing number of beads in the network, in accordance with the numerical and analytical predictions.

To this end, for each of the tested configurations we compared the velocity time series of the end beads of the excited and absorbing chains. As discussed previously, the velocity time series of the end bead of the excited chain can be estimated only indirectly based on the measurement of the corresponding transmitted force. However, given the satisfactory agreement of this estimate with the prediction of the theoretical model, it is expected that it will provide a reliable tool for studying experimental pulse equi-partition in the granular network. From the experimental results depicted in Figures 3.13a-3.16a, we can clearly observe that as the number of beads in the granular network increases, the transmitted force at the end bead of the excited chain decreases. Simultaneously, from the plots of Figures 3.13b-3.16b we deduce that the velocity of the end bead of the absorbing chain increases. These results are due to energy transfers between the two chains due to geometrical coupling, giving rise to mixed $P-$pulses and $S-$waves near the application of

the impulsive excitation, and eventual pulse equi-partition as the number of beads increases. Indeed, for the granular networks with the largest number of beads (cf. Figures 3.15 and 3.16) the velocity of the end bead of the absorbing chain exceeds in amplitude the corresponding velocity of the end bead of the excited chain, which is a clear indication that pulse (and energy) equi-partition is taking place. Once pulse equi-partition occurs in the two chains, the effect of coupling diminishes and pulses in each chain propagate independently from each other; from that point on, the velocity of the end bead of the absorbing chain does not vary much for further increase of the number of beads (compare the results of Figures 3.15 and 3.16).

3.3.3 Experimental verification of pulse equi-partition

At this point a special remark needs to be made concerning the end effects of the free boundary condition of the absorbing chain on the experimental measurements. From the theoretical results of the previous sections (e.g., see Figure 3.2a) it has been observed that pulse equi-partition in the two chains occurs when the two P −pulses (i.e., the x −solitary pulses) reach the 13th beads of the excited and absorbing chains. Since in the experimental network the end boundary condition of the absorbing chain is traction-free (in contrast to the fixed boundary condition in the theoretical model of Figure 3.1) we anticipate that end boundary effects will affect the P −pulses arriving at the ends of both chains. This is confirmed from the numerical simulations depicted in Figure 3.17 where the P −pulses at the ends of two granular networks with and without end effects are presented. In particular, we deduce that the peak value of the velocity pulse arriving at the end of the absorbing chain with end effects is significantly amplified due to the fact that the reflection of the primary pulse in that chain occurs in a traction-free boundary. However, the corresponding effect in the excited chain is almost negligible since pulse reflection in that chain occurs in a fixed boundary.
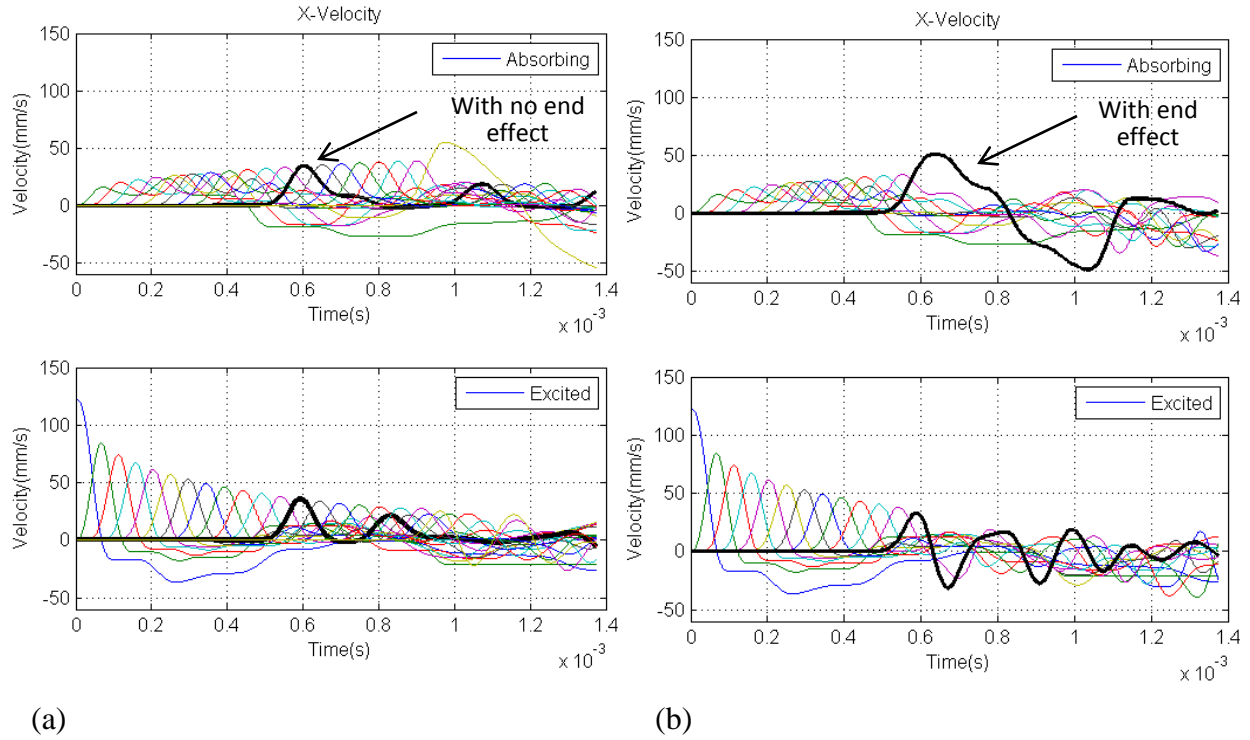
89

Figure 3.17. Numerical simulation of the velocity pulses in the $x-$direction of granular networks with, (a) 20 beads in the excited chain and 19 beads in the absorbing chain, (b) 13 beads in the excited chain and 12 beads in the absorbing chain, showing the end effects of the fixed boundary.

It follows that in order to perform the experimental pulse equi-partition study we need to compensate for the end effects in the velocity measurement of the absorbing chain by adjusting (reducing) accordingly the maximum amplitude of the measured velocity pulse. This task was accomplished by utilizing the computational responses of the experimentally validated theoretical model (3.1) to estimate the numerical difference of the velocity peak values with and without end effects in each tested network configuration, and, then, apply this difference to eliminate in each case the end effects from the experimental velocity measurement of the end bead of the absorbing chain. In Figure 3.18 we present plots of the maxima of the velocity primary pulses at the end beads of the excited and absorbing chains for the four network configurations that were tested (the horizontal axes in these plots indicate the number of beads of the excited chain in each tested
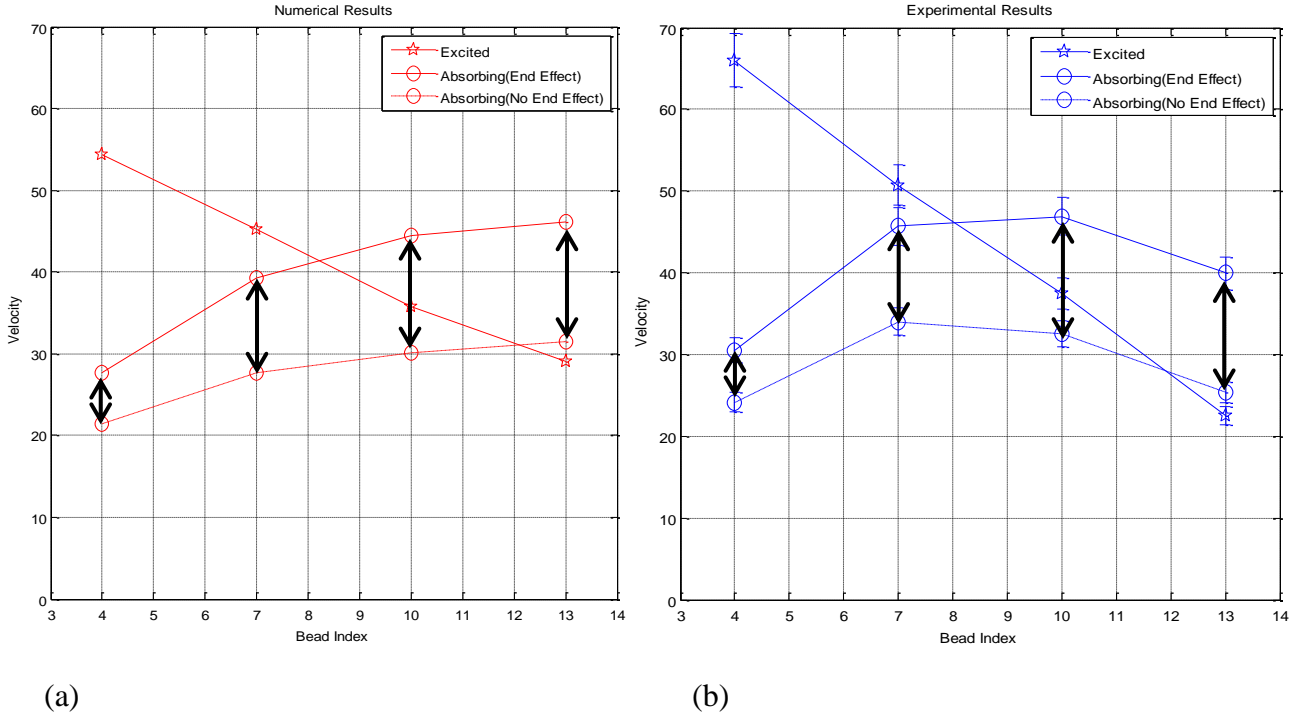
90

Figure 3.18. Peak velocities of the end beads of the excited and absorbing chains with (——) and without (-------) end effects in the four tested network configurations: (a) Computational results, (b) experimental results; note pulse equi-partion in the network with largest number of beads.

configuration). For comparison purposes, the maxima of the velocity pulses at the end beads of the absorbing chains are depicted with and without end effects, by applying the compensation scheme outlined previously. The strong energy exchanges and the primary pulse equi-partition in the network with increasing number of beads can be clearly deduced from these experimental results. It is clear that, when compensating for the end effects, primary pulse equi-partition occurs in the network with 13 beads in the excited chain, precisely as predicted by the theoretical model (3.1) (albeit of slightly different configuration) and shown in the computational results of Figure 3.2. Hence, our experimental results validate the theoretical prediction that geometrical nonlinear coupling between the chains of the two-dimensional network leads to primary pulse equi-partition in the excited and absorbing chain. Indirectly, this result validates the computational and analytical

results of Sections 3.1 and 3.2, and confirms the complicated nonlinear dynamics realized in this system.

3.4 Conclusions

In this work we studied the primary pulse transmission in a nonlinearly coupled system of granular chains under impulsive excitation. We showed that strong energy scattering occurs close to the application of the impulsive excitation, and in the early-time dynamics. This scattering is manifested through the excitation of a mixed type of nonlinear waves, consisting of oscillatory nonlinear shear waves ($S-$waves) in the transverse direction, coupled to near-zero frequency pulses ($P-$pulses) propagating in the axial direction. These mixed nonlinear waves can be regarded as perturbations due to geometric nonlinear coupling in the network of the Nesterenko solitary waves that propagate in the axial directions of the isolated (uncoupled) homogeneous chains. Our analysis extends the earlier developed, mapping technique developed for the one-dimensional granular crystals and scalar models by Starosvetsky and co-workers to two-dimensional granular networks; in the process, this analysis clarifies the strongly nonlinear mechanism that governs the formation of the mixed primary pulses in the longitudinal and transverse directions, as well as the transient energy transfers from the excited to the absorbing chain of the network. Hence, our work explores a new way of scattering of propagating solitary pulses in ordered granular media through the excitation of near-field transversal (shear) waves, and carries promising potential for future applications of multi-dimensional ordered granular materials as efficient shock and vibration mitigators.

In addition, we experimentally confirmed the theoretically predicted pulse equi-partition in granular networks with sufficiently large number of beads by testing four configurations

consisting of geometrically coupled, two-dimensional granular chains with varying number of beads. Due to pulse equi-partition, a localized excitation initially applied to the excited chain eventually "spreads" evenly to both coupled chains. In that context, the experimental study presented herein validates the computational and analytical results. Moreover, based on the experimental study we verified the accuracy of the theoretical model for primary pulse propagation in the network, and its capacity to predict the location where pulse (and energy) equi-partition in the two coupled chains occurs.

3.5 References

Ahnert, K., Pikovsky, A., "Compactons and Chaos in Strongly Nonlinear Lattices." *Phys. Rev. E.* **79**(2), 026209, 2009.

Ben-Meir, Y., Starosvetsky, Y., "Modulation of Solitary Waves and Formation of Stable Attractors in Granular Scalar Models Subjected to On-site Perturbation," *Wave Motion*, http://dx.doi.org/10.1016/j.wavwmoti.2013.12.004, 2013.

Chatterjee, A., "Asymptotic Solution for Solitary Waves in a Chain of Elastic Spheres," *Phys. Rev. E.*, **59**(5), 5912-5919, 1999.

Coste, C., Falcon, E., Fauve, S., "Solitary Waves in a Chain of Beads under Hertz Contact," *Phys. Rev. E*, **56**(5), 6104–6117, 1997.

Daraio, C., Nesterenko, V., Herbold, B., Jin, S., "Strongly Nonlinear Waves in a Chain of Teflon Beads," *Phys. Rev. E*, **72**(1), 016603, 2005.

Daraio, C., Nesterenko, V., Herbold, B., Jin, S., "Tunability of Solitary Wave Properties in One-dimensional Strongly Nonlinear Phononic Crystals," *Phys. Rev. E*, **73**(2), 026610, 2006a.

Daraio, C., Nesterenko, V., Herbold, B., Jin, S., "Energy Trapping and Shock Disintegration in a Composite Granular Medium," *Phys. Rev. Lett*., **96**(5), 058002, 2006b.

Doney, R., Sen, S., "Decorated, Tapered, and Highly Nonlinear Granular Chain," *Phys. Rev. Lett*., **97**(15), 155502, 2006.

Fraternali, F., Porter, M., Daraio, C., "Optimal Design of Composite Granular Protectors," *Mech. Adv. Mat. Str*., **17**(1), 1-19, 2009.

Hasan, M., Starosvetsky, Y., Vakakis, A., Manevitch, L., "Nonlinear Targeted Energy Transfer and Macroscopic Analog of the Quantum Landau–Zener Effect in Coupled Granular Chains," *Physica D*, **252**, 46–58, 2013a.

Hasan, M., Cho, S., Remick, K., Vakakis, A., McFarland, D., Kriven, W., "Primary Pulse Transmission in Coupled Steel Granular Chains Embedded in PDMS Matrix: Experiment and Modeling," *Int. J. Solids Struct*., **50**(20–21), 3207–3224, 2013b.

Herbold, E., Nesterenko, V., "Shock Wave Structure in a Strongly Nonlinear Lattice with Viscous Dissipation," *Phys. Rev. E,* **75**(2), 021304, 2007.

James, G., "Nonlinear Waves in Newton's Cradle and the Discrete p-Schrödinger Equation", *Math. Models Meth. Appl. Sci.*, **21**, 2335-2377, 2011.

James, G., Kevrekidis, P., Cuevas, J., "Breathers in Oscillator Chains with Hertzian Interactions," *Physica D*, **251**, 39–59, 2013.

Jayaprakash, K., Starosvetsky, Y., Vakakis, A., Peeters, M., Kerschen, G., "Nonlinear Normal Modes and Band Zones in Granular Chains with No Precompression," *Nonl. Dyn*., **63**(3), 359-385, 2011.

Jayaprakash, K., Starosvetsky, Y., Vakakis, A., Gendelman, O., "Nonlinear Resonances Leading to Strong Pulse Attenuation in Granular Dimer Chains," *J. Nonl. Science*, **23**(3), 363-392, 2013.

Job, S., Melo, F., Sokolow, A., Sen, S., "Solitary Wave Trains in Granular Chains: Experiments, Theory and Simulations," *Granular Matter*, **10**(1), 13-20, 2007.

Kopidakis, G., Aubry, S., "Discrete Breathers and Delocalization in Nonlinear Disordered Systems," *Phys. Rev. Lett.*, **84**(15), 3236-3239, 2000.

Lazaridi A., Nesterenko, V., "Observation of a New Type of Solitary Waves in a One-Dimensional Granular Medium," *J. Appl. Mech. Tech. Physics*, **26**(3), 405-408, 1985.

MacKay, R., "Solitary Waves in a Chain of Beads under Hertz Contact," *Phys. Lett. A*, **251**(3), 191-192, 1999.

Nesterenko, V., "Propagation of Nonlinear Compression Pulses in Granular Media," *J. Appl. Mech. Techn. Physics*, **24**(5), 733-743, 1983.

Nesterenko, V., *Dynamics of Heterogeneous Materials*, Springer Verlag, New York, 2001.

Potekin, R., Jayaprakash, K., McFarland, D., Remick, K., Bergman, L., and Vakakis, A., 2013, "Experimental Study of Strongly Nonlinear Resonances and Anti-resonances in Granular Dimer Chains," *Exp. Mech.*, **53**(5), 861–870.

Rosas, A., Romero, A., Nesterenko, V., Lindenberg, K., "Observation of Two-wave Structure in Strongly Nonlinear Dissipative Granular Chains," *Phys. Rev. Lett.*, **98**, 164301, 2007.

Sen, S., Manciu, M., "Solitary Wave Dynamics in Generalized Hertz Chains: An Improved Solution of the Equation of Motion," *Phys. Rev. E*, **64**(5), 056605, 2001.

Sen, S., Hong, J., Bang, J., Avalos, E., Doney, R., "Solitary Waves in the Granular Chain," *Phys. Rep.,* **462** (2), 21–66, 2008.

Starosvetsky, Y., Vakakis, A., "Traveling Waves and Localized Modes in One-Dimensional Homogeneous Granular Chains With no Pre-Compression," *Phys. Rev. E*, **82**(2), 026603, 2010.

Starosvetsky, Y., "Evolution of the Primary Pulse in One-dimensional Granular Crystals Subject to On-site Perturbations: Analytical study," *Phys. Rev. E*, **85**(5), 051306, 2012.

Starosvetsky, Y., Hasan, M., Vakakis, A., Manevitch, L., "Strongly Nonlinear Beat Phenomena and Energy Exchanges in Weakly Coupled Granular Chains on Elastic Foundations," *SIAM J. Appl. Math*., **72**(1), 337–361, 2012.

Starosvetsky, Y., Hasan, M., Vakakis, A., "Nonlinear Pulse Equi-partition in Weakly Coupled Ordered Granular Chains with no Pre-Compression," *J. Comp. Nonl. Dyn*., **8**(3), 034504–034504, 2013.

Szelengowicz, I., Hasan, M., Starosvetsky, Y., Vakakis, A., Daraio, C., "Energy Equipartition in Two-dimensional Granular Systems with Spherical Intruders," *Phys. Rev. E*, **87**(3), 032204, 2013.

Chapter 4. Coupled granular networks under harmonic excitation

In Chapter 3 we confirmed the existence of a mixture of solitary-like pulses and nonlinear shear waves in coupled granular networks under impulsive excitation. Due to strong geometric nonlinear coupling in the system clear energy exchanges between two oscillators leading to eventual energy/pulse equi-partition were noted. The near-zero frequency pulses dominate the energy propagation. However, the studies on coupled granular media considered up to now did not involve any frequency responses. Hence, in this chapter, we consider a system of coupled granular chains on elastic foundations under periodic excitations.

In Section 4.1, we review the well-known acoustic filtering properties of linear systems with spatially periodic structure. The interesting properties of phononic systems can be found in the review by Hussein et al. (2014). Perhaps the simplest model is the infinite lattice of identical particles grounded by means of linear springs and coupled through additional linear stiffnesses; the corresponding dispersion relation contains two attenuation zones (AZs) and one propagation zone (PZ) in the frequency domain (Brillouin, 1953; Mead, 1975; Vakakis et al., 2008). Moreover, the boundaries between the two AZs and the intermediate PZ correspond to in-phase and out-of-phase normal mode oscillations (Mead, 1975). The two AZs are realized at low and high frequency domains, whereas the PZ is located at intermediate frequencies.

In Section 4.2, we study the dynamics of semi-infinite nonlinear lattices on elastic foundations under suddenly applied high-frequency harmonic excitations. Yao et al. (2103) studied the high frequency responses of nonlinear systems by performing slow/fast partitions in the dynamics and showing that phase transitions can occur due to the high frequency forcing. Other works highlight the importance of high-frequency excitations, from blocking the

conduction of neural systems (Bhadra et al., 2007) and applications in magnetic force microscopy (Koblischka et al., 2006), to geophysical (Hunter et al., 2010) and biomedical applications (Ylinen et al., 1995; Levy et al., 2000). The main novel finding of this part is that it proves analytically and confirms numerically that the high rate application of a high-frequency harmonic excitation exciting a spatially periodic medium generates a dynamic overshoot phenomenon in the form of a traveling disturbance that propagates in the far field of the medium, despite the fact that the frequency of the applied harmonic load lies well inside the AZ of this medium, and, hence, no signal propagation to the far field should be expected. Hence, these results demonstrate that in addition to the frequency content of an applied harmonic excitation to an elastic medium, one should take into account the rate of application of the excitation per se in order to establish propagation of disturbances in the far field.

In the last section of this chapter we consider a special class of time-periodic responses with highly localized envelopes realized in spatially periodic media known as discrete traveling breathers (Sievers and Takeno, 1988; Campbell and Peyrard, 1990) in the intermediate PZ of granular media. A traveling breather is defined as a nonlinear oscillatory wavepacket propagating in a nonlinear medium, with its envelope possessing localized characteristics (either in amplitude or in slope). Discrete breathers are breathers realized in nonlinear lattices due to discreteness and nonlinearity (Aubry, 1997; Flach and Willis, 1998; Flach and Gorbach, 2008). It has been shown that discrete standing or propagating breathers can also form in granular networks on elastic foundations (Boechler et al., 2010; Theocharis et al., 2010; James, 2011; James et al., 2013). Starosvetsky et al. (2012) studied the dynamics of two weakly coupled, homogeneous granular chains without pre-compression, each supported by a linear distributed elastic foundation. Three different mechanisms for complete and recurrent energy exchanges between the chains were

detected, through the excitation of nonlinear beat phenomena involving spatially extended traveling waves, standing waves or propagating discrete breathers. In a continuation of that work Hasan et al. (2013) considered the same granular network excited by an impulsive force to the first bead of the excited chain, and studied targeted energy transfer between the two chains, leading to passive, irreversible pulse redirection from the directly excited chain to the chain to which it is weakly coupled. The nonlinear dynamical mechanism governing this interesting phenomenon was found to be a macroscopic analog (in space) of the Landau-Zener quantum tunneling effect (in time) (Zener, 1932; Razavy, 2003). The practical realization of the Landau-Zener effect was achieved by spatial stratification (variation) of the weak coupling between the chains or of the elastic foundation of the directly excited chain. The passive wave redirection was then realized in the form of propagating discrete breathers, which due to the spatial stratification were passively redirected from the directly excited to the indirectly excited granular chain. Hence, the propagation of discrete breathers proved to be the fundamental component of this transient passive redirection. We mention at this point that, in a more general context, nonlinear targeted energy transfer has been studied and applied to a diverse class of problems (Manevitch, 1999; Kopidakis et al., 2001; Maniadis and Aubry, 2005; Kosevich et al., 2007, 2008, 2009; Vakakis et al., 2008). Moreover, in two recent works (Vortnikov and Starosvetsky, 2015a,b) the efficacy of nonlinear energy channeling was demonstrated in two-dimensional nonlinear networks of coupled oscillators of locally resonant unit-cells incorporating internal rotators.

4.1 Aside: High-frequency dynamic overshoot in a linear lattice

The system considered in this section is linear and its configuration is shown in Figure 4.1. It consists of a semi-infinite homogeneous spring-particle lattice mounted on a linear elastic foundation. Here, we denote by $\tilde{k}_0$ and $\tilde{k}_1 = 0.1\tilde{k}_0$ the stiffness coefficients of the linear

coupling element between adjacent discrete masses, and the weak linear elastic foundation, correspondingly, and by m the mass of each particle. In addition, we assume that all particles are constrained to move in the horizontal direction only, and that no dissipative forces exist in the system. The lattice is excited by a suddenly applied harmonic force given by $\tilde{F}(t) = \tilde{F}_0 \sin(2\pi f t) H(t)$, where $\tilde{F}_0$ denotes the amplitude of the force in N, f its frequency in Hz, and $H(t)$ the Heaviside function. Finally, we assume that the system is at rest up to the time instant $t = 0-$ of application of the harmonic force.
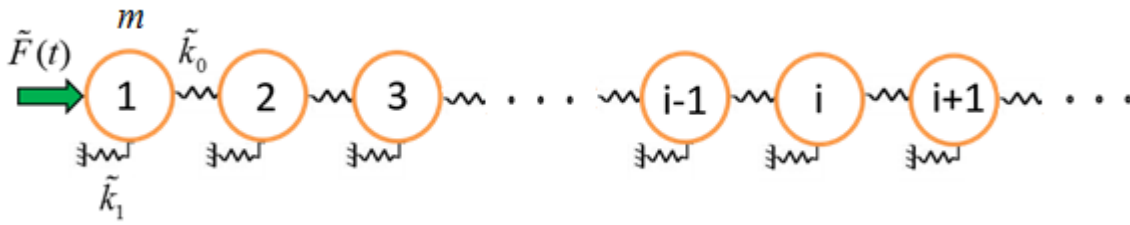

Figure 4.1. The linear spring-particle lattice under suddenly applied harmonic excitation.

According to the previous assumptions, and denoting by η_i the axial displacement from equilibrium of the i −th particle, the equations of motion of this system are given by,

$$
\begin{aligned}
m\frac{d^2\eta_1}{dt^2} &= -\tilde{k}_0(\eta_1 - \eta_2) - \tilde{k}_1\eta_1 + \tilde{F}_0 \sin\left(2\pi f t\right) H(t) \\
m\frac{d^2\eta_i}{dt^2} &= \tilde{k}_0(\eta_{i-1} + \eta_{i+1} - 2\eta_i) - \tilde{k}_1\eta_i , \qquad i = 2, 3, ...
\end{aligned}
\tag{4.1}
$$

with initial conditions $\eta_i(0-) = \dot{\eta}_i(0-) = 0, \ i = 1, 2, ...$. Since this is a linear lattice, its dynamics do not depend on the forcing level, or energy.

The equations of motion (4.1) are dimensional. For our study we consider particles composed of Poly-di-methyl-siloxane (PDMS) with density $\rho = 965 \frac{kg}{m^3}$, modulus of elasticity

$E = 1.5 \times 10^6 \ Pa$, Poisson's ratio $\nu = 0.49$, $R = 4.75 \times 10^{-3} m$; the coupling stiffness is

$\tilde{k}_0 = 4020 \frac{N}{m}$ and the foundation stiffness $\tilde{k}_1 = 402 \frac{N}{m}$. At this point we introduce the

normalizations, $z_i = \frac{\eta_i}{R}, \tau = \omega_0 t, \alpha = \frac{\tilde{k}_1}{\tilde{k}_0}, F_0 = \frac{\tilde{F}_0}{\tilde{k}_0 R}$ and $\omega = \frac{2\pi f}{\omega_0}$, where the characteristic

frequency is $\omega_0 = \left[\frac{\tilde{k}_0}{m}\right]^{1/2} \approx 3046 \ rad/s$ and the stiffness ratio is $\alpha = 0.1$. Then, the equations

of motion (4.1) can be expressed in the following normalized form,

$$
\begin{aligned}
\frac{d^2 z_1}{d\tau^2} &= -\left(1+\alpha\right) z_1 + z_2 + F_0 \sin \omega\tau \ H(\tau) \\
\frac{d^2 z_i}{d\tau^2} &= (z_{i-1} + z_{i+1}) - \left(2+\alpha\right) z_i \ , \qquad i = 2,3,\ldots
\end{aligned}
\tag{4.2}
$$

with normalized initial conditions $z_i(0) = z_i'(0) = 0, \ i = 1, 2, 3,\ldots$, where z_i denotes the

normalized axial displacements of the $i - th$ particle, the new nondimensional time variable τ is

introduced, and prime denotes differentiation with respect to this new temporal variable. Note

that in these equations the only system parameter is the stiffness ratio α , in addition to the forcing

parameters, i.e., the forcing amplitude F_0 and frequency $\omega = 2\pi f$.

4.1.1 Computational study and results

The frequency bands of periodic linear systems have been well studied. Herein, we review the

frequency acoustic bands of the linear lattice, cf. equation (4.2). Indeed, it is well known that for

$0 \le \omega \le \sqrt{\alpha}$ or $\omega > \sqrt{4+\alpha}$ the lattice supports only near field responses in the form of standing

waves with exponentially decaying envelops, defining the lower AZ and the upper AZ,

respectively. In the lower AZ adjacent particles execute in-phase motions, whereas in the upper

AZ out-of-phase. In the intermediate frequency $\sqrt{\alpha} < \omega < \sqrt{4+\alpha}$ the lattice supports traveling

101

waves that propagate unattenuated to the far field, corresponding to the PZ. The two bounding

frequencies separating the two AZs and the single PZ correspond to the in-phase normal vibration

mode, $\omega_{ip} = \sqrt{\alpha}$, and the out-of-phase mode $\omega_{op} = \sqrt{4+\alpha}$ of the lattice. Clearly, these three

different acoustic states affect the forced response of the lattice. In Figure 4.2 we study the forced

transient response of system (4.1) for three different excitation frequencies, namely at

$f = 100\ Hz$ (in the lower AZ), $f = 600\ Hz$ (in the PZ) and $f = 3,000\ Hz$ (well inside the upper

AZ), and at fixed normalized forcing amplitude $F_0 = 0.1$ (corresponding to the dimensional value

$\tilde{F}_0 = 1.9095\ N$). To this end, we depict the velocity time series of the seven leading particles of

the lattices (offset in the plots for clarity), as well as the spatio-temporal evolution of the

instantaneous kinetic energy of the 40 leading particles of the lattice. As expected, the responses

for frequencies in the lower AZ and the PZ are attenuating (cf. Figure 4.2a), and propagating (cf.

Figure 4.2b). Similar acoustic zones have been studied in nonlinear periodic systems (Vakakis

and King, 1995, 1997; Boechler and Daraio, 2009; Jayaprakash et al., 2011a), having strong

energy dependencies. The structure of the AZs and PZs strongly affect the transmission of

disturbances in the far fields of periodic media, since frequency components in AZs are blocked

from transmission, whereas components in PZs propagate through these media unattenuated. In

turn, these acoustic filtering properties drastically affect the forced responses of these media

under harmonic excitations, since only frequencies in PZs can lead to spatially extended forced

responses, whereas frequencies in AZs lead to near-field motions that are spatially localized close
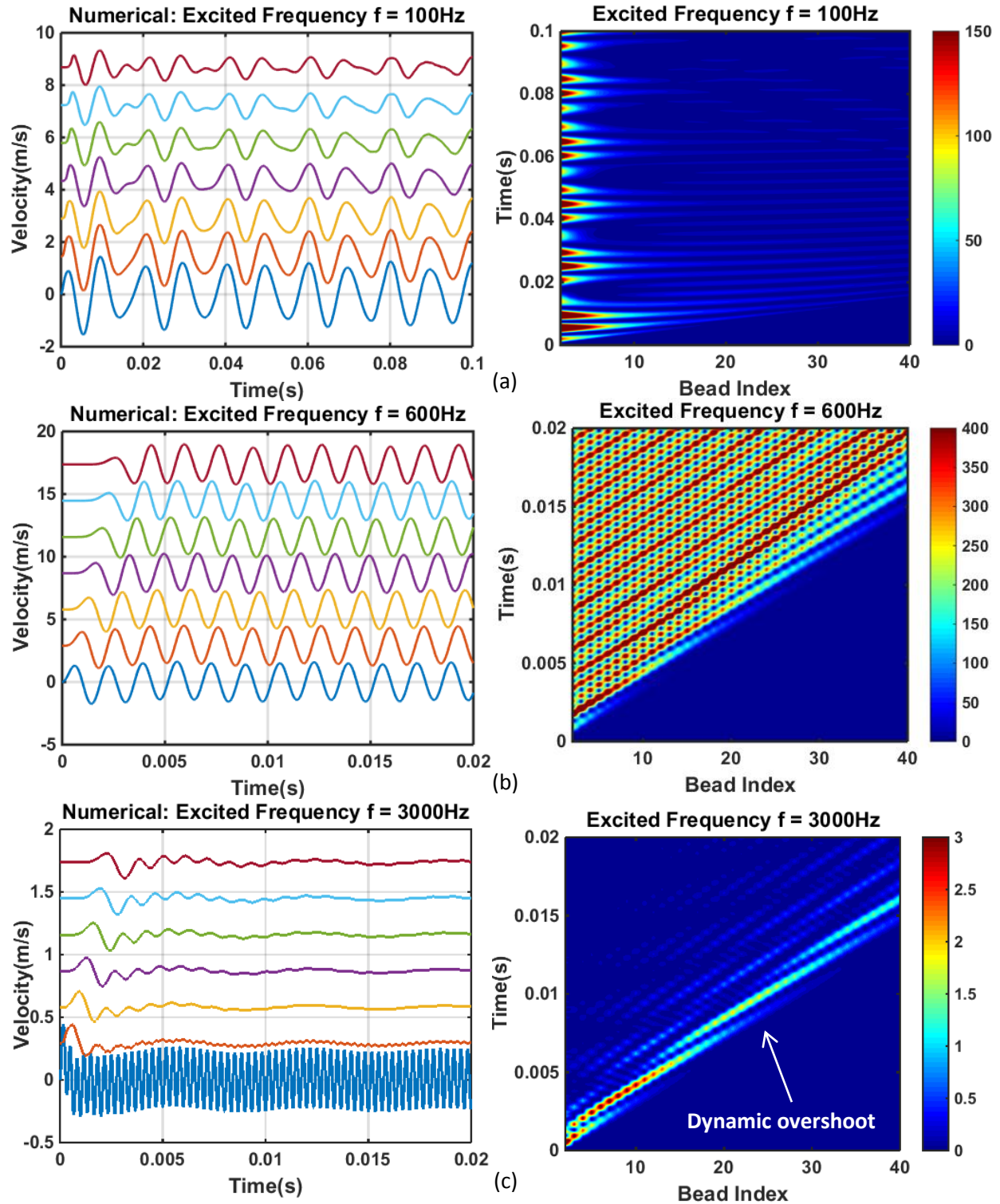
to the excitation source.

Figure 4.2. Forced transient response of system (4.1) for excitation frequency, (a) in the lower AZ, (b) the PZ, and (c) the upper AZ of the lattice; in each case the velocity time series of the seven leading particles (offset in the plot for clarity), and the spatio-temporal evolution of the instantaneous kinetic energy of the 40 leading particles are shown.

However, a rather counter-intuitive finding is depicted in Figure 4.2c. Although there occurs strong motion confinement in the first particle (as seen by its large-amplitude and high-frequency oscillation compared to the responses of the other particles of the lattice), there is still a low-frequency transient disturbance that is seen to propagate in the far field of the lattice. One would not expect such a propagating disturbance for a forcing frequency well inside the upper AZ, and this low-frequency response is precisely what we denote as "dynamic overshoot" in the lattice. In fact, this traveling disturbance resembles the response of the lattice under an impulsive excitation, rather than the high-frequency harmonic load applied in Figure 4.2c. As shown below this dynamic overshoot is the result of the high-rate of application of the high-frequency harmonic excitation at $t = 0$, and can be predicted by asymptotic analysis.

4.1.2 Asymptotic study of dynamic overshoot

We return to the normalized equations of motion (4.2), and consider the limit of high frequency of the suddenly applied harmonic excitation. The responses of the semi-infinite linear lattice can be analyzed asymptotically in terms of the corresponding Green's functions of a forced semi-infinite linear lattice derived in (Wang and Lee., 1973). To this end, considering a non-suddenly applied harmonic excitation to the first particle, the response of the $i - th$ particle is expressed as,

$$z_i(\tau) = \left[G_i(\tau)\right] * \left[F_0 \sin \omega \tau\ H(\tau)\right] \tag{4.3}$$

where $(*)$ denotes the convolution operator, and the Green's function $G_i(\tau)$ denotes the response of particle i due to an impulse applied at the left free boundary at time $\tau = 0$,

104

$$G_i(\tau) = \int_0^\tau J_0\left[\alpha\left|\tau^2 - u^2\right|\right]^{1/2}\left[J_{2i}(2u) + J_{2(i+1)}(2u)\right] du \tag{4.4}$$

and J_n is the Bessel function of $n-th$ order of the first kind. Expressing the Bessel function in integral form (or spectral representation),

$$J_{2i}(2u) = \frac{1}{\pi}\int_0^\pi \cos(i\theta)\cos\left[2u\sin(\theta/2)\right] d\theta$$

we express the Green's function in the following integral form:

$$\begin{aligned}G_i(\tau) &= \frac{1}{\pi}\int_0^\pi \cos(i\theta)\frac{\sin\left\{\tau\left[\alpha^2 + 4\sin^2(\theta/2)\right]^{1/2}\right\}}{\left[\alpha^2 + 4\sin^2(\theta/2)\right]^{1/2}} d\theta\\ &= \frac{1}{\pi}\int_0^\pi F_i(\theta)\sin\left[\omega(\theta)\tau\right] d\theta\end{aligned} \tag{4.5}$$

where $F_i(\theta) = \cos(i\theta)/\omega(\theta)$ and $\omega(\theta) = \left[\alpha^2 + 4\sin^2(\theta/2)\right]^{1/2}$. We note that the integral in (4.5) is performed within the pass band of the linear lattice since $\omega(0) = \alpha$ and $\omega(\pi) = \sqrt{4 + \alpha^2}$.

Substituting the integral expression (4.5) into (4.3), the response of the $i-th$ particle of the lattice can be expressed as:

$$\begin{aligned}z_i(\tau) &= \int_0^\tau G_i(\tau - u)F_0\sin\omega u\, H(u) du\\ &= \frac{F_0}{\pi}\int_0^\tau\int_0^\pi F_i(\theta)\sin\left[\omega(\theta)(\tau - u)\right] d\theta\sin\omega u\, du\\ &= \frac{F_0}{\pi}\int_0^\pi F_i(\theta)\int_0^\tau\sin\left[\omega(\theta)(\tau - u)\right]\sin\omega u\, du\, d\theta\\ &= \frac{F_0}{\pi}\int_0^\pi F_i(\theta)\frac{-\omega\sin\left[\omega(\theta)\tau\right] + \omega(\theta)\sin\left[\omega\tau\right]}{\omega^2(\theta) - \omega^2} d\theta\end{aligned} \tag{4.6a}$$

Considering the response in the limit of high excitation frequency, $\omega \gg \sqrt{4+\alpha} \geq \omega(\theta)$, we

expand the last relation in (4.6a) in powers of ω^{-1}, and retain the two leading-order terms:

$$
\begin{aligned}
z_i(\tau) &= \frac{F_0}{\pi} \int_0^\pi F_i(\theta) \left\{ \frac{1}{\omega} \sin\left[\omega(\theta)\tau\right] + O\left(\frac{1}{\omega^2}\right) \right\} d\theta \\
&= \frac{F_0}{\pi\omega} \int_0^\pi F_i(\theta) \sin\left[\omega(\theta)\tau\right] d\theta + O\left(\frac{1}{\omega^2}\right) = \frac{F_0}{\omega} G_i(\tau) + O\left(\frac{1}{\omega^2}\right)
\end{aligned}
\tag{4.6b}
$$

Thus, we prove that in the limit of a high frequency excitation the response asymptotically

approaches the impulse response of the lattice subject to an impulse of intensity F_0/ω.

Equivalently, the response asymptotically approaches the homogenous solution of the system

(4.2) with normalized initial conditions $z_1(0) = 0$, $z_1'(0) = F_0/\omega$, and $z_i(0) = z_i'(0) = 0$,

$i = 1, 2, 3, ...$

We note that by construction the asymptotic approximations (4.6) satisfy the initial

conditions, $z_i(0) = 0$, $i = 1, 2, 3, ...$, whereas, a straightforward computation yields,

$$
z_1'(\tau) = \frac{F_0}{\omega\pi} \int_0^\pi \{1 + \cos\theta\} \cos\left[\omega(\theta)\tau\right] d\theta + C\omega \cos\omega\tau ,
$$

so that $z_1'(0) = F_0/\omega$, and $z_i'(0) = 0$, $i = 2, 3, ...$ It follows that expressions (4.6b) provide the

complete high-frequency approximations for the responses of particles $i = 2, 3, ...$ (since they

satisfy the zero initial conditions of every particle, other than the first), whereas in order to

approximate the response of the first particle of the lattice (which is directly excited by the

suddenly applied high-frequency excitation), it is necessary to include the particular solution as

well:

$$z_1(\tau) = \frac{F_0}{\omega} G_1(\tau) + C \sin \omega\tau + O\!\left(\frac{1}{\omega^2}\right)$$

Only then we may satisfy the zero initial condition for the velocity of the first particle. This relation evaluates the unknown constant $C = -F_0/\omega^2$, and provides the complete asymptotic approximation for the response of the first particle as well. We note that this computation accounts for the sudden application of the harmonic excitation.

In summary, the asymptotic approximations for the particle responses of the linear lattice in the limit of a high-frequency, suddenly applied excitation are expressed as,

$$
\begin{aligned}
z_1(\tau) &= \frac{F_0}{\omega}\left[G_1(\tau) - \frac{\sin \omega\tau}{\omega} \right] + O\!\left(\frac{1}{\omega^2}\right) \\
z_i(\tau) &= \frac{F_0}{\omega} G_i(\tau) + O\!\left(\frac{1}{\omega^2}\right), \quad i = 2, 3, \ldots
\end{aligned}
\tag{4.7}
$$

with $G_i(\tau)$ given by (4.4) or (4.5). This indicates that, apart from the first particle which undergoes a high-amplitude, high-frequency localized oscillation, the response of the remainder of the semi-infinite lattice is approximately due to an impulse of intensity F_0/ω.

In Figure 4.3 we compare the response of the approximate asymptotic model (4.7) with the direct numerical simulation of the exact lattice model (4.2), where good agreement is noted. Hence, the high-frequency asymptotics fairly accurately capture the exact transient dynamics, and prove that the dynamic overshoot can be approximated by an initial impulsive response of the lattice in the limit of high frequency harmonic excitation. It is precisely this impulsive-like initial response of the lattice that generates the transient disturbance that propagates in the far field of the lattice, despite the fact that the forcing frequency is well inside the upper AZ. Hence,
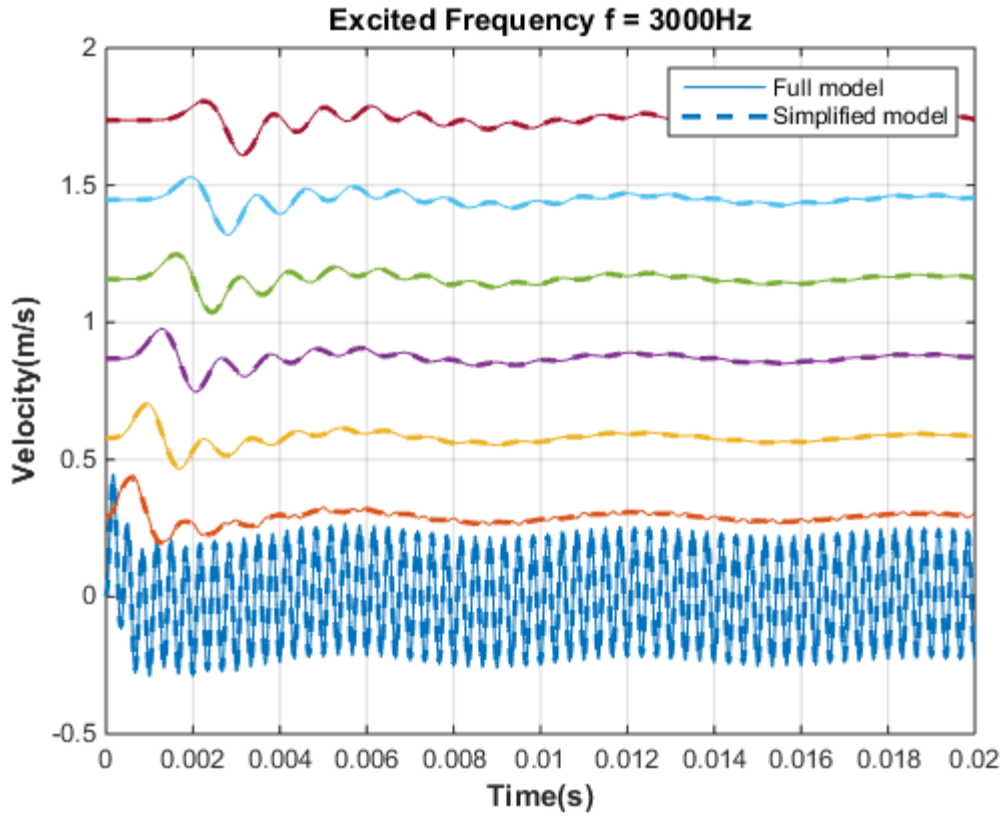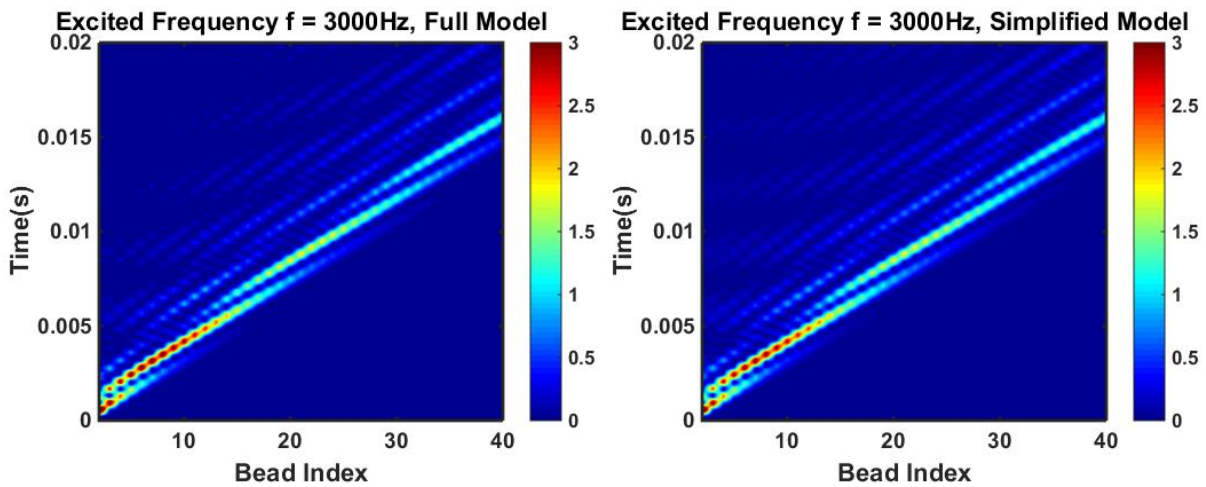
Figure 4.3. Comparison of the responses of the exact system (4.2) and the impulsively excited model (4.7): (a) Velocity time series of the leading seven particles of the exact system (———) and simplified system (-------), and (b) spatio-temporal evolution of the instantaneous kinetic energies of the 40 leading particles in the exact system (4.2) (left) and the model (4.7) (right).

it is proven that it is the high rate of application of the harmonic excitation that causes the dynamic overshoot, as conjectured previously.

These results conclude our analysis of the linear lattice under high-frequency harmonic excitation. In the next section we discuss the high-frequency dynamic overshoot of a harmonically excited strongly nonlinear, highly discontinuous, ordered system, namely a two-dimensional network of coupled granular lattices mounded on linear elastic foundations. In this case the strong nonlinearity of the granular media counterbalances the discreteness and dispersion effects and, contrary to the linear lattice, generates dynamic overshoot phenomena in the form of travelling coherent structures consisting of "pure" oscillatory wavepackets with spatially localized envelopes that propagate undistorted to the far fields of both coupled granular lattices. Moreover, intense, repetitive energy exchanges in the network are realized.

4.2 High-frequency dynamic overshoot in the granular network

In this section we consider weakly coupled granular networks under high-frequency harmonic excitation. We show asymptotically the generation of dynamic overshoot phenomena, resulting in low-frequency far-field transient wave propagation despite the high-frequency content of the applied loads. As mentioned in section 4.1, for a linear semi-infinite lattice the dynamic overshoot can be approximated in terms of the Green's function at the free end of the lattice; however, for the case of a semi-infinite ordered and weakly coupled granular network, dynamic overshoot occurs in the form of single (pure) propagating breathers. In the latter case, the strong nonlinearity of the granular network counterbalances linear dispersion, resulting in sustained single breathers that propagate unattenuated to the far field. The complexification/averaging method developed

109

by Manevitch (1999) together with a multiple scale analysis is employed in our study. Verifications of the asymptotic approximations by direct numerical simulations are performed.

4.2.1 System description

The schematic diagram of the granular network is presented in Figure 4.4. It consists of two semi-infinite, weekly coupled, uncompressed homogeneous granular lattices mounted on linear elastic foundations. Each granular chain is composed of an infinite number of identical, linearly elastic spherical granules in point contact with each other before the excitation is applied. Both chains are identical in terms of geometric and material properties. Under compressive internal forces the intra-granular interactions obey the strongly nonlinear (i.e., non-linearizable) Hertzian law. In the absence of compressive forces granule separations may occur causing possible collisions, providing an additional source of strong nonlinearity. In the model of the network, $\tilde{k}_1$ and $\tilde{k}_2$ denote the stiffness coefficients of the linear elastic foundations and the weak linear coupling, respectively, since it is assumed that $\tilde{k}_1 \gg \tilde{k}_2$. To model dissipative effects in the granular chains due to inherent structural damping within the granules, and frictional or viscoelastic effects, we introduce two types of linear viscous damping terms, with coefficients $\tilde{\gamma}_1$ and $\tilde{\gamma}_2$, representing dissipative effects in the foundation and granule interactions, and the coupling between the two chains, respectively. Moreover, we assume that the granules in both lattices are constrained to move in the horizontal direction only, so the granular network is two-dimensional. Finally, one of the lattices (designated as the "excited chain") is forced by the suddenly applied, high-frequency force $\tilde{F}(t) = \tilde{F}_0 \sin(2\pi f t) \ H(t)$ where $\tilde{F}_0$ denotes the amplitude of the force in N and $f \gg 1$ its frequency in Hz; the other lattice is initially at rest and is indirectly forced through the coupling terms (designated as the "absorbing chain").
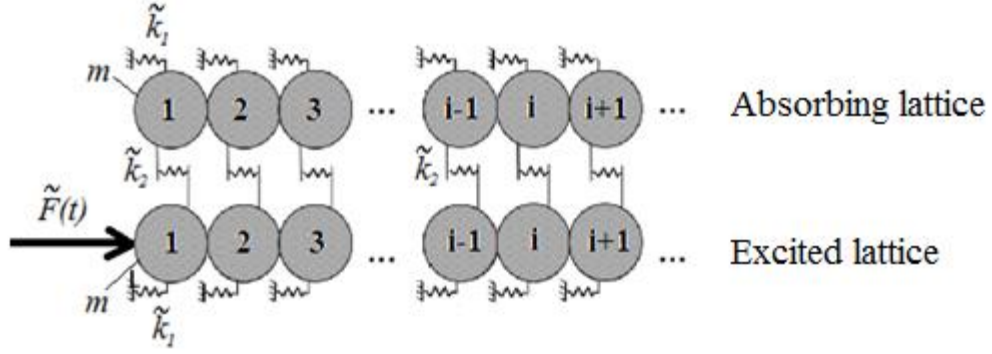
Figure 4.4. The two-dimensional weakly coupled granular network under suddenly applied, high-frequency periodic excitation.

The equations of motion of the weakly coupled granular network are strongly nonlinear and expressed as follows,

$$m\frac{d^2u_1}{dt^2} = \frac{E\sqrt{2R}}{3(1-v^2)}[-(u_1-u_2)_+^{3/2}] - \tilde{k}_2(u_1-v_1) - \tilde{k}_1u_1 - \tilde{\gamma}_2(\dot{u}_1-\dot{v}_1) - \tilde{\gamma}_1\dot{u}_1$$
$$+\tilde{F}_0\sin(2\pi ft)H(t)$$
$$m\frac{d^2u_i}{dt^2} = \frac{E\sqrt{2R}}{3(1-v^2)}[(u_{i-1}-u_i)_+^{3/2} - (u_i-u_{i+1})_+^{3/2}] - \tilde{k}_2(u_i-v_i) - \tilde{k}_1u_i - \tilde{\gamma}_2(\dot{u}_i-\dot{v}_i) - \tilde{\gamma}_1\dot{u}_i \quad (4.8)$$
$$m\frac{d^2v_1}{dt^2} = \frac{E\sqrt{2R}}{3(1-v^2)}[-(v_1-v_2)_+^{3/2}] - \tilde{k}_2(v_1-u_1) - \tilde{k}_1v_1 - \tilde{\gamma}_2(\dot{v}_1-\dot{u}_1) - \tilde{\gamma}_1\dot{v}_1$$
$$m\frac{d^2v_i}{dt^2} = \frac{E\sqrt{2R}}{3(1-v^2)}[(v_{i-1}-v_i)_+^{3/2} - (v_i-v_{i+1})_+^{3/2}] - \tilde{k}_2(v_i-u_i) - \tilde{k}_1v_i - \tilde{\gamma}_2(\dot{v}_i-\dot{u}_i) - \tilde{\gamma}_1\dot{v}_i$$

for $i = 2,3,...,$ where the variables u_i and v_i denote the axial displacements of the $i-th$ granules of the excited and absorbing lattices, respectively, and m, E, R and v the mass, elastic modulus, radius and Poisson's ratio of each of the identical granules, respectively. The subscript (+) in (4.8) indicates that only nonnegative values of the corresponding term in the parentheses should be considered, with zero values being assigned otherwise; this models the lack of interaction (and separation) between granules in the absence of compressive loads, and,

as mentioned previously, represents a source of high discontinuity and strong nonlinearity in the dynamics of the granular network.

Similar to the linear lattice in the previous section zero initial conditions are assumed for the two lattices at the beginning of application of the periodic excitation. We consider granules composed of Poly-di-methyl-siloxane (PDMS) with density $\rho = 965 \frac{kg}{m^3}$, and parameters $E = 1.5 \times 10^6 \, Pa$, $\nu = 0.49$, $R = 4.75 \times 10^{-3}$; in addition, the stiffness constants of the elastic foundation and the coupling are given by $\tilde{k}_1 = 4115 \frac{N}{m}$ and $\tilde{k}_2 = 402 \frac{N}{m}$. We assume the system is slightly damped with parameters $\tilde{\gamma}_1 = 0.0028 \frac{Ns}{m}$ and $\tilde{\gamma}_2 = 0.0069 \frac{Ns}{m}$. Furthermore, in our computational study we ensure that the applied excitation is such that the elastic deformations of the granules are sufficiently small and within the elastic limit of PDMS (i.e., bead deformations less than 2% of bead radius) and the approximations leading to the model (4.8) is valid (Zhang et al., 2015a,b).

As in the previous section the dimensional equations of motion (4.8) can be normalized by dividing each equation by the common mass of the beads, m, and introducing the re-scalings $x_n \to \frac{u_n}{R}$, $y_n \to \frac{v_n}{R}$, $\tau = \omega_0 t$ where the characteristic frequency is $\omega_0 = \sqrt{\frac{\tilde{k}_1}{m}}$:

$$
\begin{aligned}
x_1'' + x_1 + 2\varepsilon\lambda\left(x_1 - y_1\right) + 2\varepsilon^{5/2}\gamma_1 x_1' + 2\varepsilon^{5/2}\gamma_2\left(x_1' - y_1'\right) + \varepsilon^{3/4}\alpha[(x_1 - x_2)_+^{3/2}] \\
= \varepsilon^{1/2} F_0 \sin\left(\omega/\omega_0\right)\tau\, H(\tau) \\
x_n'' + x_n + 2\varepsilon\lambda\left(x_n - y_n\right) + 2\varepsilon^{5/2}\gamma_1 x_n' + 2\varepsilon^{5/2}\gamma_2\left(x_n' - y_n'\right) \\
- \varepsilon^{3/4}\alpha[(x_{n-1} - x_n)_+^{3/2} - (x_n - x_{n+1})_+^{3/2}] = 0
\end{aligned}
\tag{4.9}
$$

$$y_1'' + y_1 + 2\varepsilon\lambda\left(y_1 - x_1\right) + 2\varepsilon^{5/2}\gamma_1 y_1' + 2\varepsilon^{5/2}\gamma_2\left(y_1' - x_1'\right)$$
$$+ \varepsilon^{3/4}\alpha[(y_1 - y_2)_+^{3/2}] = 0$$
$$y_n'' + y_n + 2\varepsilon\lambda\left(y_n - x_n\right) + 2\varepsilon^{5/2}\gamma_1 y_n' + 2\varepsilon^{5/2}\gamma_2\left(y_n' - x_n'\right)$$
$$- \varepsilon^{3/4}\alpha[(y_{n-1} - y_n)_+^{3/2} - (y_n - y_{n+1})_+^{3/2}] = 0$$

(4.9 cont.)

where the variables x_i and y_i denote the normalized axial displacements of the $i - th$ granules of the excited and absorbing lattices, respectively, and prime denotes differentiation with respect to the normalized time variable τ. In (4.9), α is the normalized stiffness coefficient of the nonlinear Hertzian interaction between the beads of each lattice, λ the normalized linear coupling coefficients, $\omega = 2\pi f$ (in rad/s), and $0 < \varepsilon \ll 1$ is the small parameter of the problem scaling the weak coupling terms. Accordingly, following (Hasan et al., 2013) the stiffness, damping and forcing parameters of the granular network are scaled in terms of the small parameters as follows:

$$\tilde{\gamma}_1 = 2\varepsilon^{5/2}\gamma_1\sqrt{\tilde{k}_1 m}, \quad \tilde{\gamma}_2 = 2\varepsilon^{5/2}\gamma_2\sqrt{\tilde{k}_1 m}, \quad 2\sqrt{2}\,\mathrm{E}^* R/3\tilde{k}_1 = \varepsilon^{3/4}\alpha, \quad \tilde{k}_2/\tilde{k}_1 = 2\varepsilon\lambda, \quad \tilde{F}_0/\tilde{k}_1 R = \varepsilon^{1/2}F_0$$

Finally, we assume that the normalized excitation frequency is well inside the AZ of the network, so that $\omega/\omega_0 \gg 1$.

In recent studies it was theoretically (Jayaprakash et al., 2011b) and experimentally (Hasan et al., 2015) shown that ordered granular media such as the granular network of Figure 4.4 possess energy-tunable pass- and stop-bands similar to linear periodic systems. In low-frequency acoustic pass-bands (PZs), these highly discontinuous media support pulse-like transmission, whereas in high-frequency stop-bands (AZs), they exhibit almost complete energy filtering, preventing the transmission of induced energy. At intermediate frequency ranges (i.e., in between the pass- and stop-bands), and depending on the strength of the elastic foundation these media may support discrete breathers (Hasan et al., 2015), i.e., of stationary or travelling oscillating wavepackets with spatially localized envelopes (Sievers and Takeno, 1988; Campbell

and Peyrard, 1990); in weakly coupled networks of coupled granular lattices such as the one of Figure 4.4 such breathers lead to intense and recurrent energy exchanges between lattices.

Moreover, once the propagation of breathers has been established, passive targeted energy transfer in weakly coupled granular networks can be induced as well (Hasan et al., 2013). For example, in the network of Figure 4.4 that would amount to transient irreversible transfer of energy from the excited to the absorbing lattice. The study of passive targeted energy transfer will be explored in detail in Section 4.3. In these works the occurrence of near-complete and reversible or irreversible energy exchanges between the granular lattices of the network in the form of nonlinear beat phenomena involving traveling discrete breathers has been established. The main focus of the present section is to examine the same network under suddenly applied high-frequency harmonic excitation in order to demonstrate the existence of a nonlinear dynamical overshoot. In similarity to the linear lattice, we show that this dynamic overshoot can be analytically approximated by the impulsive response of the network; however, in contrast to the linear lattice the nonlinear overshoot in the granular network is in the form of a "pure" traveling breather, i.e., of a single oscillating wavepacket with spatially localized envelope that propagates to the far field of the network. What enables this highly coherent nonlinear response is strong nonlinearity that counterbalances discreteness and dispersion.

4.2.2 Computational study

As an example of the strongly nonlinear dynamic overshoot in the network (4.8) under suddenly applied high-frequency excitation we consider the response for $\tilde{F}_0 = 3.67 \, N$ and $f = 1.6 \, kHz$. In Figure 4.5a, we depict the velocity time series of the first seven granules of both the excited and absorbing lattices. Note that the velocity response of the first granule of the excited lattice is

114

qualitatively different from the other velocities, since after an initial transient the response is nearly harmonic with the (high) frequency of the applied excitation and amplitude that is significantly higher compared to the other responses. Following the first granule of the excited lattice, the velocity time series in Figures 4.5a clearly show the formation of a single traveling breather corresponding to nearly complete but reversible energy exchanges between the two lattices and propagating to the far fields of the two lattices. The spatio-temporal evolutions of the instantaneous kinetic energies of each lattice shown in Figure 4.5b confirm these intense energy exchanges. Despite the continuous high-frequency harmonic excitation there occurs only a "pure" (i.e., single) breather propagating in the network. It is precisely this pure breather that represents the dynamic overshoot phenomenon in the network forced by the high-frequency, suddenly applied excitation.

We emphasize at this point that the high frequency of the applied load is well within the AZ of the excited granular lattice, so transmission of energy to the far field should not be expected; as shown below, this spatially coherent traveling breather is generated at the initial phase of the high-frequency excitation of the network, and is solely caused by the high rate of application of the harmonic excitation. Indeed, as shown below, driven by the suddenly applied high frequency input, the granular network presents similar dynamic behavior to the impulsively excited network reported by Hasan et al. (2013). So, once the asymptotic reduction of the transient dynamics to an impulsive response is accomplished, we may employ directly the results of that work to analytically model the pure traveling breather shown in Figure 4.5.
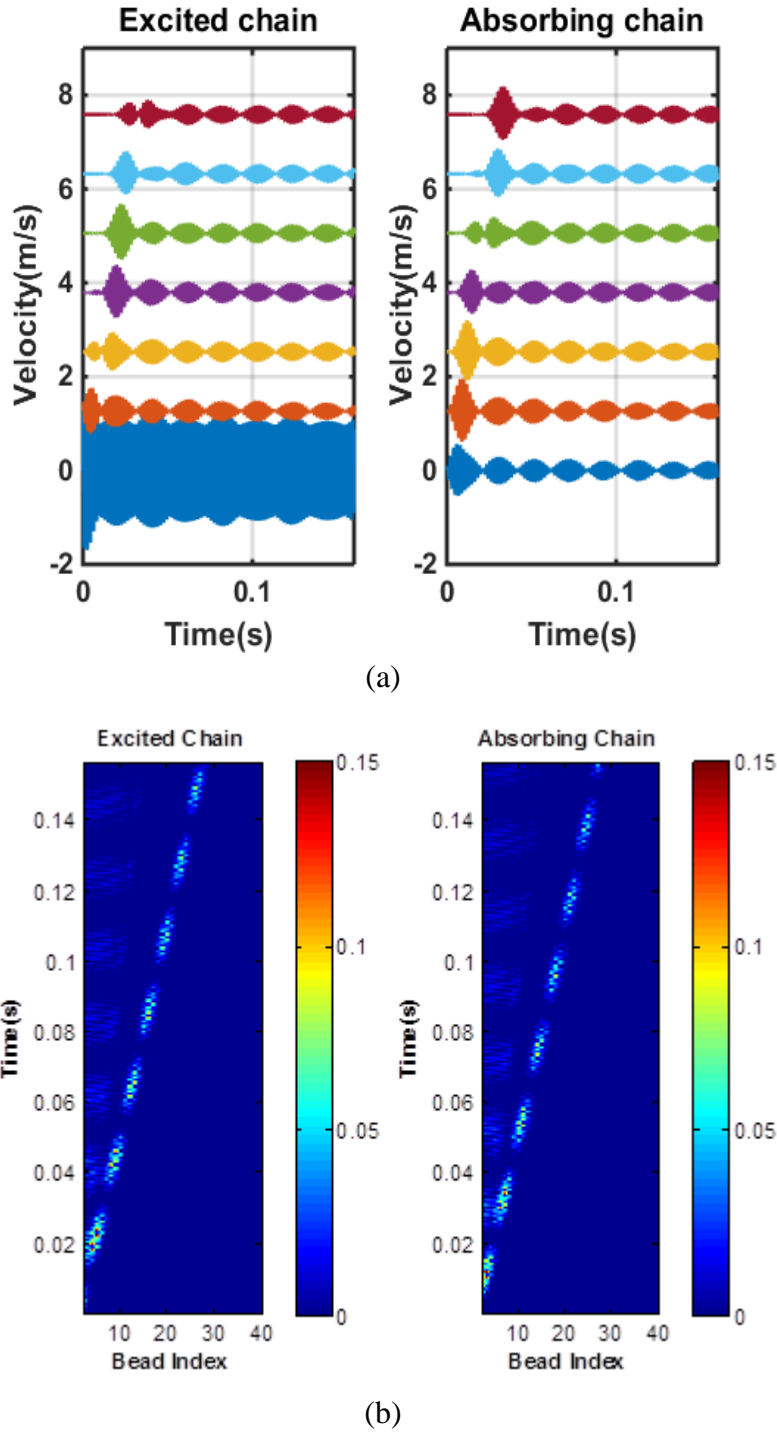
Figure 4.5. Numerical simulation of the dynamic overshoot in the granular network (4.8): (a) Velocity time series of the first seven granules of the excited and absorbing lattices, and (b) spatio-temporal evolution of the instantaneous kinetic energies of granules 2-40 of the excited and absorbing chains; the velocity times series in (a) are shifted vertically for clarity.

To further highlight the nature of the nonlinear dynamics that gives rise to the formation of the dynamic overshoot phenomenon in the granular network, in Figure 4.6 we depict the Fast Fourier Transform (FFT) of the velocity time series of the 1st, 4th and 7th granules of the excited and absorbing lattices. We deduce that the pure traveling breather is realized due to the closeness of two "fast" frequencies in the responses of both lattices: (i) The frequency of the in-phase nonlinear mode (Jayaprakash et al., 2011a) of each of the two (identical) granular lattices on its linear elastic foundation ($f_1 = (k_1/m)^{1/2}/2\pi = 508.4 \, Hz$ in this case); and (ii) the energy-dependent main fast frequency of the traveling breather characterizing the strongly nonlinear granular interactions between adjacent granules ($f_2 = 555.8 \, Hz$ for the energy level of the simulation of Figure 4.5). It turns out that the relatively small difference between these fast frequencies, $f_2 - f_1$, equals the "slow" frequency of the envelope modulation of the breather. In addition, there exist higher harmonic components in the FFTs of the velocities of the granules (other than the leading ones) of Figure 4.6; these are multiples and combinations of the aforementioned basic frequencies f_1 and f_2, and are evidenced as the periodic series of higher overtones in the FFTs. These multiple overtones are generated by the strongly nonlinear Hertzian interactions and possible granule collisions in the network, but their amplitudes are small.

It is interesting to note that these slow and fast frequency components forming the pure breather occur despite the "ultra-high" frequency of the suddenly applied harmonic excitation equaling $f = 1600 \, Hz$ in the simulation of Figure 4.5. This frequency lies well within the AZ (stop-band) of the excited granular lattice, so one would expect complete filtering of all frequency components by the granular network and absence of transmission of energy in the far field. Yet, as the numerical transient responses of Figure 4.5 and the corresponding FFTs of Figure 4.6 clearly prove, only the ultra-high excitation frequency is filtered out by the granular network, but
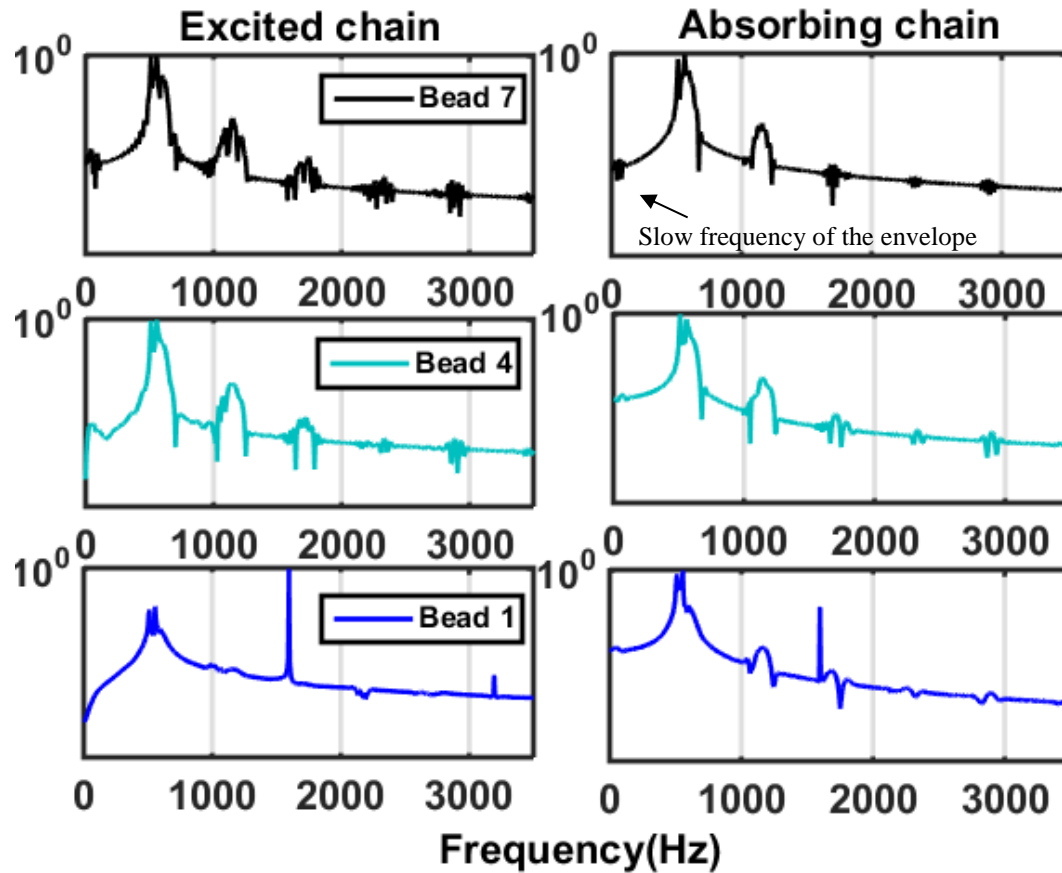
Figure 4.6. Fourier spectra of the velocity time series of the 1st, 4th and 7th granules of the excited and absorbing chains depicted in Figure 4.5 (the pure breather develops after the 1st granule of the excited lattice); note that the ultra-high excitation frequency appears only in the responses of the 1st granules and is filtered out in the responses of the other granules.

other frequency components can still propagate through the medium forming the dynamic overshoot phenomenon (the pure breather). These additional harmonic components can only be caused by the high rate of the application of the harmonic load, and as shown below, amount approximately to an impulsive response of the network.

4.2.3 Asymptotic analysis and numerical verification

Motivated by these numerical results we proceed to an asymptotic analysis of the nonlinear dynamic overshoot phenomenon shown in Figure 4.5. Based on the numerical results of Figure 4.5 and 4.6, and motivated by the analysis reported in (Hasan et al., 2013) in the following study we restrict our analysis to the regime of 1:1 internal resonance, by assuming that the oscillations of all granules of the two lattices in the granular network of Figure 4.4 possess identical fast frequencies, and apply the complexification/averaging method developed by Manevitch (1999) together with a multiple scale analysis. This is consistent with the fact that the two fast frequencies in the FFTs of Figure 4.6 are the same for the depicted responses of the excited and absorbing lattices.

To this end, we introduce the following new complex dependent variables,

$$\psi_n^x = \dot{x}_n + i x_n, \quad \psi_n^y = \dot{y}_n + i y_n \tag{4.10}$$

where $i = (-1)^{1/2}$. Then, the following multiscale expansions of these complex variables are introduced in terms of the small parameter of the problem,

$$
\begin{aligned}
\psi_n^x &= \varepsilon^{1/2} \left[\psi_{n0}^x (\tau_0, \tau_1, \ldots) + \varepsilon \psi_{n1}^x (\tau_0, \tau_1, \ldots) + O(\varepsilon^2) \right] \\
\psi_n^y &= \varepsilon^{1/2} \left[\psi_{n0}^y (\tau_0, \tau_1, \ldots) + \varepsilon \psi_{n1}^y (\tau_0, \tau_1, \ldots) + O(\varepsilon^2) \right]
\end{aligned}
\tag{4.11}
$$

where $\tau_0 = \varepsilon^0 \tau$, $\tau_1 = \varepsilon^1 \tau_0, \ldots$ are fast and slow time scales, respectively. In terms of the transient dynamics of the problem, the fast time scale is the characteristic time scale of oscillations caused by the linear foundation of both chains, whereas the slow time scale is the characteristic time scale of the dynamics governing strong energy exchanges between the two granular chains. The

derivatives with respect of τ are then expressed in terms of the new time scales, e.g.,

$\dfrac{d}{d\tau} = \dfrac{\partial}{\partial\tau_0} + \varepsilon\dfrac{\partial}{\partial\tau_1} + O\left(\varepsilon^2\right)$. Expressing the various terms in (4.9) in terms of the complex variables

(4.10) and (4.11), and collecting like-powers of the small parameter ε we obtain hierarchy of

subproblems at different orders of approximation, which are analyzed separately from each other

(since in the analysis the time scales are considered to be independent).

Considering the leading order $O\left(\varepsilon^{1/2}\right)$ terms we derive the following system:

$$\frac{\partial \psi_{10}^x}{\partial \tau_0} - i\psi_{10}^x = F\sin\left[\left(\omega/\omega_0\right)\tau\right], \quad \frac{\partial \psi_{n0}^x}{\partial \tau_0} - i\psi_{n0}^x = 0, \quad n \geq 2$$

$$\frac{\partial \psi_{n0}^y}{\partial \tau_0} - i\psi_{n0}^y = 0, \quad n \geq 1 \tag{4.12}$$

Since the leading order system is linear, the solution for ψ_{10}^x contains homogenous and particular

terms and is expressed in the form,

$$\psi_{10}^x = \left(\psi_{10}^x\right)_h + \left(\psi_{10}^x\right)_p =$$

$$= \varphi_{10}^x\left(\tau_1\right)\exp\left(i\tau_0\right) + \frac{iF}{1-\left(\omega/\omega_0\right)^2}\sin\left[\left(\omega/\omega_0\right)\tau_0\right] + \frac{F\left(\omega/\omega_0\right)}{1-\left(\omega/\omega_0\right)^2}\cos\left[\left(\omega/\omega_0\right)\tau_0\right] \tag{4.13}$$

whereas the solutions for ψ_{n0}^x, $n \geq 2$ and ψ_{n0}^y, $n \geq 1$ have only homogenous parts. The slowly

varying complex amplitude $\varphi_{10}^x\left(\tau_1\right)$ modulates the fast oscillation $\exp\left(i\tau_0\right)$, and similar

slow/fast decompositions of the homogeneous solutions are considered in the expressions of the

other leading order complex responses:

$$\psi_{n0}^x = \varphi_{n0}^x\left(\tau_1\right)\exp\left(i\tau_0\right), \ n \geq 2, \quad \psi_{n0}^y = \varphi_{n0}^y\left(\tau_1\right)\exp\left(i\tau_0\right), \ n \geq 1 \tag{4.14}$$

It follows that the fast frequency of the applied excitation appears only in the leading order approximation of the leading granule of the excited lattice, in the form of the particular solution in (4.13). This affects the solution at the next order of approximation as well. The slow modulations $\varphi_{n0}^{x}(\tau_1)$ and $\varphi_{n0}^{y}(\tau_1)$, $n \geq 1$ (representing the homogeneous terms in these approximations) cannot be evaluated at the leading order approximation, and are computed by considering terms of $\mathrm{O}(\varepsilon^{3/2})$ at the next (smaller) order.

As a result, we derive a system of complex equations governing the approximations ψ_{n1}^{x} and ψ_{n1}^{y}, in terms of the leading order solutions (4.13) and (4.14). The particular solution part of ψ_{10}^{x} (containing the "ultra-fast" excitation frequency) enters explicitly only in the higher order approximations of the responses of the leading two granules of the excited lattice and first granule of the absorbing chain. Since there are no terms with ultra-high normalized frequency (ω/ω_0) in the responses of the later granules, only the homogeneous part of (4.13) enters in the higher order analysis of these responses, and the effects of the ultra-high excitation frequency enters only implicitly in these responses.

This directly proves that the dynamic overshoot (which from the numerical simulations appears to develop in granules after the leading ones in the two lattices) is solely due to the early transient state of the network which affects the homogeneous terms and does not involve the normalized ultra-high frequency (ω/ω_0) of the excitation. This is consistent with the FFT results of Figure 4.6 and explains the lower frequency content of the pure breather representing the nonlinear dynamic overshoot.

First, we omit the response of the first granule of the excited lattice and consider the responses of the remaining granules and obtain a set of complex equations governing the $O\left(\varepsilon^{3/2}\right)$ approximations. For the excited lattice these are given by,

$$\frac{\partial\left[\varphi_{20}^{x}\exp\left(i\tau_{0}\right)\right]}{\partial\tau_{1}}+\frac{\partial\psi_{21}^{x}}{\partial\tau_{0}}-i\psi_{21}^{x}$$

$$=\alpha\left\{\frac{\varphi_{10}^{x}\exp\left(i\tau_{0}\right)-\varphi_{10}^{x*}\exp\left(-i\tau_{0}\right)-\varphi_{20}^{x}\exp\left(i\tau_{0}\right)+\varphi_{20}^{x*}\exp\left(-i\tau_{0}\right)}{2i}\right.$$

$$\left.+\frac{F}{1-\left(\omega/\omega_{0}\right)^{2}}\sin\left[\left(\omega/\omega_{0}\right)\tau_{0}\right]\right\}_{+}^{3/2}$$

$$-\alpha\left\{\frac{\varphi_{20}^{x}\exp\left(i\tau_{0}\right)-\varphi_{20}^{x*}\exp\left(-i\tau_{0}\right)-\varphi_{30}^{x}\exp\left(i\tau_{0}\right)+\varphi_{30}^{x*}\exp\left(-i\tau_{0}\right)}{2i}\right\}_{+}^{3/2}$$

$$-i\lambda\left\{\varphi_{20}^{y}\exp\left(i\tau_{0}\right)-\varphi_{20}^{y*}\exp\left(-i\tau_{0}\right)\right\}$$

$$\frac{\partial\left[\varphi_{n0}^{x}\exp\left(i\tau_{0}\right)\right]}{\partial\tau_{1}}+\frac{\partial\psi_{n1}^{x}}{\partial\tau_{0}}-i\psi_{n1}^{x}$$

$$=\alpha\left\{\frac{\varphi_{(n-1)0}^{x}\exp\left(i\tau_{0}\right)-\varphi_{(n-1)0}^{x*}\exp\left(-i\tau_{0}\right)-\varphi_{n0}^{x}\exp\left(i\tau_{0}\right)+\varphi_{n0}^{x*}\exp\left(-i\tau_{0}\right)}{2i}\right\}_{+}^{3/2}$$

$$-\alpha\left\{\frac{\varphi_{n0}^{x}\exp\left(i\tau_{0}\right)-\varphi_{n0}^{x*}\exp\left(-i\tau_{0}\right)-\varphi_{(n+1)0}^{x}\exp\left(i\tau_{0}\right)+\varphi_{(n+1)0}^{x*}\exp\left(-i\tau_{0}\right)}{2i}\right\}_{+}^{3/2}$$

$$-i\lambda\left\{\varphi_{n0}^{y}\exp\left(i\tau_{0}\right)-\varphi_{n0}^{y*}\exp\left(-i\tau_{0}\right)\right\},\quad n=3,4,... \tag{4.15a}$$

whereas for the absorbing lattice these are expressed as:

$$\frac{\partial\left[\varphi_{10}^{y}\exp\left(i\tau_{0}\right)\right]}{\partial\tau_{1}}+\frac{\partial\psi_{11}^{y}}{\partial\tau_{0}}-i\psi_{11}^{y}$$

$$=-\alpha\left\{\frac{\varphi_{10}^{y}\exp\left(i\tau_{0}\right)-\varphi_{10}^{y*}\exp\left(-i\tau_{0}\right)-\varphi_{20}^{y}\exp\left(i\tau_{0}\right)+\varphi_{20}^{y*}\exp\left(-i\tau_{0}\right)}{2i}\right\}_{+}^{3/2}$$

$$-i\lambda\left\{\varphi_{10}^{x}\exp(i\tau_0)-\varphi_{10}^{x*}\exp(-i\tau_0)+\frac{2iF}{1-(\omega/\omega_0)^2}\sin\left[(\omega/\omega_0)\tau_0\right]\right\},$$

$$\frac{\partial\left[\varphi_{n0}^{y}\exp(i\tau_0)\right]}{\partial\tau_1}+\frac{\partial\psi_{n1}^{y}}{\partial\tau_0}-i\psi_{n1}^{y}$$

$$=\alpha\left\{\frac{\varphi_{(n-1)0}^{y}\exp(i\tau_0)-\varphi_{(n-1)0}^{y*}\exp(-i\tau_0)-\varphi_{n0}^{y}\exp(i\tau_0)+\varphi_{n0}^{y*}\exp(-i\tau_0)}{2i}\right\}_{+}^{3/2}$$

$$-\alpha\left\{\frac{\varphi_{n0}^{y}\exp(i\tau_0)-\varphi_{n0}^{y*}\exp(-i\tau_0)-\varphi_{(n+1)0}^{y}\exp(i\tau_0)+\varphi_{(n+1)0}^{y*}\exp(-i\tau_0)}{2i}\right\}_{+}^{3/2} \qquad (4.15b)$$

$$-i\lambda\left\{\varphi_{n0}^{x}\exp(i\tau_0)-\varphi_{n0}^{x*}\exp(-i\tau_0)\right\},\quad n=2,3,...$$

In (4.15a,b) the superscript $(*)$ denotes complex conjugate. Upon imposing solvability conditions in (4.15), i.e., eliminating secular terms with fast frequency equal to unity (which is identical to the fast frequency on the left-hand sides) that render the solution non-uniformly valid as time tends to infinity, yields the following slow flow for the later granules in the excited and absorbing chains, which is the system of modulation equations in the slow time scale governing the (slow) evolutions of the complex amplitudes of the leading order approximations (4.13) and (4.14):

$$\frac{\partial\varphi_{n0}^{x}}{\partial\tau_1}=\alpha\left\{\frac{\varphi_{(n-1)0}^{x}\exp(i\tau_0)-\varphi_{(n-1)0}^{x*}\exp(-i\tau_0)-\varphi_{n0}^{x}\exp(i\tau_0)+\varphi_{n0}^{x*}\exp(-i\tau_0)}{2i}\right\}_{+}^{3/2}\exp(-i\tau_0)$$

$$-\alpha\left\{\frac{\varphi_{n0}^{x}\exp(i\tau_0)-\varphi_{n0}^{x*}\exp(-i\tau_0)-\varphi_{(n+1)0}^{x}\exp(i\tau_0)+\varphi_{(n+1)0}^{x*}\exp(-i\tau_0)}{2i}\right\}_{+}^{3/2}\exp(-i\tau_0)$$

$$-i\lambda\left\{\varphi_{n0}^{y}\exp(i\tau_0)-\varphi_{n0}^{y*}\exp(-i\tau_0)\right\}\exp(-i\tau_0),\quad n=2,3,...$$

$$\frac{\partial \varphi_{n0}^{y}}{\partial \tau_{1}} = \alpha \left\{ \frac{\varphi_{(n-1)0}^{y} \exp(i\tau_{0}) - \varphi_{(n-1)0}^{y*} \exp(-i\tau_{0}) - \varphi_{n0}^{y} \exp(i\tau_{0}) + \varphi_{n0}^{y*} \exp(-i\tau_{0})}{2i} \right\}_{+}^{3/2} \exp(-i\tau_{0})$$

$$-\alpha \left\{ \frac{\varphi_{n0}^{y} \exp(i\tau_{0}) - \varphi_{n0}^{y*} \exp(-i\tau_{0}) - \varphi_{(n+1)0}^{y} \exp(i\tau_{0}) + \varphi_{(n+1)0}^{y*} \exp(-i\tau_{0})}{2i} \right\}_{+}^{3/2} \exp(-i\tau_{0}) \qquad (4.16)$$

$$-i\lambda \left\{ \varphi_{n0}^{x} \exp(i\tau_{0}) - \varphi_{n0}^{x*} \exp(-i\tau_{0}) \right\} \exp(-i\tau_{0}), \quad n = 1,2,...$$

We note that the ultra-high normalized excitation frequency ω/ω_{0} does not enter in the solvability conditions (4.16) since the terms containing it are non-resonant (since by our prior assumption it holds that $\omega/\omega_{0} \gg 1$). Moreover, contrary to the leading order solutions, at this order of approximation non-smooth effects enter in the dynamics due to the possible bead separations and collisions (modelled by the subscripts (+) in (4.15a,b)). However, these non-smooth terms in the right-hand sides do not prevent the analytical study of the dynamics because they can be evaluated by Fourier expansions and averaging operations as shown in (Starosvetsky et al. 2012; Hasan et al. 2013). This analysis is not repeated here, but following this methodology we arrive to the following averaged set of modulation equations (slow flow),

$$i\frac{\partial \varphi_{n0}^{x}}{\partial \tau_{1}} \approx \tilde{\alpha} \left\{ G_{(n-1)0}^{x} \left| G_{(n-1)0}^{x} \right|^{1/2} - G_{n0}^{x} \left| G_{n0}^{x} \right|^{1/2} \right\} + \tilde{\lambda} \varphi_{n0}^{y}, \quad n = 2,3,...$$

$$i\frac{\partial \varphi_{n0}^{y}}{\partial \tau_{1}} \approx \tilde{\alpha} \left\{ G_{(n-1)0}^{y} \left| G_{(n-1)0}^{y} \right|^{1/2} - G_{n0}^{y} \left| G_{n0}^{y} \right|^{1/2} \right\} + \tilde{\lambda} \varphi_{n0}^{x}, \quad n = 1,2,...$$

$$(4.17)$$

where,

$$\tilde{\alpha} = \frac{\alpha \eta_{1}}{2\pi}, \quad \eta_{1} = \oint_{2\pi} (\cos u)_{+}^{3/2} \exp(-iu) du,$$

$$\tilde{\lambda} = \frac{\lambda \eta_{2}}{\pi}, \quad \eta_{2} = \oint_{2\pi} \cos u \, \exp(-iu) du$$

$$G_{(n-1)0}^{x} \equiv \varphi_{(n-1)0}^{x} - \varphi_{n0}^{x} = \left| G_{(n-1)0}^{x} \right| \exp(i\theta_{n-1}^{x}), \ G_{n0}^{x} \equiv \varphi_{n0}^{x} - \varphi_{(n+1)0}^{x} = \left| G_{n0}^{x} \right| \exp(i\theta_{n}^{x}), n = 1,2,...$$

$$G_{(n-1)0}^{y} \equiv \varphi_{(n-1)0}^{y} - \varphi_{n0}^{y} = \left| G_{(n-1)0}^{y} \right| \exp(i\theta_{n-1}^{y}), \ G_{n0}^{y} \equiv \varphi_{n0}^{y} - \varphi_{(n+1)0}^{y} = \left| G_{n0}^{y} \right| \exp(i\theta_{n}^{y}), n = 1,2,...$$

with the understanding that $\varphi_{00}^y \equiv 0$, so that $G_{00}^y \equiv -\varphi_{10}^y$. We note that the fast frequency of the applied excitation does not enter explicitly in the slow flow equations (4.17), but enters implicitly through the terms G_{10}^x and φ_{10}^x which depend on the slow flow of the first granule of the excited lattice (which is considered separately in this section).

Considering now the response of the first granule of the excited lattice of the network (which is the only granule of the network that is directly forced by the applied harmonic load), we express the equation governing the $O\left(\varepsilon^{3/2}\right)$ approximation as:

$$\frac{\partial\left[\varphi_{10}^x \exp\left(i\tau_0\right)\right]}{\partial\tau_1} + \frac{\partial\psi_{11}^x}{\partial\tau_0} - i\psi_{11}^x =$$

$$-\frac{\alpha}{2i}\left\{\varphi_{10}^x \exp\left(i\tau_0\right) - \varphi_{10}^{x*} \exp\left(-i\tau_0\right) + \left[2iF_0 / 1 - \left(\omega/\omega_0\right)^2\right]\sin\left(\omega/\omega_0\right)\tau_0 \right. \tag{4.18}$$

$$\left. -\varphi_{20}^x \exp\left(i\tau_0\right) + \varphi_{20}^{x*} \exp\left(-i\tau_0\right)\right\}_+^{3/2} - i\lambda\left\{\varphi_{10}^y \exp\left(i\tau_0\right) - \varphi_{10}^{y*} \exp\left(-i\tau_0\right)\right\}$$

Imposing the solvability condition for this equation we obtain the following complex slow flow equation governing the slow modulation of the response of the leading granule of the excited lattice:

$$\frac{\partial\varphi_{10}^x}{\partial\tau_1} = -\alpha\left\{\underbrace{\frac{G_{10}^x \exp\left(i\tau_0\right) - G_{10}^{x*}\exp\left(-i\tau_0\right)}{2i}}_{Term\ I} + \underbrace{F_0 \sin\left[\left(\omega/\omega_0\right)\tau_0\right]/\left[1 - \left(\omega/\omega_0\right)^2\right]}_{Term\ II}\right\}_+^{3/2} \exp\left(-i\tau_0\right)$$

$$-i\lambda\left\{\varphi_{10}^y \exp\left(i\tau_0\right) - \varphi_{10}^{y*} \exp\left(-i\tau_0\right)\right\}\exp\left(-i\tau_0\right)$$

$$\tag{4.19}$$

with $G_{10}^x \equiv \varphi_{10}^x - \varphi_{20}^x = \left|F_{10}^x\right|\exp\left(i\theta_1^x\right)$. Note that the frequency of the excitation enters now explicitly in the slow flow. However, in the limit of high frequency, $\left(\omega/\omega_0\right) \gg 1$ Term II in (4.19)

is small compared to Term I, so one can expand the power of the summation of these two Terms on the right-hand side using the binomial expansion. Then, applying the previous Fourier expansion − averaging methodology one obtains the following smooth slow flow equation,

$$i\frac{\partial \varphi_{10}^x}{\partial \tau_1} \approx -\tilde{\alpha}\left\{G_{10}^x\left|G_{10}^x\right|^{1/2} + \left(-3F_0/2(\omega/\omega_0)^{-2}\right)G_{10}^x\left|G_{10}^x\right|^{-1/2}(\eta_3/\eta_1)\right\} + \tilde{\lambda}\varphi_{10}^y$$
$$+O\left((\omega/\omega_0)^{-4}\right) \tag{4.20}$$

where,

$$\tilde{\alpha} = \frac{\alpha\eta_1}{2\pi}, \quad \tilde{\lambda} = \frac{\lambda\eta_2}{\pi}, \quad \eta_1 = \oint_{2\pi}(\cos u)_+^{3/2}\exp(-iu)\,du,$$
$$\eta_2 = \oint_{2\pi}\cos u \exp(-iu)\,du, \quad \eta_3 = \oint_{2\pi}(\cos u)_+^{1/2}\sin\left[(\omega/\omega_0)(u+\pi/2-\theta_1^x)\right]\exp(-iu)\,du$$

Equation (4.20) complements equations (4.17) and completes the derivation of the averaged slow flow at the $O(\varepsilon^{3/2})$ approximation. This slow-flow determines the complex amplitudes of the leading order solution (4.13) and (4.14), and governs the almost complete and recurrent energy exchanges between the excited and absorbing granular lattices. The set of equations (4.17) and (4.20) is free of non-smooth effects and is solved by applying appropriate initial conditions for the complex amplitudes $\varphi_{n0}^{x,y}(\tau_1)$, $n=1,2,...$. For zero initial conditions at the time instant of application of the periodic excitation, the corresponding initial conditions for the $O(\varepsilon^{3/2})$ slow flow are derived as follows:

$$\varphi_{10}^x(0) = \varphi_{10}^{x*}(0) = -F_0(\omega/\omega_0)/\left[1-(\omega/\omega_0)^2\right],$$
$$\varphi_{n0}^x(0) = \varphi_{n0}^{x*}(0) = 0, \quad n = 2,3,..., \quad \varphi_{n0}^y(0) = \varphi_{n0}^{y*}(0) = 0, \quad n = 1,2,3,... \tag{4.21}$$

This indicates that the suddenly applied, high-frequency harmonic excitation amounts to an impulsive input applied to the excited lattice. Moreover, at the leading-order approximation

126

the fast frequency of the applied force only influences the response of the first granule of the excited lattice, while the other granules of the network only sense the excitation in the form of an impulsive response generating the nonlinear dynamic overshoot.

In Figures 4.7 and 4.8 we depict the nonlinear dynamic overshoot (in the form of the pure breather) for the parameter values corresponding to the numerical results of Figure 4.5 and 4.6. The analytical results were obtained by numerically integrating the $O(\varepsilon^{3/2})$ averaged slow flows (4.17) and (4.20) subject to the initial conditions (4.21), and then substituting the results into the leading order approximations (4.13) and (4.14) taking into account the complex transformations (4.10). The results clearly show that the averaged slow flow closely captures the energy exchange phenomena between the coupled chains, and validate the theoretical prediction that the dynamic overshoot in the suddenly forced network by the high-frequency harmonic excitation amounts to an impulsive response of the same network. We note that the ultra-high excitation frequency appears mainly in the response of the first granule of the excited lattice (since it is the only granule that is directly excited by the force), and in the first granule of the absorbing lattice (which is indirectly excited by the force through its coupling with the first granule of the excited lattice); the excitation frequency does not appear in the responses of the other granules. These theoretical findings fully recover the numerical simulations of Figure 4.5 and 4.6.

Considering the FFTs of the selected velocity times depicted in Figure 4.8 we note that, although the basic harmonics that are responsible for breather formation are captured correctly by the analysis, together with the attenuation of the ultra-high excitation frequency component after the leading granules of the excited and absorbing lattices, there are some higher frequency
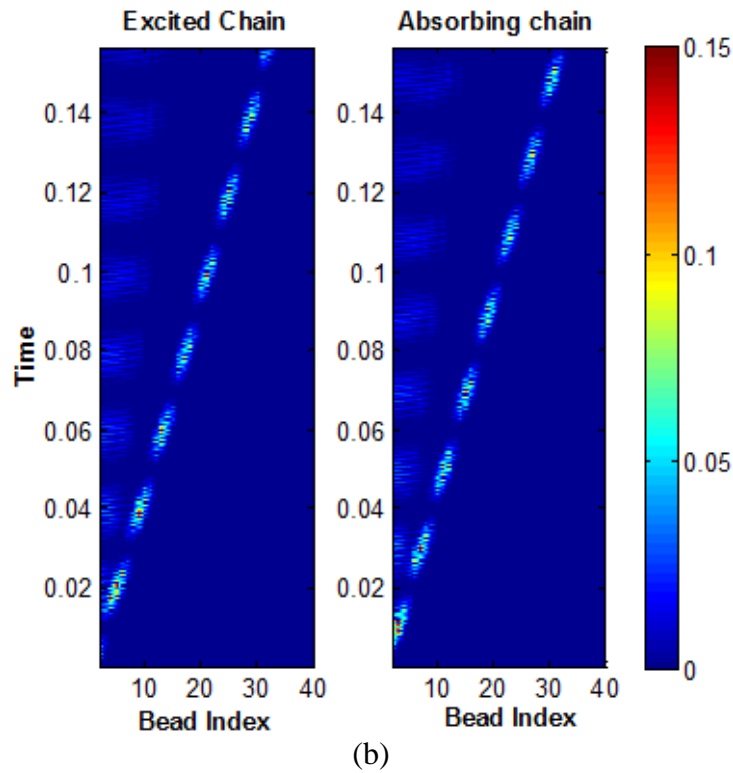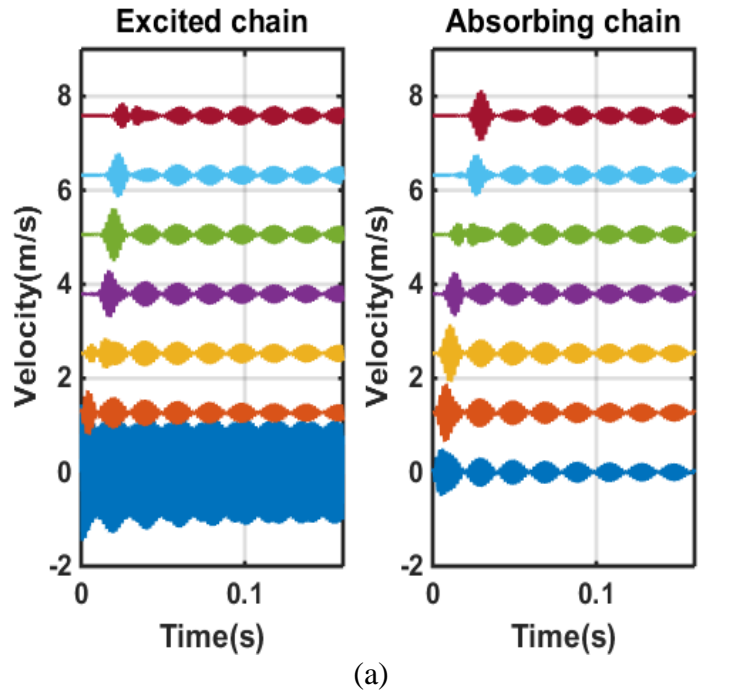
127

Figure 4.7. Analytical approximations (4.13)-(4.14) for the dynamic overshoot (pure breather): (a) Velocity time series of the first seven granules of the excited and absorbing granules, and (b) spatio-temporal evolution of the instantaneous kinetic energies of granules 2-40 of the excited and absorbing chains; the velocity times series in (a) are shifted horizontally for clarity.
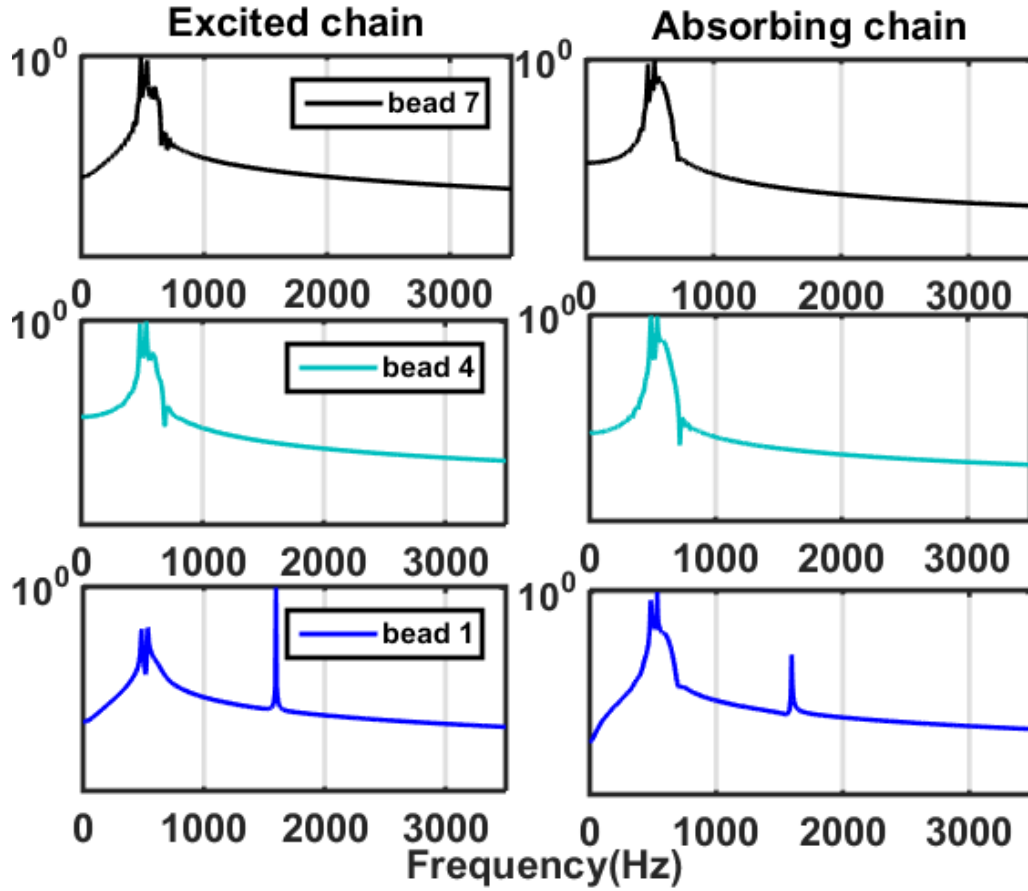
128

Figure 4.8. Fourier spectra of the analytical approximations of the velocity time series of the 1st, 4th and 7th granules of the excited and absorbing chains depicted in Figure 4.7 (the pure breather develops after the 1st granule of the excited lattice); these results should be compared to the numerical results of Figure 4.6.

discrepancies compared to the numerical FFTs of Figure 4.6. In particular, the absence of the higher overtones in the analytical predictions (corresponding to multiples and combinations of the basic frequencies of the breather) are due, (i) to the averaging operations that we performed in order to smoothen the slow flow at the $O(\varepsilon^{3/2})$ approximation, and (ii) to the fact that only the two leading order approximations were considered in the asymptotic analysis. Indeed, it is expected that as higher order terms are included, higher harmonics are added to the analytical

approximations. As a result, the analytical model turns out to be "softer" than the exact granular network.

4.3 Complete and reversible energy exchanges

In the present section we perform a computational study of the same granular network (cf. Figure 4.4) under time-periodic excitation but with lower frequency. We show that in this system there occur reversible and repeatable energy exchanges between the granular chains of the network, in the form of nonlinear beat phenomena involving traveling discrete breathers. As this is a strongly nonlinear dynamical system, its dynamics depend critically on energy and the system parameters. We study systematically the influence on the nonlinear recurring energy exchanges of the amplitude and frequency of the applied time-periodic excitation. Furthermore, we show that it is possible to achieve passive wave redirection in this granular network by inducing the Landau-Zener effect (in space) through gradual stratification of the elastic foundation of the directly excited granular chain. Complex nonlinear dynamical phenomena occur when the elastic foundation stratification is introduced, with the majority of the energy of the system is irreversibly transferred from the excited chain to the absorbing chain. The resonance capture mechanisms governing these effects are investigated in detail and the robustness of these phenomena to the system parameters is investigated.

The system considered is identical to the network in Figure 4.4, but the excited chain is forced by a periodic series of half-sine pulses, or, equivalently, by the force $\tilde{F}(t) = \tilde{F}_0 \sin(2\pi f t) H(\sin(2\pi f t))$ where $H(\cdot)$ denotes the Heaviside function, $\tilde{F}_0$ the amplitude of the force and f its frequency in Hz. The dimensional equations of motion, which are the same as equations (4.8) except the external forcing term in the first excited particle equation, can be

normalized by dividing each equation by the common mass of the beads, m, and introducing the rescalings

$$x_i \to \frac{u_i}{R}, \ y_i \to \frac{v_i}{R}, \ \tau = \frac{t}{\sqrt{A}}, \ k_{1,2} = \frac{A\tilde{k}_{1,2}}{m}, \ \gamma_{1,2} = \frac{\sqrt{A}\tilde{\gamma}_{1,2}}{m}, \ F_0 = \frac{A\tilde{F}_0}{mR} \ \text{and} \ \beta = 2\pi f \sqrt{A}$$

where the scaling factor is defined as $A = \frac{2\sqrt{2}\pi\rho R^2(1-v^2)}{E}$. Then the nondimensional equations of motion for this system can be expressed in the following form,

$$
\begin{aligned}
\frac{d^2 x_1}{d\tau^2} &= -(x_1 - x_2)_+^{3/2} - k_2(x_1 - y_1) - k_1 x_1 - \gamma_2(\dot{x}_1 - \dot{y}_1) - \gamma_1 \dot{x}_1 + + F_0 \sin(\beta\tau) H(\sin(\beta\tau)) \\
\frac{d^2 x_i}{d\tau^2} &= [(x_{i-1} - x_i)_+^{3/2} - (x_i - x_{i+1})_+^{3/2}] - k_2(x_i - y_i) - k_1 x_i - \gamma_2(\dot{x}_i - \dot{y}_i) - \gamma_1 \dot{x}_i, \\
&\quad i = 2,3,\ldots \\
\frac{d^2 y_1}{d\tau^2} &= [-(y_1 - y_2)_+^{3/2}] - k_2(y_1 - x_1) - k_1 y_1 - \gamma_2(\dot{y}_1 - \dot{x}_1) - \gamma_1 \dot{y}_1 \\
\frac{d^2 y_i}{d\tau^2} &= [(y_{i-1} - y_i)_+^{3/2} - (y_i - y_{i+1})_+^{3/2}] - k_2(y_i - x_i) - k_1 y_i - \gamma_2(\dot{y}_i - \dot{x}_i) - \gamma_1 \dot{y}_i \\
&\quad i = 2,3,\ldots
\end{aligned}
\tag{4.22}
$$

where the variables x_i and y_i denote the normalized displacements of the $i-th$ beads of the excited and absorbing chains, respectively, and the new normalized time variable τ is introduced. These equations indicate the important system parameters governing the nonlinear dynamics.

4.3.1 Propagating breathers and recurring nonlinear energy transfers

Passive nonlinear targeted energy transfer in the weakly coupled and undamped granular network of Figure 4.4 due to an initial impulse applied in the excited chain has been studied by Hasan et al. (2013). It was shown that travelling breathers could be initiated in both chains, resulting in nearly complete but reversible energy exchanges between the excited and absorbing chains. Based on these results, it was possible to achieve irreversible energy transfer from the excited to

the absorbing chain by inducing the macroscopic analog (in space) of the Landau-Zener quantum tunneling effect (in time); to achieve this a stratification (spatial variation) of the elastic foundation of the excited chain and/or the weak coupling between chains was introduced. The main focus of the present work is to investigate if similar phenomena can be obtained in the periodically forced and damped network, given the added complexity introduced by the continuous source of incoming energy in the system. Based on the results of Hasan et al. (2013), a basic prerequisite for achieving intense (reversible or irreversible) energy transfers between the two chains is the formation of propagating breathers in the system under periodic forcing. Hence, a first goal of our study is to investigate the efficacy of this type of nonlinear response in the granular network.

We analyze the frequency responses of the coupled granular chains by applying a periodic series of half-sine pulses to the excited chain, cf. equations (4.22). However, and contrary to Hasan et al. (2013), instead of the transient response we focus on the steady-state response of this granular network, i.e., on the dynamics that is eventually reached after sufficiently long time so that the initial transients have died out. Hence, unless otherwise noted a total simulation time period of $t_{total} = 50/f$ is selected. As mentioned previously, the strongly nonlinear dynamics of the coupled granular network is not re-scalable with energy, so the results are expected to depend on the input energy induced by the applied force. Taking this into account, a systematic computational study is performed to investigate the steady-state nonlinear response of the network by considering the input energy provided by each cycle of the applied excitation and considering the limiting stationary values of this input of energy per cycle. Indeed, by varying the force amplitude $\tilde{F}_0$ and frequency f we seek stationary stable steady-state responses of the network, signified by constant or periodically varying limiting levels of this input energy as the

132

normalized time increases. This indicates that the network has reached a stable steady state which is then explored in more detail.

To calculate the input energy during each cycle of the applied force, we consider the input power as the product of the velocity of the first bead of the excited chain and the applied force. Then the input energy applied by the $n-th$ half-sine pulse can be evaluated as follows (cf. Figure 4.9a),

$$E_n^{(1)} = \int_{nT}^{(n+1)T} \tilde{F}(t) \frac{du_1(t)}{dt} \, dt \, , \quad n = 0,1,2,... \tag{4.23}$$

where $T = 1/f$ is the period of the excitation and the integrand denotes the power input by the $n-th$ half-sine pulse. As an example, the case with $\tilde{F}_0 = 23.1 \, N$ and $f = 51.52 \, Hz$ is considered in Figure 4.9b where we depict the power input by the series of half-sine pulses, as well as the discrete values of input energy $E_n^{(1)}$ as computed by (4.23). In this specific example we note that the input energy per cycle tends to a constant stationary limit as the number of cycles (or time) increases, indicating that a stable steady-state response of the network has been reached.

To systematically investigate the stationary sets of $E_n^{(1)}$ for $n \gg 1$ and varying forcing parameters we study numerically their variation by defining the following two measures,

$$\Delta E^{(1)} = max_{n \geq n_c \gg 1}\{E_n^{(1)}\} - min_{n \geq n_c \gg 1}\{E_n^{(1)}\} \tag{4.24}$$

as well as its average in the limit of large number of cycles:

$$\bar{E}^{(1)} = \frac{1}{N} \sum_{n=n_c}^{n_c+N} E_n^{(1)} \tag{4.25}$$

133

In the above measures $n_c \gg 1$ represents the first cycle and N the total number of cycles considered in the computation. In our study we picked n_c and N sufficiently large (only the last third of the aforementioned time window of the simulations) in order to achieve fast convergence of the measures in the vicinity of the steady-state response of the network; this convergence is demonstrated in the discrete plot of $E_n^{(1)}$ versus n of Figure 4.9. When the convergence measure $\Delta E^{(1)}/\bar{E}^{(1)}$ reached a value below a small set tolerance, it was deemed that a stable steady state was reached and further analysis of that steady state could be initiated. It should be clear that the steady state could only be reached for specific pairs of frequency and amplitude of the harmonic excitation and the detection of these pairs was one of the main aims of this study.

We note that the previous procedure can be used to identify only stable steady-state periodic responses with the same frequency as the excitation (or period-one fixed points in the notation of discrete maps). These we denote as fundamental steady-state responses. However, subharmonic steady-state responses of the network can be similarly tracked by modifying the

discrete energy measure to $E_n^{(k)} = \displaystyle\int_{nkT}^{(n+1)kT} \tilde{F}(t)\, \frac{du_1(t)}{dt}\, dt$, $n = 0, 1, 2, ...,$ $k = 2, 3, ...$, i.e., by

computing the input energy to the granular network per k cycles of the input. Clearly, stationary values of $E_n^{(k)}$ would indicate stable responses of the network with periodicity equal to kT, i.e., with k periods of the excitation. This issue is not pursued further here, since the focus is placed on computing the fundamental steady-state responses of the granular network. In Chapter 5, we numerically prove the existence of such subharmonic resonances.
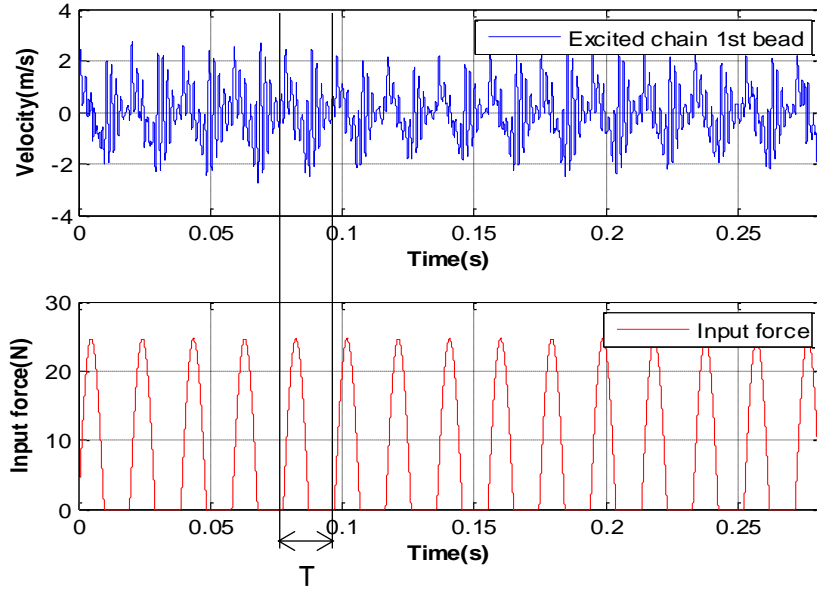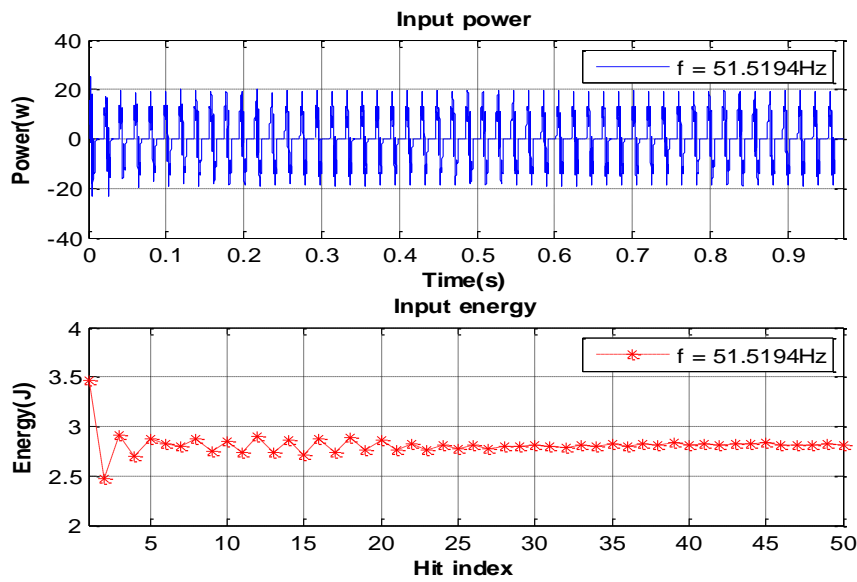
Figure 4.9. (a) Time series of the velocity of the first bead of the excited chain and of the periodic series of half-sine pulses (excitation), and (b) power (continuous in time) and energy $E_n^{(1)}$ (discrete in time) input by an applied force with parameters $\tilde{F}_0 = 23.1\ N$ and $f = 51.52\ Hz$ (ΔE indicates the tolerance for determining convergence to a steady state).
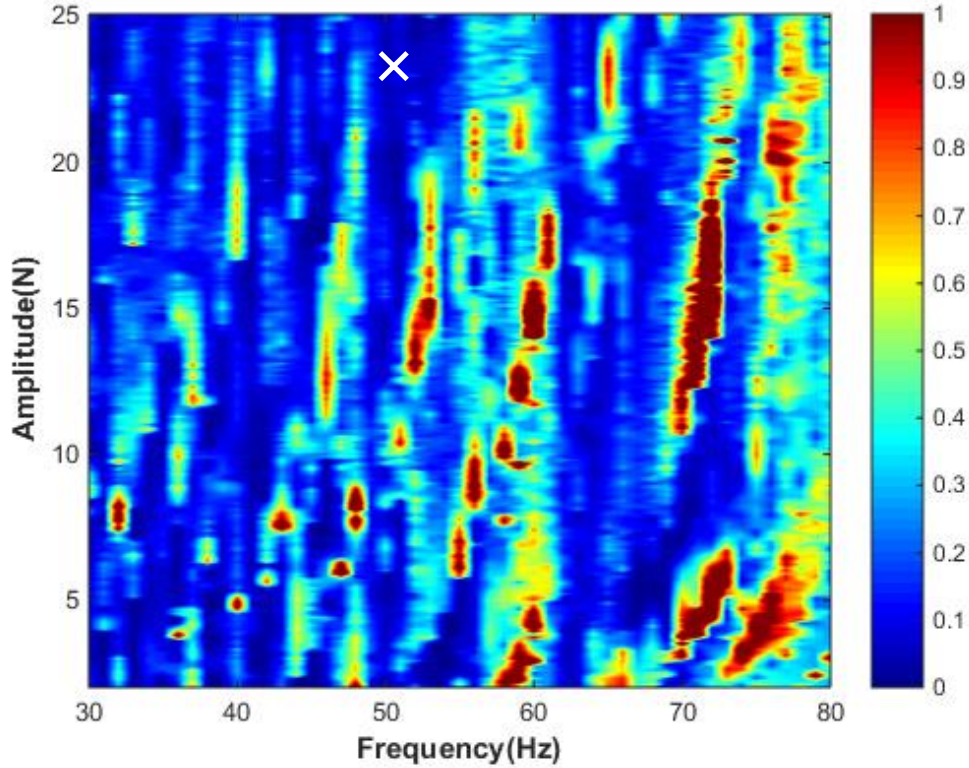
135

Contour plot of $\Delta E^{(1)}/\bar{E}^{(1)}$

Figure 4.10. Contour plot of the convergence measure $\Delta E^{(1)}/\bar{E}^{(1)}$ for varying forcing amplitude $\tilde{F}_0$ and frequency f for the granular network and maximum simulation time $t = 50/f$. Note the multiple local minima indicating the existence of multiple stable fundamental periodic responses. The case examined in detail in this and the next sections is indicated by ($\times$) (cf. Figures 4.11 and 4.12).

In Figure 4.10, we depict the contour plot of the convergence measure $\Delta E^{(1)}/\bar{E}^{(1)}$ of the granular network for varying forcing frequency in the range $30Hz \leq f \leq 80Hz$ and amplitude in the range $2N \leq \tilde{F}_0 \leq 25N$. This was computationally realized by considering $(10^3 \times 10^3)$ pairs $(\tilde{F}_0, f)$ in these ranges, simulating the dynamics of the network until steady state was reached and then evaluating the convergence measure. A convergence study was made by gradually increasing the total number of pairs $(\tilde{F}_0, f)$ in order to ensure the accuracy of the results. The specific ranges for $\tilde{F}_0$ and f were selected so that the corresponding strains in the beads were

136

constrained within the elastic limit of PDMS. In the contour plot of Figure 4.10 the multiple dark blue areas indicate local minima of variation of input energy at the steady state, which, in turn, indicate the existence of multiple stable steady-state fundamental responses. Moreover, we also deduce the existence of highly non-stationary steady responses represented as red areas where the granular network may exhibit quasi-periodic or even chaotic responses (in fact, the existence of this type of complex nonlinear dynamics is anticipated in the multi-degree-of-freedom, weakly coupled granular medium of Figure 4.4).

As an example of the strongly nonlinear dynamics of this system at a local minimum of the plot of Figure 4.10 we will focus on the stable fundamental periodic solutions for $\tilde{F}_0 = 23.1\ N$ and $f = 51.52\ Hz$. This corresponds to a nonlinear beating phenomenon involving propagating breathers in the two chains (Hasan et al., 2013), whereby there occurs recurring and nearly complete energy exchange between the excited and the absorbing chains. In Figure 4.11 we depict the spatio-temporal evolution of the instantaneous kinetic energy of each bead of the network after its dynamics has reached this fundamental steady-state response. Only the 40 leading beads of each chain are considered in that plot, and the results for the excited and absorbing chains are depicted separately, along with the time series of the applied force shown at the most left of the figure.
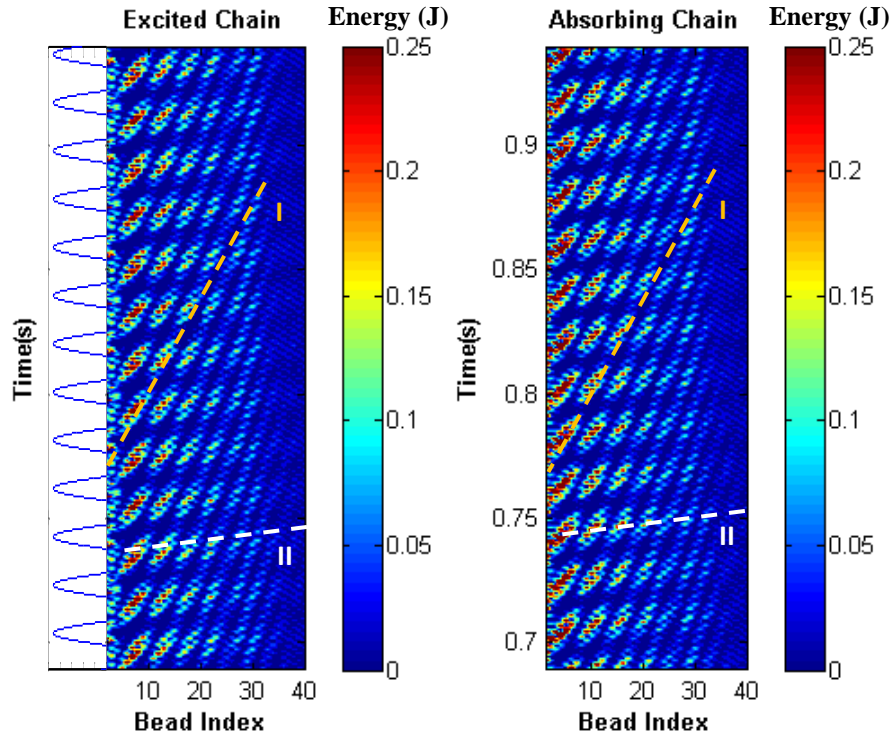
Figure 4.11. Spatio-temporal evolutions of instantaneous kinetic energies of the leading 40 beads of the excited and absorbing chains, showing nonlinear beats involving recurring energy exchanges between propagating breathers in the two chains; contour plots of kinetic energies are depicted at the steady state (for $t \geq 0.7s$) when the initial transients have died out (Lines I and II indicate the two characteristic speeds of the recurring breather formation).

Certain conclusions can be drawn based on the results of Figure 4.11. First, strong and recurring energy exchanges are noted, in the form of sequential series of nonlinear beats in terms of propagating breathers in both chains. Second, a synchronization of each applied pulse with each generated breather in the excited chain is noted, indicating the occurrence of phase locking in the dynamics. In fact, the 1:1 correspondence between each applied force pulse and a propagating breather in the excited chain signifies the realization of 1:1 resonance in the dynamics. We note at this point that as shown in Hasan et al. (2013), where a single impulse excitation was considered, the propagating breathers in the excited and absorbing chains are in

the form of fast oscillations with identical (fast) frequencies (which are influenced by the stiffness of their elastic substrates), modulated by slowly varying envelopes. Third, after the application of each forcing pulse, there occurs a periodic, nearly complete but reversible energy exchange between the two chains. At the beginning of each of these exchanges, the entire input energy is localized in the excited chain, but as time progresses, nearly all of this energy is transferred to the absorbing chain. After a period of the nonlinear beat the energy is transferred back to the excited chain, after which this type of strong energy exchange cycle repeats. Considering the plots of Figure 4.11, clear energy exchange can be seen between the initial beads of the excited and absorbing chains; for the later beads of both chains, energy exchange fades because of the energy dissipation due to bead-to-bead and bead-to-elastic foundation interactions (cf. equation (4.22)). Finally, we note that during the occurrence of the nonlinear beats the energy propagates towards the far field of both chains (albeit with diminishing intensity due to dissipation), which indicates that this regime of propagating breathers takes place in the frequency pass band of the network (Hasan et al., 2015).

There are two characteristic speeds of wavepacket transmission in the steady-state responses depicted in Figure 4.11. The smaller of the two speeds (which can be viewed as a slow local speed of wave propagation) corresponds to the propagation of each of the breathers that are generated after the application of each pulse of the periodic force. This can be estimated by the slope with respect to the vertical of lines I in the plots of Figure 4.11 and can be analytically estimated using a complexification/averaging approach similar to the one formulated in Hasan et al. (2013), where the case of a single forcing impulse was considered. The larger speed is associated with the propagation of coherent wavepackets in the network (and so it can be regarded as the fast non-local speed of wavepacket propagation). This high speed can be estimated by the
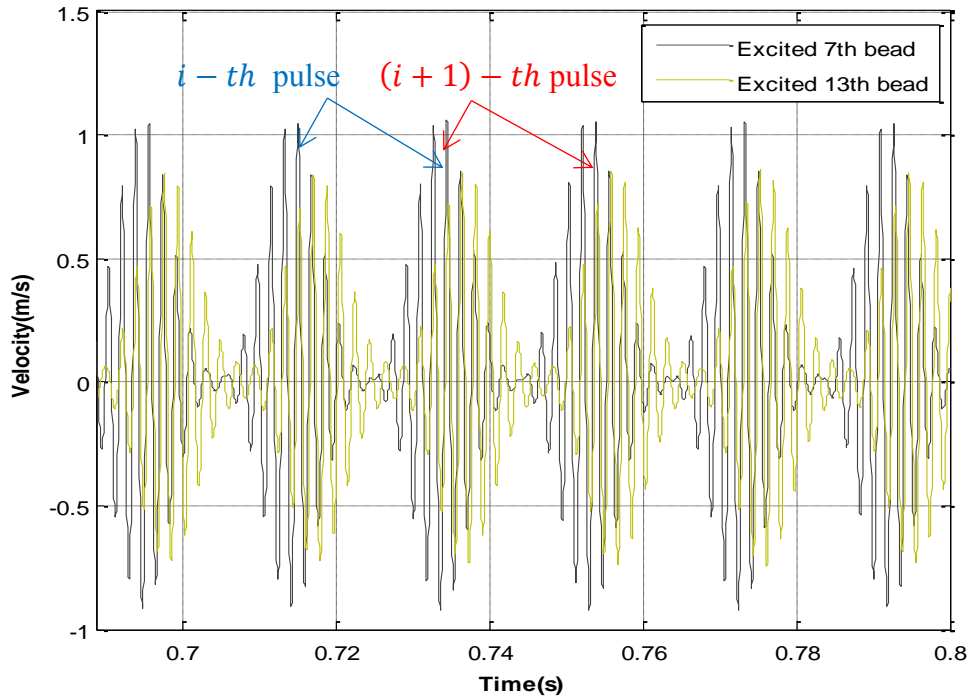
139

Figure 4.12. Steady-state velocities of the 7$^{\text{th}}$ and 13$^{\text{th}}$ beads of the excited chain.

slope of lines II in the plots of Figure 4, and corresponds to recurring (periodic) local maxima of energy localization in space and time in both the excited and absorbing chains. From the results of Figure 4.11 we note that these maxima occur starting with the 7$^{\text{th}}$ beads of the two chains and repeat every 6 beads, namely at the 13$^{\text{th}}$, 19$^{\text{th}}$,… beads. To gain insight into this fast coherent wavepacket propagation we focus on the steady-state responses of the 7$^{\text{th}}$ and 13$^{\text{th}}$ beads of the chains presented in Figure 4.12. Repeatable beating phenomena can be clearly viewed in the response of each bead. Moreover, the input energies imparted to the network by the $i - th$ and $(i + 1) - th$ half-sine pulses of the periodic force reach the 7$^{\text{th}}$ and 13$^{\text{th}}$ beads almost simultaneously. Clearly, this indicates an additional synchronization or phase-locking effect in the dynamics, and hints at a secondary resonance effect. The end result (which can also be inferred from the plots of Figure 4.11) is the steady-state fast propagation of energy quanta (or

140

coherent wavepackets) in the network. Note that the time for energy propagation from the 7th to the 13th bead remains unchanged during the time window of the simulation, indicating that the steady-state dynamics has been reached.

To further highlight the nature of the resonance phenomena that give rise to the formation of the breather in the periodically forced granular network, in Figure 4.13 we depict the fast Fourier transform of the velocity time series of the 7th bead of the excited chain. We deduce that the forced propagating breather is realized due to the closeness of three fast frequencies: (i) The frequency of the in-phase mode of each of the granular chains on its linear elastic foundation, $f_1 = (k_1/m)^{1/2}/2\pi = 515.9 \, Hz$ in our case; (ii) the energy-dependent main frequency of the breather characterizing the nonlinear granular interactions between adjacent beads, $f_2 = 567.4 \, Hz$; and (iii) the frequency of the out-phase mode of each of the granular chains, $f_3 = 618 \, Hz$. It turns out that the differences between these fast frequencies, $f_2 - f_1$ and $f_3 - f_2$, are equal to the slow frequency, f_{slow}, of the slow modulation of the developing breather, which in itself is equal to the slow frequency, f, of the applied periodic excitation. It follows that the propagating breather is realized when the slow frequency of the periodic excitation, f, equals the frequency of the slow modulation of the breather, i.e., $f = f_{slow}$, or, equivalently, when $f_2 - f_1 = f_3 - f_2 = f$. Hence, the forced steady state breather is realized when the slow frequency of the force excitation is equal to the differences between the aforementioned fast frequencies of the breather, i.e., when a combination resonance is realized in the granular network. A rigorous mathematical analysis of this resonance interaction will be performed in Chapter 5.

The results presented in this section demonstrate that strong energy transfers between the excited and absorbing chains of the network take place. These are realized at special discrete

amplitude-frequency pairs of the applied force, and take the form of propagating breathers in both chains. The resulting recurring and almost complete energy transfers between the two chains are generated by nonlinear resonances in the dynamics and are associated with phase locking and synchronization phenomena in the steady-state responses. In the next section we introduce a modification in the network, with the aim to achieve irreversible targeted energy transfer from the excited to the absorbing chain. As a result we will demonstrate that passive wave (or energy) redirection can be achieved in the periodically forced network of Figure 4.4.
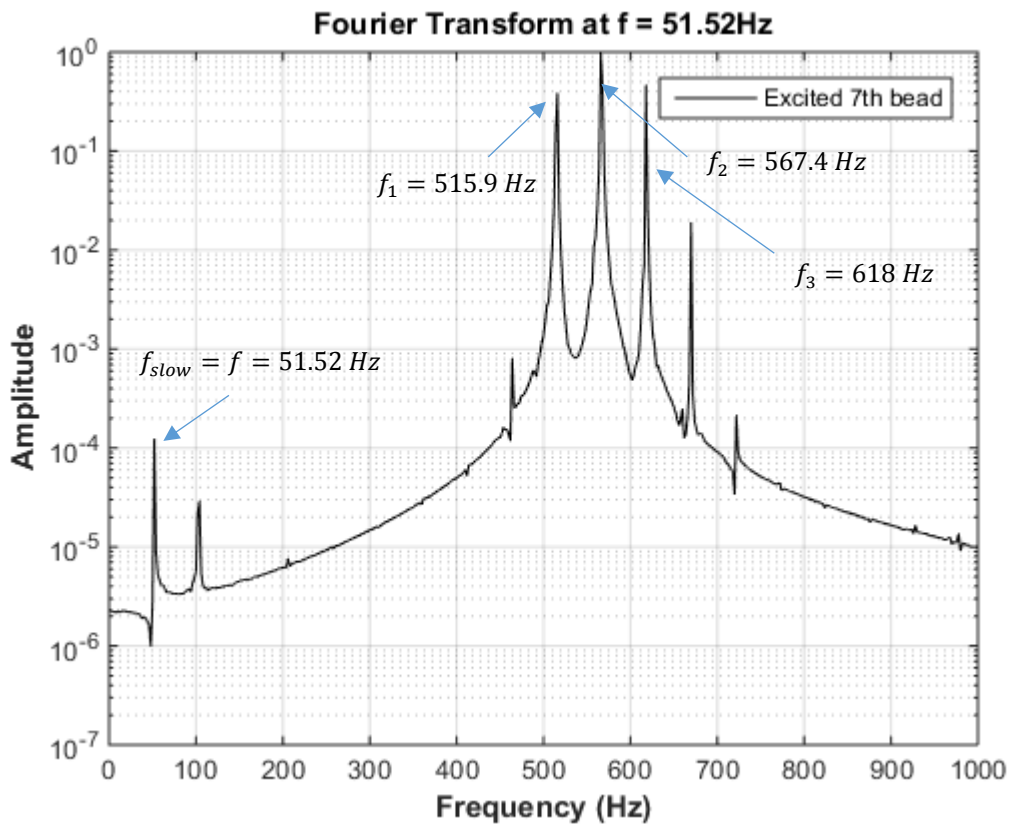
Figure 4.13. Fourier spectrum of the velocity time series of the 7th bead of the excited chain.

4.3.2 Targeted energy transfer and passive wave redirection

Motivated by the nonlinear beat phenomenon of Figure 4.11 where nearly complete but reversible energy exchanges between the two granular chains is realized, the following question naturally arises: Is it possible to structurally modify the granular network so that irreversible or targeted energy transfer from the excited to the absorbing chain is achieved, and thus passively redirect the propagating breathers to the indirectly excited part of the network? This question was first answered successfully in Hasan et al. (2013), where the transient dynamics of the same network was examined but for a single applied impulse excitation and no damping. This was performed by introducing finite spatial stratification (variation) of the elastic foundation of the excited chain (although the same effect could be achieved by stratification of the weak coupling between the chains).

The macroscopic analog of the LZT quantum effect (in time) was first studied by Kosevich et al. (2010) and Manevitch et al. (2011) in a system of two weakly coupled pendula with the length of one of the pendula varying with time. Interestingly enough, it has been proven that this macro-system has similar governing equations to those of a quantum system with the LZT effect (Kosevich et al., 2010; Manevitch et al., 2011; Kovaleva et al., 2011), proving that LZT can be realized in systems of coupled oscillators as well, with the analysis carried out in the spatial domain rather than the time domain. In the physics community LZT is known as a dynamical transition where a quantum system tunnels across an energy gap between two anti-crossed energy states (Zener, 1932; Razany, 2003). Such quantum LZT was studied in semiconductor superlattices for electrons, optical lattices for ultracold atoms and Bose-Einstein condensates (Anderson and Kasevich, 1998; Rosam et al., 2003; Sias et al., 2007). The non-adiabatic LZT effect leads to irreversible and almost unidirectional exchange of energy between

two states excited by external forcing or perturbation. The aforementioned energy exchange is suitable for oscillating systems, and one particular application is the weakly coupled granular chain system considered herein. In this system, the vibration energy induced by the periodic force input which is initially localized in the excited chain can then be irreversibly redirected to the absorbing chain. Motivated by the results of Hasan et al. (2013) we proceed to introduce a structural modification to the network of Figure 4.4 in order to achieve targeted energy transfer and passive wave redirection under periodic excitation.

Spatial stratification of stiffness elements in the network is more practical in implementation in metamaterial design, and therefore is selected in the present study. Moreover, this design enabled the implementation of the LZT effect in the impulsively forced network. Accordingly, in the following analysis, we keep the elastic foundation of the absorbing chain homogenous while spatially decreasing the stiffness of the elastic foundation of the excited chain from bead to bead by a certain percentage. According to the results of Hasan et al. (2013) this structural modification should be sufficient for inducing the LZT effect in the dynamics of the network. Revisiting the results of Figure 4.11 we note that it takes up to 4 beads for the excited chain to pass the initial transient phase, after which the propagating breather is fully developed and complete and reversible energy exchange is initiated. The dynamics in this initial transient phase is critical to the formation of reversible energy change in later beads. Hence, we will introduce spatial stratification of the stiffness of the elastic foundation supports of the leading four beads of the excited chain and express the normalized equations of motion as follows,

144

$$\frac{d^2 x_1}{d\tau^2} = -(x_1 - x_2)_+^{3/2} - k_2(x_1 - y_1) - (1 - s_1)k_1 x_1 - \gamma_2(\dot{x}_1 - \dot{y}_1) - \gamma_1 \dot{x}_1 + F_0 \sin(\beta\tau) H\big(\sin(\beta\tau)\big)$$

$$\frac{d^2 x_i}{d\tau^2} = [(x_{i-1} - x_i)_+^{3/2} - (x_i - x_{i+1})_+^{3/2}] - k_2(x_i - y_i) - (1 - s_i)k_1 x_i - \gamma_2(\dot{x}_i - \dot{y}_i) - \gamma_1 \dot{x}_i , \quad i = 2,3,...$$

$$\frac{d^2 y_1}{d\tau^2} = [-(y_1 - y_2)_+^{3/2}] - k_2(y_1 - x_1) - k_1 y_1 - \gamma_2(\dot{y}_1 - \dot{x}_1) - \gamma_1 \dot{y}_1$$

$$\frac{d^2 y_i}{d\tau^2} = [(y_{i-1} - y_i)_+^{3/2} - (y_i - y_{i+1})_+^{3/2}] - k_2(y_i - x_i) - k_1 y_i - \gamma_2(\dot{y}_i - \dot{x}_i) - \gamma_1 \dot{y}_i , \quad i = 2,3,...$$

(4.26)

where the spatial stratification parameter or spatial detuning parameter is defined as

$$s_i = \begin{cases} (i-1)s, & i = 1, 2, 3 \\ 3s, & i \geq 4 \end{cases}$$

(4.27)

and s is the spatial stratification (reduction) rate of the stiffness of the elastic foundation of the excited chain, which is chosen to be a constant in this study. It will be shown below that the spatial detuning parameters s_i, $i = 1,2,3$ have significant influence on the realization of the LZT effect and targeted energy transfer in the network.

In Figure 4.14 we present the spatial dependence of the stiffness variation that we use for the following analysis. The reduction of the stiffness parameter in space is discrete. The gradual spatial reduction rate, s, of the stiffness of the elastic foundation of the leading four beads of the excited chain is varied between 0% (for the case of an unstratified, homogeneous foundation) and the limit of 33% (maximum possible spatial stratification), since if s is larger than that value the foundation stiffness for the fourth bead of the excited chain will become negative, which is unphysical. We study the effect of the spatial stratification rate on the intensity of targeted energy transfer from the excited to the absorbing chain by computing the total kinetic energies of the

excited and absorbing chains starting from beads with $i \geq 5$, i.e., after the spatial stratification of the elastic foundation of the excited chain has been completed.
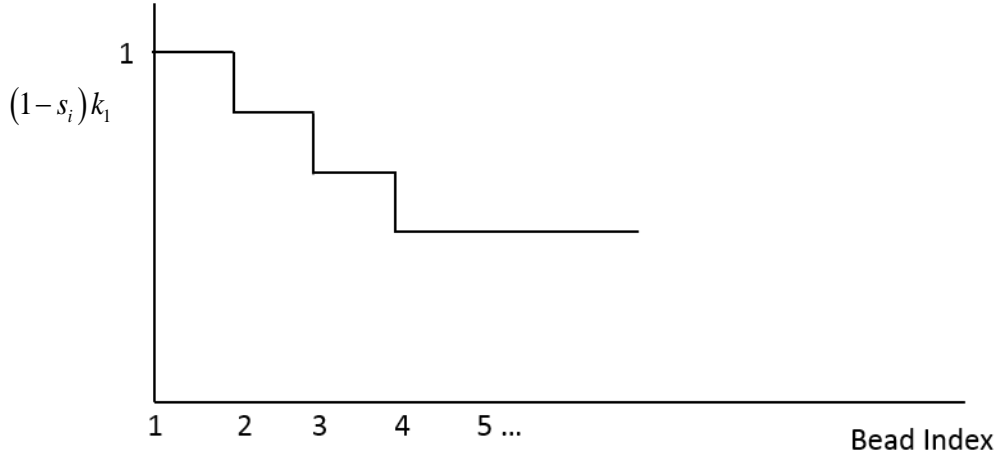

Figure 4.14. Discrete spatial stratification of the stiffness of the elastic foundation of the excited chain.

For certain stratification rates, the dynamics of the periodically forced stratified granular network can reach a steady state (as in the unstratified network discussed in the previous section), but it may take longer than in the unstratified network. In the following computational study we double the normalized simulation time to $t_{total} = 100/f$. Moreover, given the complexity of the nonlinear dynamics, steady state cannot be reached for every value of the spatial reduction rate, so we introduce the following energy measures for the excited and absorbing chains based on the instantaneous kinetic energies $T_{exc}(t)$ and $T_{abs}(t)$, respectively:

$$\bar{E}_{exc} = \frac{1}{t_{total}} \int_0^{t_{total}} T_{exc}(t) \ dt, \qquad \bar{E}_{abs} = \frac{1}{t_{total}} \int_0^{t_{total}} T_{abs}(t) \ dt \qquad (4.28)$$

These measures denote the kinetic energies of the excited and absorbing chains averaged over the total time of numerical simulation of the dynamics. It follows that by computing the ratio

$\bar{E}_{abs}/\bar{E}_{exc}$ between these two averaged kinetic energy measures we derive a scalar normalized energy measure that describes the intensity of targeted energy transfer (and passive wave redirection) in the stratified granular network at the steady state. In fact, by its definition, the greater this ratio is the more complete the targeted energy transfer from the excited to the absorbing chain is.

In Figure 4.15 we depict the averaged kinetic energy ratio $\bar{E}_{abs}/\bar{E}_{exc}$ as a function of the spatial stratification rate s, for network and forcing parameters corresponding to the local minimum of Figure 4.10 with corresponding responses presented in Figure 4.11. An initial observation is that in the unstratified network (corresponding to $s = 0\%$) the average kinetic energies of the two chains are almost identical. This is in agreement with the fact that a nonlinear beat of propagating breathers develops in the unstratified network resulting in repetitive and near-complete energy transfers between the two chains. This leads to near-equi-partition of the averaged kinetic energy between the excited and absorbing chains. As the spatial stratification rate increases from zero, energy equi-partion is nearly preserved (e.g., point III) until a sudden transition to targeted energy transfer occurs at $s \approx 26\%$ (point II), with a global maximum of the averaged kinetic energy ratio realized immediately after this transition at $s \approx 27\%$ (point I). The global maximum signifies the realization of intense passive targeted energy transfer from the excited to the absorbing chain and eventual localization of the energy in the absorbing chain. This implies passive wave redirection from the excited chain where the response initially develops to the absorbing chain through the implementation of the LZT effect in space under periodic excitation; as a result the nonlinear beat phenomenon of Figure 4.11 is eliminated, recurring energy exchange between the two chains is eliminated, and a propagating breather in the excited chain results. Obviously, two very different nonlinear dynamical steady states occur before and

after the sudden transition of Figure 4.15, and these steady states are studied separately in detail below.
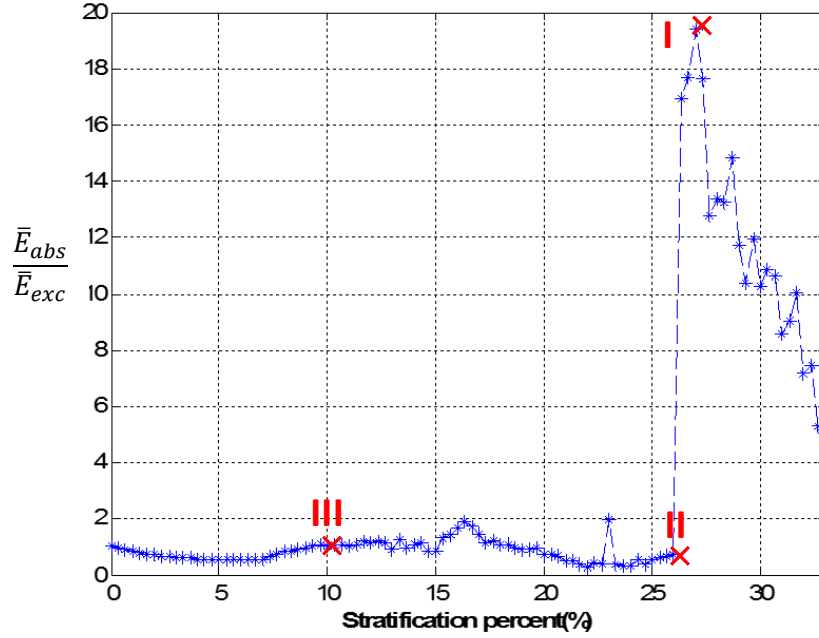

Figure 4.15. Ratio of averaged kinetic energies in the stratified granular network as function of spatial stratification rate of the elastic foundation of the leading four beads of the excited chain; points I, II and III refer to the cases discussed in detail.

In Figure 4.16, we depict the time series of the total instantaneous kinetic energies of the excited and absorbing chains for beads with $i \geq 5$ with $s = 26\%$ (Figure 4.16a) and $s = 27\%$ (Figure 4.16b). Given the highly oscillatory nature of this data and the trends of energy transmission in, and exchange within, the chains, we also compute a moving-average energy to smooth the energy time series. These are defined as follows,

$$E_{wa,exc}(t) = \frac{1}{t_w} \int_{t-\frac{t_w}{2}}^{t+\frac{t_w}{2}} T_{exc}(\tau)\ d\tau, \quad E_{wa,abs}(t) = \frac{1}{t_w} \int_{t-\frac{t_w}{2}}^{t+\frac{t_w}{2}} T_{abs}(\tau)\ d\tau \quad (4.29)$$

148
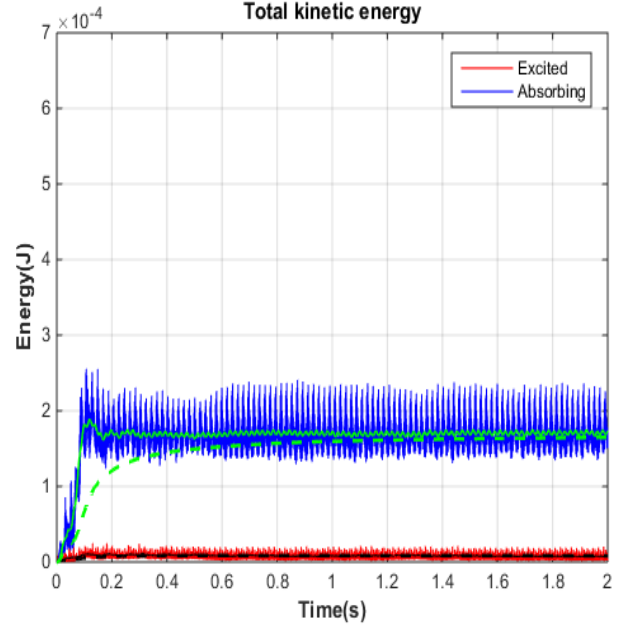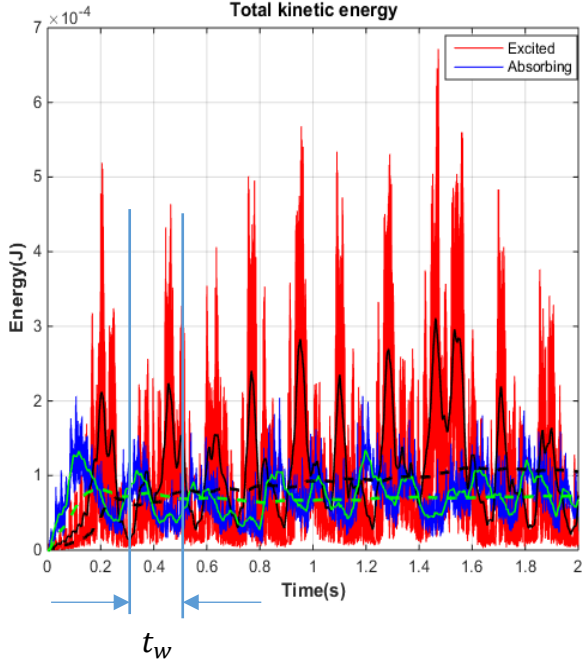
Figure 4.16. Time series of total instantaneous kinetic energies of the excited (red line) and absorbing (blue line) chains for beads with $i \geq 5$: (a) $s = 26\%$ (point II in Figure 4.15), (b) $s = 27\%$ (point I in Figure 4.15); moving-average kinetic energies are denoted by black and green solid lines for the excited and absorbing chains, respectively, whereas averaged kinetic energies are denoted by black and green dashed lines for the excited and absorbing chains, respectively.

where t_w is the length of chosen moving time window, which is $0.025 sec$ in our case. These moving-average energies are superimposed in Figure 4.16 as black and green solid lines, respectively, for the excited and absorbing chains. Satisfactory agreement between the moving-average energy and real time energy is inferred from Figure 4.16. In addition, the averaged kinetic energies,

$$E_{a,exc}(t) = \frac{1}{t}\int_0^t T_{exc}(\tau)\ d\tau, \qquad E_{a,abs}(t) = \frac{1}{t}\int_0^t T_{abs}(\tau)\ d\tau \qquad (4.30)$$

149
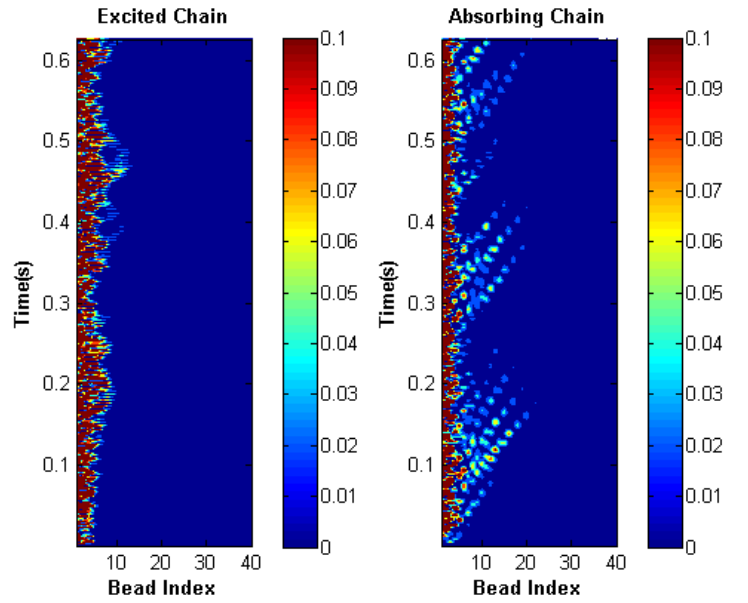
(a)
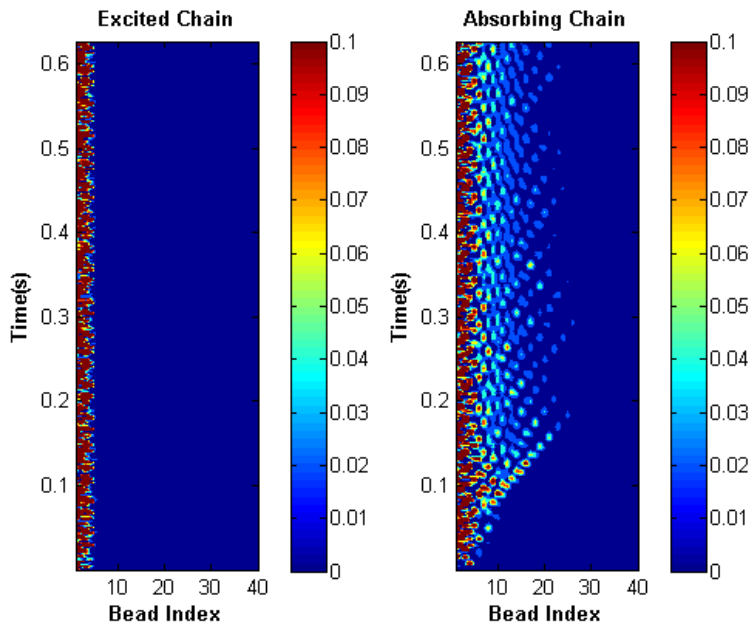
(b)

Figure 4.17. Spatio-temporal evolutions of instantaneous kinetic energies of the leading 40 beads of the excited and absorbing chains for (a) $s = 26\%$ in the regime of strong energy exchanges and (b) $s = 27\%$ in the regime of targeted energy transfer and passive wave redirection.

are also computed and are depicted as black and green dashed lines in the plots of Figure 4.16. Clearly, the constant limits of the averaged values correspond to the previous energy measures $\bar{E}_{exc}$ and $\bar{E}_{abs}$ whose ratio is presented in Figure 4.15.

Additional interesting conclusions can be drawn from Figure 4.16 considering the completely different temporal dependence of the kinetic energies for $s = 26\%$ (in the regime of strong energy exchanges between chains) and $s = 27\%$ (in the regime of targeted energy transfer and passive wave redirection). In Figure 4.16a energy exchange is observed, while energy localization is seen in Figure 4.16b. The energy plot in Figure 4.16b proves that it is possible to localize the energy in the absorbing chain so that the energy does not transfer back to the excited chain by LZT. These conclusions corroborate the spatio-temporal kinetic energy evolutions in the two chains (Figure 4.17) for $s = 26\%$ and $s = 27\%$, where wave redirection is noted in the latter case. The rapid decay of the transmitted breathers in the absorbing chain is due to viscous dissipation in the system.

4.3.3 Empirical mode decomposition and resonance captures

We now study in detail the nonlinear dynamics governing targeted energy transfer in the stratified network by analyzing the time series using empirical mode decomposition and demonstrating the occurrence of 1:1 nonlinear resonance capture in the dynamics at the spatial stratification rate of $s = 27\%$ (point I in Figure 4.15). This will prove to be the basic nonlinear dynamical mechanism governing passive targeted energy transfer in the granular network. The empirical mode decomposition (EMD), proposed by Huang et al. (1998), combined with the numerical Hilbert transform (HT), is a powerful method for decomposing oscillatory time series into a finite basis of nearly orthogonal, monochromatic oscillatory intrinsic mode functions (IMFs) each capturing

a characteristic time scale of the time series; moreover, linear superposition of the IMFs reconstructs the time series. EMD is highly suitable for applications involving nonlinear and nonstationary processes where typical linear signal analysis methods fail to capture the underlying nonlinear dynamics. In particular, EMD decomposes an oscillatory signal, $z(t)$, by using the so-called sifting algorithm consisting of the following steps:

(i) Determine all extrema of $z(t)$.

(ii) Compute two envelopes, $e_{min}(t)$ and $e_{max}(t)$, by spline interpolating the minima and maxima of the signal.

(iii) Compute the average curve between the two envelopes, $R(t) = \left(e_{max}(t) + e_{min}(t)\right)/2$.

(iv) Extract the remainder signal, $c(t) = z(t) - R(t)$.

(v) Iterate through steps (i)-(iv) until $R(t)$ is less than a prescribed tolerance, ε.

Upon satisfying these criteria, the remainder signal $c_1(t)$ is regarded as the first IMF of the original signal $z(t)$ and possesses the highest frequency. By taking the difference of the original signal and the extracted IMF, $z_1(t) = z(t) - c_1(t)$, and applying the sifting algorithm iteratively to this new signal, we can extract additional IMFs with ever decreasing frequencies. Thus, we can sequentially decompose, from high to low frequencies, the original signal into N IMFs or nearly orthogonal components that satisfy the condition

$$z(t) = \sum_{i=1}^{N} c_i(t) + R_{N+1}(t), \quad R_{N+1}(t) < \varepsilon \tag{4.31}$$

It should be noted that this process can result in spurious IMFs that do not have any physical meaning and it is necessary to disregard them. In that regard, the wavelet transform can be used to determine the temporal variation of the basic harmonic components of the signal, and to identify the physically meaningful IMFs by comparing their frequency contents to the results of the wavelet transform. Finally, an amplitude and a phase can be extracted from each physical IMF by creating an associated complex analytic signal. To this end, let $c_{i,m}^k(t)$ be the kth IMF of the $i-th$ bead of the $m-th$ chain (with $m=1$ being the excited chain and $m=2$ the absorbing one). Then its Hilbert transfrom, $\mathcal{H}[c_{i,m}^k(t)]$, is defined as

$$\mathcal{H}[c_{i,m}^k(t)] \triangleq \frac{\text{PV}}{\pi} \int_{-\infty}^{\infty} \frac{c_{i,m}^k(t)}{t-s} ds \qquad (4.32)$$

where $\mathcal{H}[\cdot]$ is the Hilbert transform and PV implies the Cauchy principal value of the integral. We form the complex analytic signal,

$$\psi_{i,m}^k(t) \equiv c_{i,m}^k(t) + j\mathcal{H}[c_{i,m}^k(t)] \qquad (4.33)$$

where $j^2 = -1$. Following this construction we may define an instantaneous amplitude $A_{i,m}^k(t)$ and an instantaneous phase $\theta_{i,m}^k(t)$ for the IMF $c_{i,m}^k(t)$ as follows:

$$A_{i,m}^k(t) = \sqrt{\left(c_{i,m}^k(t)\right)^2 + \left(\mathcal{H}[c_{i,m}^k(t)]\right)^2}, \qquad \theta_{i,m}^k(t) = \tan^{-1}\left(\frac{\mathcal{H}[c_{i,m}^k(t)]}{c_{i,m}^k(t)}\right) \qquad (4.34)$$

As shown below, when these quantities are slowly varying (compared to the fast-varying oscillations at the basic frequency of the IMF), they characterize the slow flow of the underlying dynamical process and can help us detect sustained resonance interactions between harmonics of the bead responses in the regime of targeted energy transfer.

(a)   (b)
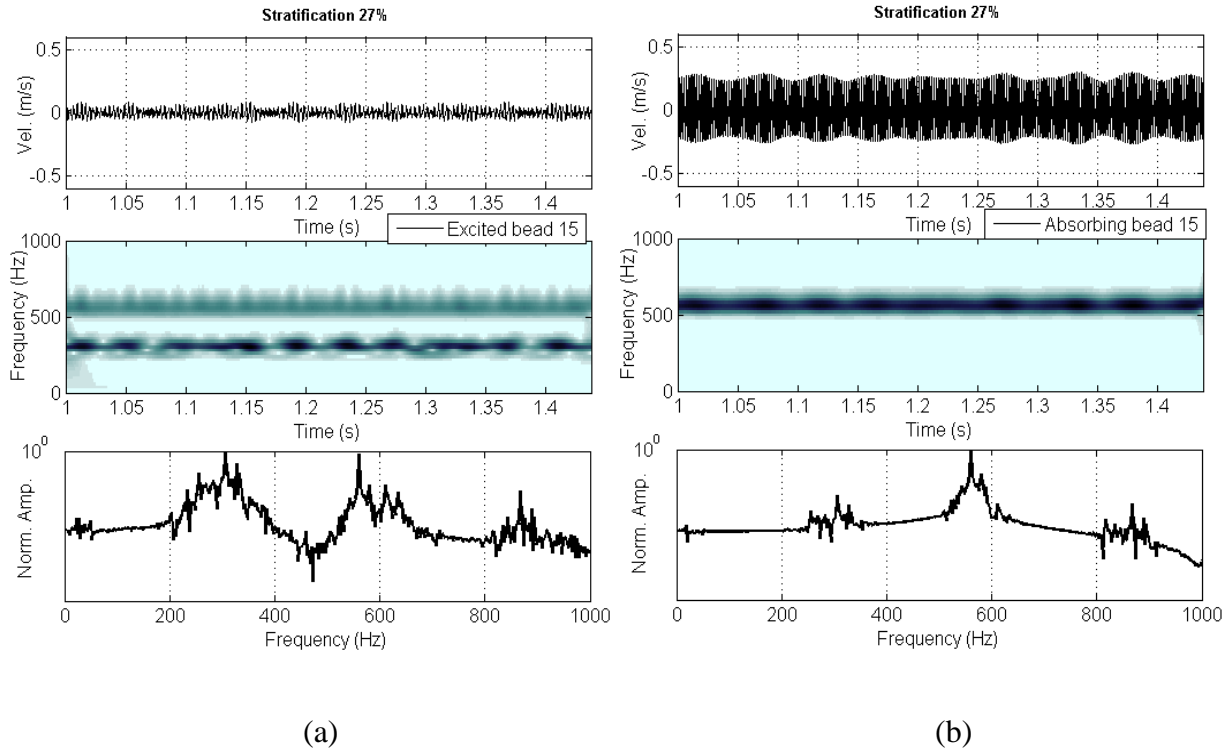
Figure 4.18. Regime of strong nonlinear targeted energy transfer and passive wave redirection (point I in Figure 4.15): Time series and wavelet transform /Fourier spectra of the velocity time series of the 15th beads of the (a) excited and (b) absorbing chains for $s = 27\%$.

As discussed in Vakakis et al. (2008), a resonance capture in the dynamics is associated with non-time-like behavior of a certain phase of the problem, and subsequent failure of the averaging theorem with respect to that "slow" phase (since for "fast" phases one can apply the averaging theorem with respect to each of them, and accordingly reduce the dimensionality of the dynamics). In the literature resonance captures have been examined based on the method of averaging (Zniber and Quinn, 2003), harmonic balance (Nandakumar and Chatterjee, 2004) or a complexification/averaging technique (Vakakis and Gendelman, 2000; Kerschen et al., 2005, 2007). In the neighborhood of a resonance manifold (Arnold, 1988), the direct averaging of the equations of motion over a slowly varying (non-time-like) phase variable cannot be applied;

154

therefore it is the existence of appropriately defined phase variables in the dynamics of a process that signifies the occurrence of resonance capture.
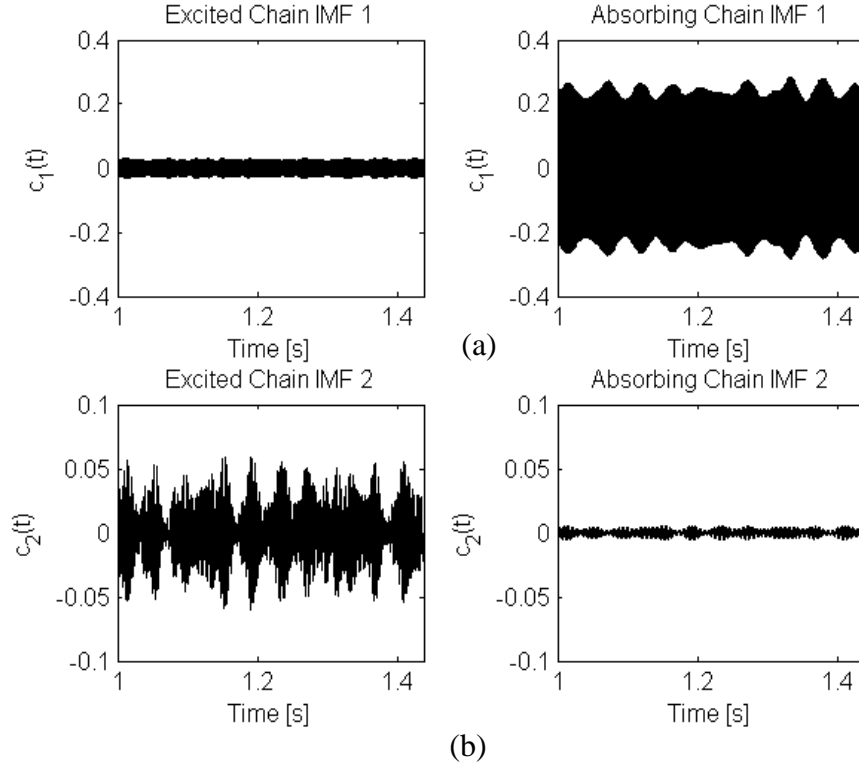
Figure 4.19. Dominant IMFs of the responses of Figure 4.18, (a) at 560 Hz and (b) at 300 Hz.

First we consider the steady-state velocity time series of the 15th beads of the excited and absorbing chains for the case of 27% spatial stratification rate, i.e., in the regime of nonlinear targeted energy transfer and the LZT effect. This case corresponds to the global maximum point I of $\bar{E}_{abs}/\bar{E}_{exc}$ in Figure 4.15. The responses together with their wavelet transform and Fourier spectra are depicted in Figure 4.18. For each time series, the two dominant IMFs at approximately 560 Hz and 300 Hz are depicted in Figure 4.19. Since the higher-frequency IMFs will be the most important for understanding the dynamical mechanism governing nonlinear targeted energy transfer in this case, we focus on these. Noting the large discrepancy of their amplitudes we deduce motion localization in the absorbing chain, signifying passive wave redirection;

155

moreover, we note that the envelopes of both IMFs are slowly varying, indicating the occurrence

of a sustained 1:1 resonance capture (Arnold, 1988) in the dynamics at that frequency.

To prove this, we study the slow-flow amplitudes and phases of the higher-frequency IMFs

through relations (4.32-4.34), and express the two higher-frequency IMFs of Figure 4.18a in the

complex form (4.33). Then we proceed to a slow/fast partition of the complexified variables as

follows,

$$\psi_{15,m}^1(t) = A_{15,m}^1(t)\, e^{j\theta_{15,m}^1(t)} \equiv \underbrace{A_{15,m}^1(t)e^{j[\theta_{15,m}^1(t)-\omega_{15}^1 t]}}_{\text{Slow component}}\ \underbrace{e^{j\omega_{15}^1 t}}_{\text{Fast component}}\ ,\ \ m = 1,2 \ \ (4.35)$$

where $\omega_{15}^1 = 2\pi * 560\ rad/s = 3518\ rad/s$ is the common (fast) frequency of the leading

IMFs in Figure 4.19a. In order to prove the occurrence of 1:1 resonance capture in the dynamics

of the 15th beads of the excited ($m = 1$) and absorbing ($m = 2$) chains it suffices to prove the

existence of a slow phase in the representations (4.35). Accordingly we consider the difference

between the phases of the two slow components in (4.35) together with its derivative,

$$\phi_{15}^1(t) = \left[\theta_{15,1}^1(t) - \omega_{15}^1 t\right] - \left[\theta_{15,2}^1(t) - \omega_{15}^1 t\right] = \theta_{15,1}^1(t) - \theta_{15,2}^1(t)$$

$$\dot{\phi}_{15}^1(t) = \dot{\theta}_{15,1}^1(t) - \dot{\theta}_{15,2}^1(t) \tag{4.36}$$

and construct the plot of $\dot{\phi}_{15}^1(t)$ vs. $\phi_{15}^1(t)$ depicted in Figure 4.20. The result proves that there

occurs a single sustained 1:1 resonance capture in the dynamics at 560 Hz; this is highlighted by

the non-time-like nature of the phase difference $\phi_{15}^1(t)$, indicating that this is a slowly varying

angle, and that the averaging theorem cannot be applied with respect to this angle (i.e., this angle

cannot be eliminated from the dynamics by averaging). Note that the oscillations of the slow

angle variable $\phi_{15}^1(t)$ are centered close to the point ($\dot{\phi}_{15}^1$, ϕ_{15}^1)= $(0,\pi)$, indicating out-of-phase

responses between the excited and absorbing chains at 560 Hz. Moreover, the characterization as 1:1 resonance capture is due to the fact that each of the two phases in the first of relations (4.36) is evident without multiplication by an integer coefficient. Revisiting the plots of Figure 4.16b, the dynamics of the stratified network reaches its steady state for $t \geq 0.6\ sec$, so the conclusions drawn by this analysis will hold at the steady state and won't change with increasing time.
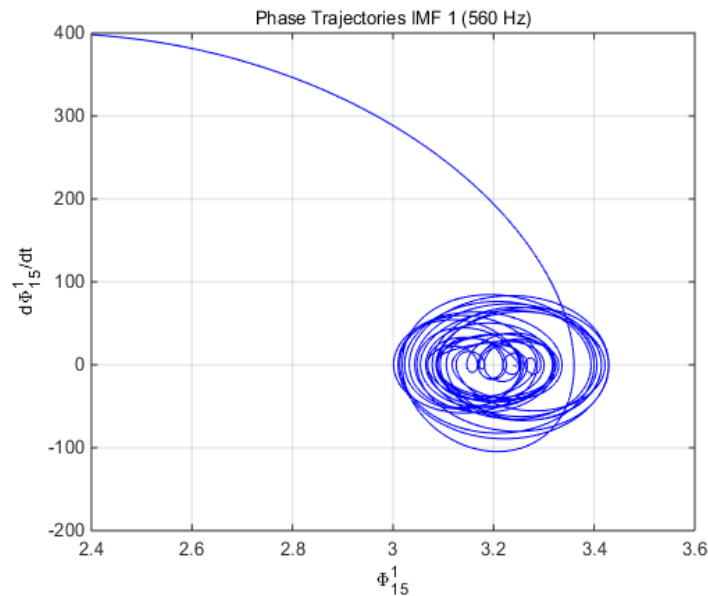

Figure 4.20. Phase plot of $\phi_{15}^1(t)$ for the highest-frequency IMFs at 560 Hz in Figure 4.19a indicating a single sustained 1:1 resonance capture.

Similar analysis can be applied for the second dominant IMFs presented in Figure 4.19b. Note that in this case a reverse energy transfer is identified, i.e., from the absorbing to the excited chain, through sustained 1:1 resonance capture at 300 Hz. However, given that the amplitudes of the IMFs at 300 Hz are comparatively small, the resulting energy exchanges at that frequency are relatively small and the targeted energy transfer is mainly influenced by the aforementioned higher-frequency resonance capture.

Summarizing, our EMD analysis coupled with a complexification methodology revealed that the LZT dynamical mechanism governing steady-state nonlinear targeted energy transfer and passive wave redirection in the stratified network with $s = 27\%$ is a sustained 1:1 resonance capture between the out-of-phase harmonic components (or the dominant IMFs) of the steady-state responses of the excited and absorbing chains at 560 Hz. Secondary sustained resonance captures might occur between different IMFs of the two chain responses at lower frequencies (e.g., between the IMFs at 300 Hz), but these give rise to less intense energy transfers since the participating IMFs are of lower amplitudes.

We now consider the case with spatial stratification $s = 26\%$ where energy exchanges between the two chains occur and there is absence of targeted energy transfer (cf. Figures 4.16a and 4.17a). This corresponds to the stratification rate just before the transition of $\bar{E}_{abs}/\bar{E}_{exc}$ to high values (point II in Figure 4.15). In that respect the dynamics of the granular network in this case is expected to be qualitatively different than the previous case with $s = 27\%$. We perform similar analysis and apply EMD to decompose the steady-state velocity time series of the 15th beads of the excited and absorbing chains, depicted in Figure 4.21. In this case, however, it appears that the steady-state responses are highly nonstationary, since they are in the form of fast oscillations modulated by strong and irregular envelopes; this contrasts with the slowly modulated, nearly uniform steady-state responses of the corresponding beads in the regime of targeted energy transfer of the network (cf. Figure 4.16). Moreover, in this case the modulated responses of the 15th beads of the excited and absorbing chains have comparable maximum amplitudes, again in contrast to the case of targeted energy transfer where steady state localization of the response in the bead of the absorbing chain was realized. Finally, there is broadband frequency content in both of these responses as evidenced by the multiple harmonics over broad

frequency ranges. Therefore, it is clear that in this case the steady-state dynamics is radically different compared to the previous case, and we proceed to an analysis based on the EMD methodology developed previously.

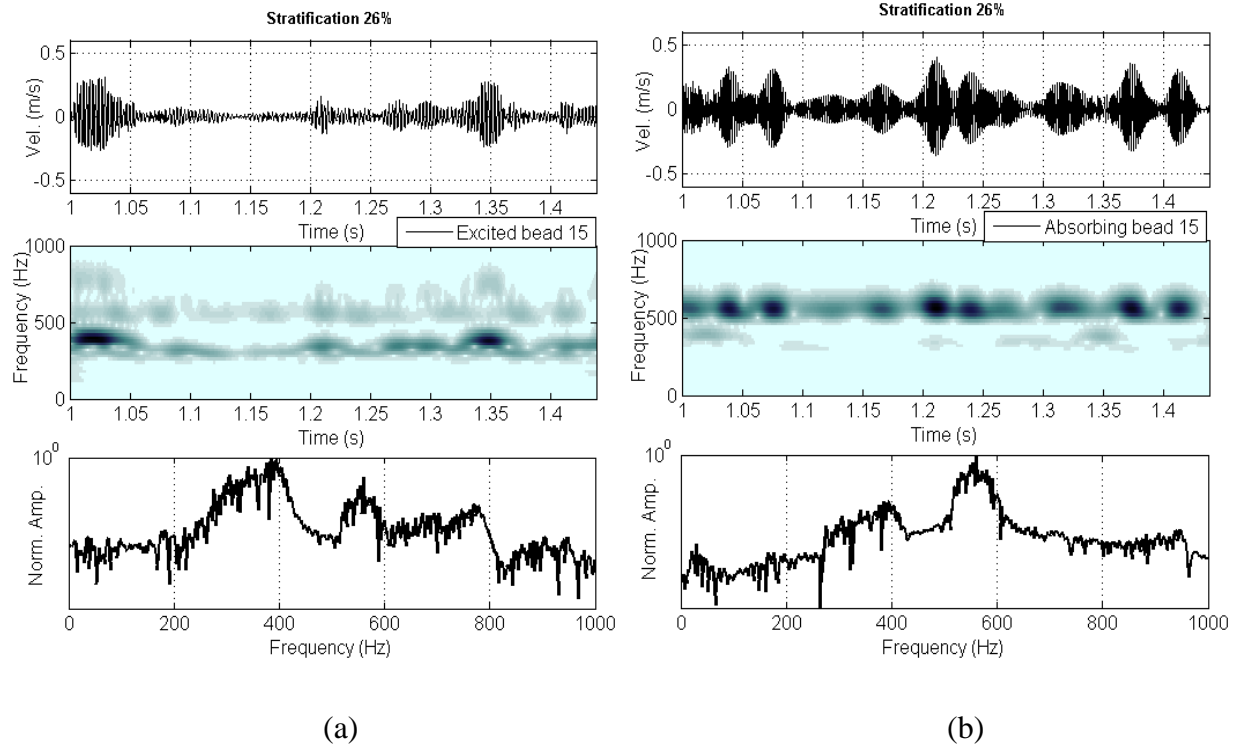(a)   (b)

Figure 4.21. Regime of energy exchanges between chains (point II in Figure 4.15): Time series and wavelet transform / Fourier spectra of the velocity time series of the 15th beads of the (a) excited and (b) absorbing chains for $s = 26\%$.

The dominant IMFs of the responses at frequencies 560 Hz and 400 Hz are depicted in Figure 4.22. We note that an additional higher frequency at approximately 780 Hz has been extracted for the response of the excited chain but since there is no corresponding IMF at that frequency in the response of the absorbing chain no energy transfer from the excited to the absorbing chain can be realized at that high frequency. Comparing the amplitudes of the first IMFs at 560 Hz we deduce that the amplitude of the IMF of the response of the excited chain is

significantly smaller than that of the absorbing chain; moreover, 1:1 resonance capture in the dynamics could occur at this frequency. In Figure 4.23 we present the phase variable $\phi_{15}^1(t)$ (computed similarly to the previous case) for the first IMFs, from which we conclude that in this case a sequence of three transient 1:1 resonance captures occurs in the network at 560 Hz in the time window considered. This is in contrast to the case of targeted energy transfer where a single sustained 1:1 resonance capture was realized at the same frequency over the entire time domain considered (cf. Figure 4.20).
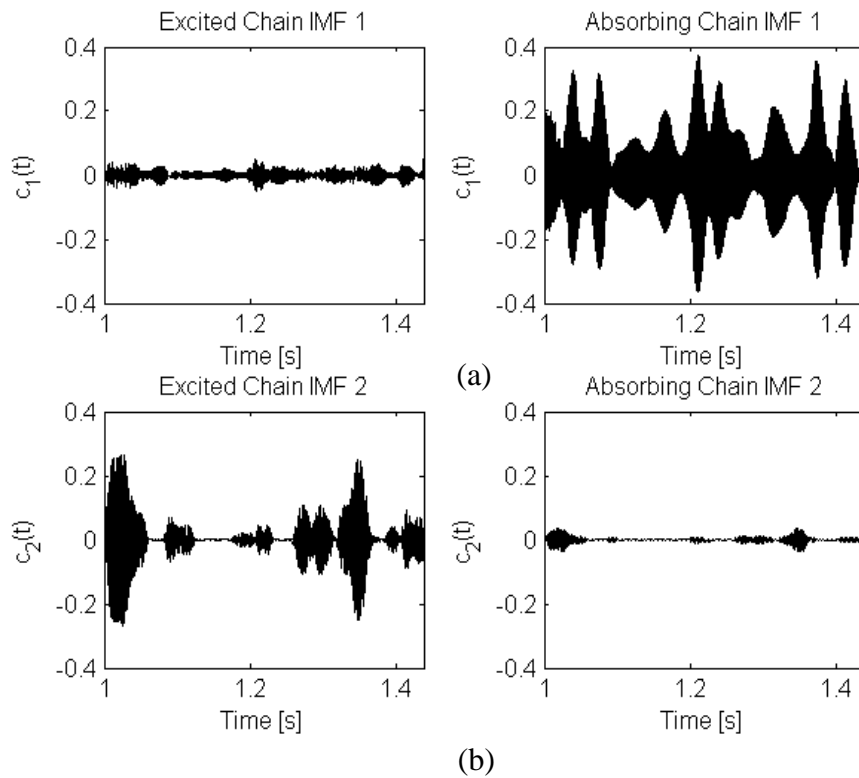
Figure 4.22. Dominant IMFs of the responses of Figure 4.21, (a) at 560 Hz and (b) at 400 Hz.

Each transient 1:1 resonance capture in Figure 4.23 is characterized by non-time-like behavior of the angle variable $\phi_{15}^1(t)$, and during this transient regime of the dynamics energy transfer from the excited to the absorbing chain takes place. However, in this case resonance

capture cannot be sustained, so it is followed by escape during which $\phi_{15}^1(t)$ has a time-like behavior and becomes a fast variable. In the escape regime no energy exchange between chains is possible until the next transient capture of the sequence occurs. These results are confirmed by the spatio-temporal kinetic energy plots of Figure 4.17a, where intermittent bursts of targeted energy transfer from the excited to the absorbing chain occur; these can be attributed to the occurrence of sequences of transient 1:1 resonance captures in the dynamics.

(a)   (b)
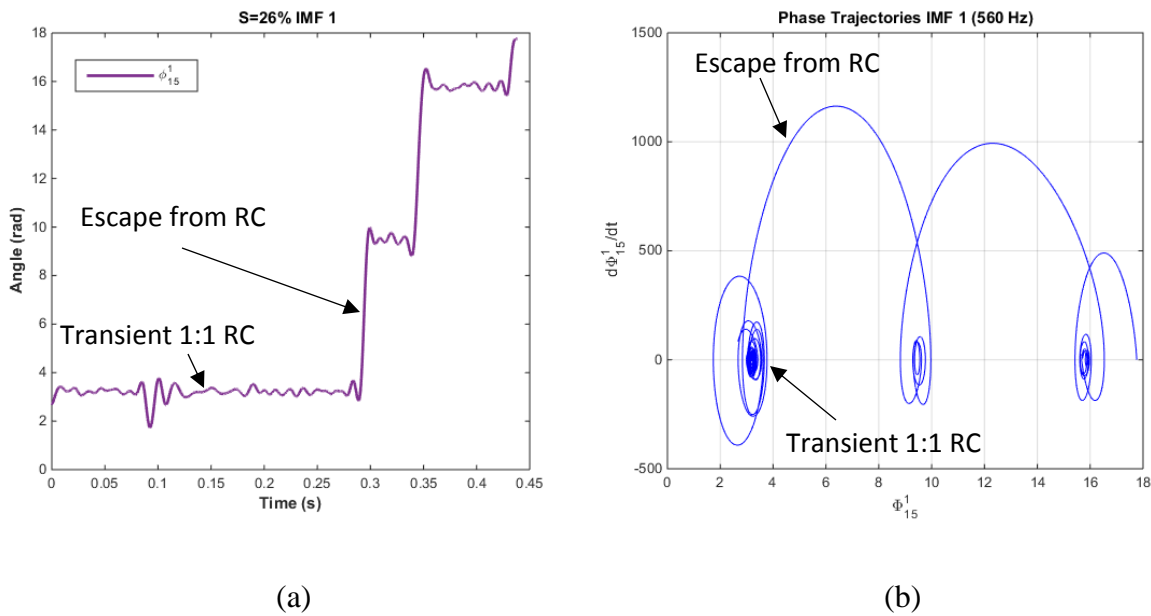
Figure 4.23. Phase variable $\phi_{15}^1(t)$ for the IMFs at 560 Hz in Figure 4.22a showing a sequence of three transient 1:1 resonance captures followed by escapes from capture: (a) Time series and (b) phase plot.

Considering the two IMFs at 400 Hz in Figure 4.22b a similar analysis indicates the absence of strong energy transfers between chains at that frequency. As shown in Figure 4.24, in this case the angle variable $\phi_{15}^2(t)$ has mostly time-like behavior (so it is mostly a fast angle). The brief periods where this angle is slowly-varying (indicating brief, transient 1:1 resonance captures in the dynamics) do not allow for strong energy transfers from the excited to the

absorbing chain. This is confirmed by the large discrepancy in the amplitudes of the two IMFs in Figure 4.22b, indicating energy localization in the excited chain and absence of intense energy exchange at this frequency.
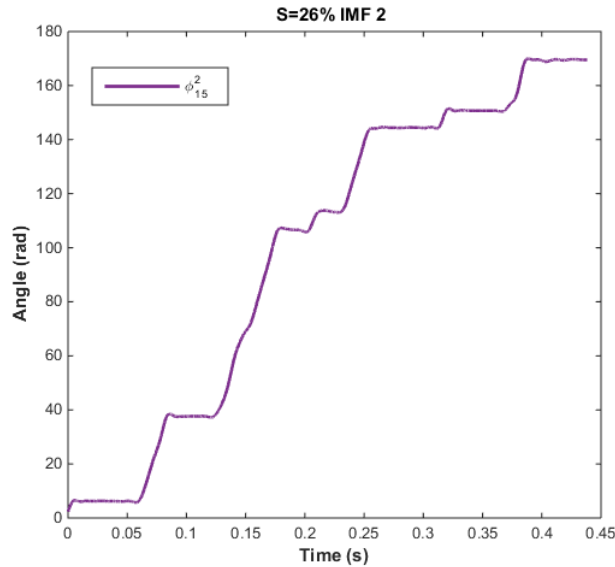

Figure 4.24. Phase variable $\phi_{15}^2(t)$ for the IMFs at 400 Hz in Figure 4.22b showing mostly time-like behavior interrupted by brief transient resonance captures.

In synopsis, the absence of targeted energy transfer from the excited to the absorbing chain in the stratified network with $s = 26\%$ is due to the absence of sustained resonance captures in the steady-state dynamics, which prevents intense directed energy transfers at the dominant frequency components of the bead responses. Instead, either there occur brief transient resonance captures involving same-frequency IMFs of the responses of the excited and absorbing chains, or there is complete absence of such resonance interactions.

A similar stratified network exhibiting an absence of targeted energy transfer and intense energy exchange with $s = 10\%$ (point III in Figure 4.15) is presented in Figure 4.25. In this case
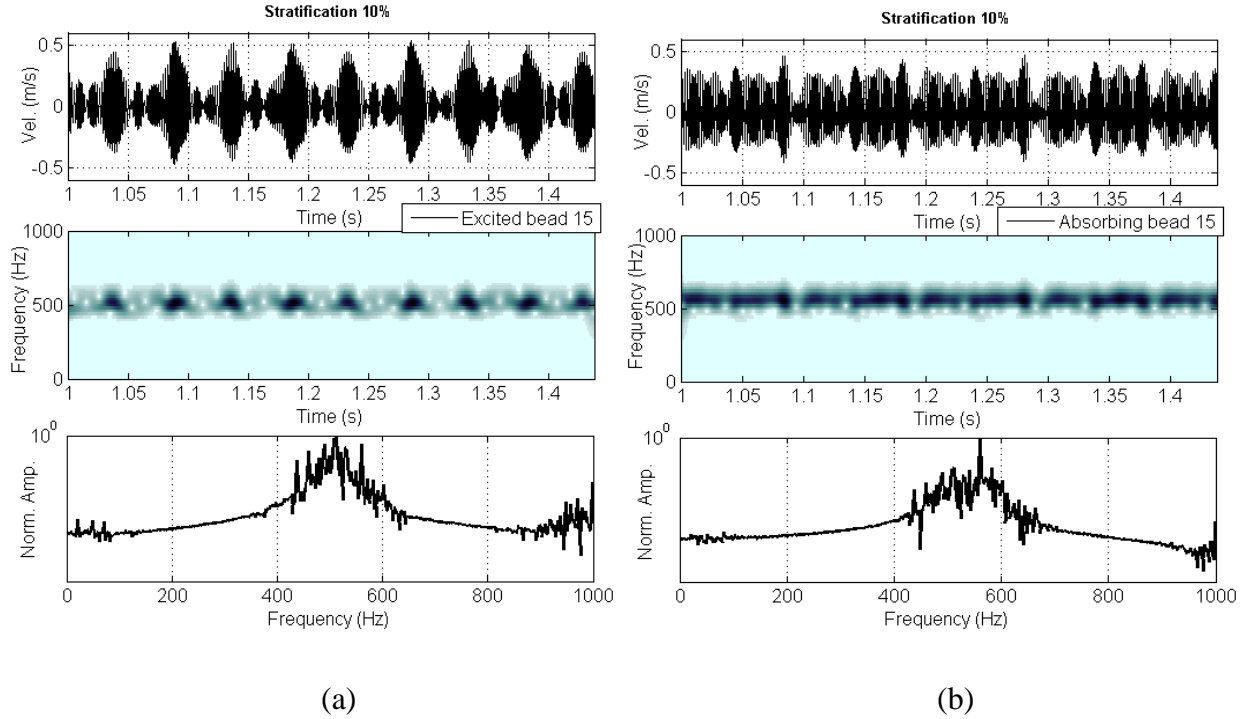
Figure 4.25. Regime of energy exchanges between chains (point III in Figure 4.15): Time series and wavelet transform / Fourier spectra of the velocity time series of the 15th beads of the (a) excited and (b) absorbing chains for $s = 10\%$.

near-equipartition of energy at the steady state between the excited and absorbing chains is noted, and this is confirmed by the fact that $\bar{E}_{abs}/\bar{E}_{exc} \approx 1$ for this spatial stratification rate. We note that in contrast to the previous cases, the steady-state dynamics are in the form of nonlinear beats (albeit of different frequency contents). Moreover, EMD analysis reveals the absence of sustained resonance captures between same-frequency dominant IMFs in the steady-state responses of the 15th beads of the excited and absorbing chains in this case.

4.4 Conclusions

The numerical and analytical findings of sections 4.1 and 4.2 proved that suddenly applied high-frequency excitations can generate interesting dynamic overshoot phenomena in spatially

periodic, linear or nonlinear media. This is contrary to what one would expect, since due to the well-known acoustic filtering properties of these media, harmonic loads with high frequencies lying well inside their attenuation zones (stop bands) should not generate disturbances capable of propagating to their far fields. Yet, as the present study shows, the high rate of application of the high frequency excitations indeed can give rise to such persistent propagating disturbances with frequencies that are well below the excitation frequency. Depending on the medium considered, these propagating disturbances, either are gradually distorted due to linear dispersion, or remain undistorted once they form (forming coherent spatial structures) due to nonlinearity that counterbalances the effects of dispersion.

It is proven that the reason for this dynamic overshoot phenomenon is the high rate of application of the high-frequency harmonic excitation, which, in essence, amounts approximately to an impulsive excitation of the periodic medium. Since such an approximate impulse is broadband, it excites frequency components in both propagation and attenuation zones of the medium, and the frequency components excited in the propagation zones generate the dynamic overshoot phenomenon. The result is the transmission of coherent wavepackets whose waveforms are, either distorted due to dispersion or remain undistorted due to the balance of dispersive effects by nonlinearity and discreteness. For the case of a one-dimensional linear lattice on elastic foundation, the high-frequency dynamic overshoot is approximately expressed in terms of the Green's function at the free end of this medium; whereas, for a two-dimensional strongly nonlinear granular network with elastic foundation the dynamic overshoot appears in the form of a "pure" traveling breather that propagates undistorted and unattenuated in the medium, representing a balance between nonlinearity, dispersion and discreteness. It is interesting that in the latter case, the excitation of the traveling breather opens the way for passive energy redirection

164

in the network through controlled spatial variation (stratification) of the coupling stiffness or of the elastic foundation of the excited lattice, which was detailed reported in section 4.3. The results in sections 4.1 and 4.2 highlight the importance of considering carefully the effects that the application rates of high-frequency excitations have on the transient dynamics of linear or nonlinear periodic systems.

We continued to study strongly nonlinear recurring energy exchanges in the same two-dimensional network of two weakly coupled, semi-infinite homogeneous granular chains on elastic foundations, with no prior compression and under low-frequency harmonic excitation in section 4.3. A computational study showed that steady-state intense and recurring energy exchanges exist for certain combinations of the amplitude and frequency of the applied excitation, in the form of propagating breathers in both chains. This leads to steady-state energy equipartition in the forced network.

Once the regime of propagating breathers is realized, targeted energy transfer and passive wave redirection can be induced by linearly stratifying the elastic foundation of the excited chain. In particular, spatial stratification in the elastic foundation of the leading four beads of the excited chain was introduced, and the steady state dynamics of the network for varying spatial stratification rate was studied. Our analysis revealed that passive wave redirection in the stratified granular network is indeed feasible, once the stratification rate exceeds a certain critical threshold. After this threshold is exceeded, sustained 1:1 resonance captures between dominant frequency components of the responses of the excited and absorbing chains were realized, leading to nonlinear targeted energy transfer from the excited to the absorbing chain, and, therefore, to passive wave redirection in the network. For spatial stratification rates below the threshold, either there occur sequences of brief, intermittent 1:1 resonance captures followed by escapes from

resonance, or there occurs absence of resonance captures. Hence, the LZT mechanism governing passive wave redirection in the stratified network consists of sustained 1:1 resonance capture between specific frequency components of the steady-state responses, which enables intense targeted energy transfer from the excited to the absorbing chain. This study contributes to the designs of acoustic metamaterials with passive wave redirection properties.

4.5 References

Anderson, B., Kasevich, M., "Macroscopic Quantum Interference from Atomic Tunnel Arrays," *Science*, **282**(5394), 1686-1689, 1998.

Arnold, V.I., *Dynamical Systems III, Encyclopaedia of Mathematical Sciences, Vol. 3*, Springer Verlag, 1988.

Aubry, S., "Breathers in Nonlinear Lattices: Existence, Linear Stability and Quantization," *Physica D*, **103**, 201-250, 1997.

Bhadra, N., Lahowetz, E. A., Foldes, S., Kilgore, K., "Simulation of High-frequency Sinusoidal Electrical Block of Mammalian Myelinated Axons," *J. Comput. Neurosci.,* **22**(3), 313-326, 2007.

Boechler, N., Daraio, C., "An Experimental Investigation of Acoustic Band Gaps and Localization in Granular Elastic Chains," *Proc. ASME IDETC*, Paper DETC2009-87427, August 30 – September 2, San Diego, CA, 2009.

Boechler, N., Theocharis, G., Job, S., Kevrekidis, P., Porter M., Daraio, C., "Discrete Breathers in One-Dimensional Diatomic Granular Crystals," *Phys. Rev. Lett*., **104**(24), 244302, 2010.

Brillouin, L., *Wave Propagation in Periodic Structures*, Dover Publication, New York, 1953.

Campbell, D., Peyrard, M., *CHAOS-Soviet American Perspectives on Nonlinear Science*, American Institute of Physics, 1990.

Flach, S., Willis, C., "Discrete Breathers," *Phys. Rep.*, **295**, 181-264, 1998.

Flach, S., Gorbach, A., "Discrete Breathers — Advances in Theory and Applications," *Phys. Rep.*, **467**(1–3), 1–116, 2008.

Hasan, M., Starosvetsky, Y., Vakakis, A., Manevitch, L., "Nonlinear Targeted Energy Transfer and Macroscopic Analog of the Quantum Landau–Zener Effect in Coupled Granular Chains," *Physica D*, **252**, 46–58, 2013.

Hasan, M., Cho, S., Remick, K., Vakakis, A., McFarland, D., Kriven, W., "Experimental Study of Nonlinear Acoustic Bands and Propagating Breathers in Ordered Granular Media Embedded in Matrix," *Gran. Matter*, **17**, 49–72, 2015.

Huang, N., Shen, Z., Long, S., Wu, M., Shih, H., Zheng, Q., "The Empirical Mode Decomposition and the Hilbert Apectrum for Nonlinear and Non-stationary Time Series Analysis," *Proc. Royal Soc. London A*, **454**(4971), 903-995, 1998.

Hunter, E., Chant, R., Wilkin, J., Kohut, J., "High-frequency Forcing and Subtidal Response of the Hudson River Plume," *J. Geophys. Res.*, **115**, C07012, 2010.

Hussein, M., Leamy, M., Ruzzene, M., "Dynamics of Phononic Materials and Structures: Historical Origins, Recent Progress, and Future Outlook," *Appl. Mech. Rev.*, **66**, 040802, 2014.

James, G., "Nonlinear Waves in Newton's Cradle and the Discrete p-Schrödinger Equation," *Math. Mod. Meth. Appl. Sci.*, **21**, 2335-2377, 2011.

James, G., Kevrekidis, P., Cuevas J., "Breathers in Oscillator Chains with Hertzian Interactions," *Physica D*, **251**, 39–59, 2013.

Jayaprakash, K., Starosvetsky, Y., Vakakis, A., Peeters, M., Kerschen, G., "Nonlinear Normal Modes and Band Zones in Granular Chains with No Precompression," *Nonl. Dyn.*, **63**(3), 359-385, 2011a.

Jayaprakash, K., Starosvetsky, Y., Vakakis, A., "A New Family of Solitary Waves in Granular Dimmer Chains with No Pre-compression," *Phys. Rev. E*, **83**, 036606, 2011b.

Kerschen, G., Lee, Y., Vakakis, A., McFarland, D., Bergman, L., "Irreversible Passive Energy Transfer in Coupled Oscillators with Essential Nonlinearity," *SIAM J. Appl. Math.,* **66**(2), 648–679, 2005.

Koblischka, M., Wei, J., Kirsch, M., Hartmann, U., "High Frequency Magnetic Force Microscopy-Imaging of Harddisk Write Heads," *Jpn. J. Appl. Phys.* **45**, 2238-2241, 2006.

Kopidakis, G., Aubry, S., Tsironis, G., "Targeted Energy Transfer Through Discrete Breathers in Nonlinear Systems," *Phys. Rev. Lett.*, **87**(16), 165501, 2001.

Kosevich, Y., Manevitch, L., Savin, A., "Energy Transfer in Coupled Nonlinear Phononic Waveguides: Transition from Wandering Breather to Nonlinear Self-trapping," *J. Phys.: Conference Series*, **92**, 012093, 2007.

Kosevich, Y., Manevitch, L., Savin, A., "Wandering Breathers and Selftrapping in Weakly Coupled Nonlinear Chains: Classical Counterpart of macroscopic Tunneling Quantum Dynamics," *Phys. Rev. E*, **77**(4), 046603, 2008.

Kosevich, Y., Manevitch, L., Savin, A., "Energy Transfer in Weakly Coupled Nonlinear Oscillator Chains: Transition from a Wandering Breather to Nonlinear Self-trapping," *J. Sound Vib.*, **322**(3), 524-531, 2009.

Kosevich, Y., Manevitch, L., Manevitch, L., "Vibrational Analogue of Nonadiabatic Landau–Zener Tunneling and a Possibility for the Creation of a New Type of Energy Traps," *Physics-Uspekhi*, **53**(12), 1281-1286, 2010.

Kovaleva, A., Manevitch, L., Kosevich, Y., "Fresnel Integrals and Irreversible Energy Transfer in an Oscillatory System," *Phys. Rev. E*, **83**(2), 026602, 2011.

Levy, R., Hutchison, W., Lozano, A., Dostrovsky, J., "High-frequency Synchronization of Neuronal Activity in the Subthalamic Nucleus of Parkinsonian Patients with Limb Tremor," *J. Neurosc.*, **20**(20), 7766–7775, 2000.

Manevitch, L., "Complex Representation of Dynamics of Coupled Nonlinear Oscillators," in *Mathematical Models of Non-Linear Excitations: Transfer, Dynamics, and Control in Condensed Systems and Other Media*, Kluwer Academic, 1999.

Manevitch, L., Kosevich, Y., Mane, M., Sigalov, G., Bergman, L., Vakakis, A., "Towards a New Type of Energy Trap: Classical Analog of Quantum Landau–Zener Tunneling," *Int. J. Non-Linear Mech.*, **46**(1), 247-252, 2011.

Maniadis, P., Aubry, S., "Targeted Energy Transfer by Fermi Resonance," *Physica D*, **202**(3-4), 200-217, 2005.

Mead, D., "Wave Propagation and Natural Modes in Periodic Systems: I Mono-coupled Systems," *J. Sound Vib.*, **40**(1), 1–18, 1975.

Nandakumar, K., Chatterjee, A., "The Simplest Resonance Capture Problem Using Harmonic Balance Based Averaging," *Nonl. Dyn.*, **37**(4), 271-284, 2004.

Razavy, M., *Quantum Theory of Tunneling*, World Scientific, 2003.

Rosam, B., Leo, K., Gluck, M., Keck, F., Korsch, H., Zimmer, F., Kohler, K., "Lifetime of Wannier–Stark States in Semiconductor Superlattices Under Strong Zener Tunneling to Above-Barrier Bands," *Phys. Rev. B*, **68**(12), 125301, 2003.

Sias, C., Zenesini, A., Lignier, H., Wimberger, S., Ciampini, D., Morsch, O., Arimondo, E., "Resonantly Enhanced Tunneling of Bose-Einstein Condensates in Periodic Potentials," *Phys. Rev. Lett.*, **98**(12), 120403, 2007.

Sievers, A., Takeno, S., "Intrinsic Localized Modes in Anharmonic Crystals," *Phys. Rev. Lett.*, **61**(8), 970-973, 1988.

Starosvetsky, Y., Hasan, M., Vakakis, A., Manevitch, L., "Strongly Nonlinear Beat Phenomena and Energy Exchanges in Weakly Coupled Granular Chains on Elastic Foundations," *SIAM J. Appl. Math.*, **72**(1), 337–361, 2012.

Theocharis, G., Boechler, N., Kevrekidis, P., Job, S., Porter, M., Daraio, C., "Intrinsic Energy Localization Through Discrete Gap Breathers in One-Dimensional Diatomic Granular Crystals," *Phys. Rev. E*, **82**(5), 056604, 2010.

Vakakis, A., King, M., "Nonlinear Wave Transmission in a Mono-coupled Elastic Periodic System", *J. Acoust. Soc. Am*., **98**(3), 1534-1546, 1995.

Vakakis, A., King, M., "Resonant Oscillations of a Weakly Coupled Nonlinear Layered System," *Acta Mech*., **128**(1-2), 59-80, 1997.

Vakakis, A.F., Gendelman, O., "Energy Pumping in Nonlinear Mechanical Oscillators: Part II—Resonance Capture," *J. Appl. Mech.,* **68**(1), 42-48, 2000.

Vakakis, A., Gendelman, O., Bergman, L., McFarland, D., Kerschen, G., Lee, Y., *Passive Nonlinear Targeted Energy Transfer in Mechanical and Structural Systems I*, Springer Verlag, 2008.

Vakakis, A., Gendelman, O., Bergman, L., McFarland, D., Kerschen, G., Lee, Y., *Passive Nonlinear Targeted Energy Transfer in Mechanical and Structural Systems II*, Springer Verlag, 2008.

Vorotnikov, K., Starosvetsky, Y., "Nonlinear Energy Channeling in the Two-dimensional, Locally Resonant, Unit-cell Model. I. High Energy Pulsations and Routes to Energy Localization," *Chaos*, **25**, 073106, 2015a.

Vorotnikov, K., Starosvetsky, Y., "Nonlinear Energy Channeling in the Two-dimensional, Locally Resonant, Unit-cell Model. II. Low Energy Excitations and Unidirectional Energy Transport," *Chaos*, **25**, 073107, 2015b.

Wang, Y., Lee, K., "Propagation of a Disturbance in a Chain of Interacting Harmonic Oscillators," *Am. J. Phys*., **41**, 51-54, 1973.

Yao, C., He, Z., Zhan, M., "High Frequency Forcing on Nonlinear Systems," *Chin. Phys. B*, **22**(3), 030503, 2013.

Ylinen, A., Bragin, A., Nadasdy, Z., Jando, Sik, A., Buzsaki, G., "Sharp Wave-Associated High-Frequency Oscillation (200 Hz) in the Intact Hippocampus: Network and Intracellular Mechanisms," *J. Neurosc.*, **15**(l), 30-46, 1995.

Zener, C., "Non-Adiabatic Crossing of Energy Levels," *Proc. Royal Soc. London A*, **137**(833), 696-702, 1932.

Zhang, Y., Hasan, M., Starosvetsky, Y., McFarland, D., Vakakis, A., "Nonlinear Mixed Solitary—Shear Waves and Pulse Equi-partition in a Granular Network," *Physica D*, **291**, 45-61, 2015a.

Zhang, Y., Moore, K., McFarland, D., Vakakis, A., "Targeted Energy Transfers and Passive Acoustic Wave Redirection in a Two-dimensional Granular Network Under Periodic Excitation," *J. Appl. Phys.*, **118**, 234901, 2015b.

Zniber, A., Quinn, D., "Frequency Shifting in Nonlinear Resonant Systems With Damping," in *ASME Int. Design Eng. Tech. Conf.*, Chicago, IL, 2003.

Chapter 5. Propagating breathers in granular networks under external excitations

In Chapter 4 we computationally studied dynamic overshoot and strongly nonlinear recurring energy exchanges in a two-dimensional network of two weakly coupled, semi-infinite homogeneous granular chains on elastic foundations. We showed that in both cases the responses were in the form of propagating breathers which enabled the realization of interesting practical applications, such as targeted energy transfer and passive wave redirection. Yet, very few works (James, 2011; James et al., 2013; Starosvetsky et al., 2012; Hasan et al., 2013) reported analytical results on the subject of propagating breathers in granular networks. Here we analytically examine the discrete breather transmission in a granular system and show that discrete breathers can exist in both one-dimensional and multi-dimensional ordered granular media with energy-tunable properties. In such a system, a complexification-averaging methodology is employed which leads to smooth slow flow reduced models of the dynamics, and reveals the nature of 1:1 resonance in the dynamic responses of the network. Our analytical study provides a predictive way to excite the system at its resonance conditions and enables the control of such nonlinear oscillatory wavepackets in both the time and frequency domains. Furthermore, based on the aforementioned analytical results we predict the existence of higher order resonances in this highly nonlinear discrete dynamical system, and provide numerical proof of these resonance phenomena. In the last section of this chapter we report a series of experimental tests performed to verify the existence of the propagating breathers and construct a mathematical model that is validated by experimental measurements. This model fully captures primary pulse transmission in the experimental network and can be employed for predictive designs involving the studied granular network.

5.1 Theoretical study

In this section we present a rigorous mathematical analysis of the dynamics of a single granular chain mounted on an elastic foundation (cf. Figure 5.1). According to the discussions in previous chapters it is evident that the dynamics of this strongly nonlinear system depend strongly on the energy level and on the system parameters. We show that under impulsive excitation, there occur propagating discrete breathers in this granular system due to the balance of nonlinearity, discreteness and the dispersion provided by the elastic foundation. As shown in Figure 5.1 the system considered in this study consists of a finite number of uncompressed homogeneous granular lattices mounted on a linear elastic foundation. Before the application of the excitation the elastic spherical granules are in point contact with each other, but separations between beads may occur after the application of the excitation.
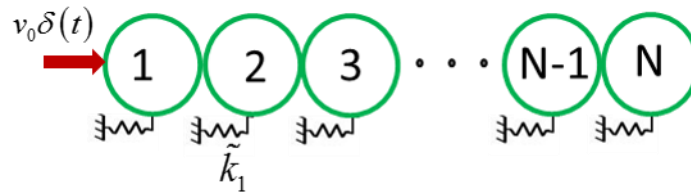
Figure 5.1. Impulsively excited single granular chain of N beads on a linear elastic foundation.

As previously, in the theoretical model of Figure 5.1, we assume nonlinear Hertzian interactions between adjacent beads governed by $F = Kd_+^{3/2}$, where d is the overlap displacement between beads, K is the coefficient of the Hertzian interaction (dependent on granule's size and material), and F is the resulting force. We also assume that the granules are constrained to move only in the horizontal direction and to be grounded by a linear elastic foundation with constant stiffness distribution $\tilde{k}_1$. Moreover, to facilitate the analysis, we do not take into account

dissipative effects in the dynamics. Under these assumptions the network can be mathematically described as follows,

$$m\frac{d^2u_1}{dt^2} = \frac{E\sqrt{2R}}{3(1-\nu^2)}[-(u_1-u_2)_+^{3/2}] - \tilde{k}_1 u_1$$

$$m\frac{d^2u_n}{dt^2} = \frac{E\sqrt{2R}}{3(1-\nu^2)}[(u_{n-1}-u_n)_+^{3/2} - (u_n-u_{n+1})_+^{3/2}] - \tilde{k}_1 u_n, \ n=2,3,... \quad (5.1)$$

$$m\frac{d^2u_N}{dt^2} = \frac{E\sqrt{2R}}{3(1-\nu^2)}[(u_{N-1}-u_N)_+^{3/2}] - \tilde{k}_1 u_N$$

where u_n is the displacement of the *n-th* granule of the chain, and m, E, R, and ν the mass, elastic modulus, radius, and Poisson's ratio of each of the identical granules, respectively. The total number of beads is equal to N, and free boundary conditions at both ends are assumed. As usual, the subscript (+) in equation (5.1) represents the Heaviside function, indicating that only nonnegative values of the corresponding term in the parentheses should be considered, otherwise zero values will be assigned; this models the lack of interaction (and possible separation) between granules in the absence of compressive loads, and, as mentioned previously, introduces a source of high discontinuity and strong nonlinearity in the dynamics of the granular network.

In this study we will consider the granular network with beads composed of poly-di-methyl-siloxane (PDMS) with parameters $E = 1.5\,\text{MPa}$, $\nu = 0.49$, $\rho = 965\,\text{kg/m}^3$ and $R = 4.75\times10^{-3}\,m$. At this point we would like to emphasize that the system considered in this section is not tied to any specific experimental setup, but rather it serves as a theoretical model used to investigate the strongly nonlinear phenomena that can be realized. As in previous chapters the dimensional equations of motion (5.1) can be nondimensionlized by dividing each equation by

175

the common mass of the granules, m, and introducing the normalizations $x_n = \frac{u_n}{R}$, $\tilde{\tau} = \omega_0 t$,

where the characteristic frequency is $\omega_0 = \sqrt{\frac{\tilde{k}_1}{m}}$:

$$
\begin{aligned}
&\ddot{x}_1 + x_1 = -\alpha \left[(x_1 - x_2)_+^{3/2} \right] \\
&\ddot{x}_n + x_n = \alpha [(x_{n-1} - x_n)_+^{3/2} - (x_n - x_{n+1})_+^{3/2}], \quad n = 2, 3... \\
&\ddot{x}_N + x_N = \alpha \left[(x_{N-1} - x_N)_+^{3/2} \right]
\end{aligned}
\tag{5.2}
$$

where the variable x_n denotes the normalized axial displacement of the n-th granule of the lattices, α denotes the normalized stiffness coefficient of the nonlinear Hertzian interaction between the beads, and overdot denotes differentiation with respect to the normalized time variable $\tilde{\tau}$. We note that there is a single nondimensional parameter, α, that depends on only the strength of the elastic foundation. In the following analysis, we focus mainly on primary pulse transmission in the granular medium; therefore, the theoretical model (5.1) or (5.2) should be capable of capturing and accounting for the strongly nonlinear bead interactions that dominate the primary propagating dynamics, but not necessarily the secondary scattering or reflections of the primary pulse at the free boundaries of the system.

5.1.1 Analytical predictions of the wave propagation speed and the frequency spectrum

The considered granular chain is at rest at $\tilde{\tau} = 0-$ and is excited by an impulse of intensity v_0 at $\tilde{\tau} = 0+$, i.e., a non-zero initial velocity v_0 is prescribed to the first bead of the chain. As an example of the strongly nonlinear dynamics of this system we perform direct numerical integration of the equations of motion (5.2) with zero initial conditions except for $\dot{x}_1(0) = 0.02$. We focus on the stable periodic solution of system (5.2) after the transient responses of the leading 3 to 4 beads have died out. In Figure 5.2 we depict the time series of the relative displacements (in

dimensionless form) between beads 10-11, 13-14, and 17-18. In the absence of dissipative forces in the system we clearly observe a propagating breather (i.e., of a nonlinear beating) denoted by a fast oscillatory response of each particle, modulated by a slowly varying envelope with constant amplitude, which is defined as a (cf. Figure 5.2).
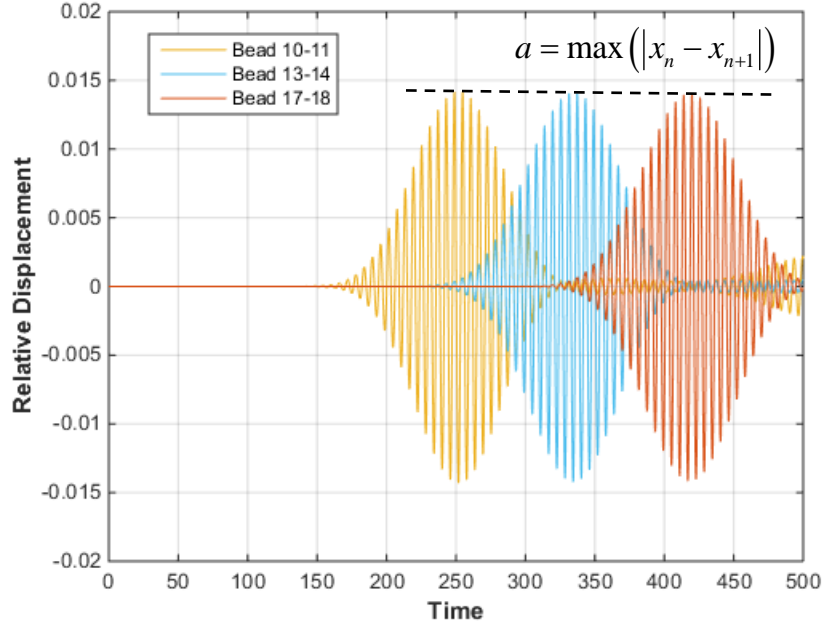

Figure 5.2. Relative displacements between beads 10-11, 13-14, and 17-18.

We note that the equations of motion (5.2) are not re-scalable with energy since not all terms are proportional to the same power of the displacement components. Then, the nonlinear dynamics of the system of Figure 5.1 are expected to depend on the specific level of energy (i.e., on the varying intensity of the applied impulse). Taking this into account, we would like to analytically study this nonlinear beating phenomenon by employing the complexification-averaging method first introduced by Manevitch (1999). We want to emphasize here that our following study is restricted to small energy levels (amplitudes) in order to ensure that the

deformations of the beads are within the elastic limit of PDMS, and to conform to the assumptions necessary for the mathematical model (5.1) or (5.2).

To apply the complexification-averaging (CX-A) method we introduce the following new complex variables,

$$\psi_n = \dot{x}_n + ix_n \quad \psi_n^* = \dot{x}_n - ix_n \tag{5.3}$$

where the asterisk denotes the complex conjugate and i is the imaginary constant. The transformation (5.3) represents the amplitude and phase variation of the oscillatory response which is referred to as the phase vector. This notation $(x_n, \dot{x}_n) \rightarrow \psi_n$ provides a convenient representation of the phase plane dynamics of the *n-th* granule which enables us to study the nonlinear dynamics in terms of slowly varying amplitudes and phases. From (5.3), we can express x_n and $\dot{x}_n$ in terms of the new complex variables as follows:

$$x_n = \frac{1}{2i}\left(\psi_n - \psi_n^*\right) \quad \dot{x}_n = \frac{1}{2}\left(\psi_n + \psi_n^*\right) \quad \ddot{x}_n = \frac{d\psi_n}{d\tau} - \frac{i}{2}\left(\psi_n + \psi_n^*\right) \tag{5.4}$$

Substituting (5.3), and (5.4) into (5.2) we obtain the following system of first order complex equations (which is exact and equivalent to the equations of motion (5.2)):

$$\frac{d\psi_n}{d\tau} - i\psi_n = \alpha \left\{ \left[\frac{\left(\psi_{(n-1)} - \psi_{(n-1)}^*\right) - \left(\psi_n - \psi_n^*\right)}{2i} \right]_+^{3/2} - \left[\frac{\left(\psi_n - \psi_n^*\right) - \left(\psi_{(n+1)} - \psi_{(n+1)}^*\right)}{2i} \right]_+^{3/2} \right\} \tag{5.5}$$

Then, the following multiscale expansions of these complex variables are introduced in terms of the small parameter of the problem,

$$\psi_n = \varepsilon \left\{ \psi_{n0}\left(\tau_0,\tau_1,...\right) + \varepsilon^{1/2}\psi_{n1}\left(\tau_0,\tau_1,...\right) + ... \right\}$$

$$\frac{d}{d\tilde{\tau}} = \frac{\partial}{\partial \tau_0} + \varepsilon^{1/2}\frac{\partial}{\partial \tau_1} + ...$$

(5.6)

where $0 < \varepsilon \ll 1$ is the small parameter scaling the amplitude of the response (assumed to be small), and $\tau_0 = \varepsilon^0\tilde{\tau}$, $\tau_1 = \varepsilon^{1/2}\tilde{\tau},...$ are the fast and slow time scales in the multi-scale dynamics, respectively. Substituting (5.6) into (5.5) and collecting like-powers of the small parameter ε we obtain a hierarchy of subproblems governing the dynamics at different order of approximations. Note that by the previous scaling we assume that the responses of the granules are small, of $O(\varepsilon)$.

Considering the leading order $O(\varepsilon)$ approximation we obtain:

$$\frac{\partial \psi_{n0}}{\partial \tau_0} - i\psi_{n0} = 0 \quad \Rightarrow \quad \psi_{n0} = \varphi_{n0}\left(\tau_1\right)\exp\left(i\tau_0\right), \quad n = 1,2,... \tag{5.7}$$

In equation (5.7) there are two time scales which represent the fast and slow dynamics of the system (5.2) or (5.5), with the complex exponential term indicating the fast oscillation parts governed by the linear foundations of the chain, and $\varphi_{n0}\left(\tau_1\right)$ the slow modulations (envelopes) of the fast oscillations. The slow modulations $\varphi_{n0}\left(\tau_1\right)$ cannot be evaluated at the leading order approximation (5.7), and are computed by considering terms at the next (smaller) order.

Proceeding to the next order of approximation, i.e., considering terms of $O\left(\varepsilon^{3/2}\right)$, we obtain the following system of equations:

$$\frac{\partial \psi_{n0}}{\partial \tau_1} + \frac{\partial \psi_{n1}}{\partial \tau_0} - i\psi_{n1} =$$

$$\alpha \left\{ \frac{\psi_{(n-1)0} - \psi_{(n-1)0}^* - \psi_{n0} + \psi_{n0}^*}{2i} \right\}_+^{3/2} - \alpha \left\{ \frac{\psi_{n0} - \psi_{n0}^* - \psi_{(n+1)0} + \psi_{(n+1)0}^*}{2i} \right\}_+^{3/2} \quad (5.8)$$

Introducing (5.7) into (5.8) and imposing solvability conditions in equation (5.8), i.e., eliminating secular terms with fast frequency equal to unity (which is identical to the fast frequency on the left-hand sides) that render the solution non-uniformly valid as time tends to infinity, yields the following slow flow, that is, the system of modulation equations in the slow time scale governing the evolutions of the complex envelops in (5.7):

$$\frac{\partial \varphi_{n0}}{\partial \tau_1} =$$

$$\alpha \left\{ \frac{\varphi_{(n-1)0} \exp(i\tau_0) - \varphi_{(n-1)0}^* \exp(-i\tau_0) - \varphi_{n0} \exp(i\tau_0) + \varphi_{n0}^* \exp(-i\tau_0)}{2i} \right\}_+^{3/2} \exp(-i\tau_0) \quad (5.9)$$

$$-\alpha \left\{ \frac{\varphi_{n0} \exp(i\tau_0) - \varphi_{n0}^* \exp(-i\tau_0) - \varphi_{(n-1)0} \exp(i\tau_0) + \varphi_{(n-1)0}^* \exp(-i\tau_0)}{2i} \right\}_+^{3/2} \exp(-i\tau_0)$$

We note that at this order of approximation there are non-smooth terms (discontinuous effects) corresponding to possible bead separations and collisions, which are represented as Heaviside functions in the original system (5.2). To evaluate the discontinuous effects we introduce Fourier expansions and averaging operations following the methodology first developed in (Starosvetsky et al. 2012; Hasan et al. 2013),

$$F_{(n-1)0} \equiv \varphi_{(n-1)0} - \varphi_{n0} = \left| F_{(n-1)0} \right| \exp(i\theta_{n-1})$$

$$F_{n0} \equiv \varphi_{n0} - \varphi_{(n-1)0} = \left| F_{n0} \right| \exp(i\theta_n) \quad (5.10)$$

When the expressions (5.10) are substituted into the non-smooth terms on the right-hand sides of (5.9), we obtain to the following expressions,

$$\left\{ \frac{F_{(n-1)0}\exp(i\tau_0) - F_{(n-1)0}^*\exp(-i\tau_0)}{2i} \right\}_+^{3/2} = \left| F_{(n-1)0} \right|^{3/2} \left\{ \sin(\tau_0 + \theta_{n-1}) \right\}_+^{3/2} = \left| F_{(n-1)0} \right|^{3/2} \left\{ \cos\phi_{n-1} \right\}_+^{3/2}$$

$$\left\{ \frac{F_{n0}\exp(i\tau_0) - F_{n0}^*\exp(-i\tau_0)}{2i} \right\}_+^{3/2} = \left| F_{n0} \right|^{3/2} \left\{ \sin(\tau_0 + \theta_n) \right\}_+^{3/2} = \left| F_{n0} \right|^{3/2} \left\{ \cos\phi_n \right\}_+^{3/2} \qquad (5.11)$$

where $\phi_k + \dfrac{\pi}{2} = \tau_0 + \theta_k$. To this end, we substitute (5.11) into (5.9). Fourier-expanding the integrands, retaining only leading order harmonics, averaging the resulting expressions with respect to the fast time scale τ_0 and rearranging terms yields the following smooth averaged slow-flow equation:

$$i\frac{\partial\varphi_{n0}}{\partial\tau_1} = \tilde{\alpha}\left\{ F_{(n-1)0} \left| F_{(n-1)0} \right|^{1/2} - F_{n0} \left| F_{n0} \right|^{1/2} \right\} \qquad (5.12)$$

where $\tilde{\alpha} = \dfrac{\alpha\eta_1}{2\pi}$ and $\eta_1 = \oint_{2\pi} \left\{ \cos\phi_n^x \right\}_+^{3/2} \exp\left[-i\phi_n^x \right] d\phi_n^x$.

Then, we express (5.12) in terms of new coordinates, namely the differences between the amplitudes $\delta_n = \varphi_{n0} - \varphi_{(n+1)0}$, and rewrite (5.12) in the form:

$$i\frac{\partial\delta_n}{\partial\tau_1} = \tilde{\alpha}\left\{ \delta_{n-1} \left| \delta_{n-1} \right|^{1/2} - 2\delta_n \left| \delta_n \right|^{1/2} + \delta_{n+1} \left| \delta_{n+1} \right|^{1/2} \right\} \qquad (5.13)$$

Equation (5.13) is the well-known single discrete nonlinear p-Schrödinger equation (DNLpS equation). In recent studies it was theoretically (Jayaprakash et al., 2011) and experimentally

181

(Hasan et al., 2015) shown that ordered granular media such as the granular network of Figure 5.1 possess energy-tunable acoustic filtering properties, whose dispersion relation contains two attenuation zones (AZs) and one propagation zone (PZ) in the frequency domain. In this nonlinear PZ we impose the following traveling wave ansatz:

$$\delta_n(\tau_1) = B e^{i(\tilde{\Omega}\tau_1 - qn)}, \quad n = 1, 2, \ldots \tag{5.14}$$

where B denotes the amplitude, $\tilde{\Omega}$ the slow modulation frequency, and q the wave number. Substituting (5.14) into (5.13) yields the following nonlinear dispersion relation for traveling waves in the homogeneous granular chain:

$$\tilde{\Omega} = 4\tilde{\alpha}B^{1/2} \sin^2(q/2) \tag{5.15}$$

It follows that the approximate periodic travelling wave solution is given by:

$$x_n - x_{n+1} = \frac{1}{2i}\left(\psi_n - \psi_n^* - \psi_{n+1} + \psi_{n+1}^*\right) \approx \frac{\varepsilon}{2i}\left\{\delta_n \exp(i\tau_0) - \delta_n^* \exp(-i\tau_0)\right\}$$
$$= a\sin(\omega\tau_0 - qn) \tag{5.16}$$

where $a = \varepsilon B$, and $\omega = 1 + 4\tilde{\alpha}a^{1/2}\sin^2(q/2)$ are the wave amplitude and oscillating frequency of $x_n - x_{n+1}$, respectively. Certain conclusions can be drawn from (5.15) and (5.16). First, the wave number q defines the frequency range of the PZ, where the in-phase mode (when $q = 0$, $\omega_{ip} = 1$) and out-of-phase mode (when $q = \pi$, $\omega_{op} = 1 + 4\tilde{\alpha}a^{1/2}$) correspond to the lower and upper bounding frequencies separating the two AZs from the single PZ. Second, the frequency ω depends on the amplitude of oscillation, which reveals the important energy-tunable acoustic filtering properties of the system. Additionally, the elastic foundation stiffness plays an important

role in determining this frequency pass band. The effect of the on-site elastic foundation is more obvious if we convert the above expression into dimensional forms:

$$q = 0, \ \tilde{\omega}_{ip} = \sqrt{\frac{\tilde{k}_1}{m}},$$

$$q = \pi, \ \tilde{\omega}_{op} = \sqrt{\frac{\tilde{k}_1}{m}\left(1 + 4\tilde{\alpha}a^{1/2}\right)} = \sqrt{\frac{\tilde{k}_1}{m}} + 0.4318 \frac{E\sqrt{RA}}{(1-v^2)\sqrt{m\tilde{k}_1}} \tag{5.17}$$

where $A = \max|u_n - u_{n+1}|$ is the dimensional amplitude of the propagating wave.
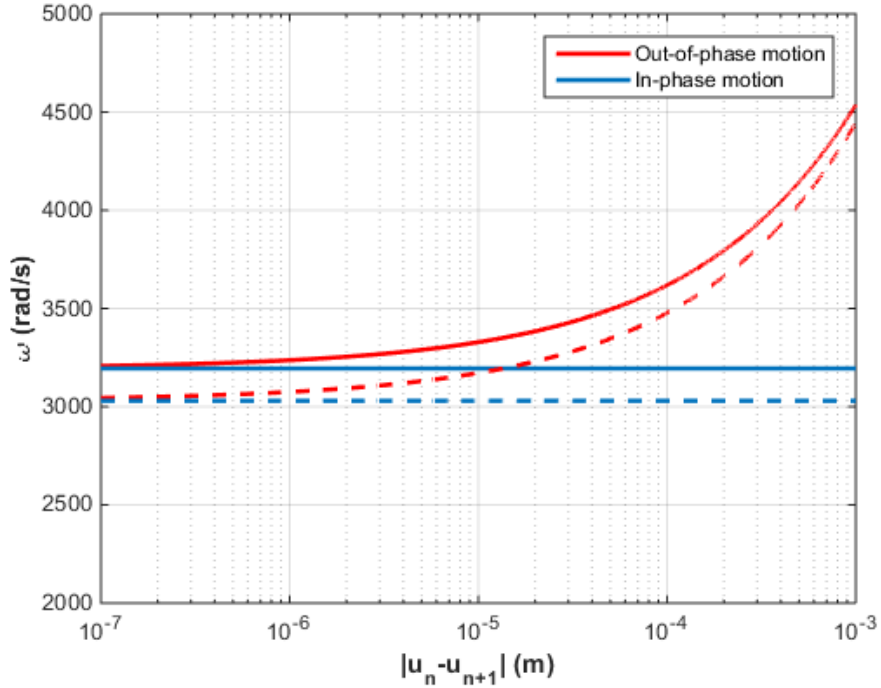
Figure 5.3. Frequency bands of the homogenous granular network as functions of wave amplitude, for different foundation stiffnesses: $\tilde{k}_1 = 4420 N / m$ (solid lines) and $\tilde{k}_1' = 3978 N / m$ (dashed lines).

In Figure 5.3, we graphically represent the frequencies of the in-phase and out-of-phase modes for varying amplitude of oscillations in the granular network mounted on two different

foundations corresponding to $\tilde{k}_1 = 4420N/m$ (solid lines) and $\tilde{k}_1' = 0.9\tilde{k}_1 = 3978N/m$ (dashed lines). An initial observation is that the frequency of the in-phase mode depends on only the strength of the elastic foundation but not the wave amplitudes, whereas the frequency of the out-of-phase mode is a function of both the foundation stiffness and the wave amplitudes. This can be explained by the fact that the in-phase mode is linear (since it does not involve compression of beads), whereas the out-of-phase mode is strongly nonlinear since it corresponds to strong compression between all adjacent beads. The area in the plot between the in-phase and out-of-phase frequencies represents the intermediate-frequency propagation zone of this nonlinear granular network.

The acoustic filtering properties of linear systems with spatially periodic structure have been well studied (Mead, 1975; Vakakis et al., 2008; Zhang et al., 2016). However, the frequency bands of linear periodic systems have no energy dependence since the frequencies of in-phase and out-of-phase modes remain constant for varying wave amplitudes, which highlights the essential nonlinear feature of granular networks. The strength of the elastic foundation can alter the PZ to different frequency ranges but will not change its shape. Herein, unless otherwise noted we select a strength of elastic foundation equal to $\tilde{k}_1 = 4420N/m$ in the analysis.

Additional interesting conclusions can be drawn from Figure 5.3 considering the PZs' separations and overlaps of two systems with different foundations at low and high energy levels. If two single chains composed of identical spherical granules but with different foundations are connected as shown in Figure 5.4, depending on the intensity of the applied impulse, the wave can localize within the initially excited region of the first chain, or propagate to the second chain. In other words, the considered system of two single chains can be designed as an energy-tunable

184

vibration filter. As an example of the dynamic response of the forced granular system we choose the foundation stiffness of the second chain to be softer, such as, $k'_1 = 0.81k_1$, as shown in Figure 5.4, and select the number of beads to $n = 15$, i.e., each chain has 15 beads for a total of $N = 30$ beads for the two chains, and excite the left end of the first chain with low ($v_0 = 10^{-3}$) and high ($v_0 = 0.06$) excitations. These conclusions corroborate the spatio-temporal kinetic energy evolutions in these two cases (Figures 5.5a and 5.5b), where wave propagation in the second chain is noted only in the latter case. This clearly indicates the energy-tunable feature of the considered granular system. In the low amplitude case the wave cannot propagate or transmit to the second chain because the PZs of two chains are completely separate; while clear energy transmission is observed for the case of higher excitation due to the overlap of two PZs. Also, as seen in Figure 5b, it is clear that nonlinear beating phenomena involving traveling discrete breathers occur in both chains but with different propagation speeds. In the following study we would like to formulate an analytical approximation for the characteristic speed of wavepacket transmission in these networks by estimating the time it takes for the propagating signal to propagate the distance between two adjacent beads of the granular chain based on the discrete DNLpS equation (5.13).
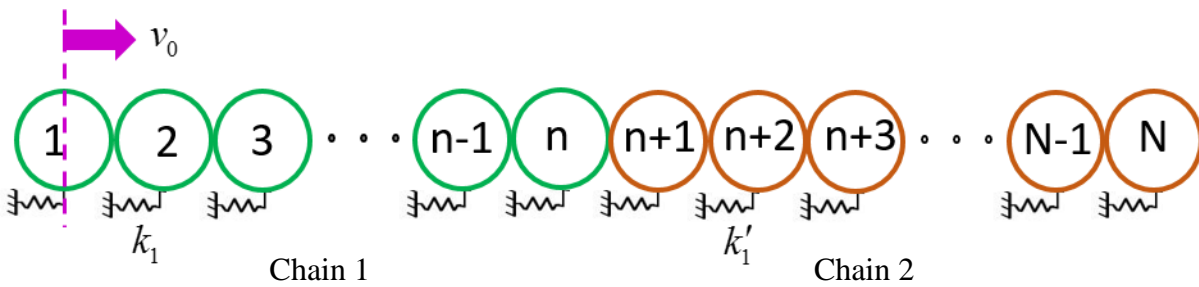
Figure 5.4. Impulsively excited network of two coupled single granular chains mounted on different linear elastic foundations.
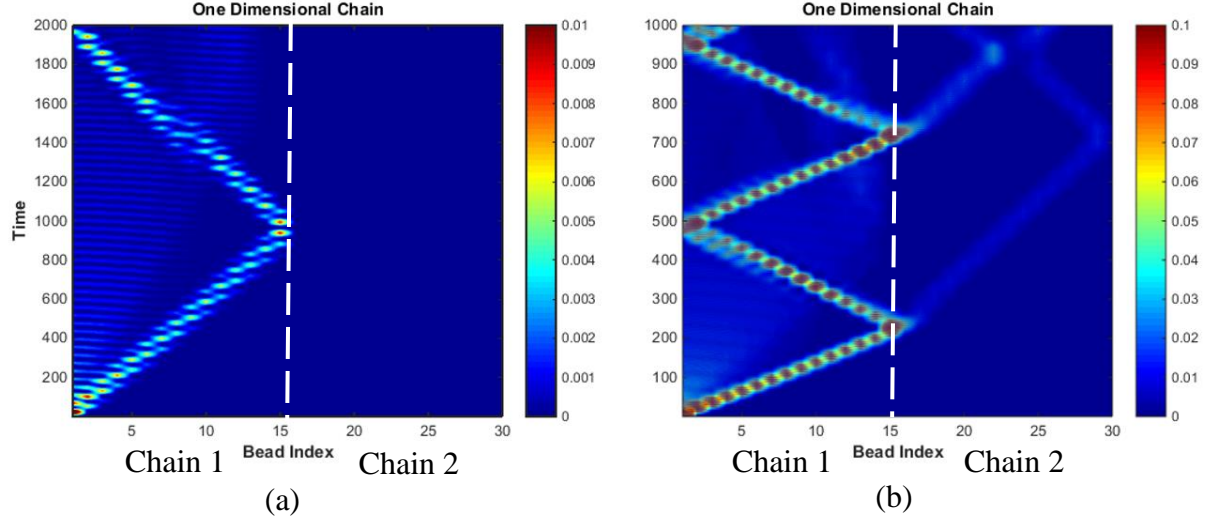
Figure 5.5. Spatio-temporal evolutions of instantaneous kinetic energies (scaled× 200) for the network of two chains for (a) low impulsive excitation, $v_0 = 10^{-3}$ (no energy transmission in chain 2), and (b) high impulsive excitation, $v_0 = 0.06$ (energy transmission in chain 2).

For the sake of simplicity, we introduce an additional time scale to the system (5.13) as $\tau = \tilde{\alpha}\tau_1$ and express (5.13) as follows:

$$i\frac{\partial \delta_n}{\partial \tau} = \left\{\delta_{n-1}\left|\delta_{n-1}\right|^{1/2} - 2\delta_n\left|\delta_n\right|^{1/2} + \delta_{n+1}\left|\delta_{n+1}\right|^{1/2}\right\} \tag{5.18}$$

In this study we will be interested in the regime of primary pulse transmission, i.e., in the leading edge of the propagating breathers, and disregard reflections from boundaries or secondary waves formed in the tails of the primary breather propagation. To this end, we recall the properties of propagating breathers and introduce the approximate *ansatz*,

$$\delta_n = B_n(\tau)\exp(-in\Omega T_1)\exp(i\Omega\tau)$$
$$B_{n-1}(\tau) = B_n(\tau - T_1) \tag{5.19}$$

into equation (5.18) and set the real and imaginary parts separately equal to zero, yielding the following set of slow modulation equations for the propagating breathers,

$$\frac{dB_n}{d\tau} = \sin\left(\Omega T_1\right)\left[B_{n-1}^{1.5} - B_{n+1}^{1.5}\right] \tag{5.20a}$$

$$-\Omega B_n = \cos\left(\Omega T_1\right)B_{n-1}^{3/2} - 2B_n^{3/2} + \cos\left(\Omega T_1\right)B_{n+1}^{3/2} \tag{5.20b}$$

where $B_n\left(\tau\right)$ is the real amplitude of the propagating solution, Ω its frequency, and T_1 a constant time delay in the slow envelope of the amplitude dynamics between two adjacent beads. Due to the time scale separation the term $\kappa = \sin\left(\Omega T_1\right)$ can be considered as constant and properly scaled out from (5.20a). Furthermore, employing the second part of the *ansatz* (5.19) and rescaling the time as $\tau^* = \kappa\tau$ we can rewrite (5.20a) and (5.20b) in the form of a time delay-advance equation as,

$$\frac{dB}{d\tau^*} = \left[B\left(\tau^* - T_1^*\right)^{3/2} - B\left(\tau^* + T_1^*\right)^{3/2}\right] \tag{5.21a}$$

$$-\kappa\sin^{-1}\left(\kappa\right)B\left(\tau^*\right)/T_1^* = \sqrt{1-\kappa^2}\left[B\left(\tau^* - T_1^*\right)^{3/2} + B\left(\tau^* + T_1^*\right)^{3/2}\right] - 2B\left(\tau^*\right)^{3/2} \tag{5.21b}$$

where $T_1^* = \kappa T_1$. An approximate solution of (5.21) has been reported by Starosvetsky et al. (2012) in the form of the following Pade' series approximation:

$$B\left(\tau^*\right) = \frac{1}{q_0 + q_2\tau^{*2} + q_4\tau^{*4} + ...} = \frac{1}{q_0\left(1 + 0.5712\tau^{*2} + 0.1915\tau^{*4} + ...\right)} \tag{5.22}$$

Here we will provide a brief summary of their main results of (Starosvetsky et al., 2012) and extend them to explicitly solve for the frequency components and wave speeds of discrete propagating

breathers in the granular network considered. We note at this point that the constant time delay $T_1^* = \kappa T_1$ (which is directly related to the speed of breather propagation) is dependent on the wave amplitude, which also reveals the energy-tunable properties of this class of strongly nonlinear granular networks.

To obtain the general relationship between the amplitude and the nontrivial time delay we introduce the rescalings $\hat{\tau} = \tau^* / T_1^*$, $\bar{B}(\hat{\tau}) = (T_1^*)^2 B(\hat{\tau} T_1^*)$ and derive the following relation,

$$(T_1^*)^2 A^* = \bar{A} = \bar{B}(0) = const \tag{5.23}$$

where A^* denotes the constant amplitude of the traveling wave $B(\tau^*)$. Equation (5.23) enables us to calculate the amplitude-time shift relationship between all members of a family of propagating breathers once a single member of that family has been computed. As a special case Starosvetsky et al. (2012) numerically obtained the time delay value corresponding to unit wave amplitude, i.e., $T_1^* = 0.6099$ when $B(0) = 1$ or $q_0 = 1$. By direct substitution into (5.23) the time delay constant in terms of the scaled time τ^* is calculated as $T_1^* = 0.6099 / \sqrt{A^*}$. Once the analytical approximation $B(\tau^*)$ is determined the value of κ can be solved numerically (Starosvetsky et al., 2012) from (5.21b). We may determine a unique value of κ by evaluating it at $\tau^* = 0$ since we are interested in the time delay at the primary peak (which occurs at $\tau^* = 0$), of the propagating solution and set $\kappa = \kappa|_{\tau^*=0} = 0.9364$. Indeed, the frequency Ω can be related to κ as follows:

$$\Omega = \frac{\kappa \sin^{-1}(\kappa)}{T_1^*} \tag{5.24}$$

In order to compare the analytical and computational results we convert the above calculations of time delay and frequencies to the fast normalized and dimensional time scales, which yields the following expressions

$$T = \frac{0.6513}{\tilde{\alpha}\sqrt{a}} \tag{5.25a}$$

$$\omega = 1 + 1.862\tilde{\alpha}\sqrt{a} \tag{5.25b}$$

or,

$$\tilde{T} = \frac{0.6513}{\tilde{\alpha}\sqrt{a}}\sqrt{\frac{m}{\tilde{k}_1}} = \frac{0.6032(1-v^2)\sqrt{m\tilde{k}_1}}{E\sqrt{RA}} \tag{5.26a}$$

$$\tilde{\omega} = \sqrt{\frac{\tilde{k}_1}{m}}\left(1 + 1.862\tilde{\alpha}\sqrt{a}\right) = \sqrt{\frac{\tilde{k}_1}{m}} + 0.2011\frac{E\sqrt{RA}}{(1-v^2)\sqrt{m\tilde{k}_1}} \tag{5.26b}$$

Equations (5.25a,b) correspond to normalized (dimensionless) coordinates where a denotes the constant amplitude of the propagating breather and $\tilde{\alpha}$ denotes the normalized stiffness coefficient of the nonlinear Hertzian interaction between the beads as defined in (5.12), whereas equations (5.26a,b) are the corresponding expressions in dimensional form with the previously defined dimensional parameters.

From a physical point of view, these two analytical measurements pave the way for predictive design for practical granular network implementations of these highly discontinuous metamaterial systems with energy-tunable wave propagation speeds and oscillation frequencies. Indeed, the constant T in (5.25a) represents the time that a moving breather takes to propagate

from one bead to its neighboring bead and is dependent on the wave amplitude and the system properties; as such, it is directly tied to the speed of breather propagation.

(a)   (b)
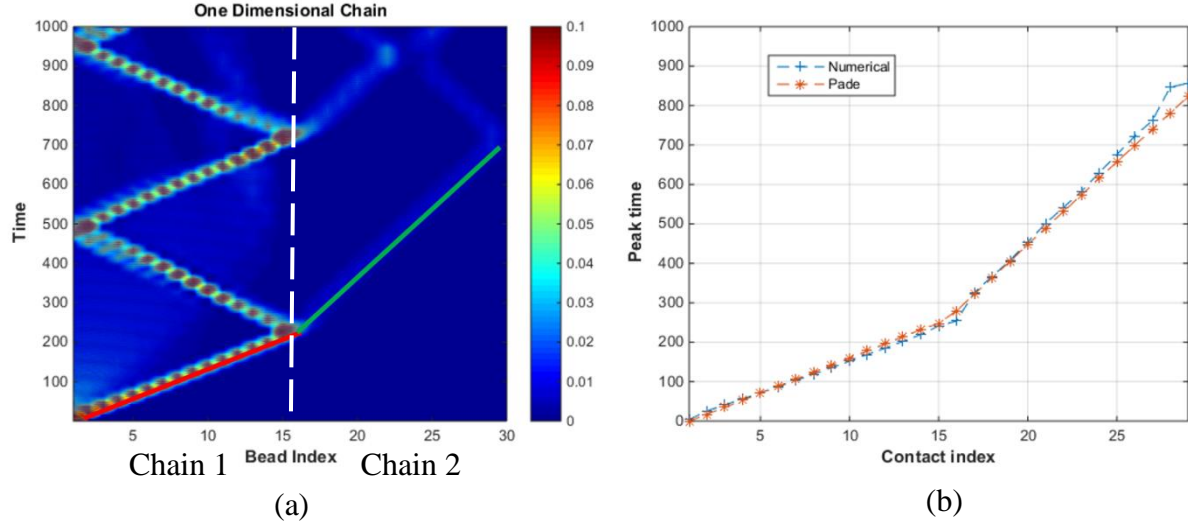
Figure 5.6. Breather propagation in the granular network of Figure 5.4 for normalized impulse $v_0 = 0.06$: (a) Spatio-temporal evolutions of instantaneous kinetic energies (scaled $\times 200$) showing breather propagation; (b) maximum amplitudes of the relative displacements during breather propagation along the nextwork: Analytical predictions based on (5.25a) (*), compared to exact numerical solutions based on (5.2) (+).

At this point we would like to reconsider the system depicted in Figure 5.4 for which the analytical prediction of normalized time delays are given by $T_1 = 15.9$ and $T_2 = 46.8$ for the (stiffer) chain 1 and (softer) chain 2, respectively.

In Figure 5.6a we replot Figure 5.5b with the paths of breather propagation in the two chains of the network where slopes represent the speeds of the breathers in the two chains. In Figure 5.6b we compare the time evolutions of the maxima amplitudes of the relative displacements predicted by the analytical approximation (5.25a) (orange line), against the results of direct numerical simulations of the full model (5.2) (blue line). Close agreement between these

two results is observed, with the analytical results fully capturing the wave propagation of the numerical results. We would like to highlight the discrepancies between the analytical predictions and numerical simulations when traveling waves reach the interface between two chains or the end of the second chain. These are attributed to the boundary effects of the system because the analytical model is developed for primary breather propagation in boundless networks and is based on the stationary responses of the middle beads in the networks away from any boundaries. Nevertheless, these boundary or end effects can be eliminated within the span of three beads and the build-up of the breather propagation is accurately predicted by the analytical model.
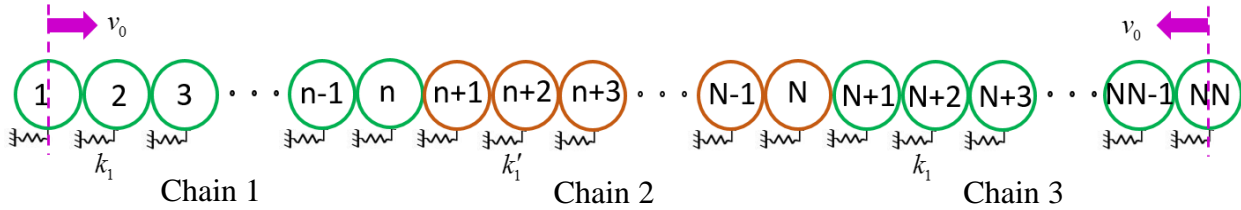
Figure 5.7. Network of three impulsively excited coupled granular chains mounted on different linear elastic foundations.

Motivated by the validation presented above, the developed analytical approximations can be used in a predictive capacity when designing granular metamaterials with prescribed properties in order to control wave propagation in granular networks. Herein, for demonstration purpose, we design the symmetric granular system depicted in Figure 5.7, which can be seen as an extension of the system in Figure 5.4, with three one-dimensional chains coupled together. This system consists of three chains where the two side chains (chains 1 and 3) are identical (i.e., they have identical beads and foundations), and both are excited by impulse excitations, whereas the middle chain (chain 2) has softer elastic foundation, namely, $k_1' = 0.81k_1$. Every chain has 15 beads and we consider only the responses under high excitations where waves can propagate between different chains, i.e., we

design the PZs of three chain to have overlapping regions; for example, we select an initial normalized impulse $v_0 = 0.06$.
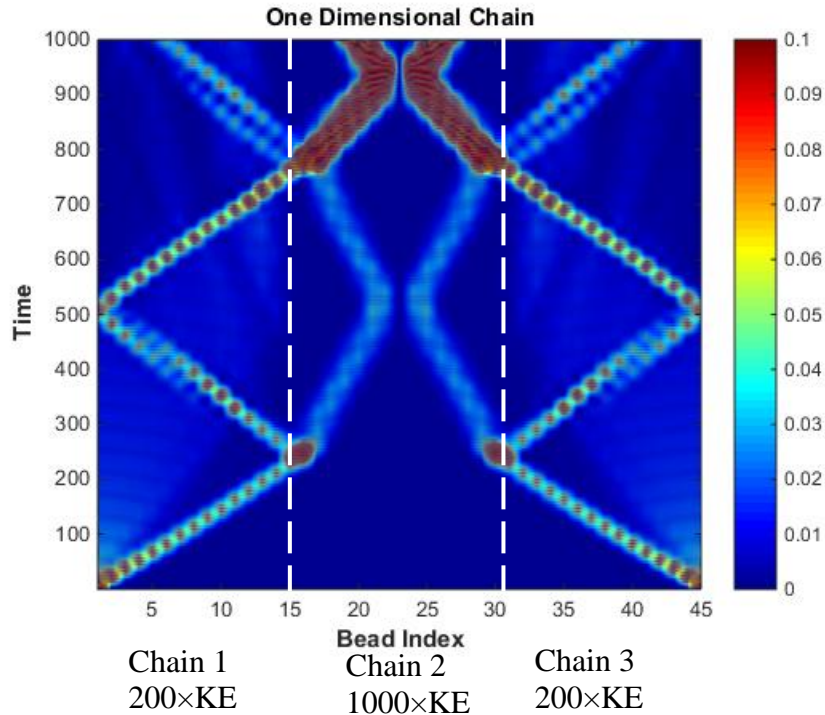
Figure 5.8. Spatio-temporal evolutions of instantaneous kinetic energies for the granular network of Figure 5.7 (scaled$\times$ 200 for the side chains and $\times 10^3$ for the middle chain)

In Figure 5.8 we depict the spatio-temporal evolution of the instantaneous kinetic energies of each bead of the network by applying impulse excitations to both ends of the system simultaneously (as shown in Figure 5.7). We note that after the application of the input pulses clear breather propagation can be seen in the two side chains and the middle chain. Interestingly enough, the 8th bead of the middle chain, which is also the central bead, remains stationary during the entire simulation time. Clearly, this is not due to the incapacity of the granular chain to transmit energy, but rather it is caused by the symmetry of the network, i.e., the negative interference effects between leftward and rightward traveling breathers at the middle chain. At the location of the 8th

bead of the middle chain the system acts as a shock absorber or attenuator since its motion is minimized (being zero). If we break the symmetry of the considered system, the response of a different bead can be minimized. To this end two possible modifications can be considered in order to introduce the desired asymmetry in the system: (a) Spatial symmetry, by using different number of beads in the three chains, and (b) temporal asymmetry by adding time delay(s) to either or both of the two applied excitations. The proposed method in the temporal domain is more feasible for practical implementation as compared to changing the physical setup. Below, we will show that it is possible to control waves by introducing suitable time delay in one of the impulsive excitations. For simplicity in this study we introduce a constant time delay, T_D, to the right excitation. It will be shown below that this temporal detuning parameter has significant influence on the system's response.
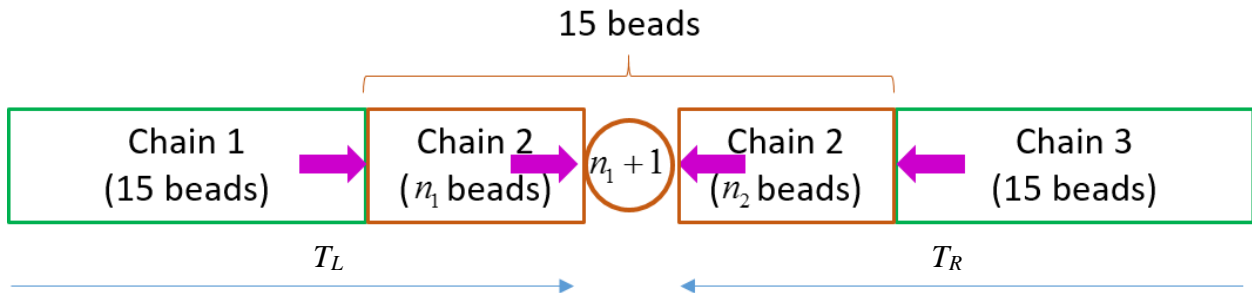
Figure 5.9. Graphical representation of traveling waves in the three chains of the network of Figure 5.7.

In Figure 5.9 we present the temporal dependence of the time delay that we use for the following analysis. We define two different normalized characteristic times of wave transmission in the system, namely, T_L and T_R, which are the times that it takes a breather traveling originating

from the left and right end, respectively, to reach the $(n_1 + 1)^{th}$ bead in the middle chain. These two propagating times can be calculated as,

$$T_L = 15T_1 + n_1 T_2$$
$$T_R = 15T_1 + n_2 T_2 + T_D$$

(5.27)

where $n_1 + n_2 = 14$; as mentioned previously, two normalized time constants, $T_1 = 15.9$ and $T_2 = 46.8$, denote the breather transmission times between neighboring beads in chains 1 and 3, and in chain 2, respectively. In the results shown in Figure 5.8, the excitations to both ends of the system are applied simultaneously, i.e., we set $T_D = 0$. Hence, the negative interference effects between left- and right-going traveling breathers happen at the center (8th) bead of the middle chain, which means that $n_1 = n_2 = 7$, and resulting in almost zero response at this center bead. By appropriately choosing the normalized delay time T_D at the right excitation the position of the stationary bead can be altered or shifted to a desired bead index. For example, if $T_D = 2\tilde{T}_2$ two waves will interact at the 9th bead of the middle chain, i.e., $n_1 = 8, n_2 = 6$. Similarly, the 10th bead will remain stationary for $T_D = 4\tilde{T}_2$. Direct numerical simulations (cf. Figure 5.10) verify these theoretical predictions. In Figures 5.10a and 5.10b we plot the spatio-temporal evolutions of the instantaneous energies of the chains of the network using the analytically predicted time delay as mentioned previously. The stationary position in the middle chain obviously shifts to the right as the positive normalized time delay T_D increases, which validates our analytical approach of calculating the time delay. Vice versa, if a negative normalized time delay T_D is applied, the position of the stationary bead will move to the left.

Another interesting observation is that the time delays we choose in the above examples are even multiples of $\tilde{T}_2$. Then, the following question naturally arises: Will the minimized motion of a desired bead be preserved if the time delay is an odd multiples of $\tilde{T}_2$? In the previous examples the local stationary bead acts as an intermediate "buffer" or "boundary" which is compressed by two traveling waves. If the time delay in the right excitation becomes an odd multiple of $\tilde{T}_2$ this boundary will be eliminated, resulting in strong interaction between the two left- and right-going propagating breathers resulting in local maximum responses of certain beads.

Chain 1	Chain 2	Chain 3	Chain 1	Chain 2	Chain 3
200×KE	1000×KE	200×KE	200×KE	1000×KE	200×KE
	(a)			(b)	
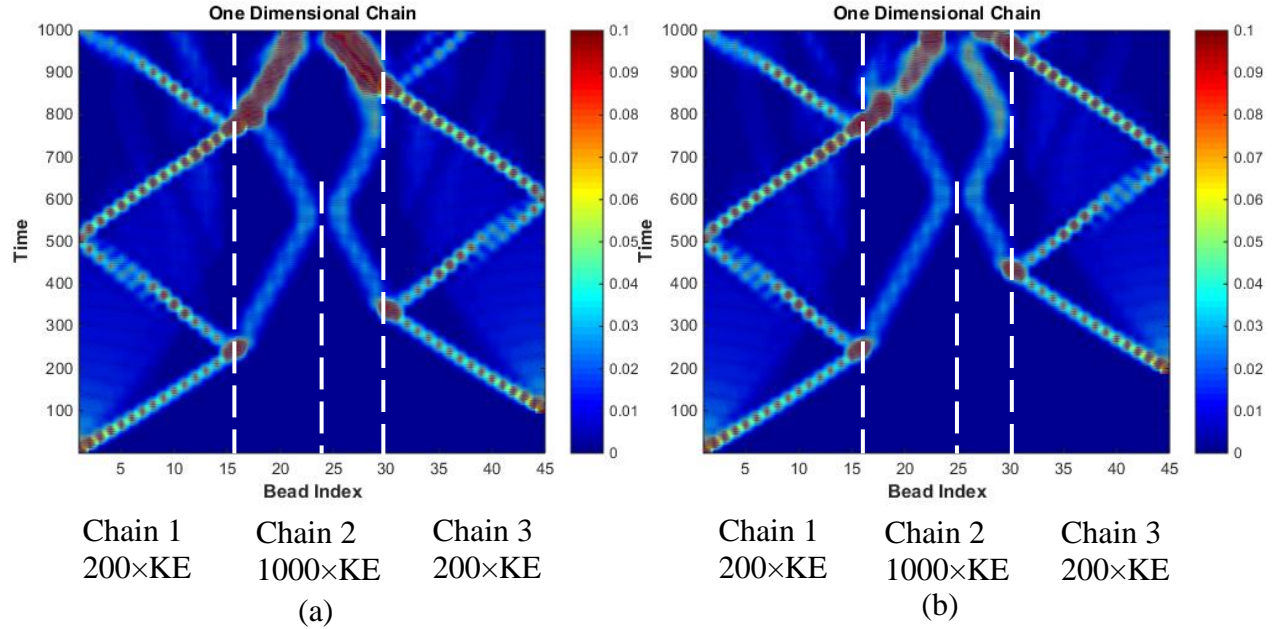
Figure 5.10. Spatio-temporal evolutions of instantaneous kinetic energies for the network of Figure 5.7 for time delays: (a) $T_D = 2\tilde{T}_2$ and (b) $T_D = 4\tilde{T}_2$.

The previous assertions can be directly verified from the numerical results presented in Figures 5.11a and 5.11b. In Figure 5.11a, the right-going and left-going propagating waves interact at beads 8 and 9 with $T_D = \tilde{T}_2$, leading to local large-amplitude oscillations of these two beads. The positions or bead indices which experience the local maximum oscillations can be shifted by

increasing T_D, as shown in Figure 5.11b. The results confirm the "movability" of this local peak for different time delay. Hence, when the time delay in the right impulsive excitation is an odd multiple of $\tilde{T}_2$ the system can be regarded as a local oscillation amplifier rather than a shock absorber.

Chain 1   Chain 2   Chain 3
200×KE   1000×KE   200×KE
                   (a)

Chain 1   Chain 2   Chain 3
200×KE   1000×KE   200×KE
                   (b)
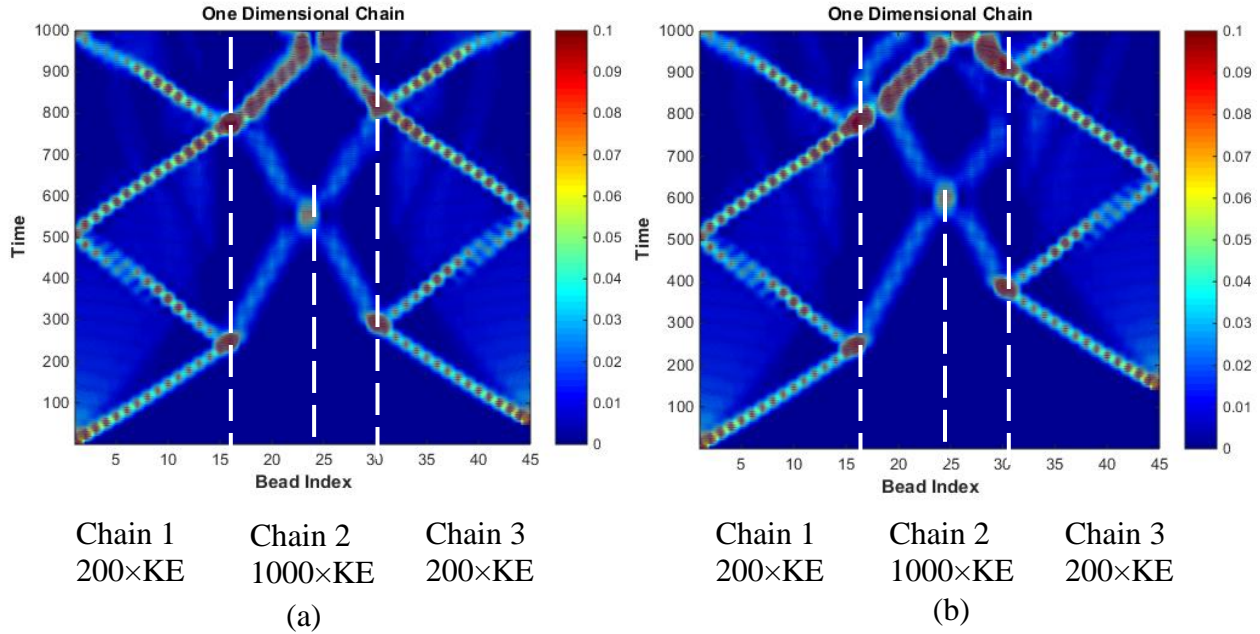
Figure 5.11. Spatio-temporal evolutions of instantaneous kinetic energies for the network of Figure 5.7 for time delays: (a) $T_D = \tilde{T}_2$ and (b) $T_D = 3\tilde{T}_2$.

5.1.2 Computational study of resonance phenomena

In this section we would like to analyze the dynamic responses of one-dimensional granular lattices under harmonic excitations. In equation (5.25) or (5.26) the frequency component ω (normalized) or $\tilde{\omega}$ (dimensional) reveals the nature or mechanism of the propagating breather. This nonlinear phenomenon is due to the closeness of three *fast frequencies*: (i) The frequency of the in-phase mode of the granular chain on its linear elastic foundation, equaling $\omega_1 = 1$ or $\tilde{\omega}_1 = \sqrt{k_1/m}$; (ii)

the energy-dependent main frequency of the breather characterizing the strongly nonlinear granular interactions between adjacent beads, that is, $\omega_2 = 1 + 1.862\tilde{\alpha}\sqrt{a}$ or

$$\tilde{\omega}_2 = \sqrt{\frac{\tilde{k}_1}{m} + 0.2011\frac{E\sqrt{RA}}{(1-v^2)\sqrt{m\tilde{k}_1}}}\ ;\text{ and (iii) the frequency of the out-of-phase mode of the granular}$$

chain, equaling $\omega_3 = 1 + 4\tilde{\alpha}a^{1/2}$ or $\tilde{\omega}_3 = \sqrt{\frac{\tilde{k}_1}{m} + 0.4318\frac{E\sqrt{RA}}{(1-v^2)\sqrt{m\tilde{k}_1}}}$. It turns out that two

differences between these fast frequencies, namely the differences $\omega_2 - \omega_1$ and $\omega_3 - \omega_2$, are almost identical and are equal to the *slow frequency* ω_{slow}, of the slow modulation of the developing breather. This leads to 1:1 internal resonance resonance, which is the nonlinear mechanism that governs breather propagation in this case. Under appropriate low-frequency external excitation at frequency ω_{slow} a combination resonance is realized in the granular network initiating propagation of the traveling breather, as numerically verified by Zhang et al. (2015). To gain insight into the frequency response of the granular network we relate the constant amplitude of the traveling breathers to the aforementioned three fast frequencies and depict the corresponding normalized results in Figure 5.12a and the dimensional results in Figure 5.12b (the same parameters corresponding to the bands of Figure 5.3 are used with elastic foundation $\tilde{k}_1 = 4420N/\text{m}$). These results provide for predictive design of breather formation in this class of ordered granular media. Indeed, motived by the results of Hasan et al. (2013) and Zhang et al. (2015), which, in fact, were special examples of realizations of propagating breathers, we proceed to introduce a general realization of traveling breathers in a granular network based on the previous analytical results.

197
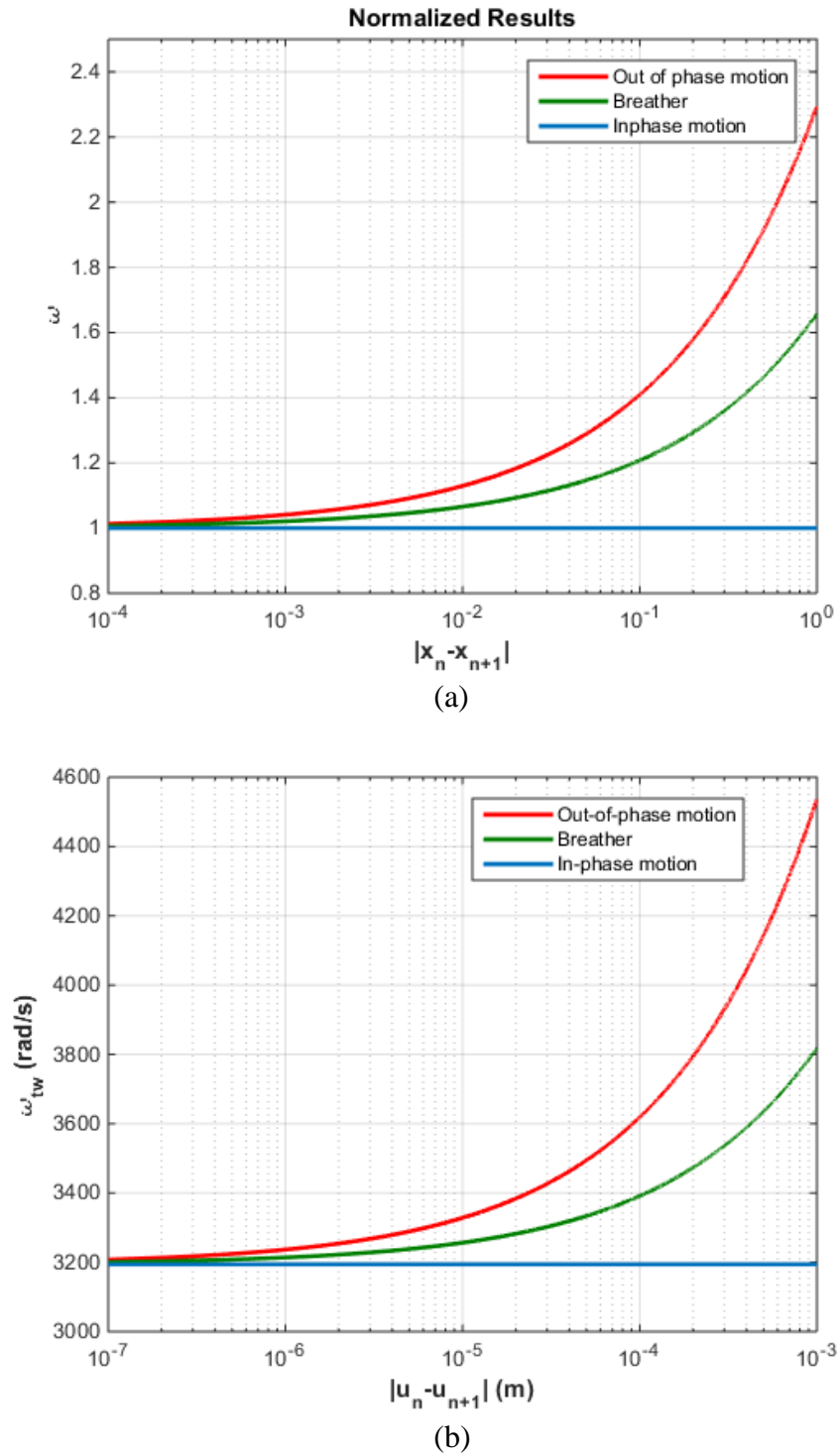
Figure 5.12. The three fast frequency components of the homogenous granular network as functions of the amplitude of the traveling breather: (a) Normalized results; (b) dimensional results with foundation stiffness $\tilde{k}_1 = 4420 N/\text{m}$.
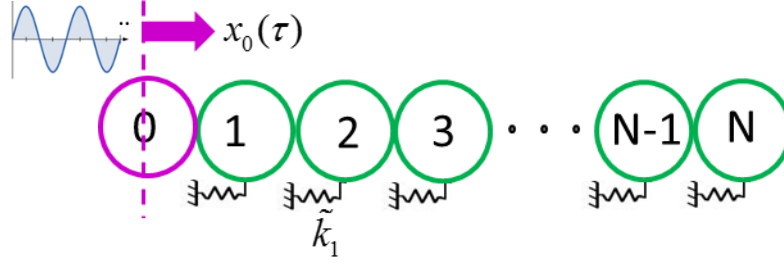
Figure 5.13. The one-dimensional homogeneous granular network mounted on a uniform linear elastic foundation under harmonic excitation.

In the present section we perform a computational study of the granular network under time-periodic excitation. A schematic of the considered one-dimensional granular network is presented in Figure 5.13. It is similar to the system in Figure 5.1, but excited by the motion of a zero-th bead with prescribed harmonic displacement. In the previous derivations no dissipative effects were taken into account; this is a limitation since such dissipative effects are present in every practical granular network. Accordingly, in the following analysis we consider the dissipative effects in the granular chains due to inherent internal structural damping within the material of the beads, frictional effects during bead interactions or viscoelastic effects in the foundation. To this end, we introduce two types of linear damping terms in the model, with dimensional coefficients $\tilde{\gamma}_1$ and $\tilde{\gamma}_2$. The viscous damping terms with coefficient $\tilde{\gamma}_1$ model dissipation in the elastic foundation, whereas the damping terms with coefficient $\tilde{\gamma}_2$ model dissipation during the Hertzian interactions between adjacent granular beads. Performing the same normalizations as in equation (5.2), the dimensionless governing equations of motion are expressed as follows:

$$\ddot{x}_1 + x_1 = \alpha \left[(A_0 \sin(\omega_{ex}\tau) - x_1)_+^{3/2} - (x_1 - x_2)_+^{3/2} \right] - \gamma_1 \dot{x}_1 +$$
$$\gamma_2 \left\{ (A_0 \omega_{ex} \cos(\omega_{ex}\tau) - \dot{x}_1) H(A_0 \sin(\omega_{ex}\tau) - x_1) - (\dot{x}_1 - \dot{x}_2) H(x_1 - x_2) \right\}$$

$$\cdots$$

$$\ddot{x}_n + x_n = \alpha \left[(x_{n-1} - x_n)_+^{3/2} - (x_n - x_{n+1})_+^{3/2} \right] - \gamma_1 \dot{x}_n +$$
$$\gamma_2 \left\{ (\dot{x}_{n-1} - \dot{x}_n) H(x_{n-1} - x_n) - (\dot{x}_n - \dot{x}_{n+1}) H(x_n - x_{n+1}) \right\} \tag{5.28}$$

$$\cdots$$

$$\ddot{x}_N + x_N = \alpha \left[(x_{N-1} - x_N)_+^{3/2} \right] - \gamma_1 \dot{x}_N +$$
$$\gamma_2 \left\{ (\dot{x}_{N-1} - \dot{x}_N) H(x_{N-1} - x_N) \right\}$$

where the variable x_n denotes the normalized axial displacement of the n-th granule, and α denotes the normalized stiffness coefficient of the nonlinear Hertzian interaction between the beads. In (5.28), A_0 and ω_{ex} are the normalized amplitude and frequency of the excitation, respectively, and γ_1 and γ_2 are the normalized linear viscous damping coefficients.

We analyze the frequency responses of the system by applying a harmonic displacement excitation, cf. equation (5.28), and focus on the steady-state response of this granular network, i.e., on the dynamics that is eventually reached after a sufficiently long time so that the initial transients have died out. However, as mentioned previously, the strongly nonlinear dynamics of the granular network is not re-scalable with energy, so the results are expected to depend on the external excitations. Indeed, only under certain combinations of amplitude A_0 and frequency ω_{ex} can the system reach a regular steady state. Taking this into account, we investigate the steady-state nonlinear response of the network by considering the input energy provided during each cycle of the applied excitation and consider the limiting stationary values of the input energy per cycle. To calculate the input energy during each cycle of the applied excitation, we consider the input power as the product of the velocity of the first bead and the effective applied force from the prescribed

motion of the zero-th bead. Then the input energy applied during the $n-th$ cycle can be evaluated as follows,

$$E_n^{(1)} = \int_{nT_0}^{(n+1)T_0} \alpha \left(x_0 - x_1 \right)_+^{3/2} \frac{dx_1}{d\tau} d\tau, \quad n = 0,1,2,... \tag{5.29}$$

where T_0 is the normalized period of the excitation and the integrand denotes the power input by the $n-th$ sine pulse. As an example, the case with $A_0 = 2.69$ and $\omega_{ex} = 0.112$ is considered in Figure 5.14 where we depict the normalized power input by the series of sine pulses, as well as the discrete values of input energy $E_n^{(1)}$ as computed by (5.29). In this specific example we note that the input energy per cycle tends to a constant stationary limit as the number of cycles (or time) increases, indicating that a stable steady-state response of the network has been reached.
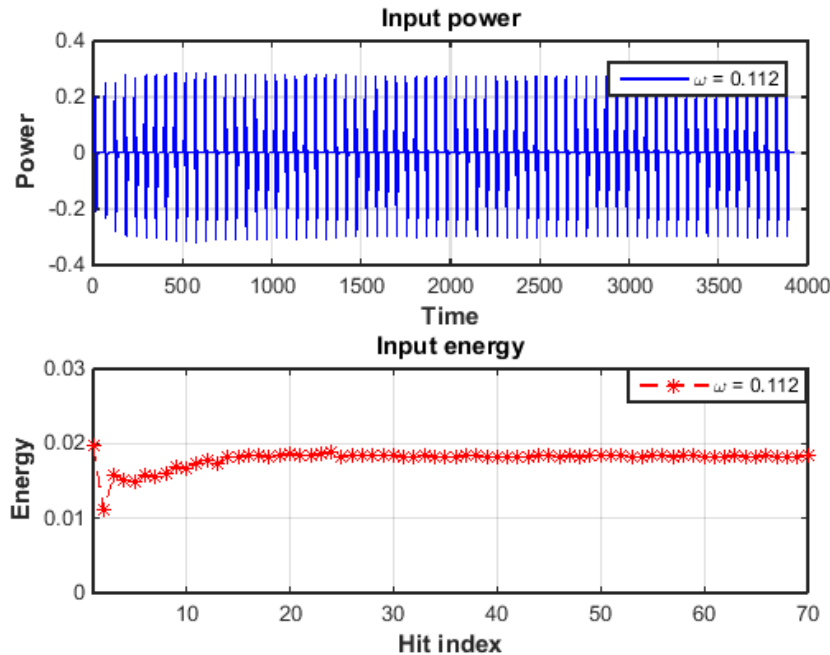
Figure 5.14. Normalized power (continuous in time) and energy $E_n^{(1)}$ (discrete in time) input by an applied displacement with parameters $A_0 = 2.69$ and $\omega_{ex} = 0.112$.

We now focus on this stable fundamental periodic solution with the aforementioned excitation parameters. This corresponds to a nonlinear beat phenomenon involving propagating breathers in the chain. In Figure 5.15a we depict the spatio-temporal evolution of the instantaneous kinetic energies of the 20 leading beads of the network after its dynamics has reached this fundamental steady-state response, along with the time series of the applied harmonic excitation shown at the left of the figure. Certain conclusions can be drawn based on the results of Figure 5.15a. First, clear energy propagation is noted, in the form of a sequence of nonlinear beats in the form of propagating breathers. Similar to the previous impulse excitation example, after 3 to 4 beads the transient response of the chain dies out and propagating breathers are formed in the granular system. During the occurrence of the nonlinear beats the energy propagates towards the far field (albeit with diminishing intensity due to dissipation), which indicates that this regime of propagating breathers takes place in the frequency pass band of the network (Hasan et al., 2015), confirming our analytical results of Figure 5.12. Second, there is one characteristic speed of breather transmission in the steady state. This can be analytically estimated using the analysis of the time delay between neighboring beads of Section 5.1.1, i.e., equation (5.25a) or (5.26a). Finally, a synchronization of each applied pulse with each generated breather in the chain is noted, indicating the occurrence of phase locking in the dynamics. In fact, the 1:1 correspondence between each applied pulse and a propagating breather in the chain signifies the realization of 1:1 resonance in the dynamics. A last note is about the dissipation effects in this harmonically excited system. In the previous results where no damping terms were included in the equations of motion, i.e., no energy dissipation was considered, the breather's amplitude remained constant after the transient response of the initial 3 to 4 beads died out.
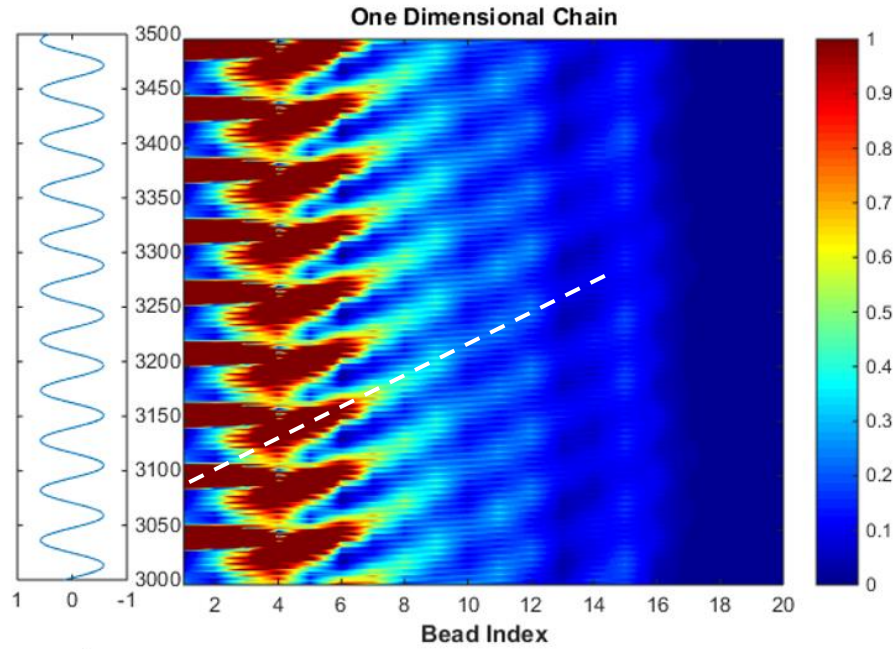
(a)
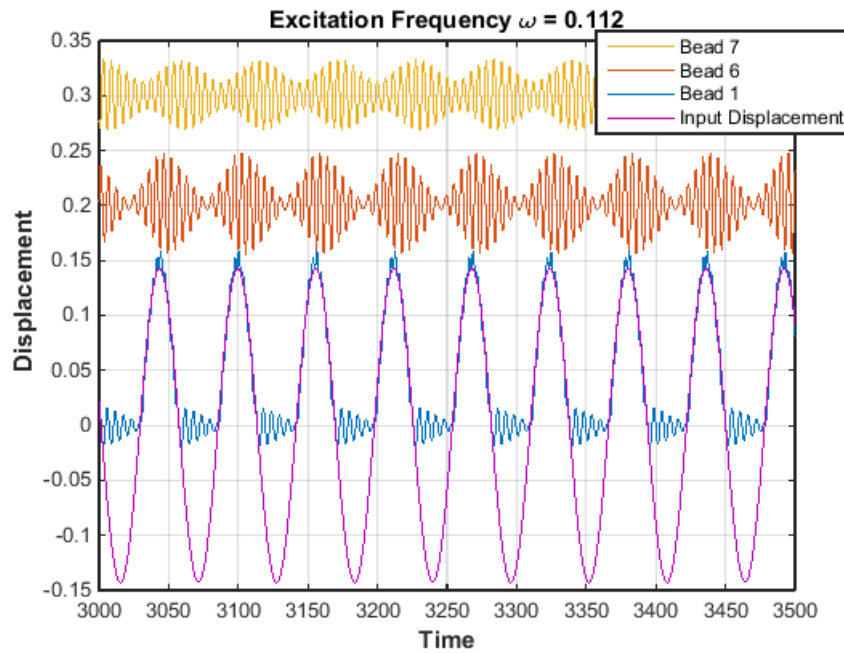
(b)

Figure 5.15. Breather propagation in the harmonically forced granular system due to 1:1 resonance: (a) Spatio-temporal evolutions of the instantaneous kinetic energies of the leading 20 beads, showing propagating breathers in the chain at the steady state, and (b) steady-state displacements of the 1st, 6th and 7th beads.
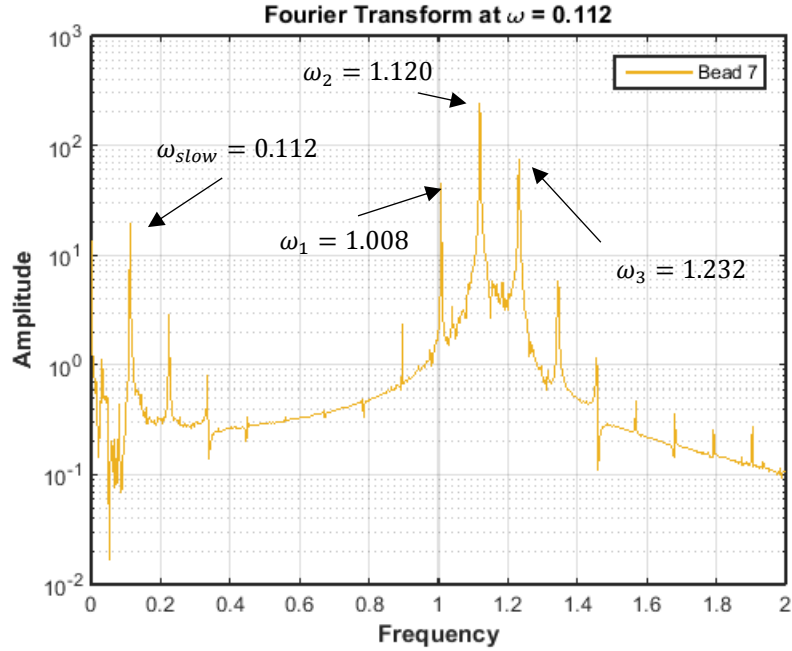
Figure 5.16. Fourier spectrum of the velocity time series of the 7th bead.

However, in the present study, the intensity of propagating energy diminishes due to the presence of damping. Accordingly, in order to employ the previous analytical results in Figure 5.12, a new measure of the amplitude of the relative displacement is defined. Instead of using the amplitude of the slowly varying envelope of the steady relative displacement $|x_n - x_{n+1}|$ (where n is the bead index), in the present harmonically excited system we use instead the amplitude of the difference of the amplitudes between the 5th and 6th beads, i.e., $|x_5 - x_6|$, unless otherwise noted, to minimize the effect of dissipation and ensure the elimination of any transients in the steady state response.

To gain insight into the propagating breather, in Figure 5.15b we depict the steady-state responses of the 1st, 6th and 7th beads of the chain as well as the harmonic input signal. Repetitive beating phenomena can be clearly viewed in the response of each bead, where fast oscillations are

modulated by slow envelopes. To further highlight the nature of the resonance phenomena that give rise to the formation of the breather in the periodically forced granular network, in Figure 5.16 we depict the fast Fourier transform amplitude spectrum of the 7th bead's response in the chain. As mentioned previously, three dominant fast frequencies and one slow modulation frequency can be directly inferred from it. As predicted by our analysis, the differences between any two neighboring fast frequencies is equal to the slow frequency of the slow modulation of the developing breather, which in itself is equal to the excitation frequency, ω_{ex}, of the applied periodic excitation. It follows that the propagating breather is realized when the slow frequency of the periodic excitation, ω_{ex}, equals the frequency of the slow modulation of the breather, i.e., when $\omega_{ex} = \omega_{slow}$, or, equivalently, when $\omega_2 - \omega_1 = \omega_3 - \omega_2 = \omega_{ex}$. This also reveals the nature of 1:1 resonance in the system. These analytical predictions regarding the three fast frequencies have been derived in the previous section and can be directly estimated from the amplitude- frequency plot (cf. Figure 5.12b), as $\omega_1^a = 1$, $\omega_2^a = 1.116$ and $\omega_3^a = 1.228$. The errors between the analytically predicted values and the direct numerical computations have been calculated to be less than 0.8%.

Due to the essential nonlinearities of the system, steady state responses in which resonances exist can only be reached for specific pairs of frequency and amplitude of the harmonic excitation. The analytical results presented in Figure 5.12 provide a predictive way for choosing the excitation parameters to realize such breathers corresponding to 1:1 resonance in the dynamics. For a given amplitude level the difference between neighboring fast frequencies, which is equal to the slow modulation frequency, can be found. We can prescribe a harmonic excitation with its frequency equaling this slow frequency and tune its amplitude until 1:1 resonance is reached. Motivated by the successful prediction of 1:1 resonance, where the dominant, amplitude-dependent frequency

of the breather partitions the passband, i.e., the area between in-phase and out-of-phase frequencies, into two equal parts (cf. Figure 5.12), we proceed to numerically verify the existence of higher order resonances, for example, 1:2 and 1:3 resonances. The expressions of these higher resonance solutions are expected to have similar forms as 1:1 resonance and the passband of granular network to be partitioned into $n+1$ nearly equal pieces for the $1:n$ resonance case. This means in this case there are n additional fast frequency components (which together with the in-phase and out-of-phase mode frequencies provide a total of $n+2$ fast frequencies in the breather) generated by the nonlinear interactions between granular particles. For example, in the 1:1 resonance case, the only fast frequency caused by the nonlinear bead interactions is ω_2. In the general case, the $n+2$ fast frequencies in the breather corresponding to $1:n$ resonance can be approximated as follows,

$$\omega_n^i \approx \omega^{in} + i \cdot \frac{\omega^{out} - \omega^{in}}{n+1}, \quad i = 0, ..., n+1 \tag{5.30}$$

where $\omega_n^0 = \omega^{in}$ and $\omega_n^{n+1} = \omega^{out}$ are the normalized in-phase and out-of-phase fast frequencies corresponding to the first and last fast frequency components. In this case the slow frequency is given by $\omega_{slow} \approx \frac{\omega^{out} - \omega^{in}}{n+1}$, whereas the slow frequency of external harmonic excitation is equal to $\omega_{ex} \approx n \frac{\omega^{out} - \omega^{in}}{n+1}$. The graphical representation of the normalized amplitude-frequency relations for 1:2 and 1:3 resonances are depicted in Figures 5.17a and 5.17b, respectively.
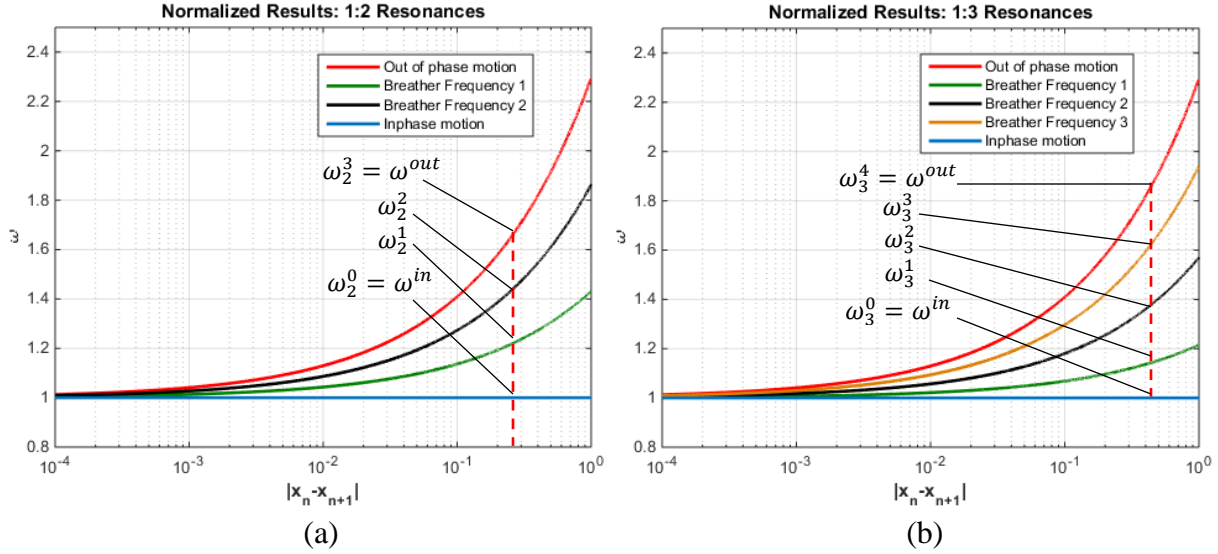
Figure 5.17. Normalized amplitude-frequency relations for breather formation corresponding to higher order resonances of the homogeneous granular network: (a) 1:2 resonance; (b) 1:3 resonance; the corresponding fast frequencies of the breathers are indicated.

Considering the case of 1:2 resonance, the differences between adjacent fast frequencies are almost identical as well. As an example, we consider the case where this difference is about $\omega_{slow} = 0.06$. Then, the forced steady state breather is expected to be realized when the frequency of the harmonic displacement excitation is equal to two times this difference. Hence, the (normalized) excitation frequency is chosen to be $\omega_{ex} = 2\omega_{slow} = 0.12$ and the corresponding (normalized) amplitude is given by $A_0 = 2.94$. The power input by the series of applied harmonic excitation and the corresponding discrete values of input energy are depicted in Figure 5.18a, and the spatio-temporal evolutions of instantaneous kinetic energies of the leading beads of the homogeneous chain in Figure 5.18b. Unlike the nearly constant stationary energy input depicted in Figure 5.14 the discrete values of input energy exhibit a period-2 cycle, repeating every two periods of the excitation; this clearly reveals the nature of 1:2 resonance realized for this breather

formation. A cycle of high and low input energies provides the total energy required to form a propagating breather under condition of 1:2 resonance at the steady state.
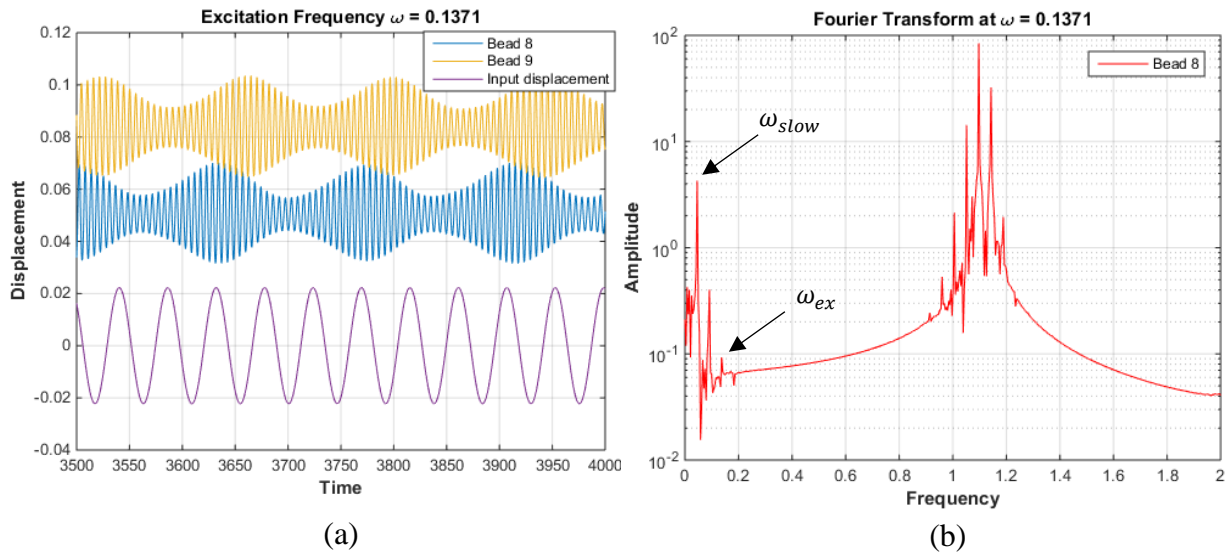

(a)

(b)

(c)
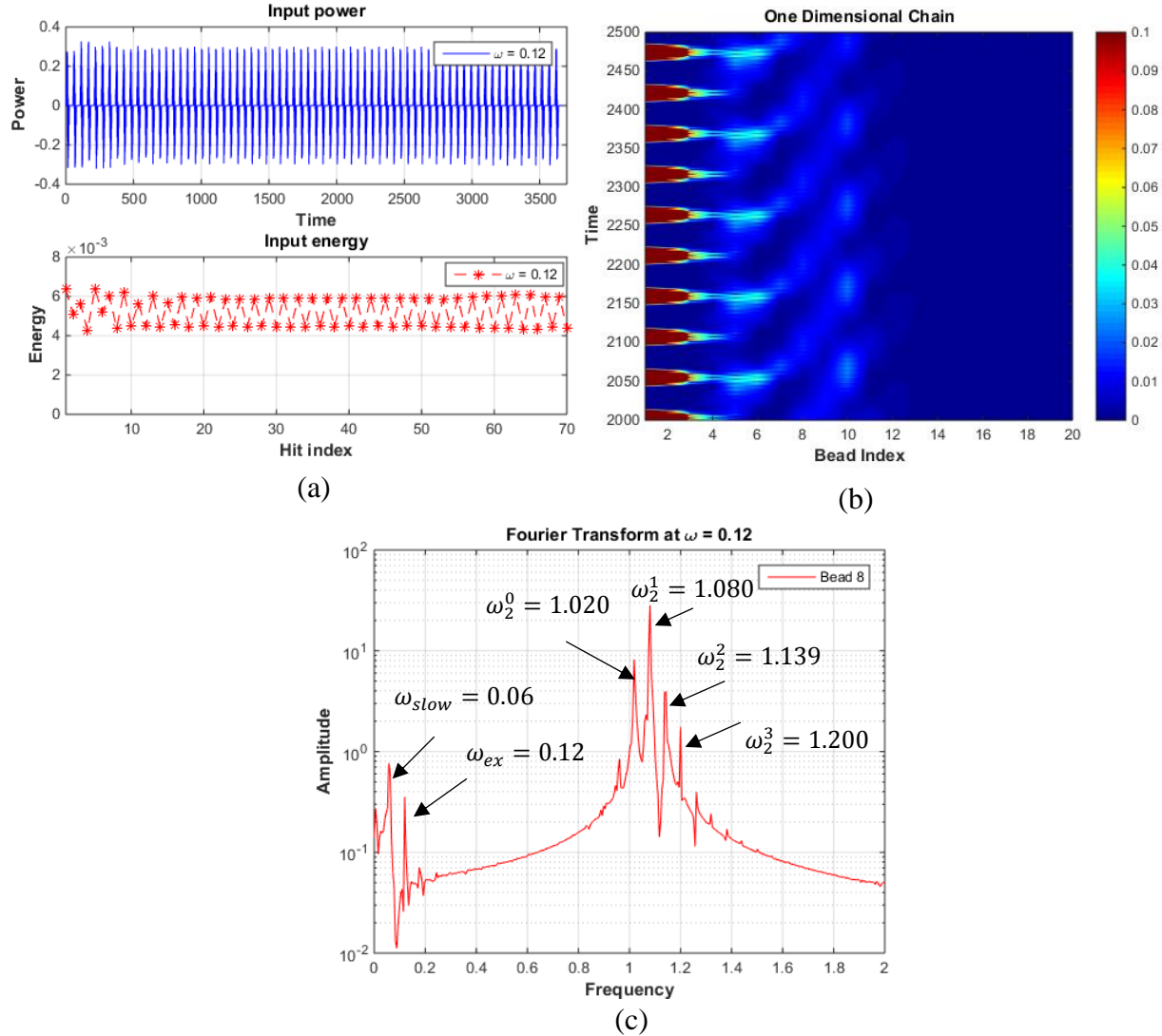
Figure 5.18. Breather formation under condition of 1:2 resonance, for prescribed harmonic displacement of the zero-th bead with normalized amplitude $A_0 = 2.94$ and slow normalized frequency $\omega_{ex} = 0.12$: (a) Normalized power and energy input by the harmonic excitation, (b) spatio-temporal evolutions of the instantaneous kinetic energies of the leading 20 beads of the homogeneous chain, and (c) Fast Fourier spectrum of the response of the 8th bead.

This can be more clearly viewed in Figure 5.18b, where the 1:2 correspondence between the propagating breathers and applied pulses in the chain is noted. Similar frequency analysis is performed and depicted in Figure 5.18c. Indeed, we note that a new breather is formed every two cycles of the applied harmonic excitation. Compared to the fundamental 1:1 resonance considered previously, there is an additional fast frequency component in the breather as expected. The same methodology can be applied to breathers corresponding to 1:3 resonance and the results are shown in Figure 5.19. The 1:3 correspondence between the breather formation and the applied harmonic excitation can be deduced from both the time series and the frequency content, where two additional fast frequency components are detected.

(a)   (b)

Figure 5.19. Breather formation under condition of 1:3 resonance, for prescribed harmonic displacement of the zero-th bead for slow normalized excitation frequency $\omega_{ex} = 0.1371$: (a) steady-state displacements of the input, and breather responses at the 8th and 9th beads, (b) Fast Fourier spectrum of the response of the 8th bead.

The results presented in this section show that a countable infinity of breathers can be realized in the harmonically excited homogeneous granular chain on elastic foundation,

corresponding to $1:n$ nonlinear resonance phenomena between the applied slow harmonic excitation and the differences of the fast frequency components of the modulated responses. As a result, strong energy propagation takes place in the granular system. Each family of breathers corresponding to a specific resonance is tunable with energy, and is realized at specific amplitude-frequency relationships of the applied harmonic input. The formation of these countable infinities of breathers can be predicted by the presented asymptotic analysis, which paves the way for predictive design of granular networks to exhibit the desired nonlinear resonances and breather propagation. The existence of breathers corresponding to 1:1 fundamental resonance has also been reported by Zhang et al. (2015), and these nonlinear phenomena were associated with phase locking and synchronization in the steady-state responses. The analytical study the present work allows for a predictive design to realize such resonances in practical settings. In the next section we provide experimental evidence of the theoretically predicted breathers in a granular network on linear elastic foundation.

5.2 Experimental study

In Section 5.1 we examined a homogeneous granular chain on a linear elastic foundation under impulsive excitation and analytically studied properties of propagating breathers. In this section we experimentally study the formation of discrete breathers in this highly nonlinear acoustic metamaterial and prove the existence of traveling breathers in this system. Two different experimental setups are considered in our study and propagating breathers are robustly detected in each case. Moreover, we extend the theoretical model, i.e., equation (5.2) developed in Section 5.1, in order to recover the experimentally detected response. We show that our developed mathematical model is fully validated by experimental results.
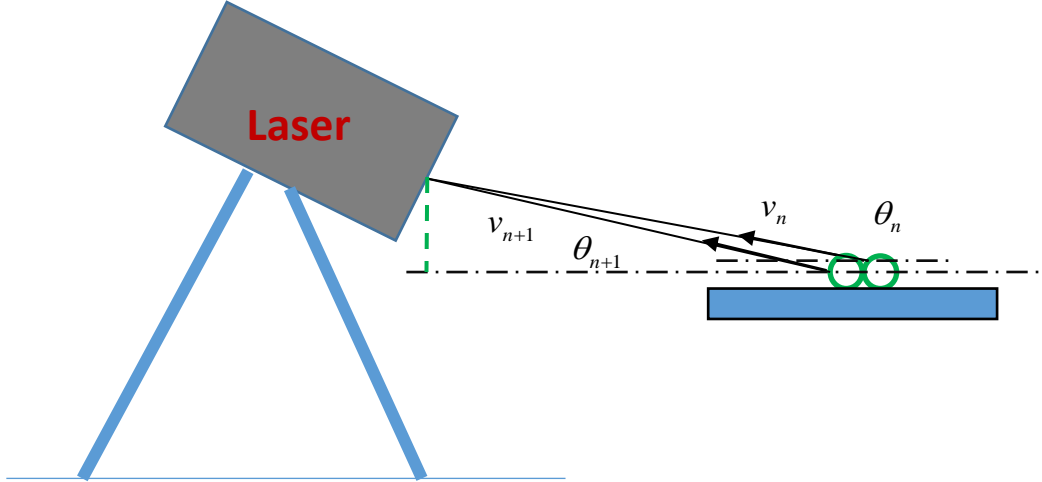
Figure 5.20 A schematic of the granular beads and the laser vibrometer

In this study we will be interested only in primary pulse transmission, i.e., only in the propagation of the generated primary waves through the chain, but not in secondary scattering of these waves once they encounter the boundaries of the chain. We will use a non-contacting laser vibrometer (Polytec® model PSV-400) to measure the velocities of each bead; the methodology adopted for these measurements is presented in the schematic of Figure 5.20. To measure the middle beads' velocities the head of the laser vibrometer is setup with an initial angle (cf. Figure 5.20) in order to account for the presence of the later beads. However, it should be noted that the laser vibrometer is measured only the component of the bead velocity in the direction of the laser beam (velocity component v_n in Figure 5.20). Hence, the axial velocity of each bead can be obtained using the trigonometric relation, $v_n^x = v_n / \cos(\theta_n)$, where θ_n is the scanning angle of the laser beam for the *n-th* bead. According to the geometric configuration of our experimental setup the maximum scanning angle corresponds to the last bead and is given by $\theta_{max} = 0.0479 rad$ or $\cos(\theta_{max}) = 0.999$ in our experimental setup. Hence, we estimate $v_n \approx v_n^x$ in the following analysis. The data is then post-processed using Matlab®.

211

Two different experimental fixtures were considered in the following study, designated as experimental setups I and II. In the setup I the elastic foundation was achieved using a glue, whereas in setup II it was realized by means of stiff cylindrical rods. In both cases breather formation was detected robustly, however, the excess damping introduced by the grounding glue in Setup I restricted the study. The two setups are discussed in detail below.

5.2.1 Experimental setup I

In this section we perform a series of experimental tests with the first setup, with the aim to observe propagating breathers in the homogeneous granular chain. Motived by previous numerical results of homogeneous granular chains under impulse excitation we consider impulsive response of a granular network to verify the existence of discrete breathers and validate our previous computational model. The experimental setup I is depicted in Figure 5.21. Similar to the theoretical study, we consider a granular chain consisting of a number of identical beads composed of type 302 stainless steel (McMaster Carr®, 9291K31) with common radius $R = 9.5\,mm$, modulus of elasticity $E = 193\,GPa$, density $\rho = 8000\,Kg\,/\,m^3$ and Possion's ratio $\nu = 0.3$. To provide the on-site potentials as in the theoretical study the beads are attached/glued to the steel base using JB Welding. The impulsive excitation is provided by means of a pendulum with a bead (identical to the beads of the chain) attached at its end. In addition to the laser measurement mentioned above another laser vibrometer (Polytec® model PSV-300-U) is employed to measure the pendulum motion in order to estimate the initial velocity of the first bead after the applied impulse; the two vibrometers are synchronized. Since the laser can measure only one bead's response at a time, we have to repeat the experiment at the same level of applied impulse multiple times in order to measure all the bead velocities.
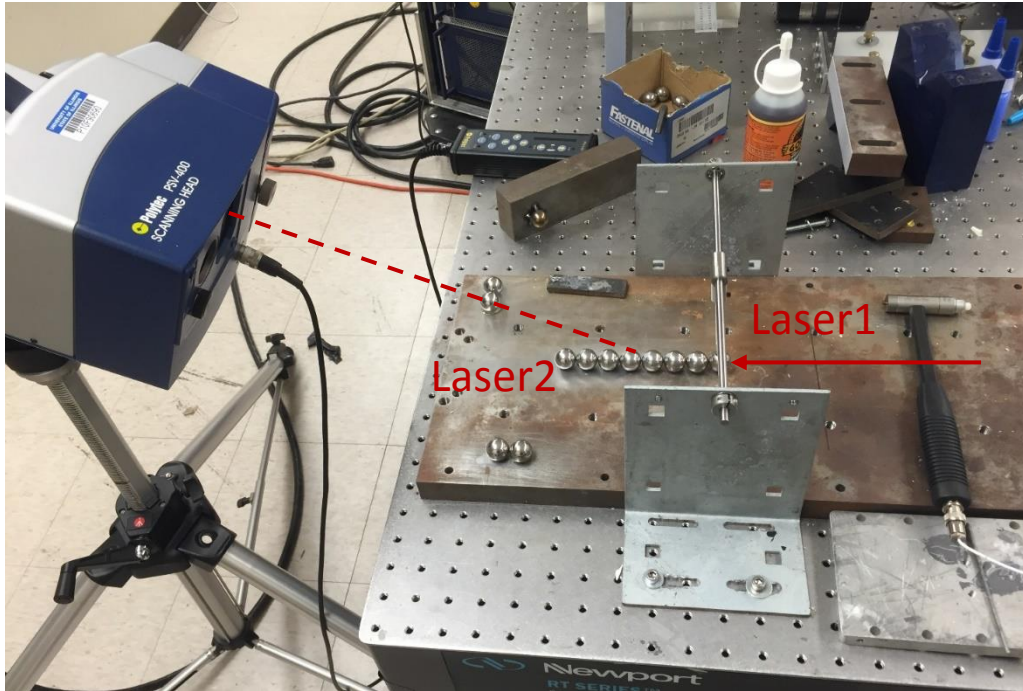
212

Figure 5.21 Side view of experimental setup I for the impulsively excited granular network.

In the experimental setup, the dissipative effects in the dynamics are always present. Although an attempt is made to minimize the frictional contacts in the experimental fixture, complete elimination of friction and other sources of damping in the experiments is seldom possible. In particular, friction forces are expected due to relative rotations between adjacent beads or between beads and their foundations; moreover, inherent internal structural damping in the material of the beads is anticipated as an additional source of damping in the experimental system. In the original models (cf. equation (5.1) or (5.2)) we did not take into account such dissipative effects. To address this issue we add linear viscous damping terms proportional to the relative velocities between adjacent beads and between the beads and the foundation. The foundation stiffness and damping can be chosen by reconciling the numerical and experimental results for a single bead response, as shown in Figure 5.22. This leaves the bead-to-bead damping term as a parameter to be determined

213

later by matching the numerical and experimental results for an impulsively excited homogenous granular chain composed of 10 beads.
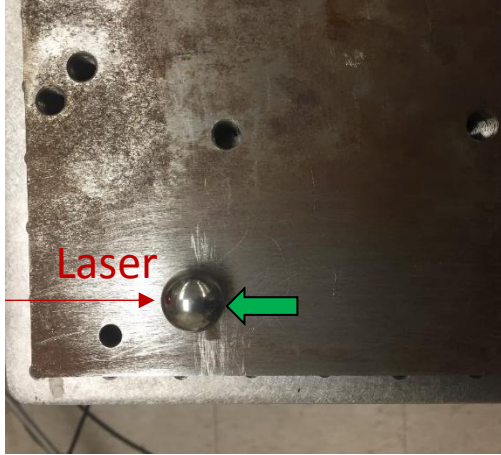
(a)
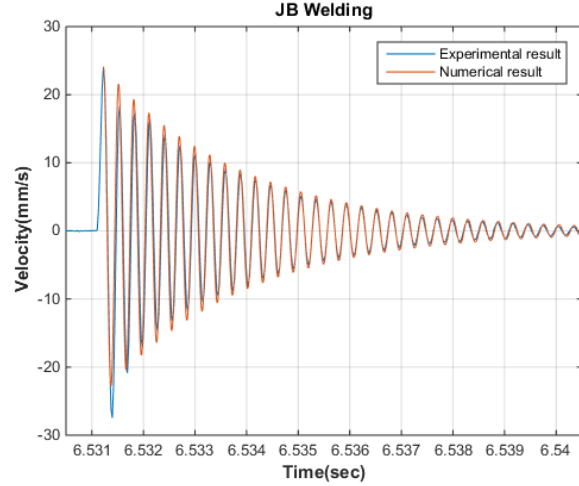
(b)

Figure 5.22. (a) Top view of the experimental fixture for the single bead testing, and (b) experimental (blue line) and numerically reconstructed (orange line) velocity of the tested bead.

In the single bead testing the bead is modeled as a linear mass-spring system with non-zero initial velocity, governed by the following second-order differential equation:

$$m\ddot{u} + \tilde{c}_1 \dot{u} + \tilde{k}_1 u = 0; \, u(0) = 0, \, \dot{u}(0) = v_0 \qquad (5.31)$$

where $m = 0.0287 kg$ is the bead's mass, v_0 the initial velocity which can be estimated directly from the experimental measurement, and $\tilde{k}_1$ and $\tilde{c}_1$ are the stiffness and viscous damping coefficients, respectively, of the foundation which need to be determined. In Figure 5.22b, the experimental measurement (blue line) is reconciled with the theoretical prediction incorporating viscous damping (orange line) by selecting the stiffness and viscous damping coefficient of the theoretical model as $\tilde{k}_1 = 1.33 \times 10^7 \, N / m$ and $\tilde{c}_1 = 21.23 Ns / m$. We would like to point out that

this viscous damping is associated with the choice of foundation. To achieve a stiffer foundation, in addition to the steel base, we glue beads to one and two rigid side walls, respectively. Following the same method, in these two cases the foundation stiffnesses are determined as $2.8 \times 10^7 \, N/m$ and $3.62 \times 10^7 \, N/m$, with corresponding damping coefficients $88 Ns/m$ and $153.7 Ns/m$, respectively. However, in order to observe clear energy or wave transmission, lower damping is desired. Hence, a tradeoff is made here by using the system with one side wall with $\tilde{k}_1 = 2.8 \times 10^7 \, N/m$ and $\tilde{c}_1 = 88 Ns/m$ to continue our study of the one-dimensional chain. These two values are used for the duration of this section for the simulations used for comparing theoretical and experimental results.

Figure 5.23. Top view of the experimental setup I for the impulsively excited granular chain.

In particular, we consider the response of a homogeneous chain composed of 10 beads (cf. Figure 5.23) and superimpose the velocity time series of each bead measured by a non-contacting laser vibrometer with numerical simulations of the corresponding theoretical model. In Figure 5.24 we compare the experimental measurements and numerical predictions for each bead in the granular network. The numerical results are obtained by numerically integrating the following theoretical model,

$$m\frac{d^2u_1}{dt^2} = \frac{E\sqrt{2R}}{3(1-v^2)}[-(u_1-u_2)_+^{3/2}]-\tilde{k}_1u_1-\tilde{c}_1\dot{u}_1+\tilde{c}_2(\dot{u}_1-\dot{u}_2)\mathrm{H}(u_1-u_2)$$

$$\cdots$$

$$m\frac{d^2u_n}{dt^2} = \frac{E\sqrt{2R}}{3(1-v^2)}[(u_{n-1}-u_n)_+^{3/2}-(u_n-u_{n+1})_+^{3/2}]-\tilde{k}_1u_n-\tilde{c}_1\dot{u}_n$$
$$+\tilde{c}_2\left\{(\dot{u}_{n-1}-\dot{u}_n)\mathrm{H}(u_{n-1}-u_n)-(\dot{u}_n-\dot{u}_{n+1})\mathrm{H}(u_n-u_{n+1})\right\},\quad n=2,3,...9 \tag{5.32}$$

$$\cdots$$

$$m\frac{d^2u_{10}}{dt^2} = \frac{E\sqrt{2R}}{3(1-v^2)}[(u_9-u_{10})_+^{3/2}]-\tilde{k}_1u_{10}-\tilde{c}_1\dot{u}_{10}+\tilde{c}_2(\dot{u}_9-\dot{u}_{10})\mathrm{H}(u_9-u_{10})$$

where $u_n(t)$ denotes the displacement of the *n-th* bead. In equation (5.32) $\tilde{k}_1$ and $\tilde{c}_1$ (which have been experimentally obtained by single bead testing) represent the stiffness and linear viscous damping of the foundation, respectively; $\tilde{c}_2$ is the coefficient of linear viscous damping modeling energy dissipation in interactions between adjacent beads, chosen to be $20 Nm/s$ to reconcile the numerical and experimental results; and m, R, E and v are properties of the bead as defined in a previous section. In the comparisons depicted in Figure 5.24 the theoretical predictions are in satisfactory agreement with the experimental measurements. The localized propagating wavepackets are clearly evident from the experimental measurements depicted in Figure 5.24, indicating the formation of a propagating breather in the impulsively excited granular chain. Obvious energy propagation towards the far field is noted (albeit with diminishing intensity due to dissipation). At later beads, such as beads 9 and 10, the motions are almost negligible due to the energy dissipation effects.
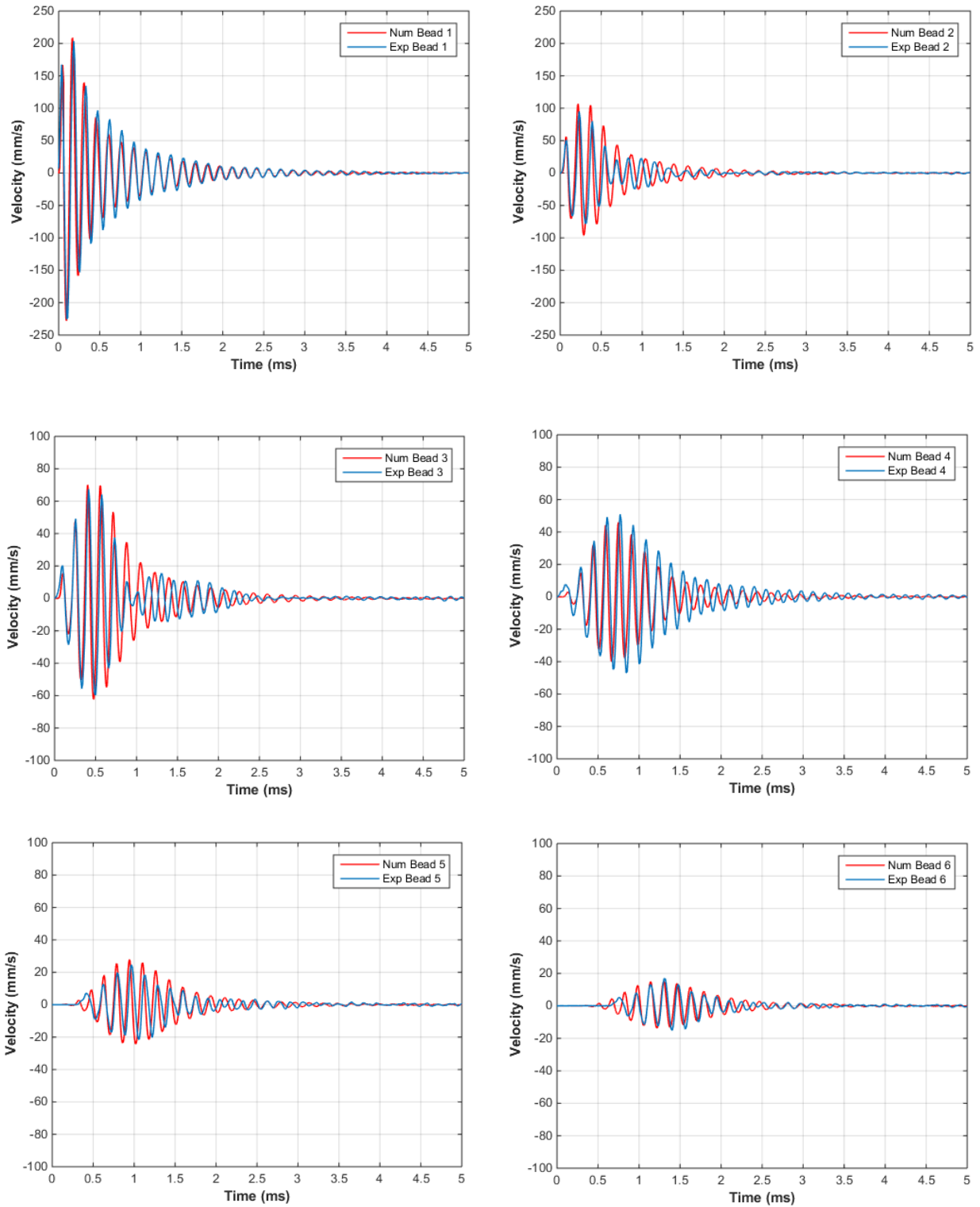
Figure 5.24. Comparisons between experimental measurements (blue lines) and numerical results (red lines) for the granular network with 10 beads: Velocity time series of beads 1-6.
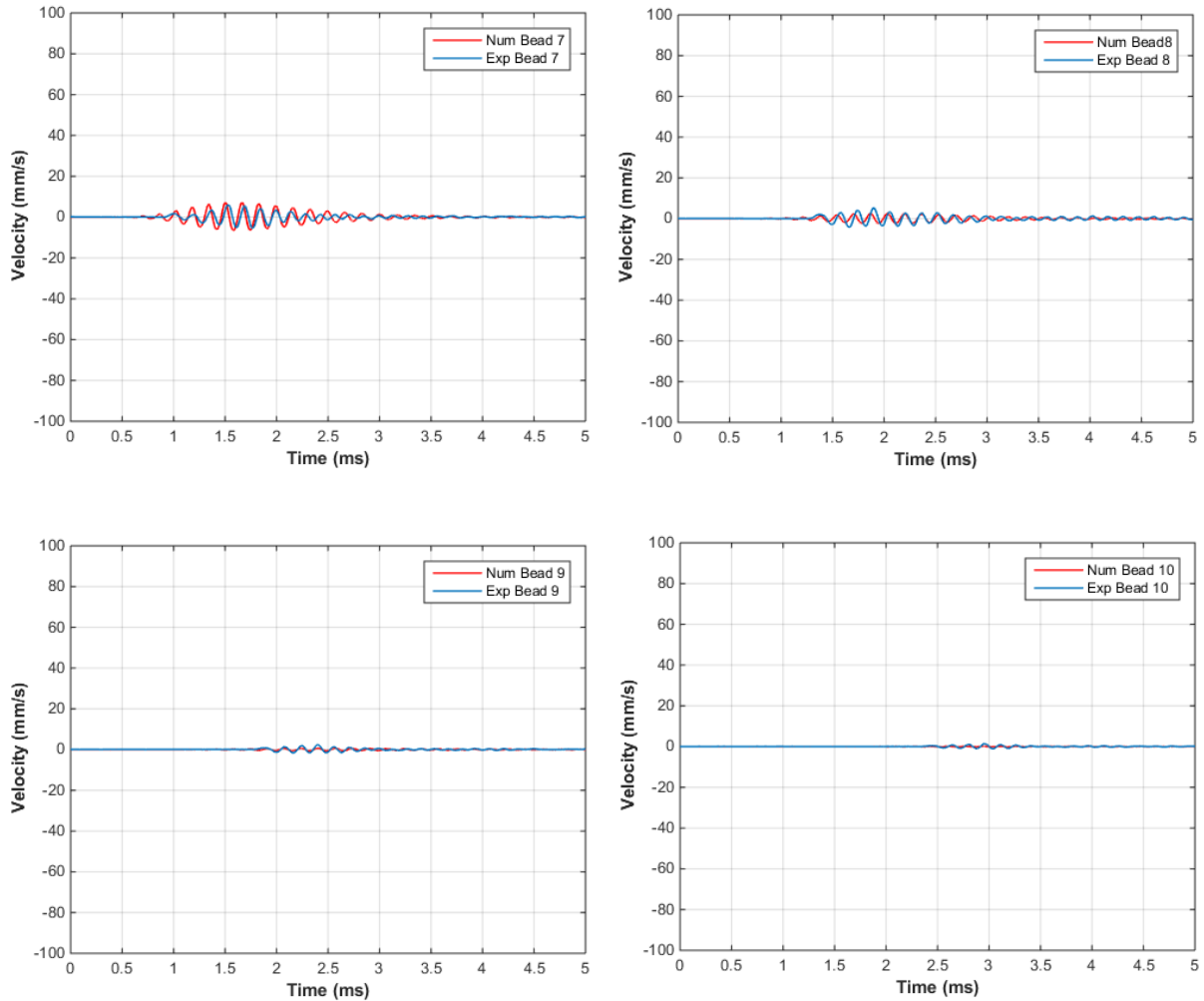
Figure 5.24 (cont.) Comparisons between experimental measurements (blue lines) and numerical results (red lines) for the granular network with 10 beads: Velocity time series of beads 7-10.

From a physical point of view, the formation of the breather is caused by the balance of competing dynamical effects, such as the elastic foundation of the sample, the strongly nonlinear Hertzian interactions between granules, and the discreteness of the granular chain. We emphasize that the nonlinearity, the discreteness and the on-site potential are prerequisites for the realization of these types of modulated oscillatory responses. The oscillatory response of each bead, modulated by a slowly varying envelope, is fully captured by the theoretical results. All numerical simulations follow the same trends as the experimental results. The deviations between theory

and experiment may be attributed to the approximation of viscous damping in the theoretical model which is incapable of fully capturing the nonlinear dissipative effects such as friction and plasticity; and also to inherent bead misalignments in the experimental networks that can have an effect on the experimental results. Even more important, perhaps, is that these experimental results verify numerical predictions of a traveling breather in a homogenous chain with an elastic on-site potential.

Motived by the previous study of the single homogeneous chain and the theoretical results reported in (Hasan et al., 2013; Zhang et al., 2015) we extend our experimental analysis to a two-dimensional network of coupled ordered granular chains. In particular, in the following study we experimentally study a system consisting of two weakly coupled, uncompressed, ordered, homogeneous granular chains mounted on linear elastic foundations and coupled by weak linear stiffnesses. Each chain consists of a number of identical linearly elastic spherical granular beads, which are in touch with one another, so their Hertzian interactions are essentially nonlinear (i.e., non-linearizable); moreover, in the absence of compression, bead separations may occur leading to collisions and providing an additional source of strong nonlinearity. Here, we denote by k_1 and k_2 the stiffness coefficients of the linear elastic foundations and of the linear coupling elements, respectively, and assume weak coupling by imposing the condition that $k_2 << k_1$. In addition, as in the previous section we assume that the beads in both chains are constrained to move in the horizontal direction only. Such a network has been studied theoretically by Hasan et al. (2013) and Zhang et al. (2015) under impulsive and harmonic excitations. In the present work, we aim to experimentally establish breather formation in this coupled granular network. The schematic and the actual experimental setup are depicted in Figure 5.25.
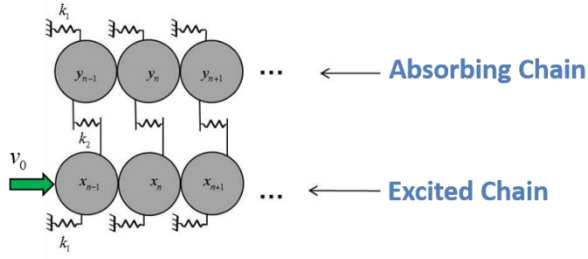
Figure 5.25. Schematic and top view of experimental fixture for the network of coupled granular chains.

The equations of motion for this system can be expressed in following non-dimensional form,

$$
\begin{aligned}
&\ddot{x}_n + k_1 x_n = \alpha\left[(x_{n-1}-x_n)_+^{3/2} - (x_n - x_{n+1})_+^{3/2}\right] - k_2(x_n - y_n) \\
&-c_1\dot{x}_n + c_2\left\{(\dot{x}_{n-1}-\dot{x}_n)\mathrm{H}(x_{n-1}-x_n) - (\dot{x}_n - \dot{x}_{n+1})\mathrm{H}(x_n - x_{n+1})\right\} - c_3(\dot{x}_n - \dot{y}_n) \\
&\ddot{y}_n + k_1 y_n = \alpha\left[(y_{n-1}-y_n)_+^{3/2} - (y_n - y_{n+1})_+^{3/2}\right] - k_2(y_n - x_n) \\
&-c_1\dot{y}_n + c_2\left\{(\dot{y}_{n-1}-\dot{y}_n)\mathrm{H}(y_{n-1}-y_n) - (\dot{y}_n - \dot{y}_{n+1})\mathrm{H}(y_n - y_{n+1})\right\} - c_3(\dot{y}_n - \dot{x}_n);
\end{aligned}
\tag{5.33}
$$

where the variables x_n and y_n denote the displacements of the $n-th$ beads for the excited and absorbing chains, respectively. Comparing equation (5.33) to equation (5.32) there are two more parameters, k_2 and c_3, namely, the stiffness and damping coefficients of the linear coupling elements. Similar to the single chain testing discussed previously, these two coefficients can be determined by reconciling the numerical and experimental results by testing a single pair of beads, as shown in Figure 5.26. In this setup all beads are glued only to the steel base using JB Welding and the effective foundation stiffness and damping have been recorded as the single bead testing (cf. Figure 5.22). The linear stiffness and damping of

the coupling between the two chains are obtained numerically as $\tilde{k}_2 = 2.5 \times 10^6 \, N/m$ and

$\tilde{c}_3 = 30 Ns/m$, by matching the experimental results with numerical simulation of the

theoretical model (cf. Figure 5.26b). Then, the bead number is gradually increased to eight

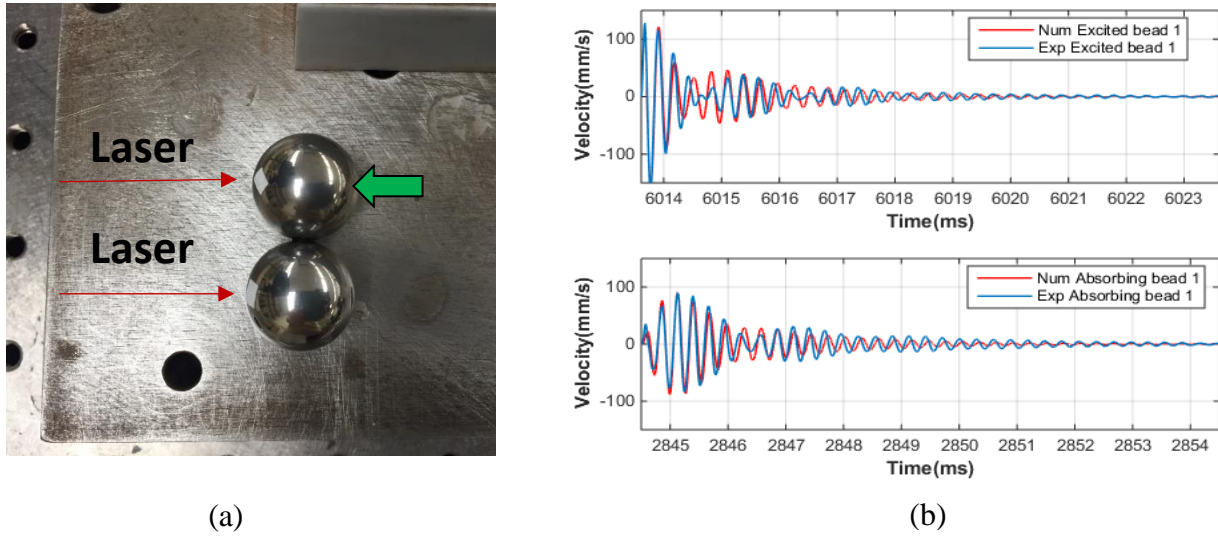and the responses of the two chains are depicted in Figure 5.27.

(a)   (b)

Figure 5.26. Experimental setup I: (a) Top view of experimental fixture for single pair of beads testing, and (b) experimental (blue line) and numerical (red line) velocity of the tested beads.
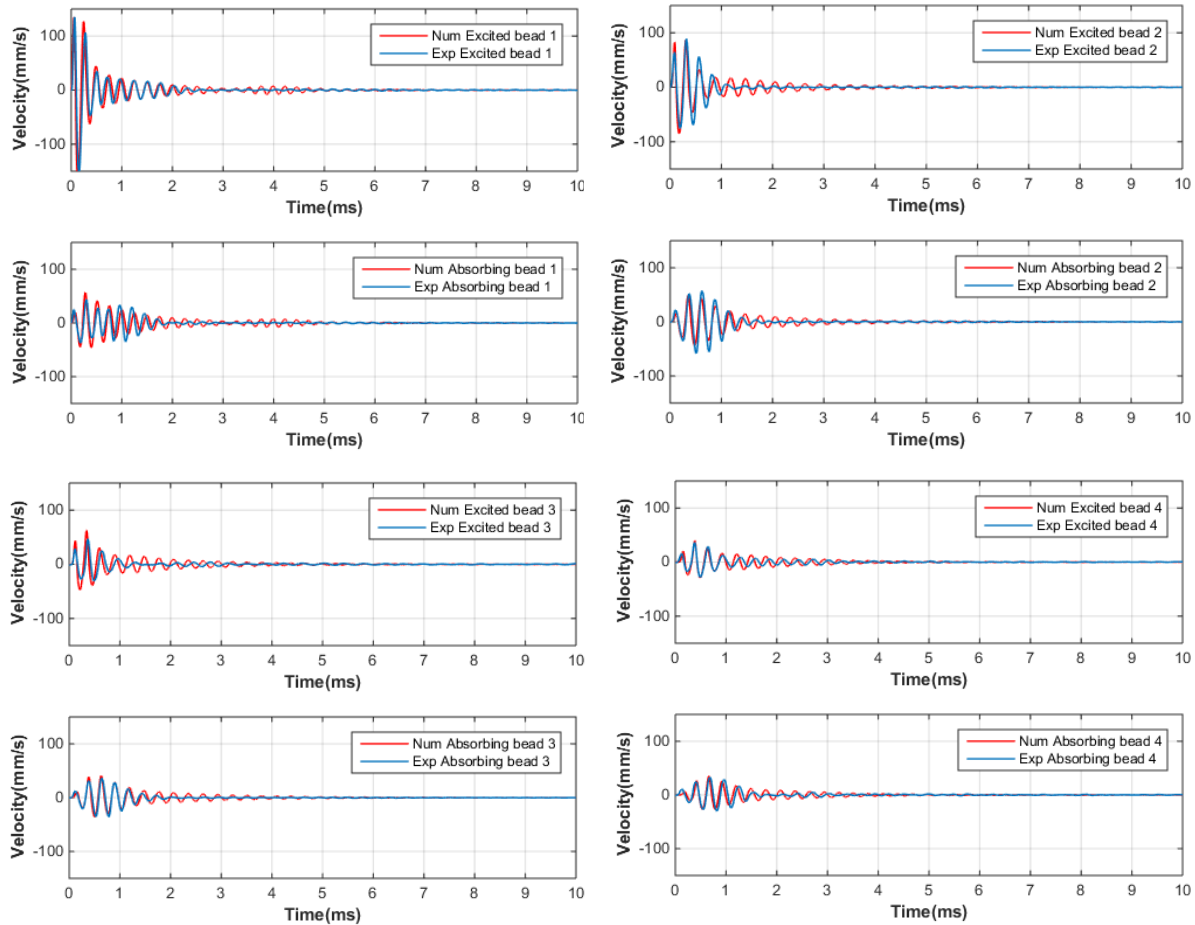
Figure 5.27. Comparisons between experimental measurements (blue lines) and numerical results (red lines) for the coupled granular network with 8 beads in each chain: Velocity time series of beads 1-4.

Certain conclusions can be drawn considering these experimental results. First, the results clearly depict that energy exchanges are occurring between the two coupled chains. Initially the entire input energy is localized in the first bead of the excited chain, but with progressing time this energy gets transferred to the later beads of the excited chain (through Hertzian interactions) and of the absorbing chain (through the weak linear coupling between the two chains). Second, in the previous theoretical studies, the discrete breather persisted for a relatively long time as compared to the breather observed in our experiment. This discrepancy is due the lack of

222

dissipative effects in most of the theoretical models, such as the work reported by Hasan et al. (2013). However, in the experimental system dissipative effects cannot be ignored and play an important role in the wave or energy propagation. To highlight these effects we have added three different types of damping terms as mentioned before. Finally, our numerical simulations are in satisfactory agreement with experimental measurements, which validates the computational models.
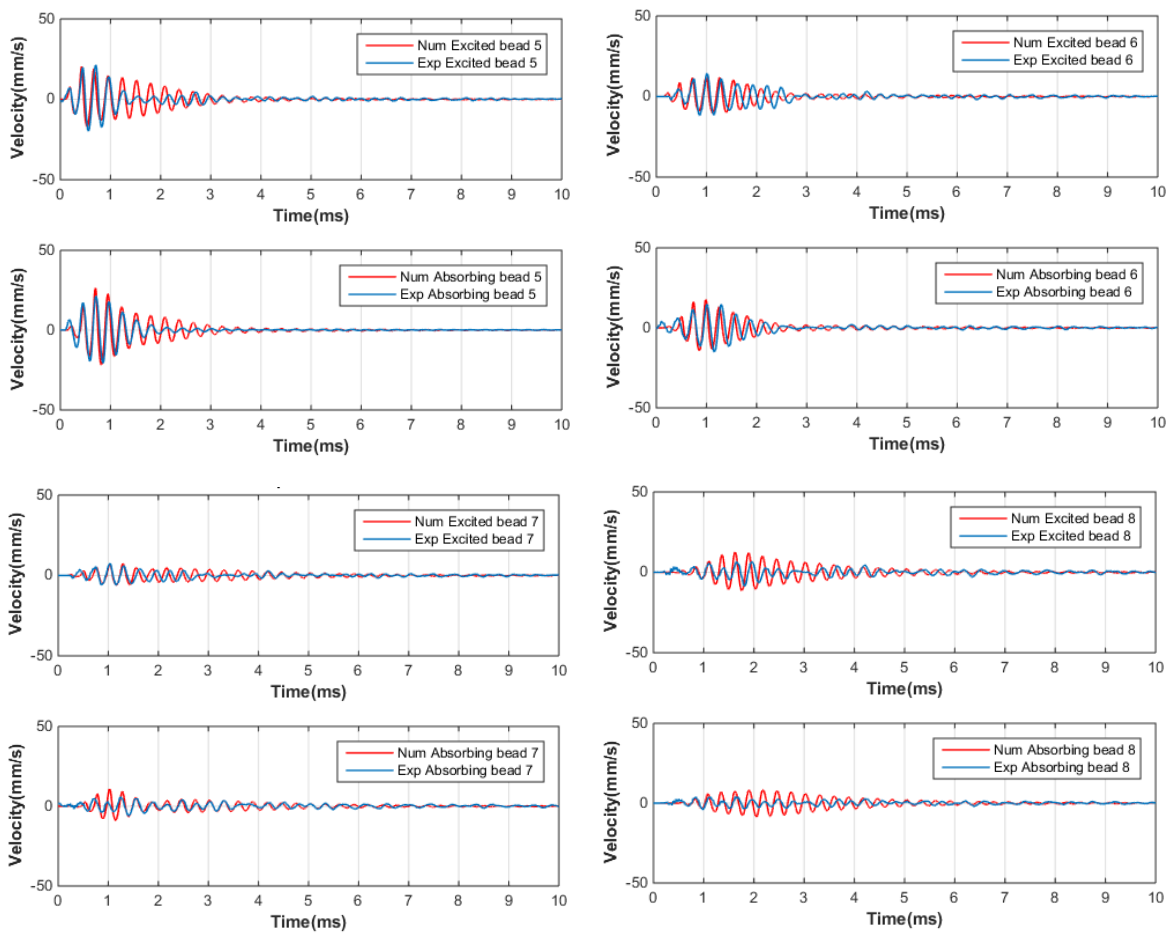

Figure 5.27 (cont.). Comparisons between experimental measurements (blue lines) and numerical results (red lines) for the coupled granular network with 8 beads in each chain: Velocity time series of the beads 5-8.

5.2.2 Experimental setup II

In the previous experimental setup propagating breathers were observed in the initial granules of the tested granular systems but near-zero responses were noted at the later beads due to the strong energy dissipation. As mentioned previously, lower damping is desired for clear energy or wave transmission. To address this issue we fabricate a different experimental fixture as shown in Figure 5.28. In this new fixture the homogeneous granular chain consists of 7 spherical granules composed of bearing-quality aircraft-grade E52100 alloy steel of common radius $R = 12.7\ mm$, modulus of elasticity $E = 210\ GPa$, density $\rho = 7850\ Kg\,/\,m^3$ and Poisson's ratio $\nu = 0.3$. Each bead is fabricated with a $6\ mm$ diameter through-hole to which a steel rod is rigidly welded to its middle and aligned horizontally and vertically with the neighboring beads. These supporting rods, made of grade 304 stainless steel, provide the linear on-site potentials (elastic foundations) as in the theoretical study. Each rod has diameter $6\ mm$ and both ends are placed in a slot of two side holders. After completing the alignment of the granular chain the holders are firmly bolted and rigidly fastened to the steel base. One end of the chain is excited by an impulsive force applied with a pendulum whose mass is equal to the mass of the each bead of the chain. The initial drop angle of the pendulum, measured using a protractor mounted at the pivotal axis of the pendulum, can be used to estimate the impact velocity or the intensity of the applied impulse. As in the previous experimental fixture a laser vibrometer (Polytec® model PSV-400) is employed here to measure the velocity of each bead. The data is then post-processed using Matlab®.
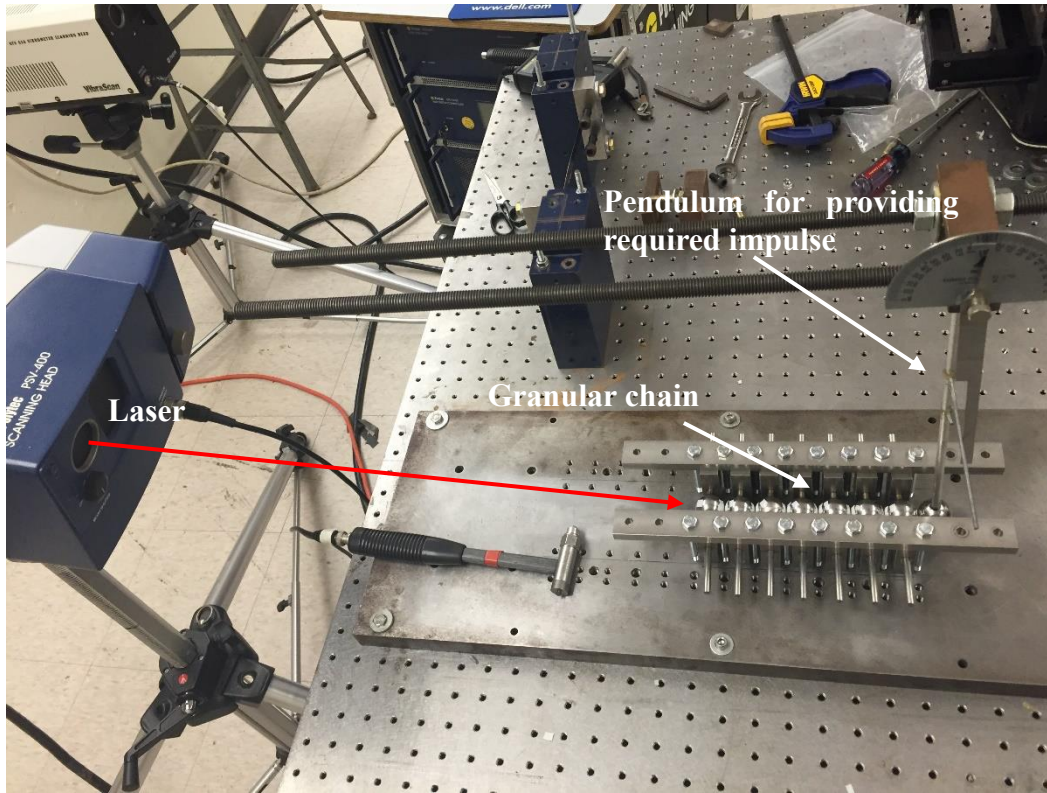
Figure 5.28. Experimental setup II composed of a single granular chain on supporting rods, a pendulum and a laser vibrometer.

Proceeding with our theoretical model (5.32) we reevaluate the damping coefficient and effective stiffness of the supporting rods, which can be seen as inherent properties of the linear elastic foundations. We perform a single bead test as in Section 5.2.1 and reconcile the experimental measurements with the numerical results that are obtained from model (5.31). In Figure 5.29 the numerical results (red) are superimposed onto the experimental results (blue) by selecting the stiffness and viscous damping coefficient of the theoretical model as $\tilde{k}_1 = 1.7 \times 10^7 \, N/m$ and $\tilde{c}_1 = 16 Ns/m$. Good agreement is noted here and these two values are used for the rest of the beads as well. The linear viscous damping between adjacent beads in a one dimensional chain composed of steel beads has been reported by Herbold et al. (2007) as

225

32.15 Ns/m, and by Potekin et al. (2013), as 35.4 Ns/m. Regarding the numerical value of the damping coefficient, we use the estimated value by Potekin et al. (2013), i.e., $\tilde{c}_2 = 35.4 Ns/m$ which was derived for identical steel beads.
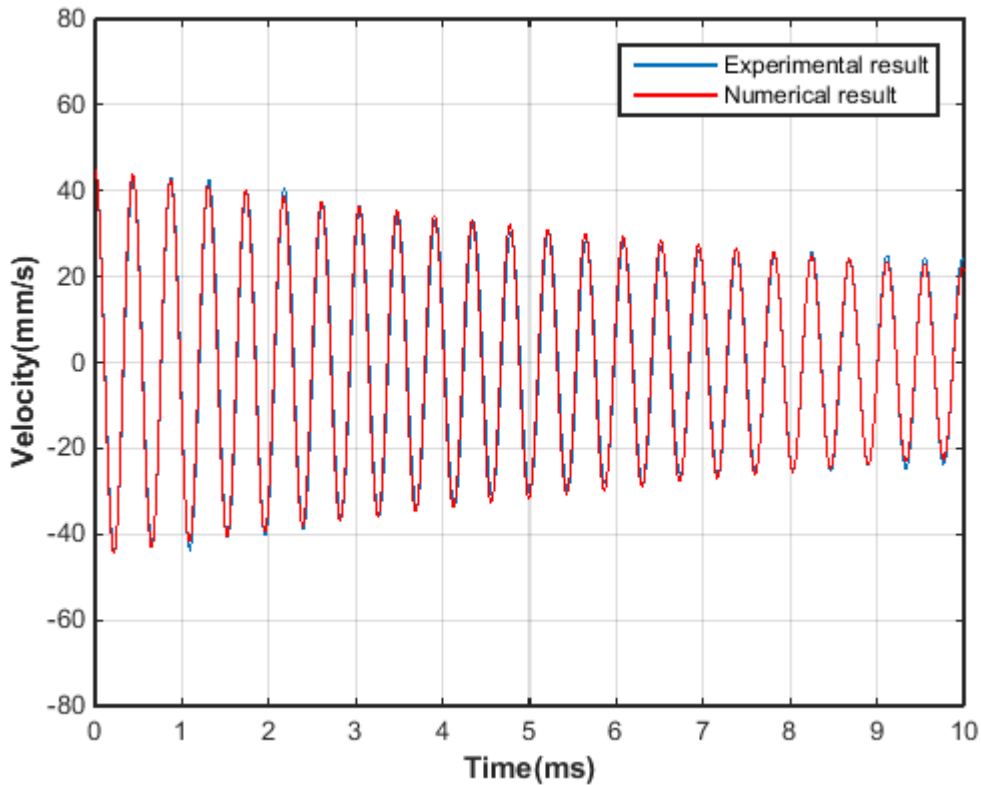

Figure 5.29. Comparison of experimental measurements and numerical simulations of the velocity of a single bead with supporting rod.

Since the tested granular system is essentially nonlinear, its dynamics is expected to be highly dependent on the level of energy; moreover, our analysis is restricted to small energies which ensures that the deformations of the beads are well within the elastic deformation range. To study the energy dependence of breather formation in our experimental study we consider three different levels of (low) excitation corresponding to initial drop angles of the forcing pendulum equaling $\theta_0 = 1°$ (designated as forcing level 1 – providing an initial velocity to the

first bead of the chain equal to $40mm/s$), $\theta_0 = 2°$ (forcing level 2 –initial velocity $55mm/s$)

and $\theta_0 = 3°$ (forcing level 3 –initial velocity $80mm/s$), where θ_0 is the initial drop angle of the

pendulum (the length of the pendulum is chosen equal to $302mm$). Then, these results are

compared with our numerical solutions where the dynamical interactions between the beads are

governed by Hertzian contact law and onsite foundations are modeled as linear grounded springs.

Furthermore, the considered chain is of finite length with its left and right boundaries free. These

considerations are very much commensurate with the experimental setup which we elaborated in

the previous section.

In Figure 5.30 we depict the comparison between the numerical (red) and experimental

(blue) results for the seven beads at the lowest impulse excitation (forcing level 1). The numerical

results are obtained by direct integration of the theoretical model (5.32) with the aforementioned

parameters. We superimpose the experimental and computational velocity time series of the

seven beads in Figures 5.30a-g. Satisfactory agreement is observed, with the computational

predictions fully capturing the primary propagating modulated wavepackets of the experimental

measurements. Moreover, comparisons of the experimental and computational spatiotemporal

variation of the instantaneous kinetic energies of the 7 beads are depicted in Figures 5.30h and

5.30i, respectively. It is apparent that the response of the chain is in the form of waves that are

initiated at the forced end of the chain and propagate to the other end. Examining the wave forms

depicted in these plots, we deduce that all numerical simulations reproduce accurately the

experimental measurements, following the same trends and even reproducing the wave

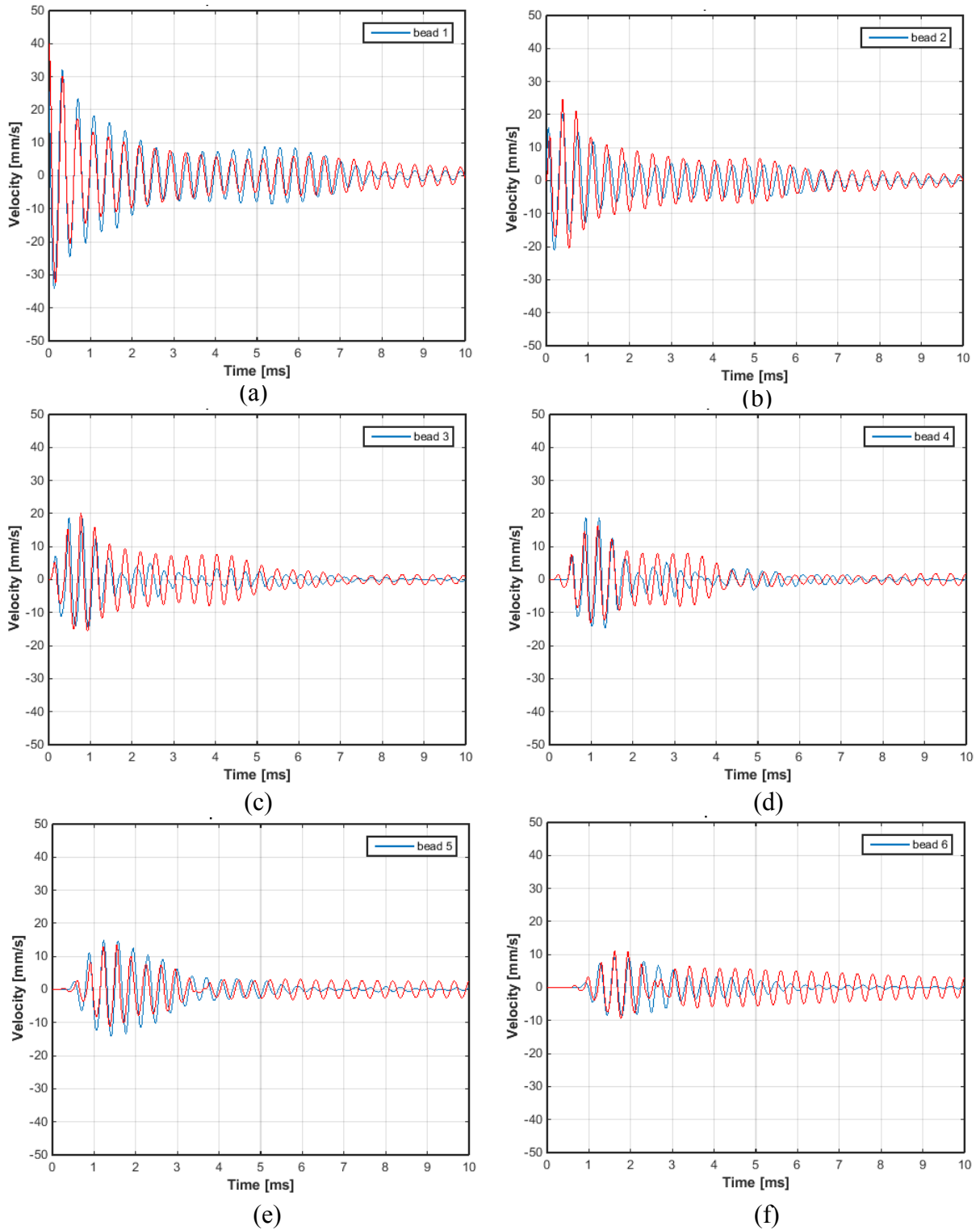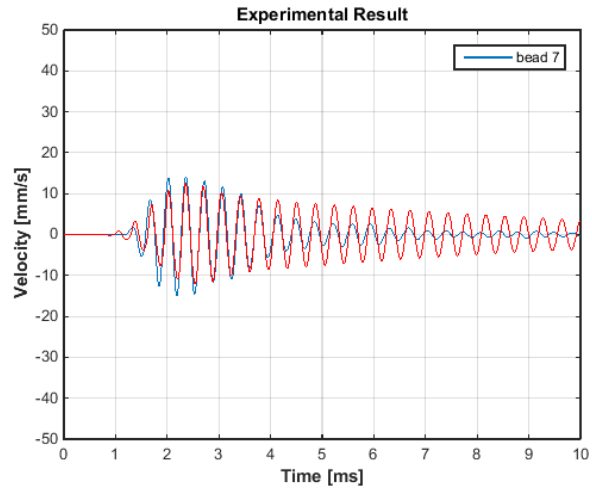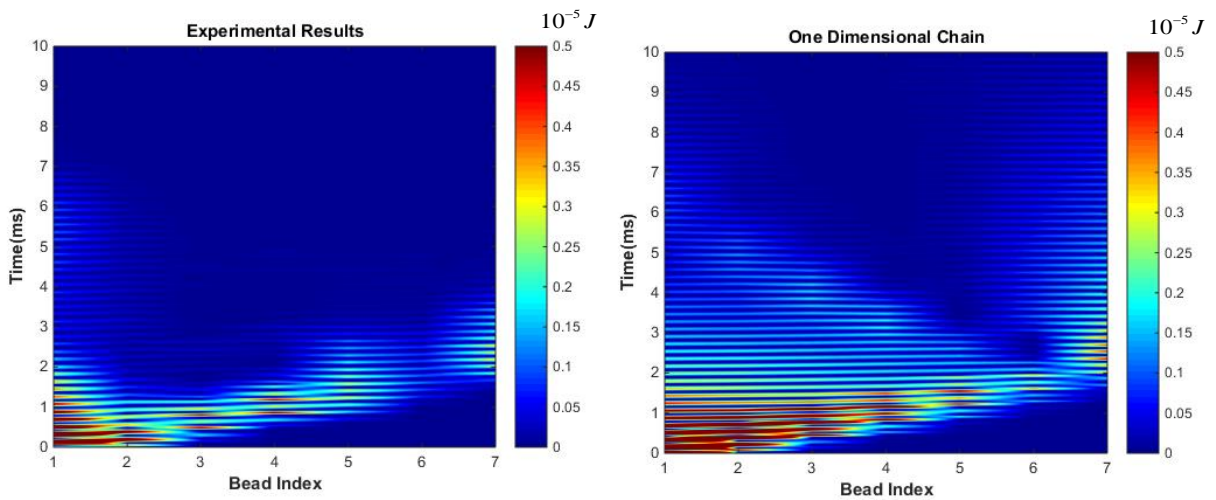reflections after the primary propagating waves reach the boundary of the chain.

Figure 5.30. Comparison of experimental measurements and numerical simulations for the lowest impulse (forcing level 1): (a)-(g) Experimental (blue) and numerical (red) velocity time series of the beads 1-7, (h) experimental and (g) numerical spatio-temporal evolution of the kinetic energy in the granular system.

228

(g)

(h)   (i)

Figure 5.30 (cont.). Comparison of experimental measurements and numerical simulations for the lowest impulse (forcing level 1): (a)-(g) Experimental (blue) and numerical (red) velocity time series of the beads 1-7, (h) experimental and (g) numerical spatio-temporal evolution of the kinetic energy in the granular system.
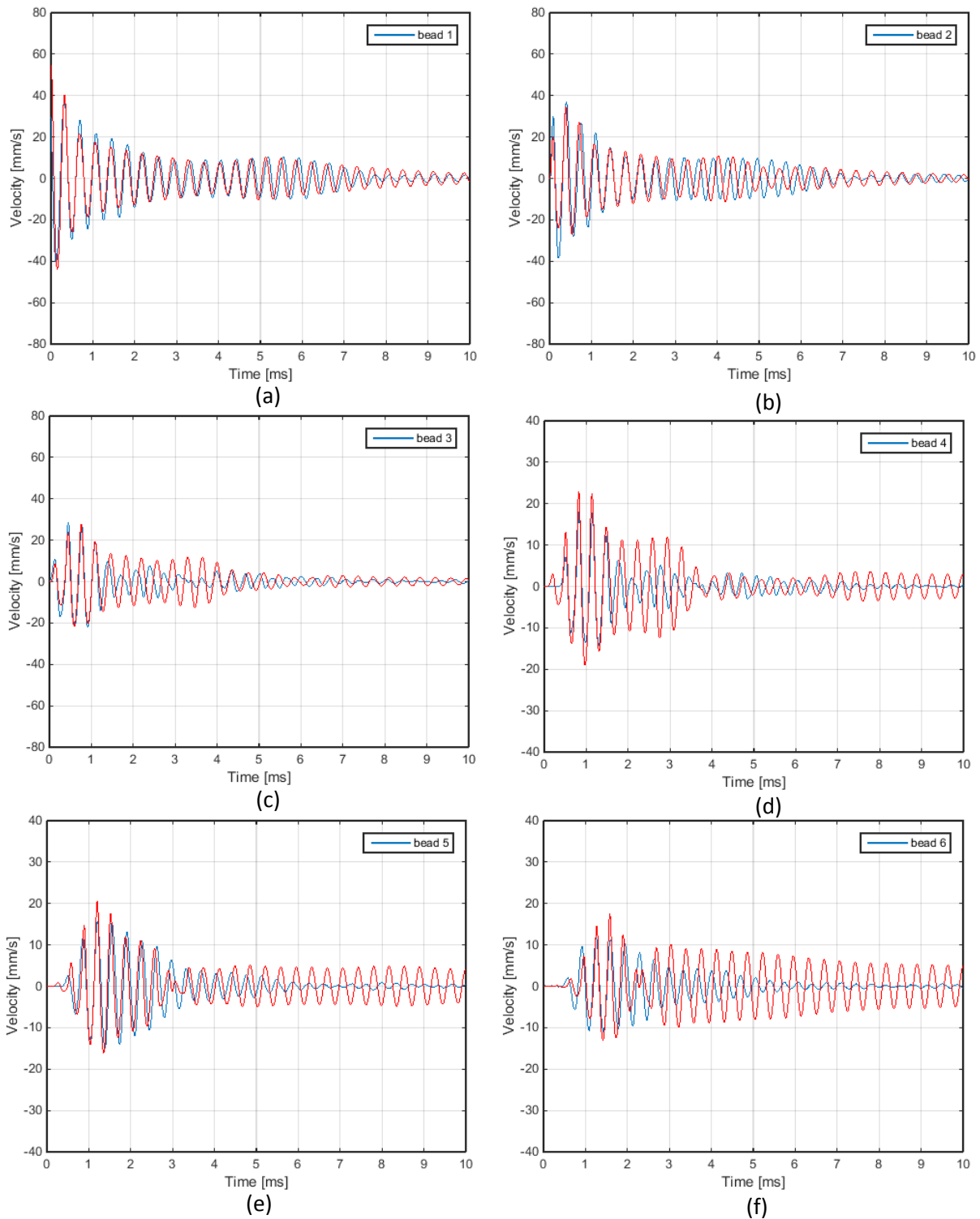
Figure 5.31. Comparison of experimental measurements and numerical simulations for the medium impulse (forcing level 2): (a)-(g) Experimental (blue) and numerical (red) velocity time series of the beads 1-7, (h) experimental and (g) numerical spatio-temporal evolution of the kinetic energy in the granular system.
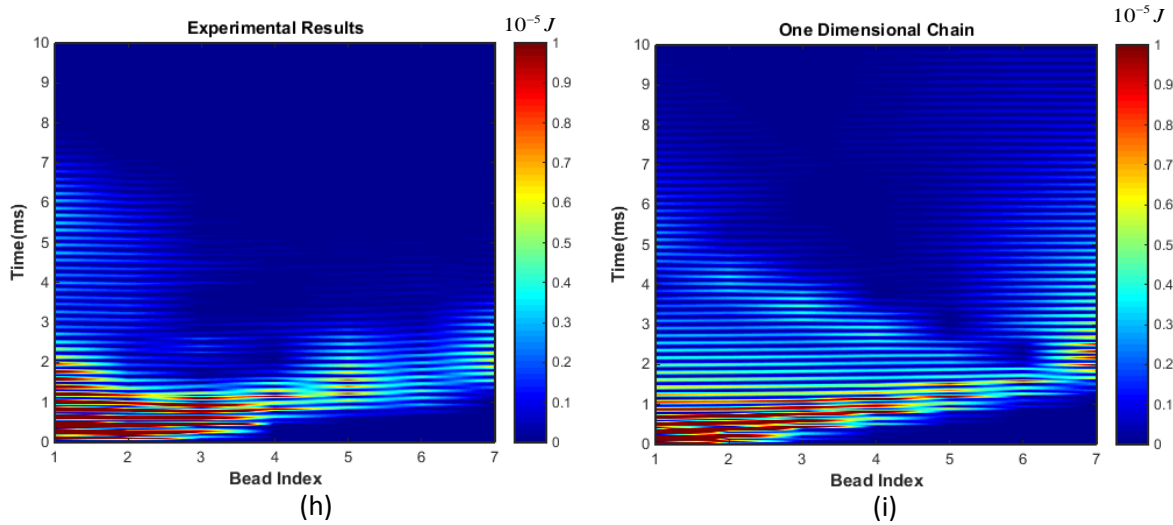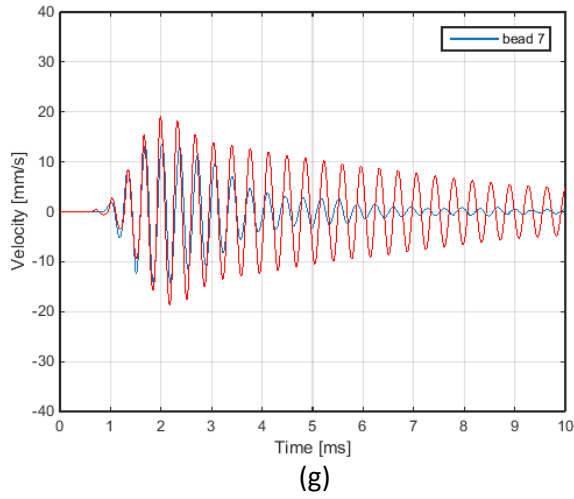
(g)

(h)

(i)

Figure 5.31 (cont.). Comparison of experimental measurements and numerical simulations for the medium impulse (forcing level 2): (a)-(g) Experimental (blue) and numerical (red) velocity time series of the beads 1-7, (h) experimental and (g) numerical spatio-temporal evolution of the kinetic energy in the granular system.
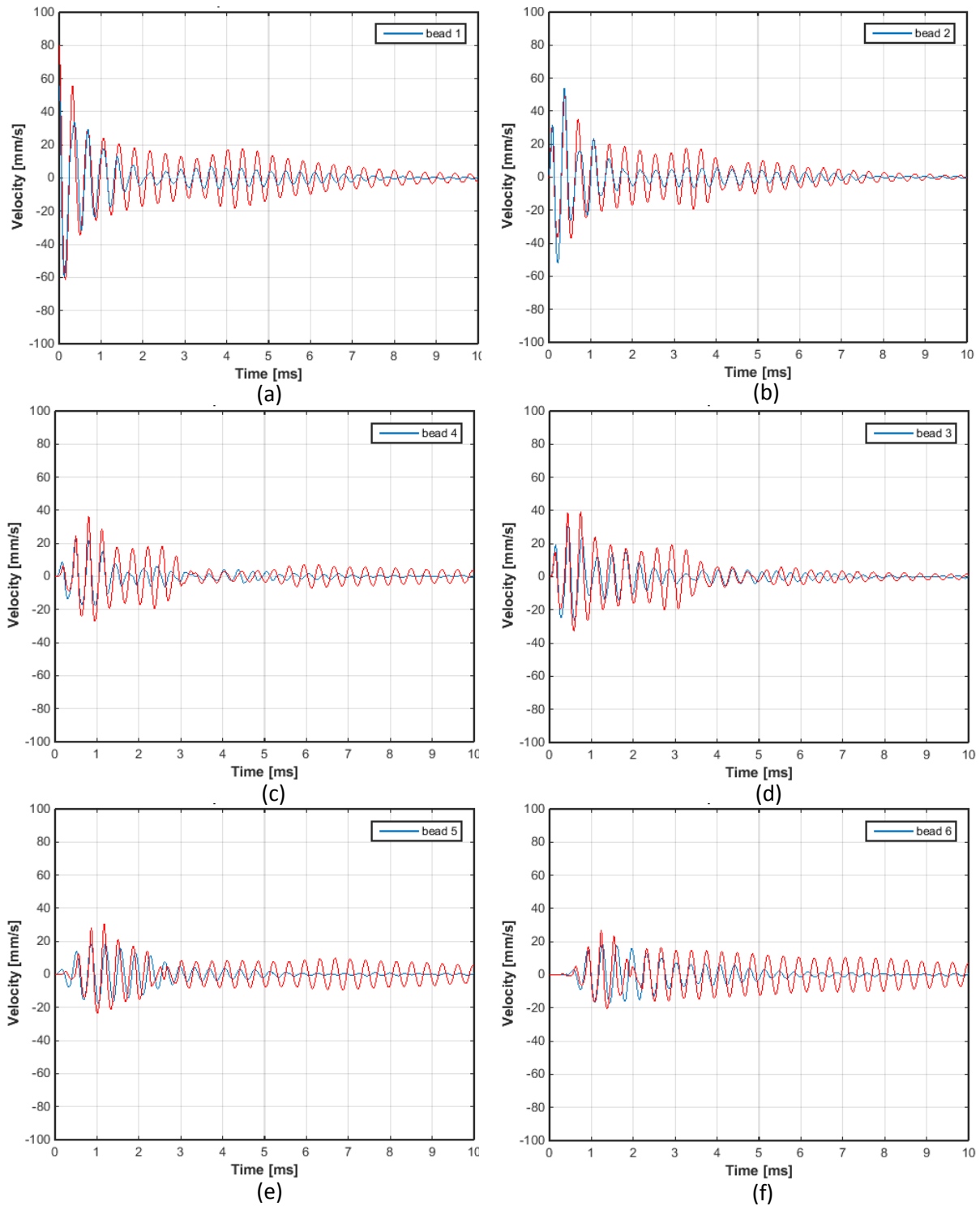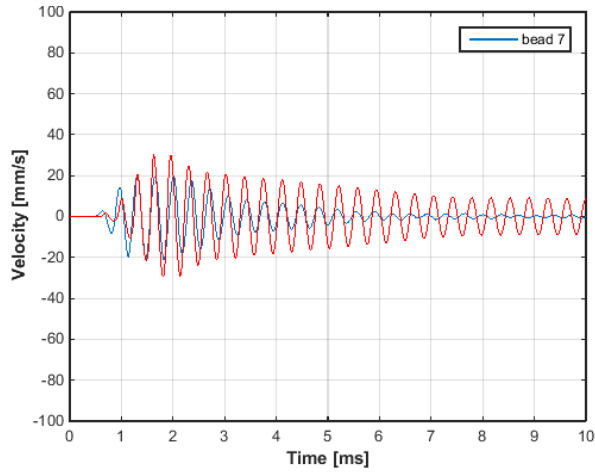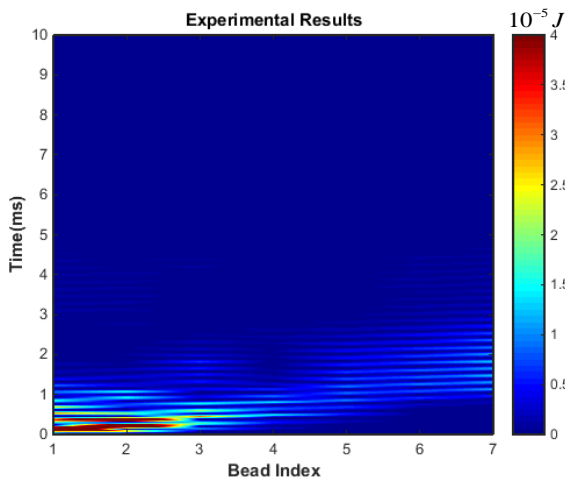
231

Figure 5.32. Comparison of experimental measurements and numerical simulations for the highest impulse (forcing level 3): (a)-(g) Experimental (blue) and numerical (red) velocity time series of the bead 1-7, (h) experimental spatio-temporal evolutions of the kinetic energy, and (g) numerical spatio-temporal evolutions of the kinetic energy.
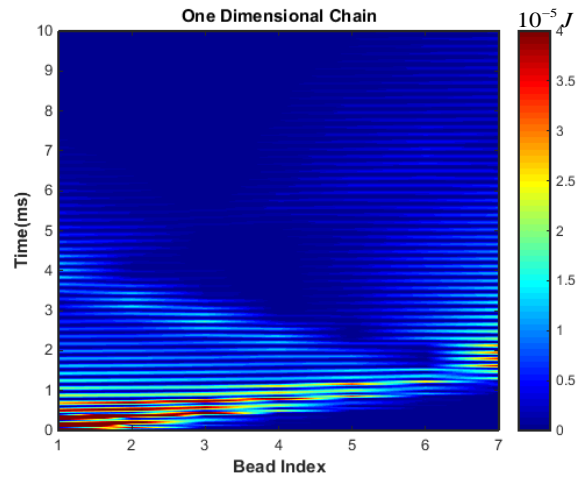
(g)

(h)

(i)

Figure 5.32 (cont.). Comparison of experimental measurements and numerical simulations for the highest impulse (forcing level 3): (a)-(g) Experimental (blue) and numerical (red) velocity time series of the bead 1-7, (h) experimental spatio-temporal evolutions of the kinetic energy, and (g) numerical spatio-temporal evolutions of the kinetic energy.

As shown in Figures 5.31 and 5.32, similar good agreement between experimental and numerical results is deduced for the other two forcing levels (levels 2 and 3). However, we would like to point out the deviations between the experimental and computation results in the cases of stronger impulses. These can be attributed to possible misalignments in the experimental fixture, as well as to the assumption of impulsive excitation provided by the forcing pendulum. In addition,

deviations between experiments and numerical simulations can be attributed by the approximation of the dissipative effects in the theoretical model by linear viscous damping (cf. equations (5.32)). Clearly, such linear viscous damping appears to be incapable of fully modeling the nonlinear dissipative effects present in the breather formation such as friction and plasticity effects. At the lowest forcing case (forcing level 1) our numerical model overestimates the amplitudes, while at the highest forcing level (forcing level 3) it seems to underestimate the responses. Nevertheless, the computational results are in satisfactory agreement with the experimental measurements regarding the initial breather formation in the granular chain, with discrepancies between theory and experiment appearing at later times when the nonlinear damping effects affect significantly the response.

A last note concerning the theoretical and experimental comparisons has to do with the initial velocity prescribed in the computational model. In the results of Figures 5.30-5.32 we employed the following estimates the initial velocities: $40mm/s$ (forcing level 1), $55mm/s$ (forcing level 2), and $80mm/s$ (forcing level 3). These estimates were derived by best reconciling the experimental measurements and numerical simulations in the initial stage of the breather formation. Clearly, alternative estimates of the initial velocities can be derived directly from the initial drop angles of the forcing pendulum. Given that the length of the pendulum has length $h = 302mm$ we can theoretically calculate the applied initial impulse (and, approximately, the initial velocity of the first bead of the chain) based on energy conservation as follows, $v_0 = \sqrt{2gh\left(1 - \cos\left(\theta_0\right)\right)}$ where g is the gravitational constant. This, however, is an approximate estimate since it ignores the mass of the pendulum bar, and friction losses at the pivot of the pendulum; moreover, it assumes that the entire momentum of the pendulum is transferred exclusively to the first bead of the chain and omits losses in momentum transfer due

to elastic deformations of the contacting beads and also due to "spillover" of momentum to the second and other beads of the chain. Finally, there is a third way to estimate the initial velocity of the first bead, by experimentally measuring the pendulum responses at the three forcing levels directly using a laser vibrometer. Such measurements of the velocities of the pendulum are depicted in Figure 5.33, from which we observe very clear applications of impact. Again, these measurements assume exclusive transfer of momentum from the pendulum exclusively to the first bead of the granular chain. The assumption that the applied initial impulse is equal to the initial velocity of the first bead is based on no energy loss during the interaction between the chain and pendulum, which is practically impossible.

Table 5.1. Initial velocities for three forcing levels approximated by different methods.

Forcing level	Numerical estimation	Theoretical calculation	Experimental testing
Level 1	$40mm/s$	$30.3mm/s$	$39.7mm/s$
Level 2	$55mm/s$	$60.6mm/s$	$61.3mm/s$
Level 3	$80mm/s$	$91.0mm/s$	$86.5mm/s$

In Table 5.1 we summarize the estimated initial velocities for the three forcing levels using the aforementioned methods. We note that the effects of friction and energy loss are not significant given the closeness of the results from the three different methods.
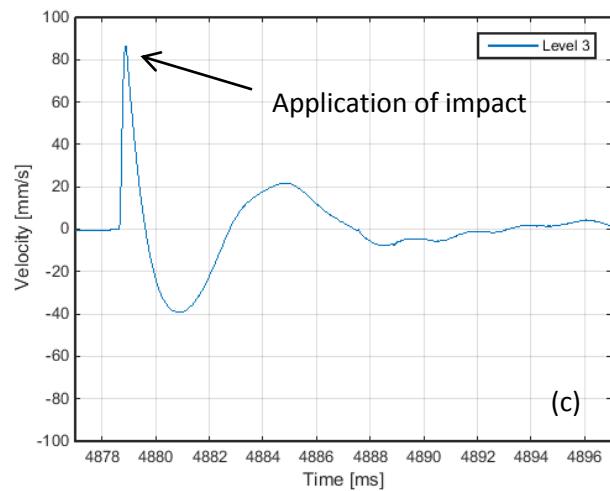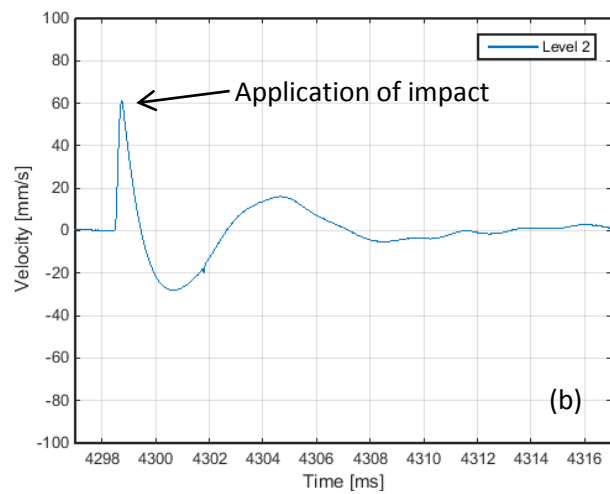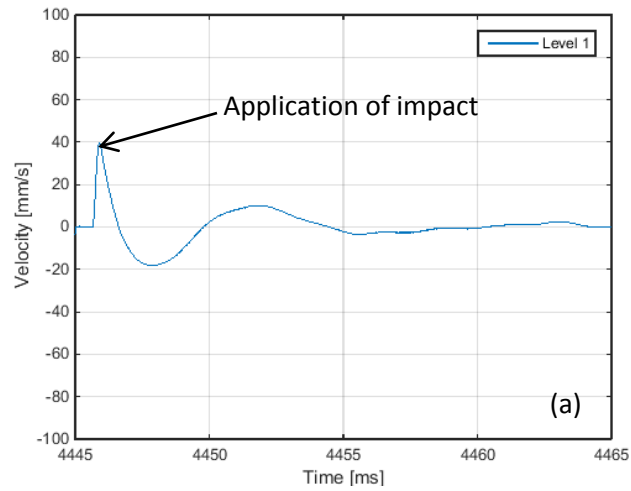
Figure 5.33. Typical laser vibrometer measurement of the velocity of the pendulum for the different forcing levels: (a) level 1, (b) level 2, and (c) level 3.
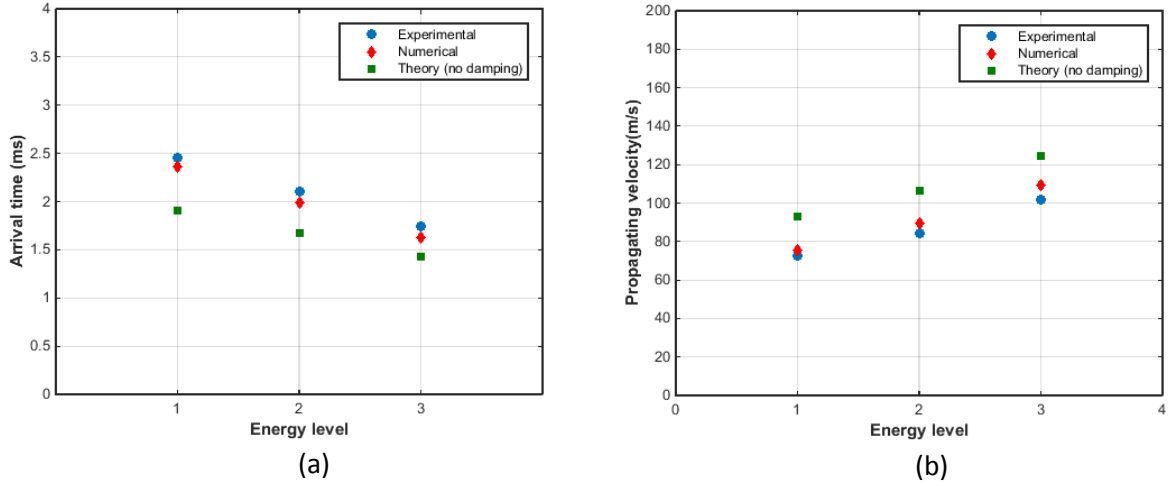
Figure 5.34. Propagating breather in the homogeneous granular chain on elastic foundation: (a) arrival time of the breather at the end bead, and (b) corresponding breather propagation speed; Experimental measurements (●), computation results based on system (5.31) (◊), and analytical preditions besed on equation (5.33) (□).

Finally, we consider the wave propagation speed in the chain for the three different forcing levels. As mentioned previously, the granular system without pre-compression is strongly nonlinear with energy-dependent properties such as the speed of wave propagation. To prove this energy-tunable dynamical property, and to validate our previous analytical study, we compare the arrival times of the breather reaching the end bead from the experimental results, numerical simulations and theoretical predictions. For the experimental and numerical results the arrival time for the three different excitation levels can be directly read from the 7th bead response as depicted in Figure 5.34a (the horizontal axis indicates the excitation level). The analytical prediction in Figure 5.34a is calculated from,

$$T_{theory} = 7 \times \frac{6.0394(1-v^2)\sqrt{m\tilde{k}_1}}{E\sqrt{RA}} \tag{5.34}$$

where all parameters are previously defined. Again, good agreement between the experimental measurements and the numerical simulations are clearly deduced. We note that there is an obvious discrepancy between the analytical prediction and the other two results, which is attributed to the assumption of zero damping in the analytical study. However, the trend of the decreasing propagation time as the excitation level increases is fully captured by the analytical model. Then, the speed of wave propagation can be directly calculated by dividing the distance traveled, which equals the total length of the chain (7 inches or 177.8 mm), by the arrival time. We depict the resulting wave speed in Figure 5.34b.

5.3 Conclusions

We have studied propagating discrete breathers in externally excited homogenous nonlinear granular media on elastic foundations, with no pre-compression. We analytically proved that the propagating breathers are due to nonlinear resonances in the dynamics. In fact, the propagating breathers are formed by a dynamical balance of the nonlinear Hertzian interactions in the granular chains, the on-site elastic potentials and the discreetness of the media. Moreover, our analytical models successfully predict the wave propagation speed and frequency components of the discrete breathers. Then, a computational study was performed to validate the analytical results. Utilizing these analytical predictions we have shown multiple potential applications in the design of acoustic shock absorbers or amplifiers, and we have numerically proven the existence of countable infinities of breathers caused by higher order resonances. We emphasize that due to the strong nonlinearity of the granular dynamics, the above results are dependent on the intensities (magnitudes) of the applied excitations, so the stationary dynamics are passively tunable with energy.

In agreement with the theoretical predictions we experimentally demonstrated propagating breathers in these highly discontinuous granular media under impulsive excitation. The propagating breathers were robustly excited in a single granular chain at different levels of impulsive excitation, provided that it was sufficiently small. Furthermore, our experimental results fully validated the computational and analytical results (at least for the primary propagating breathers). To the authors' knowledge, the findings in this work are the first experimental evidence of propagating discrete breathers in this class of strongly nonlinear metamaterials. The formation of propagating breathers in granular chains paves the way for practical implementations of passive wave redirection in granular metamaterials, as discussed in Chapter 4, by employing spatial Landau-Zener tunneling. In general, the results of this section can be applied to the design of practical nonlinear granular metamaterials which are adaptive to different external excitations and tunable to energy.

5.4 References

Hasan, M., Starosvetsky, Y., Vakakis, A., Manevitch, L., "Nonlinear Targeted Energy Transfer and Macroscopic Analog of the Quantum Landau–Zener Effect in Coupled Granular Chains," *Physica D*, **252**, 46–58, 2013.

Hasan, M., Cho, S., Remick, K., Vakakis, A., McFarland, D., Kriven, W., "Experimental Study of Nonlinear Acoustic Bands and Propagating Breathers in Ordered Granular Media Embedded in Matrix," *Gran. Matter*, **17**, 49–72, 2015.

Herbold, E., Nesterenko, V., "Shock Wave Structure in a Strongly Nonlinear Lattice with Viscous Dissipation," *Phys. Rev. E,* **75**(2), 021304, 2007.

James, G., "Nonlinear Waves in Newton's Cradle and the Discrete p-Schrödinger Equation," *Math. Mod. Meth. Appl. Sci.*, **21**, 2335-2377, 2011.

James, G., Kevrekidis, P., Cuevas J., "Breathers in Oscillator Chains with Hertzian Interactions," Physica D, **251**, 39–59, 2013.

Jayaprakash, K., Starosvetsky, Y., Vakakis, A., Peeters, M., Kerschen, G., "Nonlinear Normal Modes and Band Zones in Granular Chains with No Precompression," *Nonl. Dyn.*, **63**(3), 359-385, 2011.

Manevitch, L., "Complex Representation of Dynamics of Coupled Nonlinear Oscillators," in *Mathematical Models of Non-Linear Excitations: Transfer, Dynamics, and Control in Condensed Systems and Other Media*, Kluwer Academic, 1999.

Mead, D., "Wave Propagation and Natural Modes in Periodic Systems: I Mono-coupled Systems," *J. Sound Vib.*, **40**(1), 1–18, 1975.

Potekin, R., Jayaprakash, K., McFarland, D., Remick, K., Bergman, L., and Vakakis, A., "Experimental Study of Strongly Nonlinear Resonances and Anti-resonances in Granular Dimer Chains," *Exp. Mech.*, **53**(5), 861–870, 2013.

Starosvetsky, Y., Hasan, M., Vakakis, A., Manevitch, L., "Strongly Nonlinear Beat Phenomena and Energy Exchanges in Weakly Coupled Granular Chains on Elastic Foundations," *SIAM J. Appl. Math.*, **72**(1), 337–361, 2012.

Vakakis, A., Gendelman, O., Bergman, L., McFarland, D., Kerschen, G., Lee, Y., *Passive Nonlinear Targeted Energy Transfer in Mechanical and Structural Systems: I and II*, Springer Verlag, 2008.

Zhang, Y., Moore, K., McFarland, D., Vakakis, A., "Targeted Energy Transfers and Passive Acoustic Wave Redirection in a Two-dimensional Granular Network Under Periodic Excitation," *J. Appl. Phys*., **118**, 234901, 2015.

Zhang, Y., Vakakis, A., "High-Frequency Dynamic Overshoot in Linear and Nonlinear Periodic Media," *J. Comput. Nonlinear Dynam.*, **12**, 011012, 2016.

Chapter 6. Conclusions and suggestions for further work

In this work, we aimed to study the essentially nonlinear dynamics and acoustics of uncompressed granular networks with or without external excitation. In this regard we have considered both one-dimensional and multi-dimensional networks of granular metamaterials. Without seeking the continuum limit approximations the exact discrete and non-smooth equations of motion were directly employed in our theoretical study. Further, our experimental studies recovered some of the intriguing theoretical findings. In this chapter we provide a synopsis of above derived results as well as some directions for future research work.

6.1 Conclusions

In the first part of the dissertation, we studied the stationary-state dynamics of one-dimensional finite homogeneous granular chains with no prior compression and under time-periodic excitations. We theoretically confirmed two types of resonance motions involving harmonic or subharmonic traveling pulses in the granular chain, as well as a state of anti-resonances or chimera states. These nonlinear dynamical states corresponded to local maxima and minima, respectively, of the maximum transmitted force at the right end of the chain. Furthermore, we experimentally verified the existence of two strongly nonlinear resonance peaks and one anti-resonance valley between them. Our experimental results which were found to be in good agreement with the theoretical computational results, proved that a strongly nonlinear medium (with complete absence of linear acoustics and linear resonance spectrum) can support a strongly nonlinear resonance spectrum, tunable with energy. To our knowledge this is the first such experimental result reported in the literature. The findings represented in this part have multiple potential applications in the design of strongly nonlinear acoustic metamaterials as energy

absorbers when they are excited at anti-resonance frequencies, or, on the contrary, as efficient energy transmitters at resonance frequencies.

The second granular network under consideration in this dissertation was a granular network composed of a nonlinearly coupled system of two granular chains. We developed a semi-analytical method for studying the primary pulse transmission in these coupled granular chains subjected to impulsive excitation. In the early-time responses of the network strong energy scattering close to the application of the impulsive excitation was deduced due to the formation of a mixed type of nonlinear waves involving oscillatory nonlinear shear waves (S −waves) in the transverse direction and near-zero frequency pulses (P − pulses) propagating in the longitudinal direction. Our computational results showed that pulse (or energy) equi-partition occurred in the considered granular network because of strong energy transfers from the excited to the absorbing chain. The P −pulses dominated energy transmission to the far field of the granular network, and can be seen as perturbations of the well-known Nesterenko solitary waves which propagate in single homogenous granular chains. Moreover, we introduced an analytical mapping approach which revealed the strongly nonlinear mechanism that leads to the formation of the mixed nonlinear waves in the longitudinal and transverse directions. Experimental energy transfers from the excited to the absorbing chains and eventual pulse equi-partition were also presented. We tested four experimental configurations consisting of geometrically coupled, two-dimensional granular chains with varying number of beads, and impulse excitation applied to one of the chains. In granular networks with sufficiently large number of beads the theoretically predicted pulse equi-partition was observed experimentally. Moreover, our experimental results validated the proposed theoretical model which could reliably capture primary pulse propagation

in the coupled granular chains. This model provided a new avenue of understanding and analyzing energy scattering in two- or multi-dimensional ordered granular networks.

Then, we aimed to study intense nonlinear recurring energy exchanges in weakly coupled, strongly nonlinear granular chains mounted on linear elastic foundations (i.e., linear on-site potentials), without prior compression and under harmonic excitation. Depending on the frequency of the excitation such ordered granular media possess energy-tunable pass and stop bands similar to linear periodic systems. We analyzed the strongly nonlinear dynamics of granular chains in two frequency ranges, namely, (i) the high-frequency attenuation zone; and (ii) the intermediate-frequency propagation zone. In the second scenario, we successfully realized targeted energy transfer (TET), i.e., one-way, irreversible energy transfer from an "excited" to an "absorbing" granular chain. We showed that once discrete breathers are formed in this granular network almost complete and irreversible energy transfers from one of the interacting granular chains to another weakly coupled chain can be achieved through stratification of the on-site elastic foundation. The governing nonlinear dynamical mechanism for this targeted energy transfer phenomenon is the Landau-Zener tunneling (LZT) effect in space.

Moreover, we detected interesting and counterintuitive dynamic overshoot phenomena in both linear and nonlinear periodic media when they were excited by suddenly applied high-frequency excitations. In the far fields of these media we numerically detected transient (nonstationary) propagating disturbances even though the excitation frequency was located well inside the attenuation zone of these systems. From an analytical point of view, we showed that the dynamic overshoot for a linear semi-infinite lattice can be approximated in terms of the Green's functions at the free end of the lattice or, equivalently, by an impulsive response of the lattice in the limit of high frequency harmonic excitation. We compared this asymptotic model

244

with the results of direct numerical simulations and good agreement was deduced. Contrary to the linear case, in the nonlinear granular medium the dynamic overshoot was realized in the form of a pure stationary breather, i.e., of an oscillatory wavepacket with localized envelope, resulting from the balance of dispersion, nonlinearity and discreteness. Employing the complexification/averaging method together with a multiple scale analysis we were able to asymptotically prove the dynamic overshoot was solely due to the early transient state of the network. In similarity to the linear lattice, the suddenly applied, high-frequency harmonic excitation eventually amounted to an impulsive input applied to the excited lattice. Thus, after the asymptotic reduction of the transient dynamics to an impulsive response was accomplished, we could directly apply the results reported by Hasan (2013) for passive energy redirection based on the excitation of the traveling breather.

In the intermediate frequency range, a systematically computational study of the above weakly coupled granular network was presented. Contrary to the study for high-frequency excitation, we focused on the steady-state response of this granular network under harmonic excitation with relatively slow frequency, i.e., on the dynamics that was eventually reached after sufficiently long time has passed so that the initial transients have died out. For certain combinations of the amplitude and frequency of the applied excitation the network reached a stable steady-state response where a periodic, nearly complete but reversible energy exchange between the two chains occurred. Energy localization, in the form of propagating breathers, which was generated by nonlinear resonances in the dynamics and was associated with phase locking and synchronization phenomena in space and time in both the excited and absorbing chains was noted.

Motivated by the realization of nonlinear beat phenomena in this weakly coupled granular network, we introduced a linear spatial stratification of the elastic foundation of the excited chain, which was a necessary step towards the practical implementation of the Landau-Zener effect in space and the realization of targeted energy transfer and passive wave redirection in the weakly coupled granular network. The steady state dynamic responses of the network for varying spatial stratification rate (from 0% to 33%) were then studied. Intense passive targeted energy transfer from the excited to the absorbing chain and eventual localization of the energy in the absorbing chain was archived at the spatial stratification rate of 27%. Employing the empirical mode decomposition (EMD) together with the numerical Hilbert transform (HT) we were able to reveal the nonlinear dynamical mechanism governing this passive wave redirection in the stratified granular network. At the spatial reduction rate of 27% we showed the occurrence of sustained 1:1 resonance captures between dominant frequency components of the responses of the excited and absorbing chains leading to nonlinear targeted energy transfer in the network. For other spatial stratification rates either no resonance captures occurred, or transient 1:1 resonance captures were realized followed by escapes from resonance. Based on these results we concluded that intense targeted energy transfer from the excited to the absorbing chain was due to sustained 1:1 resonance captures between specific frequency components of the steady-state responses of the beads of the excited and absorbing chains. The study of practical realization of the Landau-Zener effect indicated the feasibility of implementing passive wave redirection in practical acoustic metamaterials.

In the last part of the dissertation, we focused on analytical and experimental studies of propagating discrete breathers in homogenous granular media mounted on elastic foundations. Under the assumption of small energy (amplitude) we were able to reduce the nonlinear dynamics

of a homogeneous granular chain to a single discrete nonlinear p-Schrödinger equation (DNLpS equation); to perform this we employed the complexification-averaging method. This well-known DNLpS equation allowed us to derive the nonlinear dispersion relation for traveling waves and propagating breathers in the homogeneous granular chain, from which energy-tunable and foundation-dependent acoustic filtering properties, i.e. pass- and stop-bands, of the ordered granular network could be deduced. We analytically studied the propagating breathers, in the form of oscillatory wavepackets with localized envelopes, the in pass-band of the granular medium. Explicit expressions for the wave propagation speed and the frequency components of the localized propagating breathers were derived. Our study in the frequency domain revealed the nature of the nonlinear beating phenomena, namely that they were due to a combination of internal and external resonances whereby the (slow) frequency of the harmonic excitation equals a fraction of the difference between certain fast frequency components. Hence, a countable infinity of families of breathers parametrized by energy was detected, with each family corresponding to $1/n, n = 1, 2, \dots$ combination resonances. Some of these breathers were numerically studied. Moreover, we experimentally detected propagating breathers in a one-dimensional granular chain under impulsive excitation, which validated our computational and analytical studies. Two experimental setups were constructed for this purpose and the realization of propagating breathers was robustly detected.

Summarizing, in this dissertation we reported both theoretical and experimental results on the free and forced dynamics of granular networks composed of weakly coupled ordered granular chains. We investigated and developed a predictive framework for wave propagation in granular networks and acoustic metamaterials for effective wave tailoring. These results can be utilized for the design of practical implementations employing granular media for shock

247

mitigation, wave redirection, and energy-tunable acoustic filtering. This dissertation contains novel concepts, new analytical methodologies and new experimental studies for studying this new class of strongly nonlinear acoustic metamaterials with unprecedented dynamical properties.

6.2 Suggestions for further research

Regarding suggestions for future work, there are numerous possible extensions of the topics discussed in this dissertation. The concept of resonances and anti-resonances in one-dimensional granular chains discussed in Chapter 2 can be extended to higher dimensions, for example, hexagonal or square lattices. It would be interesting to perform a systematical study to show how input energy from the external excitation or any other system parameters could influence the formations of nonlinear resonances and anti-resonances. Such analysis could potentially contribute to the design of practical implementations of nonlinear acoustic metamaterials, such as sound attenuators or amplifiers, with properties adaptive to different types of external excitations.

For the case of "dry" coupled granular chains discussed in Chapter 3 we mainly focused on the near-zero frequency primary pulses propagation in the longitudinal direction. However, the system could potentially reach resonance conditions if the frequencies of the vertical shear oscillatory waves match or are close to the characteristic frequencies of the coupled granular chains. As a result, at least in principle, strong energy scattering in the vertical motion could be observed and small amounts of residual energy would be left to propagate in the axial direction. Moreover, we only considered homogenous chains, while granular dimer chains exhibit interesting intrinsic responses which are dependent on the mass ratio between the light and heavy beads. For a one-dimensional chain the properties of any light intruders (dimer beads) can

drastically affect the transmitted energy in the system (Jayaprakash et al., 2013; Potekin et al., 2016). In multi-dimensional networks of granular metamaterials, such as the coupled chains considered herein, light granules could be placed between heavy beads in the same chain or between two different chains, which would introduce additional coupling effects. In each case the dynamical mechanism governing the nonlinear scattering of the applied impulsive energy in both directions would change. Hence, it would be informative to extend the study of the homogenous granular coupled chains to dimer chains in order to establish possible quantitative or qualitative changes in wave propagation and energy transfer.

Finally, in Chapters 4 and 5 we mounted granular networks on elastic foundations compared to the "dry" chains considered in previous Chapters. It would be interesting to know if the onsite potentials are prerequisites for the realization of targeted energy transfer (TET). Moreover, for practical implementations of the findings of this work, experimental validation of the theoretical models is required. The experimental study in Chapter 5 for discrete propagating breathers in a single granular chain with homogenous elastic foundation can be further developed to verify the Landau-Zener Tunneling effect (as discussed in Chapter 4), leading to TET or passive wave redirection. However, it could be practically difficult to obtain gradually stratified foundations as we considered in theoretical study. Hence, it would be desirable to theoretically study similar systems as discussed in Section 4.3 but with simpler stratification schemes for the onsite potentials of excited chain, in order to verify if TET can still be realized in these cases.

6.3 References

Jayaprakash, K., Starosvetsky, Y., Vakakis, A., Gendelman, O., "Nonlinear resonances leading to strong pulse attenuation in granular dimer chains," *J. Nonl. Science*, **23**(3), 363-392, 2013.

Potekin, R., McFarland, D., Vakakis, A., "Nonlinear wave scattering at the flexible interface of a granular dimer chain," *Granular Matter*, **18**(68), 2016.